Solution Methodologies for the Population Balance Equations Describing the Hydrodynamics of Liquid-Liquid Extraction Contactors

Vom Fachbereich für Maschinenbau und Verfahrenstechnik
der Technischen Universität Kaiserslautern
zur Erlangung des akademischen Grades

Doktor – Ingenieur (Dr.-Ing.)

genehmigte Dissertation

Vorgelegt von

M. Sc. Chem. Eng. Menwer Attarakih

aus Amman - Jordanien

Eingereicht am: 19.05.2004
Mündliche Prüfung am: 01.07.2004

Promotionskommission:

Vorsitzender: Prof. Dr.-Ing. P. Steinmann
Referenten: Prof. Dipl.-Ing. Dr. techn. Hans-Jörg Bart
Associated Prof. Naim M. Faqir

Dekan: Prof. Dr.-Ing. P. Steinmann

D 386
2004

ACKNOWLEDGMENT

This work is performed during my stay as a Ph.D. student at the University of Kaiserslautern / Germany at the Institute of Process Engineering chaired by Prof. Dipl.-Ing. Dr. techn. Hans-Jörg Bart.

I would like first to thank my advisor Prof. Hans-Jörg Bart for his permanent and extensive support to accomplish this work. I highly appreciate his excellent advice and guidance during all the stages of this long term project, and in particular for his contributions to my publications.

I would like also to express my deep thanks to Associated Prof.. Naim Faqir from the University of Jordan/ Chem. Engng. Dept. for his valuable remarks, patience, and his contributions for preparing my publications during his many research visits to the Institute of Thermal Process Engineering here at the University of Kaiserslautern.

Second I am very grateful to Prof. Dr.-Ing. P. Steinmann and the Associated Prof. Naim M. Faqir for serving as Committee Members.

This work is partially supported by the German Academic Exchange Service (DAAD), the precious scholarship from my home University: Al-Balaqa Applied University as well as the financial support granted by the chairman of the Institute of Process Engineering: Prof. Hans-Jörg Bart, to all those I gratefully acknowledge this support.

I am deeply indebted to all my colleagues at the Institute of Process Engineering and especially the Extraction Group (Martin Simon and Stephan Schmidt) whose continuous help greatly facilitated my research.

I would like to thank Mr Dennis Bosse for translating the abstract, and Mrs Schneider for her help in checking the language of some parts of this thesis. The help of Dr. Krätz is also greatly acknowledged.

To my mother that she has been suffering for more than three years without any chance to see me; to the whole members of my family who are still waiting for me; I say to all of them ″PLEASE FOREGIVE ME″.

Finely, I am thankful to my wife: Feda′ for her endless patience and continuous support, to my little children: Balqees, Maya and Kariem for their ever shining smiles of kindness and love.

Kaiserslautern, in July 2004

Menwer Attarakih

To my mother, wife and the little children: Balqees, Maya and Kariem

ABSTRACT

Solution Methodologies for the Population Balance Equations Describing the Hydrodynamics of Liquid-Liquid Extraction Contactors

The polydispersive nature of the turbulent droplet swarm in agitated liquid-liquid contacting equipment makes its mathematical modelling and the solution methodologies a rather sophisticated process. This polydispersion could be modelled as a population of droplets randomly distributed with respect to some internal properties at a specific location in space using the population balance equation as a mathematical tool. However, the analytical solution of such a mathematical model is hardly to obtain except for particular idealized cases, and hence numerical solutions are resorted to in general. This is due to the inherent nonlinearities in the convective and diffusive terms as well as the appearance of many integrals in the source term.

In this work two conservative discretization methodologies for both internal (droplet state) and external (spatial) coordinates are extended and efficiently implemented to solve the population balance equation (PBE) describing the hydrodynamics of liquid-liquid contacting equipment. The internal coordinate conservative discretization techniques of Kumar and Ramkrishna (1996a, b) originally developed for the solution of PBE in simple batch systems are extended to continuous flow systems and validated against analytical solutions as well as published experimental droplet interaction functions and hydrodynamic data. In addition to these methodologies, we presented a conservative discretization approach for droplet breakage in batch and continuous flow systems, where it is found to have identical convergence characteristics when compared to the method of Kumar and Ramkrishna (1996a).

Apart from the specific discretization schemes, the numerical solution of droplet population balance equations by discretization is known to suffer from inherent finite domain errors (FDE). Two approaches that minimize the total FDE during the solution of the discrete PBEs using an approximate optimal moving (for batch) and fixed (for continuous systems) grids are introduced (Attarakih, Bart & Faqir, 2003a). As a result, significant improvements are achieved in predicting the number densities, zero and first moments of the population.

For spatially distributed populations (such as extraction columns) the resulting system of partial differential equations is spatially discretized in conservative form using a simplified first order upwind scheme as well as first and second order nonoscillatory central differencing schemes (Kurganov & Tadmor, 2000). This spatial discretization avoids the characteristic decomposition of the convective flux based on the approximate Riemann Solvers and the operator splitting technique required by classical upwind schemes (Karlsen et al., 2001).

The time variable is discretized using an implicit strongly stable approach that is formulated by careful lagging of the nonlinear parts of the convective and source terms.

The present algorithms are tested against analytical solutions of the simplified PBE through many case studies. In all these case studies the discrete models converges successfully to the available analytical solutions and to solutions on relatively fine grids when the analytical solution is not available. This is accomplished by deriving five analytical solutions of the PBE in continuous stirred tank and liquid-liquid extraction column for especial cases of breakage and coalescence functions.

As an especial case, these algorithms are implemented via a windows computer code called LLECMOD (Liquid-Liquid Extraction Column Module) to simulate the hydrodynamics of general liquid-liquid extraction columns (LLEC). The user input dialog makes the LLECMOD a user-friendly program that enables the user to select grids, column dimensions, flow rates, velocity models, simulation parameters, dispersed and continuous phases chemical components, and droplet phase space-time solvers. The graphical output within the windows environment adds to the program a distinctive feature and makes it very easy to examine and interpret the results very quickly. Moreover, the dynamic model of the dispersed phase is carefully treated to correctly predict the oscillatory behavior of the LLEC hold up. In this context, a continuous velocity model corresponding to the manipulation of the inlet continuous flow rate through the control of the dispersed phase level is derived to get rid of this behavior.

Key words: Liquid-liquid dispersion; Hydrodynamics; Population balance; Droplet breakage; Droplet coalescence; Conservation laws; Numerical Solution.

KURZFASSUNG

Lösungsansätze zur Beschreibung der Hydrodynamik in der Flüssig-flüssig Extraktion auf Basis von Populationsbilanzen

Der poyldisperse Charakter von turbulenten Tropfenschwärmen in gerührten Extraktionsapparaten erschwert deren mathematische Modellierung sowie das Finden von geeigneten Lösungsstrategien. Mit Hilfe von Populationsbilanzen (PBE) können solche Systeme als eine Verteilung von Tropfen mit unterschiedlichen internen Eigenschaften, z.B. Konzentration oder Temperatur, zeit- und ortsaufgelöst mathematisch beschrieben werden. Aufgrund der mathematischen Komplexität können nur für wenige Spezialfälle die PBE analytisch gelöst werden und es müssen numerische Lösungstrategien entwickelt werden. Diese Schwierigkeiten sind vor allem auf Nichtlinearitäten in den konvektiven und diffusiven Termen sowie auf die große Anzahl von Integralen in den Quelltermen zurückzuführen.

In dieser Arbeit wurden zwei konservative Diskretisierungsmethoden zur Beschreibung des internen (Tropfenzustand) und des externen (Kolonnenhöhe) Koordinatensystems weiterentwickelt, um die Hydrodynamik von Flüssig-flüssig-Kontaktoren mit Hilfe von PBE effizient vorausberechnen zu können. Für die interne Diskretisierung wurde die Methodik von Kumar und Ramkrishna (1996a, b), die einfache Batchsysteme mit PBE erfolgreich beschreibt, auf kontinuierliche Prozesse erweitert und mit Hilfe von analytischen Lösungen sowie experimentellen Daten validiert. Darüber hinaus wurde eine Diskretisierungsmethode für den Tropfenzerfall in kontinuierlichen und in Batchsystemen entwickelt, die die gleichen Konvergenzeigenschaften aufweist wie die Methode von Kumar und Ramkrishna (1996a).

Unabhängig von den gewählten Diskretisierungsmethoden ist die numerische Lösung von PBE immer mit Ungenauigkeiten behaftet. Daher wurden für die Minimierung des numerischen Gesamtfehlers für Batchsysteme bewegliche Gitter und für kontinuierliche Systeme fixierte Gitter eingeführt (Attarakih, Bart & Faqir, 2003a). Mit den gewählten Gittertypen konnten signifikante Verbesserungen bei der Anzahldichte sowie dem nullten und ersten Moment der Verteilung erreicht werden.

Für ortsaufgelöste Tropfenverteilungen, wie sie z.B. in Extraktionskolonnen vorkommen, wurde das resultierende partielle Differentialgleichungssystem mit Hilfe eines einfachen First-Order-Upwind-Verfahrens und einem nichtoszillatorischen Differenzenverfahrens (erster und zweiter Ordnung) (Kurganov & Tadmor, 2000) örtlich diskretisiert. Diese Art der örtlichen Diskretisierung vermeidet die charakteristische Spaltung des konvektiven Stromes, wie er bei der Anwendung des Riemann Solvers oder bei klassischen Upwind-Verfahren (Karlsen et al., 2001) entsteht.

Die Zeitvariable wird mittels eines stabilen, impliziten Verfahrens diskretisiert, das die nichtlinearen Anteile des konvektiven Terms sowie der Quellterme zeitlich verzögert betrachtet.

Für die Verifikation der vorgestellten Algorithmen wurden analytische Lösungen der PBE für fünf Spezialfälle abgeleitet, die sowohl Tropfenzerfall als auch Koaleszenz in kontinuierlichen Rührkesseln und Extraktionskolonnen betrachten. In allen Fällen konvergierten die eingesetzten Diskretisierungsmethoden erfolgreich gegen die analytische Lösungen und auch zu Lösungen für sehr feine Gitter, für die keine analytischen Lösungen existieren.

Die vorgestellten Algorithmen wurden in ein Windows-basiertes Simulationstool mit dem Namen LLECMOD (Liquid-Liquid Extraction Column Module) implementiert, um die Hydrodynamik beliebiger Extraktionskolonnen simulieren zu können. Das benutzerfreundliche Interface von LLECMOD gestattet dem Benutzer die Auswahl der Gitter, Kolonnendimensionen, Ströme, Geschwindigkeitsmodelle, Simulationsparameter, chemische Komponenten der kontinuierlichen und der dispersen Phase, sowie des Solvers für die orts-zeit-aufgelöste Beschreibung der Dispersphase. Die graphische Ausgabe erlaubt die schnelle Auswertung der Simulationsergebnisse. Darüber hinaus wurde darauf geachtet, dass das dynamische Modell auch das oszillatorische Verhalten des Dispersphasenholdups korrekt vorausberechnet

Keywords: Flüssig-flüssig Dispersion; Hydrodynamik; Populationsbilanzen; Tropfenzerfall; Tropfenkoaleszenz; Erhaltungsgleichungen; Numerische Simulat

Contents

List of Publications

This thesis is based on the following publications that are referred to in the text using the standard literature citing employed in this overview.

I Attarakih, M. M., Bart & Faqir, N. M. (2002). An approximate optimal moving grid technique for the solution of discretized population balances in batch systems. *European Symposium on Computer Aided Process Engineering-12,* Editors:Grievink, J. and Schijndel, J. Elsevier, Amsterdam, pp.823-828.

II Attarakih, M. M., Bart, H. J., & Faqir, N. M. (2003a). Optimal moving and fixed grids for the solution of discretized population balances in batch and continuous systems: droplet breakage. *Chem. Engng. Sci.*, **58,** 1251-1269.

III Attarakih, M. M., Bart, H.-J., & Faqir, N. M. (2003b). Solution of the population balance equation for liquid-liquid extraction columns using a generalized fixed-pivot and central difference schemes. Kraslawski, A. & Turunen, I. (Ed.), *European Symposium on Computer Aided Process Engineering-13*, Computer-aided chemical engineering 14 (pp. 557-562). Elsevier, Amsterdam.

IV Attarakih, M. M., Bart, H. J., & Faqir, N. M. (2004a). Solution of the droplet breakage equation for interacting liquid-liquid dispersions: a conservative discretization approach. *Chem. Engng. Sci.*, **59**, 2547-2565.

V Attarakih, M. M., Bart, H.-J. & Faqir, N. M. (2004b). Numerical solution of the spatially distributed population balance equation describing the hydrodynamics of interacting liquid-liquid dispersions. *Chem. Engng. Sci.* **59**, 2567-2592.

VI Attarakih, M. M., Bart, H.-J., & Faqir, N. M. (2004c). LLECMOD: a windows-based program for hydrodynamics simulation of liquid-liquid extraction columns. submitted to the *Chem. Engng. Procc. Journal*.

List of Symbols

$\boldsymbol{A}$	breakage interaction matrix, Eq.(9)
A_c	column cross sectional area
D_c, D_d	diffusion coefficients for the continuous and dispersed phases respectively, $m^2.s^{-1}$
D_R, D_s	rotor and stator diameters respectively, m
$\boldsymbol{d}$	characteristic droplet diameter vector
d, d'	droplet diameter, mm
d_0	mean droplet diameter of the initial or feed droplet distribution, mm
d_i, $d_{i+1/2}$	the characteristic droplet diameter and the right boundary of the ith subdomain respectively, mm
d_{min}, d_{max}	minimum and maximum droplet diameters, mm
$d30$, $d32$	mean droplet diameters, mm
$\overline{d30}$	mean droplet diameter with respect to d and column height, mm
F	the convective flux: $U_d n$, $s^{-1}m^{-3}$
FDE^L, FDE^U	average lower and upper finite domain errors, Eqs.(25) and (26)
g	the acceleration of gravity, $m.s^2$
H, H_c	column and single compartment heights respectively, m
$\boldsymbol{I}$	vector whose components are the integral quantities, I_i
I_i	integral quantity based on the property $u_m(d_i)$ in the ith subdomain
K_b, K_c	breakage and coalescence frequency constants
L	number of external (spatial) coordinate cells
M_x	number of subdomain of the internal coordinate (pivots)
M_0, M_1	zero and first moments of the discrete number density, $m^{-3}$and (-)
M_0^c, M_1^c	zero and first moments of the number density as obtained from the continuous distribution.
M_0^d, M_1^d	zero and first moments of the number density as obtained from the discrete distribution.
N_0^f	number concentration in the inlet feed, m^{-3}
N_i	droplet number concentration in the ith subdomain, mm^{-3}
N^*	rotor speed, s^{-1}
n	number distribution function, m^{-4}
n^{feed}	feed number distribution function, m^{-1}
$\boldsymbol{P}$	physical properties vector
P_r	breakage probability, Eq.(49)
Q_d	dispersed phase flow rate, $m^3.s^{-1}$
Q_c,	continuous phase flow rate, $m^3.s^{-1}$
Q_t	dispersed phase flow rate at top of the column, $m^3.s^{-1}$
$\boldsymbol{r}$	external coordinate vector:[x, y, z]
S	local propagation speed, Eq.(43)
t	time, s
U_c	continuous phase velocity relative to the column walls, $m.s^{-1}$
U_d	dispersed phase velocity relative to the column walls, $m.s^{-1}$
U_r	relative droplet (slip) velocity, $m.s^{-1}$
U_t	terminal droplet velocity, $m.s^{-1}$
u_m	any property associated with single droplet
v,v'	droplet volumes, m^3
v_0, v_f	mean droplet volume of the initial condition and feed distributions, m^3
v_{min}, v_{max}	minimum and maximum droplet volume, m^3
$v_{\min}^*$	optimal minimum droplet volume, m^3
v_i, $v_{i+1/2}$	the characteristic droplet volume and the right boundary of the ith subdomain respectively, m^3
x_i	the characteristic droplet volume in the ith subdomain, m^3
z	spatial coordinate, m
z_d	dispersed feed inlet, m

Greek symbols

α	parameter in the Weibull and inlet feed distributions
β	parameter in the Weibull distribution
β_n	daughter droplet distribution based on droplet number, mm^{-1}
δ_{l,l_d}	the Kronecker delta
Γ	droplet breakage frequency, s^{-1}
$\boldsymbol{\Psi}^{<i>}$	the *i*th coalescence interaction matrix whose elements are given by Eq.(13)
ϕ, $\boldsymbol{\Phi}$	dispersed phase hold up
φ_i	dispersed phase hold up in the *i*th subdomain
$\gamma_i^{<i-1>}$, $\gamma_i^{<i>}$	linear functions satisfying Eq.(7)
ρ_c, ρ_d	density of the continuous and dispersed phases respectively, $kg.m^{-3}$
μ_c	continuous phase viscosity, $kg.m^{-1}.s^{-1}$
ω	droplet coalescence frequency, $m^3.s^{-1}$
ω_R, $\omega_{R,crit}$	rotor and critical rotor speeds respectively, s^{-1}
σ_{cd}	interfacial tension, $N.m^{-1}$
σ	geometric grid factor
$\boldsymbol{\zeta}$	vector of external and time coordinates [*x, y, z, t*]
ξ	as defined by Eq.(12)
τ	residence time, s
θ	TVD parameter between 1 and 2.
$\vartheta(v')$	average number of droplets produced when mother droplet of volume, v', is broken

An Overview

Solution Methodologies for the Population Balance Equations Describing the Hydrodynamics of Liquid-Liquid Extraction Contactors

1. Introduction

In liquid-liquid contacting equipment such as completely mixed and differential contactors, droplet population balance based-modeling is now being used to describe the complex hydrodynamic behavior of the dispersed phase. This is due to the complex nature of the macroscopic dispersed phase interactions in a continuously turbulent flow field. These macroscopic interactions such as droplet breakage and coalescence result in a distributed population of droplets. This population is distributed not only in the spatial domain of the contacting equipment, but also randomly distributed with respect to the droplet state (properties) such as size, concentration and age. Within this framework it appears that Hulburt and Katz (1964) and Valentas and Amundson (1966) were among the first who introduced the population balance equation (PBE) into the modeling of chemical engineering processes involving dispersed phase operations. Such processes include unit operations carried out in batch and continuous stirred tanks as well as in differential contacting equipment such as crystallization (Motz, Mitrovic & Gills, 2002; Puel, Fevotte & Klein, 2003), bubble (Campos & Lage, 2003) and liquid-liquid extraction columns (LLEC) (Modes et al., 1999; Gerstlauer, 1999). In such unit operation equipment the dynamically changing behavior of the dispersed particles, or strictly speaking droplets (or bubbles), makes it necessary to consider a detailed mathematical rather than lumped modeling approach. These details are necessary to describe the discontinuous events occurring due to the interaction of the turbulent continuous and the dispersed phases constituents (droplets) such as breakage and coalescence. Loosely speaking, the term breakage considers the interaction of a single droplet with the turbulent continuous phase where the droplet undergoes breakage if the turbulent kinetic energy transmitted to the droplet exceeds its surface energy (Coulaloglou & Tavlarides, 1977). On the other hand, droplet coalescence is expected to occur due to the interaction between two droplets and the turbulent continuous phase. The coalescence between these two droplets is considered to occur if the intervening liquid film has sufficient contact time to be drained out (Chatzi & Lee, 1987). Consequently, it is expected to find a droplet size distribution along the spatial coordinate of the liquid-liquid contacting equipment making the models inherently assuming uniform droplet size distribution or based on some mean droplet diameter (*d32*) of little practical value (Alatiqi et al., 1995, Weinstein, Semiat & Lewin, 1998). Accordingly, the promising modeling of these phenomena, based on the population balances, offers not only the dispersed phase hold-up (volume concentration) but also any integral property associated with the resulting particle (droplet) distribution such as the mean droplet size and the specific interfacial area required for the calculation of mass and heat fluxes (Al Khani, Gourdon & Casamatta, 1988; Tsouris, Kirou & Tavlarides, 1994; Alopaeus et al., 2002). The population balance approach could be applied for modeling the behavior of the interacting liquid-liquid dispersions in either two basic ways, namely; the stagewise and the differential models. In the stagewise (Tsouris, Kirou & Tavlarides, 1994; Kentish, Stevens & Pratt, 1998; Steiner, Balmelli & Hartland, 1999) the multistage column is represented by a sequence of interacting stirred tanks with forward and backward flow components to compensate for the nonideal behavior of each tank. Practical examples of such columns are the perforated plate column, pulsed sieve plate column, Scheible column and mixer and settler cascades. In this sense a population balance equation has to be written for each tank with the required boundary conditions. In the differential model approach the phases are continuously contacted and allowed to separate only at the exit from the contactor such as the spray column, the rotating disc contactor (RDC), pulsating plate, Kühni and the Oldshue-Rushton column. In such equipment, the PBE is usually formulated as a conservation law in terms of volume concentration (mass for constant dispersed phase density) (Casamatta & Vogelpohl, 1985; Al Khani, Gourdon & Casamatta,

1988, 1989; Cabassud, Gourdon & Casamatta, 1990; Modes et al., 1999). The resulting differential model takes into account the droplet transport; breakage and coalescence as well as the necessary boundary conditions, though the latter are not clearly stated in the published literature. For a comprehensive review of mathematical modeling of liquid-liquid extraction columns, their advantages and disadvantages, the interested reader could refer to Mohanty (2000).

The application of the population balance approach is expected to provide invaluable information if no careful modeling of the breakage and coalescence as well as droplet transport laws is taken into consideration. However, due to the recent extensive research for determining the kinetics of droplet breakage and coalescence as well as droplet transport from single and swarm droplet experiments, it becomes more possible than before to introduce more realistic models for these kinetic parameters and the transport laws (Cauwenberg, Degreve & Slater, 1997; Kentish, Stevens & Pratt,1998; Colella et al., 1999; Modes, 2000; Alopaeus et al. 2002; Biggs & Lant, 2002; Bart, 2003; Desnoyer, Masbernat & Gourdon, 2003; Mignard, Amin, & Ni, 2003, Simon, Schmidt & Bart, 2003). Actually, this detailed level of information is at the expense of the mathematical complexity and thus demands a high computational cost since no analytical solution is known for the general population balance equation. Consequently, a numerical solution is required if precise simulation of the dispersed phase processes is required. In the last two decades there are many published papers concerned with the numerical solution of many special cases of the PBE arising from the modeling of many chemical and physical processes (Gelbard & Seinfeld, 1978; Gelbard, Tambour & Seinfeld, 1980; Sastry & Gaschignard, 1981; Casamatta & Vogelpohl, 1985; Al Khani, Gourdon & Casamatta, 1988; Hounslow, Marshal & Ryall, 1988; Marchal et al., 1988; Al Khani, Gourdon & Casamatta, 1989; Guimaraes et al., 1990; Hounslow, 1990; Kronberger et al., 1994; Hill & Ng, 1995; Kronberger et al., 1995; Ribeiro et al., 1995; Zimmermann et al., 1995; Hill & Ng, 1996; Kumar & Ramkrishna, 1996a, b; van Peborgh Gooch & Hounslow, 1996; Zamponi et al., 1996; Kumar & Ramkrishna, 1997; Hill & Ng, 1997; Liou, Srienc & Fredrickson, 1997; Ribeiro et al., 1997; Song, Steif & Weinspach, 1997; Nicmanis & Hounslow, 1998; Toutain et al., 1998; Vanni 1999; Bennett & Rohani, 2001; Liu & Cameron, 2001; Vanni, 2000; Lee et al., 2001; Wulkow, Gerstlauer, Nieken, 2001; Diemer & Olson, 2002a, b; Lim et al., 2002; Mahoney & Ramkrishna, 2002; Motz, Mitrovic, & Gills, 2002; Verkoeijen et al., 2002; Attarakih, Bart & Faqir, 2003a, b, 2004a; Compas & Lage, 2003; Goodson & Kraft, 2003). Despite this intensive research, no general numerical approach exists that is applicable to the general PBE when multivariate population distributions are necessary to be taken into account. The dependence of the average number distribution on droplet size, concentration and perhaps age (Ribeiro et al., 1995; Gerstlauer, 1999) is an example of such multivariate distribution in liquid-liquid dispersions. Moreover, the problem becomes more complicated when external coordinates appear as in the case of differential population balance models. By external coordinate it is meant the physical space (continuous phase), which is occupied by the droplets and hence is distinguished from the internal coordinates describing the droplet properties such as size, concentration, age etc. (Hulburt & Katz, 1964). This independent set of coordinates is often referred to in the population balance literature as the droplet (particle) phase space. One attractive approach to reduce the dimensionality of the population balance equation is by averaging it with respect to selected internal coordinate through the use of the method of moments (Randolph & Larson, 1988; Diemer & Olson, 2002). The method of moments is considered very attractive from computational point of view especially when specific average properties of the population are the target of the calculations. Unfortunately, the method of moments is not without inherent problems due to the closure and the distribution reconstruction intricacies (Diemer & Olson, 2002).

1.1 Review of the available numerical methods

Apart from the method of moments, the most frequently used numerical methods for the solution of the PBE could be grouped into three categories: stochastic, higher order and zero order methods.

1.1.1 Stochastic methods

Stochastic approaches as differentiated from finite difference methods are simulation techniques designed to artificially realize the system behavior through the generation of random numbers used for the identification of the probability functions governing the system behavior (Ramkrishna, 2000). This stochastic simulation approach has the advantage of being capable of simulating the multivariate PBE with respect to internal coordinate when the other numerical methods become extremely expensive. A presentation of two currently used algorithms for stochastic simulation of the PBE in a batch stirred tank: the direct simulation and the mass flow algorithms is found in Goodson and Kraft (2003).

1.1.2 Higher order methods

Most of the higher order methods try to approximate the distribution function by a set of linearly independent functions of order greater than zero through the finite element method. Gelbard and Seinfeld (1978) solved the PBE for droplet coalescence in batch stirred tank using the orthogonal collocation on finite elements with cubic polynomials and by scaling the droplet diameter logarithmically. Nicmanis and Hounslow (1998) solved the PBE for continuous stirred tank at a steady state using the mixed Galerkin and the orthogonal collocation methods on finite elements with cubic polynomials. Despite their accuracy, the major disadvantage of these methods is the excessive computational load imposed by evaluation of double integrals. This is particularly when the breakage and coalescence functions are dependent on some integral property associated with the population such as the dispersed phase hold-up (time dependent). Mahoney and Ramkrishna (2002) addressed this issue in addition to the difficulties associated with singularities of the integrand where suggestions are presented to remove these singularities for specific coalescence frequencies. Wulkow, Gerstlauer and Nieken (2001) solved the PBE for crystallization process using the Galerkin method on finite elements, which is adaptive in both droplet size and order (Galerkin-h-p). The major drawback of this method is the difficulty to decouple the time dependent frequencies (coalescence and breakage) from the time dependent variables, and hence the computational cost is increased excessively especially when more than one coordinate in the PBE is involved. An extensive review of these methods could be found in Ramkrishna (1985, 2000).

1.1.3 Zero order methods

Zero order methods as referred to by Kostoglou and Karabelas (1994) are methods concerned with representing the population distribution after dividing the droplet size into finite number of classes by a constant value (zero order polynomial) in each class. In this way the original integro-partial differential equation is transformed into a system of ODEs for which the numerical solution is well established. Zero order methods could be classified into two broad classes according to Kumar and Ramkrishna (1996a): internally consistent and inconsistent discretization schemes with respect to selected integral properties. By internal consistency it is meant that the desired integral property associated with the average number concentration obtained from the discrete PBE should be the same as that obtained from its continuous counterpart. This internal consistency is found to predict accurately the desired integral properties and at the same time improves the accuracy of the predicted droplet distribution on coarse grids (Hounslow, Marshal & Ryall, 1988; Lister, Smit & Hounslow, 1995; Kumar & Ramkrishna, 1996a, b; Attarakih, Bart & Faqir, 2003a, b, 2004a). Hounslow, Ryall and Marshal (1988) are the first who introduced an internally consistent set of discrete PBEs with respect to total number and volume for droplet coalescence in batch stirred tank using a geometric grid of constant factor 2. Unfortunately, this method is not amenable to grid refinement and it was extended to variable geometric factor by a set of more complicated discrete equations by Lister, Smit and Hounslow (1995). Hill and Ng (1995, 1996) followed this line and derived a discretized PBE for droplet breakage and coalescence in a batch stirred tank with a major flaw that it is dependent on the type of the breakage functions for droplet breakage and the type of the grid for droplet coalescence. Their simple extension to continuous stirred tank is considered to be internally inconsistent, as will be shown in this work. One of the earliest works to force internal consistency by conserving total droplet number and volume is presented in the paper by Sastry and Gaschignard (1981). These authors introduced two coupled sets of discrete PBEs for droplet coalescence in terms of number and volume balances with the appearance of double integrals in the source and sink terms and thus showing an excessive computational costs. Kumar and Ramkrishna (1996a) used the advantage of internal consistency and introduced a general framework of zero order discretization that is internally consistent with respect to any two integral properties irrespective of the grid structure. This scheme is called the fixed-pivot technique because it concentrates the droplet population in a given size range at a single point (called the pivot) through the use of Dirac delta function. The underlying idea in this approach is that when a droplet is formed by either breakage or coalescence on a discrete grid its resulting characteristic volume will never coincide with any of the representative volumes except for the linear grid. In the classical discretization approaches the resulting droplet volume is assigned to the nearest pivot and hence it could be shown that only one integral property could be conserved (Attarakih, Bart & Faqir, 2004a) (see chapter 3). To conserve at least two integral properties the resulting droplet volume is linearly interpolated between two adjacent pivots such that any two integral properties are conserved. The fixed-pivot technique is found to be very powerful not only in predicting the unimodal but also the bimodal distributions when the other zero order methods fail to do that or become computationally expensive (Vanni, 2000). Another variation of this approach is introduced by the same authors (Kumar &

Ramkrishna, 1996b) making use of the idea of Sastry and Gaschignard (1981) and that of internal consistency through the so-called moving-pivot technique. For example, when both total number and mass are the desired quantities to be conserved, the technique results in two sets of number and volume balances coupled through the pivots. These pivots are now dynamic quantities and change their positions to reflect the changes in the average number distribution. Attarakih, Bart and Faqir (2003a) extended recently the moving-pivot technique to a continuous stirred tank with only droplet breakage. Despite the high accuracy of the scheme it is considered computationally expensive when applied to PBEs showing spatial variation of the distribution. Lee et al. (2001) exploited the advantages of the fixed-pivot technique and coupled it with an adaptive mesh method and the method of characteristics to simulate a batch crystallizer of potassium sulfate. Lim et al. (2002) also made use of the fixed-pivot technique and weighted essentially non-oscillatory (WENO) scheme applied to the growth term to solve the PBE for a batch crystallizer of potassium sulfate. Although these authors claimed that their method conserves the total crystal number and mass, the discrete equations for agglomeration and breakage they used conserve only the total number due to the erroneous expressions resulting when the size coordinate is transformed from mass to length. Most recently, Campos and Lage (2003) have also used the fixed-pivot technique in the simulation of a bubble column through a mixed Euler-Lagrangian formulation. However, they failed to take into account the problem of internal consistency due to the presence of the feed distribution. This means that the extension of either the fixed-pivot or moving-pivot techniques to continuous flow systems is not simply by plugging the discrete equations of the source term in the model. In the present work (see chapters 2 and 5 for details) it has been shown how the moving and fixed-pivot techniques could be *correctly* extended to the continuous flow systems.

It is worthwhile to mention some of the internally inconsistent methods such as the Galerkin method on finite elements with zero order polynomials (Kronberger, 1995), the finite difference method of Ribeiro (1995) and the wavelet-based method presented by Liu and Cameron (2001). The first method was introduced to discretize the PBE describing the hydrodynamics of liquid-liquid extraction columns. The method is not only less accurate than the fixed-pivot technique, but also it is computationally less efficient due to the many double integrals in the source term. Ribeiro et al.(1995) presented a simple first-order finite difference scheme for both droplet size and time to simulate the hydrodynamics of a continuous stirred tank. The algorithm is also extended to three internal coordinates: droplet volume, age and concentration where the method is only consistent with respect to total droplet volume (Ribeiro et al., 1997). The wavelet-based method is used to discretize the PBE by approximating the average number concentration and the coalescence frequency using a series of wavelets. Liu and Cameron (2001) reported that the resulting computational matrices resulting from the wavelet collocation algorithm are computed offline for time independent coalescence frequencies. The method is shown to have good prediction of the average number concentration and its associated moments when sufficient number of collocation points are used (greater than 67 for the case of constant coalescence frequency). The method was only compared to some analytical solutions and not with any competing approach for the solution of the PBE to assess its performance. Bennet and Rohani (2001) used the combined Lax-Wendroff and Crank-Nicholson methods to simulate an evaporative cooling crystallizer with fines dissolution. The convergence and accuracy of the method for general cases including breakage and coalescence were not considered. Motz, Mitrovic and Gilles (2002) applied the space-time conservation element and solution element (CE/SE) (Chang, Wang & Chow, 1999) to crystallization process with only crystal growth, attrition, dissolution and nucleation. Their numerical results for crystal growth simulation showed that this method is much superior to a second-order flux-limited upwind scheme (Koren, 1993), however; the method was not extended to include crystal agglomeration or breakage.

Compared to the above literature concerning the solution of the PBE of one internal coordinate, there is a few numbers of numerical studies with regard to PBE showing external coordinate dependency when interacting liquid-liquid dispersions are considered. For the numerical solution of stagewise models the interested reader could refer to Gerstlauer (1999) and Mohanty (2000). For differential PBE models, Al Khani, Gourdon and Casamatta (1988), Gourdon and Casamatta (1994) and Milot et al. (1990) used the finite difference methods for discretizing both the internal and external coordinate; however, they presented no detailed information about the algorithms. Milot et al. (1990) reported that the spatial finite difference scheme that he used shows spurious numerical oscillations unless fine grid is used around the dispersed and continuous phase inlets. Kronbeger et al. (1994, 1995) solved the PBE with spatial dependency using the Galerkin and the finite volume methods for discretization of the internal and external coordinates respectively. The resulting discrete set of PBEs was treated as a system of conservation laws. They used a first-order upwind scheme with flux vector splitting based on the sign of the local droplet velocity. However, the approximate Riemann solver of Roe they used requires the estimation of the eigenvalues of the convective flux Jacobian, which is computationally very expensive

for large systems. At a steady state where mild gradients exist they reported that both schemes produced identical results. Moreover, the aforementioned authors used a limited flux-extrapolation scheme of second order accuracy. In spite of limiting the numerical flux it still shows spurious oscillations at the dispersed phase inlet especially during the transient period where large gradients are expected to occur.
Apart from interacting liquid-liquid dispersions, recently Campos and Lage (2003) presented a mixed Euler-Lagrange formulation for solving the PBE of a bubble column including bubble breakage, coalescence and absorption. They considered only positive bubble velocities and used third order TVD (Total Variation Diminishing) scheme to discretize the convective term.
In this work comprehensive numerical algorithms (methodologies) have been developed to solve the PBE describing the hydrodynamics of interacting liquid-liquid dispersions, which shows both spatial and time dependencies as well as droplet interactions (breakage and coalescence) (chapters 4 and 5). The underlying idea of this work is presented briefly by Attarakih, Bart and Faqir (2002, 2003b) and is extended, numerically tested and experimentally validated in this work (Attarakih, Bart and Faqir, 2004b) (see chapter 5). From the literature review above, it is clear that the fixed-pivot offers the advantages of being relatively simple, accurate and computationally efficient and hence it is *correctly* extended and efficiently applied to continuous flow systems. Unlike the previous works reported for spatial discretization, which usually use upwind differencing schemes, a couple of first and second order accuracy central differencing schemes recently developed by Kurganov and Tadmor (2000) has been utilized. These schemes offer the advantage over the upwind schemes that they are free of any approximate Riemann solvers and hence are not tied to the eigenvalue structure of the Jacobian of the convective flux. In addition to these two central schemes a simple first-order upwind differencing scheme with flux vector splitting is derived based on the transport phenomena of the dispersed phase in a general liquid-liquid extraction column.
The remaining body of this review is arranged as follows: in section 2 the general PBE for continuous flow systems is presented. The generalization of the fixed-pivot technique to continuous flow systems will be presented in section 3 stressing on how the feed source term is treated. In this section, the coalescence and breakage matrices are restructured to improve the scheme performance with special attention is paid to the finite domain error. Moreover, a conservative discretization approach for droplet breakage in continuous flow systems is also derived and validated. In section 4 the semi-discrete PBEs, based on the LLEC transport and the interactions of the dispersed and continuous phases along with the introduction of the central first and second order semi-discrete schemes, are derived. In section 5 the time discretization of the resulting system of ODEs is introduced. Section 6 is devoted to test the validity of the discrete models using three of the analytical solutions derived by Attarakih, Bart and Faqir (2004b) that are listed in chapter 5. The experimental realization of the model is dealt with in section 7 by considering a laboratory scale LLEC of rotating disc type (RDC) for which the steady state hydrodynamic experimental data is available (Modes 2000). In section 8 the LLECMOD program is briefly introduced, and finally in section 9, the conclusions and recommendations are presented.

2. The population balance equation (PBE)

The PBE describing the hydrodynamics of a dispersed phase in a continuous flow system in the absence of other transport phenomena such as mass transfer (no convective flux along the droplet internal coordinate) could be written as:

$$\frac{\partial n(v;\boldsymbol{\zeta})}{\partial t} + \nabla \cdot [\boldsymbol{F} - \boldsymbol{D}_d \nabla n(v;\boldsymbol{\zeta})] = \rho\{n(v;\boldsymbol{\zeta}), v\} \tag{1}$$

where v is the droplet volume, $\boldsymbol{\zeta} = [\boldsymbol{r}, t]$, is a vector of external and time coordinates specifying the variation of n. $n(v,\boldsymbol{\zeta})\delta v = N(\boldsymbol{\zeta}) f(v) \delta v$ is the average number concentration associated with droplets having a volume between $v \pm \delta v$ at the time instant t and position in space $\boldsymbol{r}$ and its corresponding total number concentration is $N(\boldsymbol{\zeta})$ while $f(v)$ is the average number density. The first part of the second term on the left hand side represents the droplet transport by convection through a surface of a given volume in space with velocity $\boldsymbol{U_d} = [U_{d,x}, U_{d,y}, U_{d,z}]$. The second part of this term is the droplet transport by diffusion characterized by the random movement of the individual droplets, in contrast to the convective transport by the turbulent eddies. The coefficient $\boldsymbol{D}_d$ appearing in this term is the Fick's diffusion tensor. The last term on the right hand side is the net number of droplet produced by either breakage or coalescence per unit time and unit volume and is given by (Valentas & Amundson, 1966):

$$\rho\{n,v\} = -\Gamma(v,\phi)n(v;\zeta) + \int_{v}^{v_{\max}} \Gamma(v',\phi)\beta_n(v \mid v')n(v';\zeta)\delta v' - n(v;\zeta)\int_{v_{\min}}^{v_{\max}-v} \omega(v,v-v',\phi)n(v-v';\zeta)\delta v' + \frac{1}{2}\int_{v}^{v_{\max}} \omega(v,v-v',\phi)n(v-v';\zeta)n(v';\zeta)\delta v' \quad (2)$$

The first and third terms in the above expression represent the rate at which the droplets are lost by breakage and coalescence per unit volume respectively, while the second and the fourth terms account for the rate of formation of droplets by breakage and coalescence per unit volume respectively. The breakage and coalescence frequencies are given by the functions, Γ and ω respectively and are dependent on the agitation intensity, internal tank (column) geometry and the dispersed phase hold-up that is given by:

$$\phi(\zeta) = \int_{v_{\min}}^{v_{\max}} vn(v;\zeta)\delta v \quad (3)$$

Note that the function $\beta_n(v|v')$ represents the distribution of the daughter droplets, given that a mother droplet of volume v' is broken and is assumed independent of time, but it may be function of the energy input and the system physical properties. This function should satisfy the usual number, volume and the physical ($\beta_n(v|v')=0$, $v>v'$) constraints (Ramkrishna, 2000).

3. The PBE discretization with respect to internal coordinate

3.1 The generalized fixed-pivot technique (GFP)

The population balance model given by Eq.(1) represents a nonlinear integro-partial differential equation (IPDE) of convective-diffusion type, where the source of nonlinearity is due to the convective and the source terms. To project this IPDE onto a finite set of PDEs, we discretize the droplet internal coordinate, v, according to the following discrete set: $\{v_{i-1/2} \mid i = 1, \ldots. M_x + 1\}$ with $v_{\min} = v_{1/2} < v_{3/2} < \ldots < v_{M_x+1/2} = v_{\max}$. Let the ith subdomain be defined as $V_i = [v_{i-1/2}, v_{i+1/2})$, $\mathrm{i} = 1,\ldots M_x$ and the population of the ith subdomain be concentrated at the middle of this subdomain such that $x_i = (v_{i-1/2} + v_{i+1/2})/2 = \pi d_i^3/6$. Then the droplet size distribution is expanded using a point wise sampling of the distribution at the middle of the ith subdomain (also called the pivot) according to the following relation:

$$n(v;\zeta) = \sum_{i=1}^{M_x} N_i(\zeta)\delta(v - x_i) \quad (4)$$

where δ refers to the Dirac delta function and the set of the unknown coefficients, $N_i(\zeta)$, refers to the total number concentration in the ith subdomain. Let us define the total quantity of droplets associated with a single droplet property $u_m(v)$ in the ith subdomain by:

$$\mathrm{I}_i(z,t) = \int_{v_{i-1/2}}^{v_{i+1/2}} u_m(v)n(v;\zeta)dv = u_m(x_i)N_i(\zeta),\ m = 1,2 \quad (5)$$

where the volume fraction, $\varphi_i(z,t)$, in the ith subdomain follows directly by substituting $u_2(v)=v$ in the last equation.

Kumar and Ramkrishna (1996a) showed that when the source term given by Eq.(2) is discretized by integrating it from $v_{i-1/2}$ to $v_{i+1/2}$ with respect to v, the source of internal inconsistency as described in section 1.1.3 results mainly due to the formation terms of breakage and coalescence but not due to the loss terms. They solved this problem through modifying the formation terms due to breakage and coalescence by multiplying them with a triangular function that we may define as:

$$w_i(v) = \begin{cases} \gamma_i^{<i-1>}(v), & x_{i-1} \le v < x_i \\ \gamma_i^{<i>}(v), & x_i \le v < x_{i+1} \end{cases} \quad (6)$$

The set of linear functions, $\gamma_i^{<i-1>}(v)$ and $\gamma_i^{<i>}(v)$ should satisfy the constraints imposed by the conservation of any two integral properties associated with the number distribution function obtainable from those associated with the single droplet, $u_1(v)$ and $u_2(v)$:

$$\gamma_{i-1}^{<i-1)}(v)u_m(x_{i-1}) + \gamma_i^{<i-1>}(v)u_m(x_i) = u_m(v),\ m = 1,2 \tag{7}$$

Making use of these ideas we can integrate Eqs.(1) and (2) with respect to v from $v_{i-1/2}$ to $v_{i+1/2}$ with the aid of Eq.(4) through (6), and then multiplying both sides by the general desired discrete quantity, $u_m(x_i)$, to get the following system of discrete PDEs:

$$\frac{\partial I_i(\boldsymbol{\zeta})}{\partial t} + \nabla \cdot [\boldsymbol{F}_i - \boldsymbol{D}_d \nabla I_i(\boldsymbol{\zeta})] = \rho\{\boldsymbol{I}(\boldsymbol{\zeta}), u_m(\boldsymbol{x})\},\quad i = 1,2,...M_x \tag{8}$$

The source term takes into account the conservation of any two integral properties, u_1 and u_2 and is given by (Attarakih, Bart & Faqir, 2004b) (see chapter 5):

$$\boldsymbol{\rho}(\boldsymbol{I}) = \begin{pmatrix} \boldsymbol{I}^T\left[\left(\boldsymbol{\omega} \bullet \boldsymbol{\Psi}^{<1>}\right)\boldsymbol{I}\right] \\ \boldsymbol{I}^T\left[\left(\boldsymbol{\omega} \bullet \boldsymbol{\Psi}^{<2>}\right)\boldsymbol{I}\right] \\ ..... \\ \boldsymbol{I}^T\left[\left(\boldsymbol{\omega} \bullet \boldsymbol{\Psi}^{<M_x>}\right)\boldsymbol{I}\right] \end{pmatrix} - \boldsymbol{I}^T \bullet \left[\boldsymbol{\omega}\left(\boldsymbol{\xi} \bullet \boldsymbol{I}\right)\right] + \boldsymbol{A}[\boldsymbol{\Gamma} \bullet \boldsymbol{I}] \tag{9}$$

where:

$$A_{i,k} = \begin{pmatrix} \left[\pi_{i,i}^{<m>} - 1\right] \\ \pi_{i,k}^{<m>} \end{pmatrix},\quad i = 1,2..M_x, k = i, i+1...M_x \tag{10}$$

$$\pi_{i,k}^{<m>} = \int_{d_{i-1}}^{d_i} \gamma_i^{<i-1>}(d)[\frac{u_m(d_i)}{u_m(d_k)}]\beta_n(d \mid d_k)\delta d + \int_{d_i}^{\min(d_k, d_{i+1})} \gamma_i^{<i>}(d)[\frac{u_m(d_i)}{u_m(d_k)}]\beta_n(d \mid d_k)\delta d \tag{11}$$

$$\xi_k = \frac{1}{u_m(x_k)} \tag{12}$$

$$\Psi_{k,j}^{<i>} = \begin{cases} \left[1 - \frac{1}{2}\delta_{k,j}\right]\frac{u_m(x_i)}{u_m(x_j)u_m(x_k)}\gamma_i^{<i-1>}(x_k + x_k), & \text{if}\quad d_{i-1}^3 \le d_j^3 + d_k^3 < d_{i-1}^3 \\ \left[1 - \frac{1}{2}\delta_{k,j}\right]\frac{u_m(x_i)}{u_m(x_j)u_m(x_k)}\gamma_i^{<i>}(x_k + x_k), & \text{if}\quad d_i^3 \le d_j^3 + d_k^3 < d_{i+1}^3 \end{cases} \tag{13}$$

$$\Gamma_i = \Gamma(d_i, \phi(\boldsymbol{\zeta})),\quad i = 1,2,...M_x \tag{14}$$

$$\omega_{i,k} = \omega(d_i, d_k, \phi(\boldsymbol{\zeta})),\quad i,k = 1,2,...M_x \tag{15}$$

Note that the above mathematical model conserves the total droplet number and volume by setting $u_1 = 1$and $u_2 = v$ and the symbol $\bullet$ appearing in Eq.(9) denotes an element by element matrix multiplication.
The inlet feed distribution is treated as a point source term and hence its conservative discrete form is given by:

$$I_i^{feed} = \int_{d_{i-1}}^{d_i} \gamma_i^{<i-1>}(d)[u_m(d_i)]f^{feed}(d)\delta d + \int_{d_i}^{d_{i+1}} \gamma_i^{<i>}(d)[u_m(d_i)]f^{feed}(d\mid)\delta d \tag{16}$$

Note that the recognition of the sparse structure of the coalescence interaction matrix ($\boldsymbol{\Psi}$) makes it possible to reduce the computational time drastically. The first double summation in Eq.(9) recognizes only the triangular structure of the *i*th interaction coalescence matrix ($\boldsymbol{\Psi}^{<i>}$) and ignores its sparse nature. This sparse nature is due to the definite number of droplets falling in the *i*th subdomain through coalescence of droplets from the *k*th and *j*th subdomains. The significance of introducing the coalescence interaction matrix has two distinctive advantages over the original formulation of Kumar and Ramkrishna (1996a). The first one is that this three dimensional matrix is decoupled from the time dependent variables, $\boldsymbol{\omega}$ and $\boldsymbol{I}$ and hence it is always evaluated offline once a time.

Second the *i*th coalescence interaction matrix, $\boldsymbol{\Psi}^{<i>}$, has a size $i \times i \times i$ which grows linearly as *i* increases and hence this saves the storage requirement instead of storing an $M_x \times M_x \times M_x$ matrix for each *i*. Moreover, the sparse nature of the *i*th coalescence interaction matrix is found to reduce considerably the execution time as shown in Fig.(1). This is because we carry the above summations only when the resulting volume of any two droplets of volumes x_k and x_j falls in the *i*th subdomain. This strategy is called the restructuring of the interaction coalescence matrices.

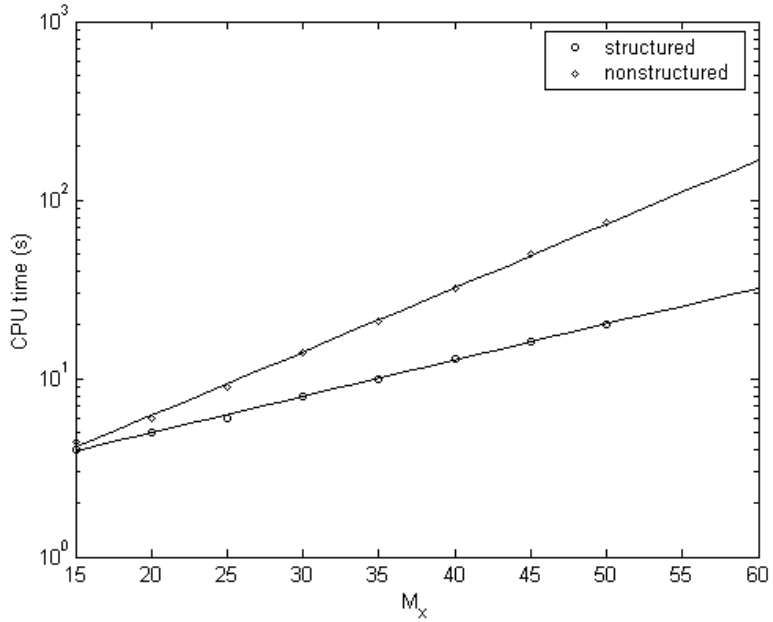

Fig.(1): The effect of restructuring the coalescence interaction matrices on the CPU time requirements for droplet coalescence in a CST (Pentium III 750 MHz).

3.2 The generalized moving-pivot technique (GMP)

The idea of the moving-pivot technique is first introduced by Kumar and Ramkrishna (1996b) for simple batch systems. This technique is generalized to continuous flow systems by carrying out simultaneous number and volume balances in the case of total number and volume conservation. These balances are then coupled through the representative droplet volumes (pivots) and hence they are allowed to move to reflect the changes in the number density as a function of space and time. This is done by solving the two system of PDEs given by Eq.(8) for $I_i^{<1>}(\zeta) = N_i(\zeta)$ and $I_i^{<2>}(\zeta) = \int_{v_{i-1/2}}^{v_{i+1/2}} vn(v;\zeta)\delta v$, i = 1, 2, …. M_x followed by solving for the moving-pivots using the following relation:

$$x_i(\zeta + \Delta\zeta) = \begin{cases} I_i^{<2>}(\zeta) / I_i^{<1>}(\zeta), \ if \ I_i^{<1>}(\zeta) > 0 \\ x_i(\zeta), \ otherwise \end{cases}, \ i = 1, 2, ...M_x \tag{17}$$

However, this system of equations could be simplified for the especial case of droplet breakage in a continuous stirred tank to the following system of ODEs (Attarakih, Bart and Faqir, 2003a):

$$\frac{dN_i(t)}{dt} = \lambda_i^c N_i(t) + \sum_{k=i+1}^{M_x} \pi_{0,i,k}\Gamma_k N_k(t) + \frac{N_i^{feed}}{\tau}, \qquad i = 1, 2, \ .....M_x \tag{18}$$

$$\frac{dx_i(t)}{dt} = \chi_i + \frac{1}{N_i(t)} \sum_{k=i+1}^{M_x} (\pi_{1,i,k} - x_i\pi_{0,i,k})\Gamma_k N_k(t), \qquad i = 1, 2, \ .....M_x \tag{19}$$

where:

$$\pi_{m,i,k} = \int_{v_{i-1/2}}^{u_{i+1/2}} v^m \beta(v \mid x_k) dv, \qquad \begin{cases} u_{i+1/2} = x_i, & k = i \\ u_{i+1/2} = v_{i+1/2}, & k > i \end{cases} \tag{20}$$

$$\lambda_i^c = \Gamma_i(\pi_{0,i,i} - 1) - \frac{1}{\tau} \tag{21}$$

$$\chi_i = (\pi_{1,i,i} - x_i\pi_{0,i,i})\Gamma_i + \frac{x_i^{feed} - x_i}{\tau}\left(\frac{N_i^{feed}}{N_i}\right) \tag{22}$$

3.3 The finite domain error

In discretizing an equation defined over an infinite domain an inherent error is incurred due to the failure of taking into account the portion of the function lying outside the domain of discretization. This error is termed the total FDE and is represented by (Sovova and Prochazka, 1981):

$$\varepsilon_0(t) = \int_0^{v_{\min}} n(v,t)dv + \int_{v_{\max}}^{\infty} n(v,t)dv = FDE_0^L + FDE_0^U \tag{23}$$

Note that for a given number of intervals, M_x, and interval width, Δv, an optimal minimum droplet volume, v_{min}, exists and could be found by differentiating Eq. (23) with respect to v_{min} and set the result equal to zero:

$$n(v_{\min}^*, t) - \frac{dv_{\max}}{dv_{\min}} n(v_{\max}^*, t) = 0 \tag{24}$$

For droplet breakage in batch systems and according to Eq. (24), the optimal minimum droplet volume must decrease as function of time to account for the increasing number density at the lower size range. This suggests the use of optimal moving grid for droplet breakage, which moves from the upper to the lower size ranges as function of time. Consequently, Eqs.(18) through (22) and Eq.(24) must be solved simultaneously at each instant of time to find such an optimal moving grid. Unfortunately, the solution is iterative by solving Eq. (24) at each integration step, and might mask the benefits gained by using the optimal moving grid. To compensate for this drawback, an approximate optimal moving grid technique is derived in the following section.

3.4 An approximate optimal moving grid for droplet breakage in batch systems

The total finite domain error, as defined above, will be close to the minimum value when both residuals are equal, which leads to an approximate optimal minimum droplet volume and hence optimal moving grid. This optimal moving grid should keep the number of intervals constant during grid movement, and hence redistribution of the population between the old and the newly formed grids is essential. This should be performed by conserving any two moments of the population in order to be consistent with Eqs.(18) and (19).

Now consider a typical geometric grid ($v_i(t)=\sigma^{i-1}v_{min}(t)$) at two instants of time: t and $t+\Delta t$ where the optimal minimum droplet volume moves from $v^*_{\min}(t)$ to $v^*_{\min}(t+\Delta t)$. Let $\gamma_i^{<i>}(t)$ be the fraction of droplets at the pivot $x_i(t)$ to be assigned to the pivot $x_i(t+\Delta t)$ and $\gamma_{i+1}^{<i>}(t)$ be the fraction of droplets at the pivot $x_i(t)$ to be assigned to the pivot $x_{i+1}(t+\Delta t)$. These fractions are found such that both number and volume of these droplets are conserved after redistribution (see Eq.(7)). Accordingly, the discrete lower and upper residuals at this instant of time are given by (see chapter 2 for details):

$$FDE_0^L(t+\Delta t)=\gamma_1^{<0>}N_0(t) \tag{25}$$

$$FDE_0^U(t+\Delta t)=\sum_{i=M_x+1}^{\infty}\gamma_i^{<i-1>}N_{i-1}(t)+\gamma_i^{<i>}N_i(t) \tag{26}$$

where only the (M_x+2)th term in the summation above has a significant value for sufficiently large M_x or geometric factor σ. The optimality condition implied by Eq.(24) could be approximately satisfied by forcing both sides of Eqs.(25) and (26) to be equal, which after some algebraic manipulation using a geometric grid: $v_i=\sigma^{i-1}v_{\min}$ yields Eq.(27) below. This equation specifies the approximate path followed by the geometric grid such that the finite domain error is approximately minimum. The lower and upper residuals, $N_0(t)$ and $N_{M_x+1}(t)$ could be estimated by making number and volume balances on the zero and last intervals by extending the PBEs given by Eqs.(18) and (19) (see chapter 2 for details).

$$\frac{v^*_{\min}(t+\Delta t)}{v^*_{\min}(t)}=\frac{\frac{1}{\sigma-1}N_{M_x}(t)+\frac{1}{\sigma}N_0(t)}{\frac{\sigma+1}{\sigma}N_0(t)+\frac{1}{\sigma-1}N_{M_x}(t)-N_{M_x+1}(t)} \tag{27}$$

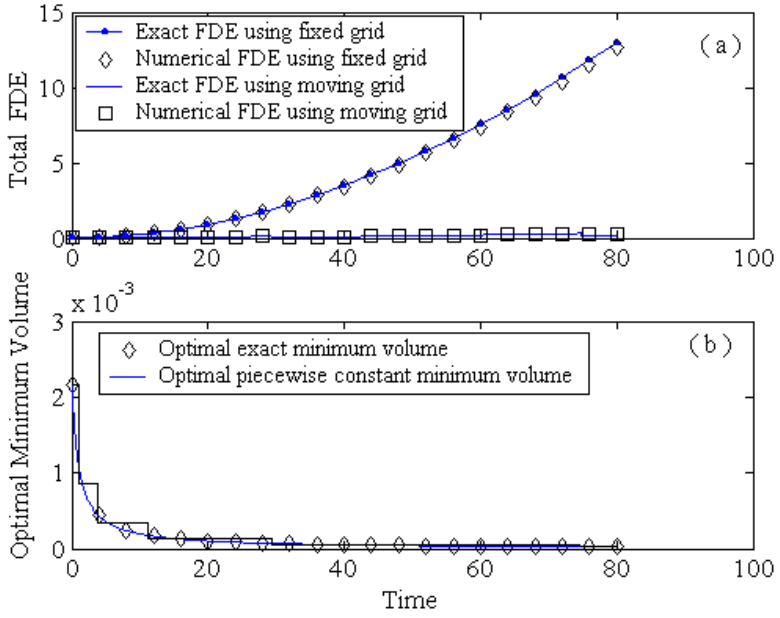

Fig.(2): a-The effect of the optimal grid movement on the total finite domain error. b- The approximate and exact optimal minimum droplet volume profiles for droplet breakage in a batch vessel using a geometric grid with factor $\sigma = 2.5$, $M_x = 10$, binary breakage, $\Gamma=v$, $\beta(v|v')=1/v'$, and exponential initial condition. The analytical solution is given by Ziff and McGrady (1985).

Fig.(2) shows the effect of the approximate optimal moving grid on the finite domain error when compared to a fixed grid. As expected the total FDE for a fixed grid increases with time due to the failure of taking into account the increasing number density in the small size range. Note that the piecewise constant path followed by the grid approximates well the exact one. This approximate technique could be extended to droplet coalescence in batch systems as well or when both droplet breakage and coalescence mechanisms are active. However the extension to continuous flow systems is not possible due to the fixed nature of the inlet feed distribution.

3.5 Optimal fixed grid for droplet breakage in continuous flow systems

In the development of the moving grid technique for batch systems, we sought to minimize the total finite domain error based on the number density, FDE_0. However, there is still a finite domain error induced by excluding droplet volumes due to the failure of extending the domain of the internal coordinate to 0 and ∞. This is actually the total FDE based on the volume or the first moment of the distribution, and could be defined by an analogy to the zero FDE (Eq. (23)):

$$\varepsilon_1 = FDE_1^L(v_{\min},t) + FDE_1^U(v_{\min},t) \tag{28}$$

where FDE_1^L and FDE_1^U are defined based on the first moment of the distribution.

Since droplet breakage in batch systems leads to a population density that is skewed to the left, small volume of droplets are lost due to the failure of extending the droplet volume to infinity. However, for continuous systems the zero and first moments of the feed do affect the zero and first moments of the distribution in the vessel. Hence, where the feed distribution is constant as stated above, appreciable errors would result due to the exclusion of numbers and volumes from the domain. This marked influence of the feed density function on the moments of the distribution lends itself to consider both finite domain errors based on the zero and first moments in seeking an optimal grid for discretization. In other words, we seek a grid that minimizes the time-averaged of the sum of the FDE based on both zero and first moments of the distribution. This total FDE is found by adding Eqs. (23) and (28) and the result could be related to the continuous zero and first moments of the distribution as follows:

$$M_0^d(v^*_{\min.}(0),t) + M_1^d(v^*_{\min.}(0),t) = M_0^c(t) + M_1^c(t) - [\varepsilon_0(v^*_{\min.}(0),t) + \varepsilon_1(v^*_{\min.}(0),t)] \tag{29}$$

Note that minimizing the total FDE (the term in square brackets) is equivalent to maximizing the sum of the left hand side at any instant of time since the continuous zero and first moments of the distribution are functions of time only. Since the proposed optimal grid is fixed as mentioned above, it is recommended to maximize the time-averaged of the left hand side of Eq. (29). This could be posed as a constrained one dimensional nonlinear optimization problem as follows (Attarakih, Bart & Faqir, 2003a):

$$\underset{\sigma}{\text{maximize}} \left(\frac{\int_0^{t_f} [M_0^d(\sigma,t) + M_1^d(\sigma,t)]}{t_f} dt \right) \tag{30}$$

subject to Eqs.(18) and (19) and:

$$M_0^d(\sigma,t) + M_1^d(\sigma,t) = \boldsymbol{N}^T(t)\boldsymbol{N}(t) + \boldsymbol{x}^T(t)\boldsymbol{N}(t), \quad 1 < \sigma \le \sigma_{\max.} \text{ for all } t \in [0, t_f].$$

The effect of the optimal geometric factor and hence v_{min} and v_{max} on the total zero and first moments of the distribution as well as the mean droplet volume using this strategy is shown in Fig.(3) (see chapter 2). Note that the above formulation is general and not restricted to the type of the flow system or the droplet interaction mechanism prevailing in it. However, it becomes more expensive especially when the droplet population shows spatial dependency. A more computationally effective procedure to minimize the total FDE based on any two integral quantities associated with the single droplet is described in chapter 5.

3.6 A conservative discretization approach for the PBE: droplet breakage

It should be first emphasized that the recovery of internal consistency with respect to certain integral properties does not necessarily require the same number distribution function. This means that one could estimate, for example, one integral property from two number distributions that are slightly different.
Now, an infinite number of these number density curves could be generated but still having the same total area. It then appears that it is feasible to solve a modified but slightly different PBE with the property that the discrete set of equations (with respect to number concentration) of this slightly modified PBE is internally consistent with respect to any two integral properties. However, this does not mean that the slightly modified PBE will converge to a completely different or erroneous number distribution. This is because we enforce the slightly modified PBE to be identical to its original counterpart at least with respect to the desired integral properties. It should also be stressed that the discrete solution generated by these discrete equations should converge to the solution of its continuous counterpart as the grid is made fine.
To proceed further, a pair of auxiliary functions: $\eta(v)$ and $\alpha(v)$ is introduced to account for the intra-interval problem (Hill & Ng, 1995; Attarakih, Bart & Faqir, 2004a, see also chapter 3) when the PBE is transformed from the continuous to the discrete domains. So, the proper choice of placing these functions is at the loss and formation terms so that the following modified PBE for droplet breakage could be obtained:

$$\frac{dI_i(t)}{dt}=\frac{1}{\tau}\left(I_i^{feed}(t)-I_i(t)\right)-\eta(x_i)\Gamma(x_i)I_i(t)-\sum_{k=i}^{M_x}\alpha(x_k)\Gamma(x_k)I_k(t)\left(\frac{u_m(x_i)}{u_m(x_k)}\right)\int_{v_{i-1/2}}^{\min(x_k,v_{i+1/2})}\beta_n(v\mid x_k)dv \qquad (31)$$

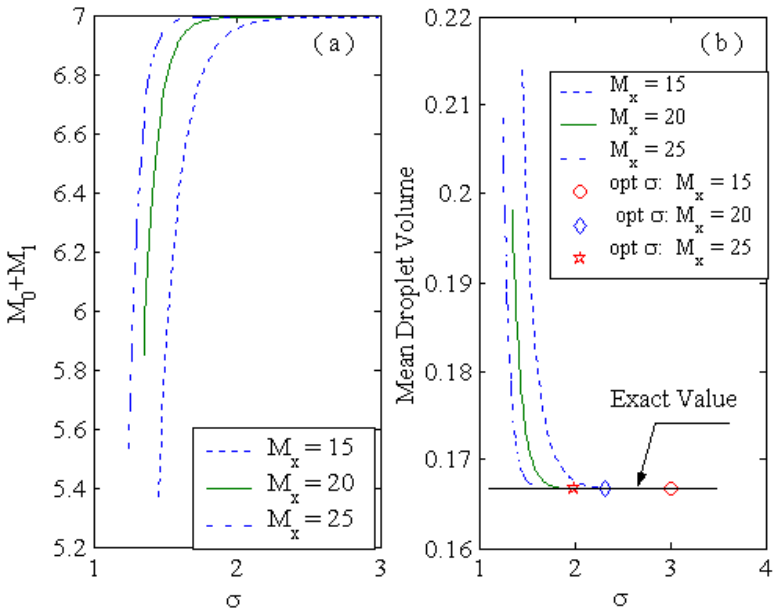

Fig(3): The effect of the optimal geometric grid factor on: a-The steady state sum of zero and first moments of the distribution. b- The mean droplet volume for droplet breakage in a continuous vessel with $\Gamma=v$ and $\beta(v|v')=1/v'$, binary breakage, $\tau = 5$, and exponential feed distribution.

Now we are ready to determine the form of the discrete functions $\eta(x_i)$ and $\alpha(x_i)$ by enforcing internal consistency of Eq.(31) with respect to any two integral properties:$u_1(v)$ and $u_2(v)$ that are associated with the number distribution. This is could be simply accomplished by equating the two desired integral properties obtained form Eq.(31) to that obtained from its continuous counterpart to get the following three constraints presented in chapter 3 and in Attarakih, Bart and Faqir (2004a):

$$u_m(x_i)N_i^{feed}=\int_{v_{i-1/2}}^{v_{i+1/2}}u_m(v)n^{feed}(v)dv \qquad (32)$$

$$\alpha(x_i) = \frac{q_2(x_i) - q_1(x_i)}{r_2(x_i) - r_1(x_i)} \tag{33}$$

$$\eta(x_i) = 1 + \left[\alpha(x_i) r_2(x_i) - q_2(x_i)\right] \tag{34}$$

$$r_m(x_i) = \sum_{k=1}^{i} \left(\frac{u_m(x_k)}{u_m(x_i)}\right) \int_{v_{k-1/2}}^{\min(x_i, v_{k+1/2})} \beta_n(v \mid x_i) dv, \ m = 1, 2 \tag{35}$$

$$q_m(x_i) = \sum_{k=1}^{i} \int_{v_{k-1/2}}^{\min(x_i, v_{k+1/2})} \left(\frac{u_m(v)}{u_m(x_i)}\right) \beta_n(v \mid x_i) dv, \ m = 1, 2 \tag{36}$$

and for i=2,...M_x and $\eta(x_i) = \alpha(x_i) = 1$ for i=1.

Note that this discretization approach (as well as the GFP technique) could not exactly conserve the desired integral properties exactly due to what we called the *intrinsic discretization error*: *IDE*; but instead it conserves one of them approximately. The reason for this approximation is the loss of linear dependency in the first subdomain for Eqs.(33) and (34). For this case we choose to conserve the total number concentration, $N(t)$, and leave the total volume concentration, $\phi(t)$, approximately conserved.

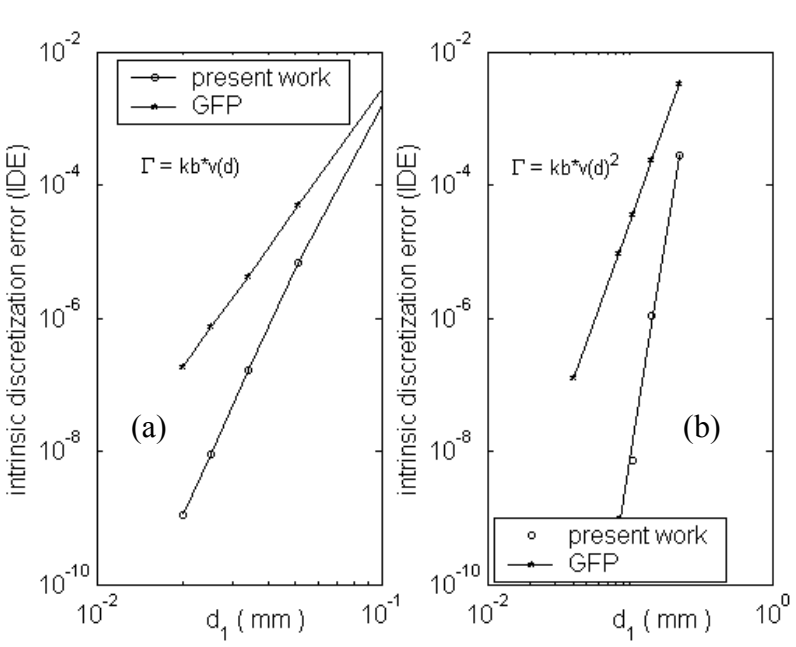

Fig.(4): The steady state intrinsic discretization error (*IDE*) using the present approach and the GFP technique: a- $\Gamma(d) = k_b \left(\pi d^3 / 6\right)$. b- $\Gamma(d) = k_b \left(\pi d^3 / 6\right)^2$ where k_b = 1, τ = 100 s, and the inlet feed distribution is given by $n^{feed}(d) = 3d^2 N_0^f / d_0^3 \exp\left(d / d_0\right)^3$ with d_0=1 and N_0^f=1.

Note that at a steady state the *IDE* could be accurately estimated from Eq.(31) according to the following relation (Attarakih, Bart & Faqir, 2003a) (see chapter 3 for details):

$$IDE(x_1) = \tau x_1 \Gamma(x_1) \left(\vartheta(x_1) - 1\right) N_1(t \to \infty) = \left|\phi^{feed} - \phi(t \to \infty)\right| \tag{37}$$

A similar relation could be easily derived for the GFP technique (Attarakih, Bart & Faqir, 2003a) where Fig.(4) shows a comparison between these *IDE*s for two cases of droplet breakage frequencies.

It is clear that the present conservative discretization approach has a lower value of *IDE* when compared to the GFP technique. The convergence characteristics of the present approach and the GFP technique using theoretical and practical case studies are shown in Fig.(5). It is clear that the two approaches have a convergence rate that is approximately inversely proportional to the square of the number of pivots. The predicted dynamic evolution of the droplet volume density is shown in Fig.(6) as compared to the analytical solution (Attarakih, Bart & Faqir, 2003a). The prediction of the GFP technique is found almost identical to the present approach and hence it is omitted for the sake of clarity.

4. The PBE discretization with respect to external coordinate

The discrete set of partial differential equations given by Eqs.(8) is now in terms of any discrete quantity, $u_m(d_i)$ associated with the discrete number concentration, $N_i(\boldsymbol{\zeta})$. The question that presents itself at this stage is which discrete quantity, $u_m(d_i)$ that is suitable for the discretization of Eq.(8) with respect to the external coordinate? This question might be answered if we are guided by the PBE volume approach of Verkoeijen et al. (2002). These authors has pointed out that the volume distribution based on droplet volume as an internal coordinate is the most suitable when the PBE is coupled with a fluid dynamics model such that in our case. Here the volume distribution becomes inevitable since the finite volume schemes are the most feasible one for external coordinate discretization for the system of conservation laws given by Eq.(8) when $u_m(v) = v$. So, the finite volume numerical approach is used to discretize the PBEs with respect to the external coordinate using a volume distribution function by setting $u_1(v)=1$ and $u_2(v)=v$ corresponding to total number and volume conservation and hence: $I_i = \varphi_i(\boldsymbol{\zeta}) = x_i N_i(\boldsymbol{\zeta})$. This system of PDEs is simplified to model the hydrodynamics of interacting liquid-liquid dispersion in a typical LLEC as follows (see chapter 5):

$$\frac{\partial \varphi_i(\boldsymbol{\zeta})}{\partial t} + \frac{\partial}{\partial z}[F_i - D_d \frac{\partial \varphi_i(\boldsymbol{\zeta})}{\partial z}] = \frac{Q_d \varphi_i^f}{A_c}\delta(z - z_d) + \rho\{\boldsymbol{\varphi}(\boldsymbol{\zeta}), \boldsymbol{x})\}, \quad i = 1,2,...M_x \tag{38}$$

where the inlet feed distribution is modeled as a point source term at the location z_d of the column. Note that the positive coordinate coincides with the dispersed flow direction from the bottom to the top of the column. To complete the model the Danckwert's boundary conditions are utilized for this model by considering the LLEC with an active height H to behave like a closed vessel between 0^+ and H^- (Wilburn, 1964).

The above system of conservation laws is actually dominated by the convective term for typical values of D_d which are in the order of $10^{-4} m^2/s$ (Modes, 2000) (Peclet No. $\approx 1\times10^3 H$ - $2\times10^3 H$). Due to this and the presence of the feed point source term it is expected that the total transient hold-up (and hence the hold-up of the different internal subdomains) will move along the column height with a steep front. Accordingly, high-resolution schemes are required to capture this moving front since first order schemes are known to suffer from excessive numerical diffusion (front smearing) (Toro, 1999). However, it will be very useful in the first step of spatial discretization is to consider only a first-order accurate scheme that is based on droplet volume balance on discrete space (spatial cell).

4.1 Spatially first order discrete scheme

Consider the general staggering spatial grid (cell-centered finite volume approach) given by $z_{l\pm1/2} = z_l \pm \Delta z_l / 2,\ l = 1,2..L$ and let the average cell hold-up be defined as:

$$\varphi_{i,l}(t) = \frac{1}{\Delta z_l}\int_{z_{l-1/2}}^{z_{l+1/2}} \varphi_i(z,t)dz \tag{39}$$

Now it is possible to consider the unsteady state droplet volume balance across the *l*th cell boundaries and the net volume (mass) generation of the dispersed phase in it. This cell volume could be considered small enough so that the spatial variation within it could be neglected and hence we get (see chapter 5):

$$\frac{d\varphi_{i,l}}{dt} + \frac{F_{i,l+1/2} - F_{i,l-1/2}}{\Delta z_l} = \frac{D_d \partial \varphi_i / \partial z)_{l+1/2} - D_d \partial \varphi_i / \partial z)_{l-1/2}}{\Delta z_l} + \frac{Q_d \varphi_i^{feed}}{A_c}\frac{\delta_{l,l_d}}{\Delta z_l} + \rho(\boldsymbol{\varphi}_l) \tag{40}$$

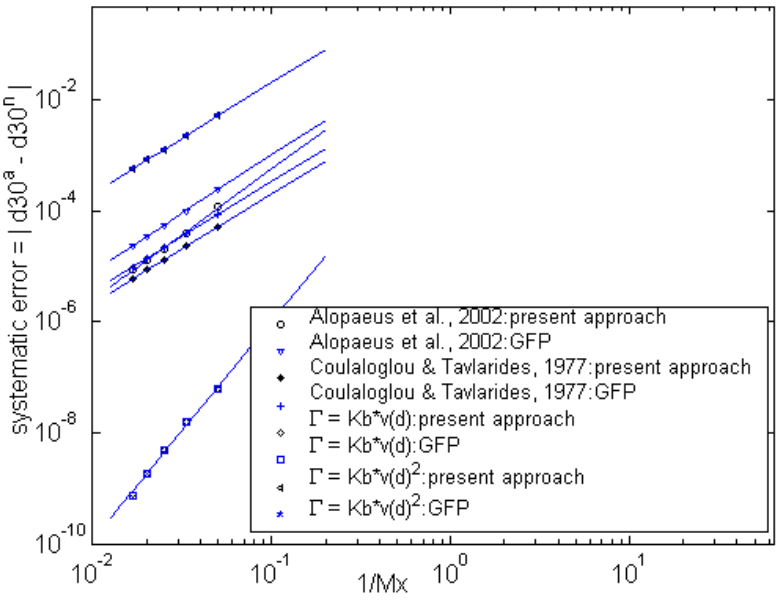

Fig.(5): The convergence characteristics of the present discretization approach and the GFP technique as measured by the systematic error for cases at a steady state with τ = 100 s.

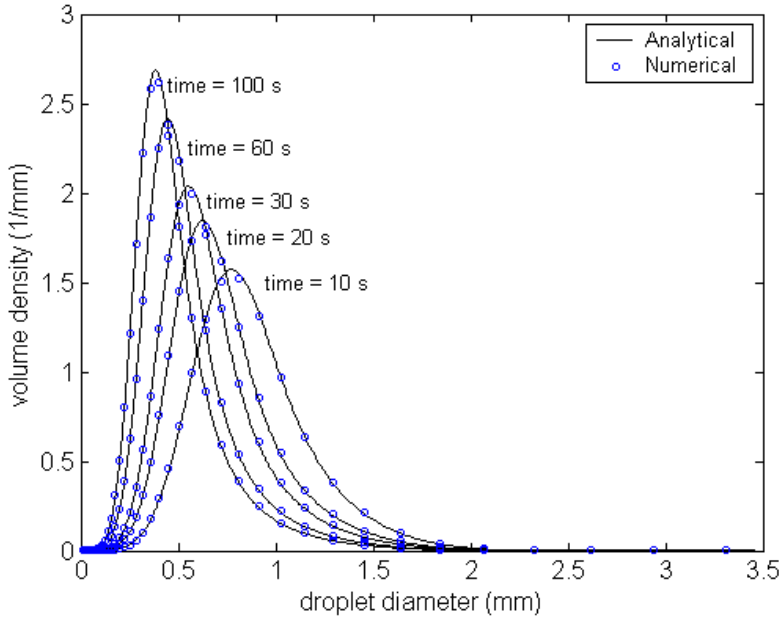

Fig.(6): The dynamic evolution of the droplet volume density using the present discretization approach, where the inlet feed distribution is given by $n^{feed}(d) = 3d^2 N_0^f / d_0^3 \exp\left(d/d_0\right)^3$ with d_0=1, N_0^f=1, $\Gamma(d) = k_b\left(\pi d^3/6\right)$ with k_b = 1, τ = 100 s, and M_x = 50. The analytical solution is given in chapter 3.

Since the droplet rise velocity, $U_i = U_r(d_i, z, \phi) - U_c$, might be negative at any cell boundary due to the effect of the droplet swarm and/or the continuous phase velocity, it is necessary to split the convective flux into negative and positive components:

$$F_{i,l+1/2} = max\left(U_i(d_i, \phi_l(t))\varphi_{i,l}(t), 0\right) + min\left(U_i(d_i, \phi_{l+1}(t))\varphi_{i,l+1}(t), 0\right) \tag{41}$$

The spatial derivatives of the diffusive flux might be approximated as a difference between the centers of two adjacent cells where the hold-up values are known.
The relative velocity U_r could be simply adapted to the type of the column and the chemical system under investigation in the following form:

$$U_r(d, z, \phi) = K_v U_t(d, \boldsymbol{P}) f(\phi) \tag{42}$$

In the above equation K_v is the droplet slowing factor having a value between zero and one which takes into account the internal column geometry and might be dependent on energy input, and the droplet diameter (Modes, 2000). U_t is the single droplet terminal velocity and is adequately described by some correlation such as Klee and Treybal (1956), Vignes (1965) and Grace, Wairegi and Nguyen (1976) depending on the system physical properties (Gourdon and Casamatta, 1994). The function $f(\phi)$ takes into account the effect of droplet swarm and is generally taken as $(1-\phi)^m$, where m is an empirical exponent (Godfrey and Slater, 1991), while the vector $\boldsymbol{P}$ may consist of all the system physical properties.
To circumvent the problem of numerical diffusion inherently existing in the first-order schemes, high-resolution schemes are required to lessen this numerical diffusion and hence sharpen the predicted moving front. This is done by increasing the order of spatial discretization of the numerical flux without violating the physical behavior of the phenomena under investigation. This violation comes from the fact that *linear* differencing schemes of order greater than one introduces spurious oscillation around large gradients according to the Godunov's theorem (Toro, 1999). Thus higher order upwind numerical fluxes are nonlinear and require more information by resorting to a complicated characteristic decomposition of the numerical flux more than the simplified approach presented above. It should be mentioned that this model is exactly the same as that derived by Kronberger et al. (1995) and Kronberger (1995) based on first-order upwind differencing and flux vector-splitting scheme.

4.2 Spatially second order discrete scheme

Recently, Kurganov and Tadmor (2000) presented a high-resolution central difference scheme of second order accuracy. This central differencing scheme offers universal black-box solver for general systems of conservation laws such that given by Eq.(38). Moreover, the use of central differencing schemes in the presence of the diffusion as well as the source terms does not call for the operator splitting technique suffering from the traditional splitting limitations; that is, it requires small time step that is comparable to the diffusion time scale (Karlsen et al., 2001). Unlike the upwind differencing schemes, the central differencing schemes do not require the time-consuming characteristic decomposition called for by the approximate Riemann solvers (Toro, 1999). Additionally, the spatial numerical derivatives required for the high-resolution implementation could be evaluated in a componentwise manner in a way similar to the scalar nonlinear limiters. Similarly, the evaluation of the numerical flux Jacobian is not necessary, but instead the approximate flux derivatives are evaluated in a componentwise manner based on the neighboring discrete values of the numerical flux: $F(\varphi_{i,l-1}, \phi_{l-1}), F(\varphi_{i,l}, \phi_l)$ and $F(\varphi_{i,l+1}, \phi_{l+1})$.

The main idea behind these central differencing schemes is in the way that it evolves in time the reconstructed piecewise-polynomial values at the cell boundary from their known values at the cell centers. This evolution step is realized by sampling the reconstructed values at the cell boundaries by including more precise information about the local propagation speeds ($S_{l\pm1/2}$). Kurganove and Tadmor (2000) used these ideas to construct the following numerical flux approximation:

$$F_{i,l+1/2} = \frac{F(\varphi^+_{i,l+1/2}) + F(\varphi^-_{i,l+1/2})}{2} - \frac{S_{i,l+1/2}}{2}\left(\varphi^+_{i,l+1/2} - \varphi^-_{i,l+1/2}\right) \tag{43}$$

where:

$$\varphi^{+}_{i,l+1/2} = \varphi_{i,l+1} - \frac{\Delta^{*} z_{l+1}}{2} \frac{\partial \varphi_i}{\partial z}\bigg|_{l+1} \text{ and } \varphi^{-}_{i,l+1/2} = \varphi_{i,l} + \frac{\Delta^{*} z_{l}}{2} \frac{\partial \varphi_i}{\partial z}\bigg|_{l}$$

The spatial derivatives appearing in the above equations are evaluated using a minmod-like limiter (Kurganov & Tadmor, 2000) with a TVD parameter $\theta \in [1, 2]$.
In this work, the estimation of the local propagation speeds (see chapter 5), $S_{i,l\pm1/2}$, is carried out based on a crude estimation of the convective flux Jacobian such that its eigenvalues are approximately given by: $\lambda_i \approx U_{d,i}, i = 1, 2..M_x$.

Note that $\Delta z_l = z_{l+1/2} - z_{l-1/2}$ is the same as $\Delta^{*} z_l = z_{l+1} - z_l$ only for uniform spatial cells where the above numerical flux could be reduced exactly to that of Kurganov and Tadmor (2000) when uniform spatial grid is used. Moreover, the above central differencing scheme could be made first order by setting the spatial derivatives to zero.

5. The PBE discretization with respect to time

The semi-discrete model given by the set of ODEs (Eq.(40)) (as especial case of the PBE given by Eq.(8)) and the corresponding numerical fluxes (Eqs.(41) and (43)) admit the use of efficient time discretization schemes by contrast to its fully discrete versions. Although higher order time differencing schemes offer high accuracy and time step control, they may violate the solution positivity especially at high level of space discretization unless very small time steps are to be used. So, as a first simple time discretization, we apply the implicit Euler method by lagging the nonlinear terms appearing in the convective and source terms. The discrete system could be written in a standard tridiagonal form in space for each internal coordinate subdomain as follows:

$$-q^{n}_{i,l,l-1}\varphi^{n+1}_{i,l-1} + q^{n}_{i,l,l}\varphi^{n+1}_{i,l} - q^{n}_{i,l,l+1}\varphi^{n+1}_{i,l+1} = \varphi^{n}_{i,l} + \Delta t R^{n}_{i,l}, \quad i = 1, 2..M_x,\ l = 1, 2..L,\ n = 0, 1..N_t \tag{44}$$

where:

$$q^{n}_{i,l,l-1} = \Delta t a(\varphi^{n}_{i,l-1}),\ q^{n}_{i,l,l} = 1 + \Delta t b(\varphi^{n}_{i,l}),\ q^{n}_{i,l,l+1} = \Delta t c(\varphi^{n}_{i,l+1}) \tag{45}$$

The nonlinear terms *a*, *b*, *c*, and *R* appearing in the above equations are dependent on the numerical flux type and could be easily deduced by comparing Eqs.(44) and (45) with the time-discretized version of Eq.(40).
The above tridiagonal system could be resolved using the standard Thomas algorithm at each time step followed by the fixed-point iteration method to improve the predicted solution due to lagging of the nonlinear terms. An accelerating convergence technique such as the bounded Wegstein method may be used. This iterative technique is required only for unsteady state simulations, since for steady state calculations the above algorithm converges always to the solution irrespective of the time step size. Moreover, since the above tridiagonal system is diagonally dominant (Kronberger, 1995) with positive right hand side, it is found to converge to the steady state solution without any risk of having negative values ensuring the solution positivity.

6. Discrete model validation

The convergence and accuracy of the discrete model in both internal and external coordinates is tested against analytical solutions whenever it is possible. A sample problem of four case studies is considered of which three have analytical solutions. The first three cases are devoted to test the GFP as well as the spatial discretization schemes for the LLEC model where analytical solutions were derived in chapter 5. These case studies are summarized in Table 1. In all the cases that follow we assume zero initial condition at the instant where the dispersed phase feed is switched on.
The column dimensions used for validation are that of a laboratory scale RDC column (Modes, 2000), whereas the chemical system used is the EFCE test system: water-toluene whose physical properties are available online (http://www.dechema.de/Extraktion).
The spatial numerical schemes are denoted as follows: the first order upwind scheme with flux vector splitting is UW1FVS, the first and second order central differencing schemes of Kurganov and Tadmor

(2000) are denoted by KT1 and KT2 respectively. The TVD parameter θ used in the reconstruction step of the KT2 method is set 1.7 as a compromise value between dissipative and oscillatory free solution behavior. Also, the two dimensional grid with respect to spatial and droplet diameter is denoted as $L \times M_x$ respectively.

6.1 Case 1: zero droplet breakage and coalescence in a LLEC

First, the solution of the PBE given by Eq.(40) is considered by dropping the diffusive and source terms, with the assumption that the dispersed phase is flowing through a stagnant continuous phase (Q_c=0) at low hold-up such that the swarm effects are negligible.
Fig.(7) shows the dispersed phase hold-up and the number concentration profiles at t = 15 s as compared to the analytical solution (Attarakih, Bart & Faqir, 2004b) (see also chapter 5). First, the two first order upwind and central differencing schemes (UW1FVS and KT1) show identical predictions of the profiles on a two-dimensional grid of size 150×30. This is because it is easy to show that the central first order scheme is reduced exactly to the first order upwind scheme for linear convective problems (Kurganov and Tadmor, 2000). Due to their first order accuracy the two schemes show numerical diffusion around the sharp moving front as expected. The use of the second order central differencing scheme (KT2) eliminates almost the entire diffusing luggage accompanying the first order schemes.
Fig.(8) shows the exact and numerical average volume distribution along the column height at t =15 s using the KT2 scheme. The two solutions are almost identical and the forward mixing of the dispersed phase is also predicted. The large droplets travel faster than the small ones and hence they posses different residence times as it is observed experimentally (Zhang et al., 1985; Qian & Wang, 1992).
Fig.(9) shows the convergence characteristics of the central differencing schemes KT1 and KT2. It is clear that both methods are converging in the sense of the L1-error. The KT2 has an L1-error that is about 40% less than that of KT1. The L1-error for the UW1FVS is the same as that of KT1 and so it is not shown here.

Table 1: Case studies for the discrete model validation of a laboratory scale RDC LLEC.

Case	Active mechanism	U_t	U_c	Feed distribution
1	no breakage or coalescence	Rigid sphere law (Wesselingh & Bollen, 1999)	Zero	$n^{feed} = \alpha\beta d^{\beta-1} e^{-\alpha d^{\beta}}$ $\alpha = 1.1\times10^{-3}$ and $\beta = 8$
2	breakage	Q_d/A_c	Zero	$n^{feed} = N_0^f e^{-\alpha v(d)/v_0} / v_0$ $v_0 = \alpha^2 / N_0^f$, $N_0^f = 1$ and $\alpha = 1$
3	coalescence	Q_d/A_c	Zero	the same as case 2
4	Breakage + coalescence	Rigid sphere law (Wesselingh & Bollen, 1999)	Attarakih, Bart & Faqir (2004b)	the same as case 1

6.2 Case 2: droplet breakage in a LLEC

In this case the total volume and number concentration profiles have a discontinuity that is moving along the column with a speed $U_d=Q_d/A_c$. This hypothesized problem is very difficult to solve because of this moving discontinuity and hence it represents a severe test to the spatial discretization schemes as well as the GFP. Fig.(10) shows the analytical (Attarakih, Bart & Faqir, 2004b) and the predicted volume and number concentrations using the GFP technique and the UW1FVS, KT1 and KT2 schemes. It is clear that the first order schemes are suffering from some numerical diffusion and need more spatial grid points to reduce it. On the other hand, the second order scheme has a much better performance near the discontinuities in both volume and number concentrations. In comparison to case 1 we need only 150

compared to 300 spatial cells to almost eliminate the numerical diffusion because the moving front is rather flat than in this case. Moreover, it seems that both droplet breakage and the nonuniform velocity distribution that are responsible for the nonuniform volume concentration profile. This is because when a volume concentration is obtained from the PBE, the source term due to droplet breakage disappears to satisfy the conservation of volume (mass), but this is not the case for the total number concentration. Hence, the total number concentration increases linearly along the column height.

6.3 Case 3: droplet coalescence in a LLEC

Fig.(11) shows the predicted total volume (Φ) and number (N) concentrations using UW1FVS, KT1, and KT2 along with the analytical solution derived in chapter 5. As in case 2, since the dispersed phase velocity distribution is uniform, both these profiles move along the column with a discontinuity having a speed of $U_d=Q_d/A_c$. This makes the numerical solution using the first order schemes more dissipative than the second order one (KT2). Since the total volume of droplet is conserved its concentration profile along the column is uniform; however, the number concentration profile is proportional to the inverse of z since droplet coalescence is accompanied by droplet number reduction.

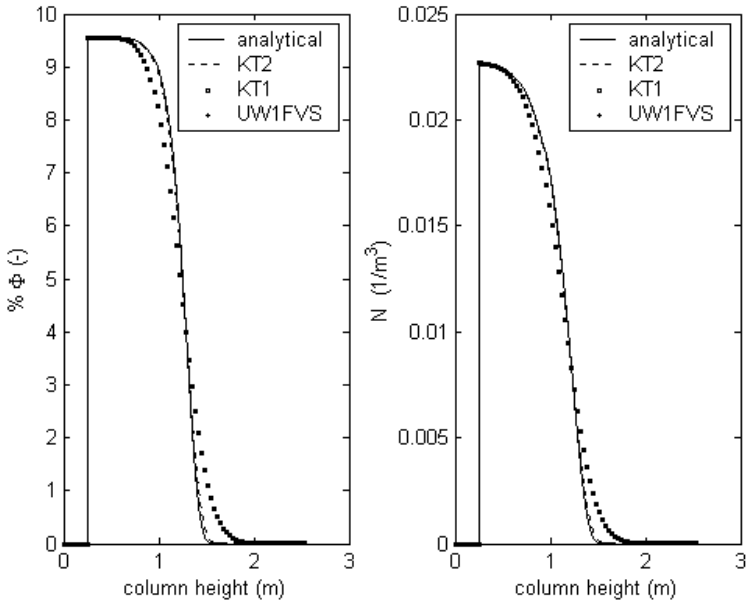

Fig.(7): Validation of the spatial discretization algorithms with grid dimensions:150×30 for internal and external coordinates respectively, t =15s, Δt =0.05s, rigid sphere law terminal velocity, Q_c=0 and Q_d=1.111×10^{-4}m^3/s.

6.4 Case 4: droplet breakage and coalescence in a LLEC

In this case we consider a more realistic case including droplet breakage and coalescence as well as the swarm effect function $f = (1-\phi)$ and slowing factor K_v = 1. The breakage frequency is given by $\Gamma = \frac{\pi^2 K_b}{36} d^6$ s^{-1} where K_b = 0.02 m^{-6}/s, d is in mm and the daughter droplet distribution is $\beta_n(d \mid d') = 6d^2 / d'^3$. The coalescence frequency is given by $\omega = K_c(d^3 + d'^3)$ with K_c = 0.5 m^{-6}/s where d is in mm and the dispersion coefficients are D_c=D_d = 10^{-4} m^2/s (Modes, 2000). The minimum and maximum droplet diameters are 0.25 and 4 mm where breakage and coalescence are active, and 0.25 and 6.5 mm when only droplet coalescence is active. The time step is taken 2 s for the steady state simulation with tolerance 10^{-6} as a criterion for steady state approach. Since no analytical solution is available for this case, the numerical convergence is tested through doubling the grid dimensions such that the two consecutive grids produce almost the same solution.

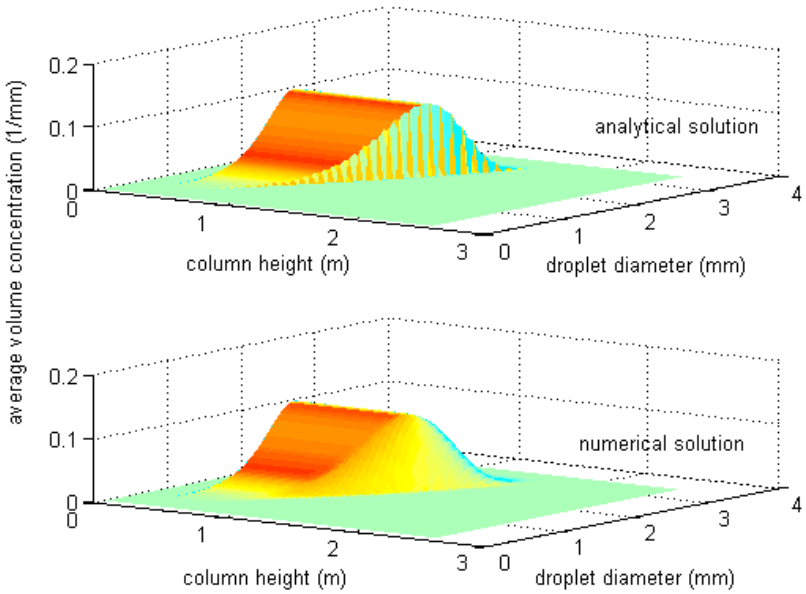

Fig.(8): Comparison of the numerical and exact transient behavior of the average volume concentration using the GFP and the second order central difference scheme (KT2) with grid dimension:150×30 for internal and external coordinates respectively, t = 15 s, Δt =0.05s, Q_c=0 and Q_d=1.111×10^{-4}m^3/s.

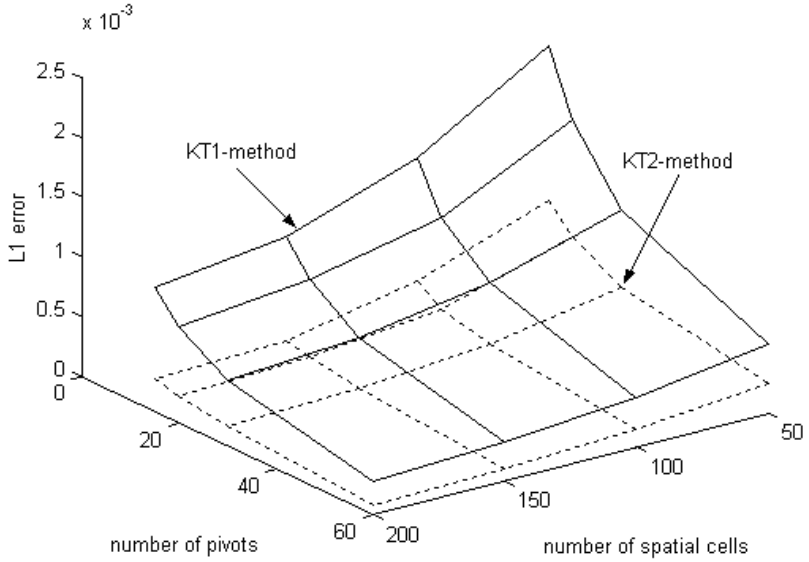

Fig.(9): The convergence characteristics of the first and second order (KT1 & KT2) central differencing schemes at t = 10 s, Δt =0.05 s, uniform droplet diameter, nonuniform spatial grids, Q_c=0.0 and Q_d=1.111×10^{-4}m^3/s and $L_1(t) = \sum_{i=1}^{M_s}\sum_{l=1}^{L} | \varphi_{i,l}^{<analyt>}(t) - \varphi_{i,l}^{<num>}(t) | \Delta d_l \Delta z_i$.

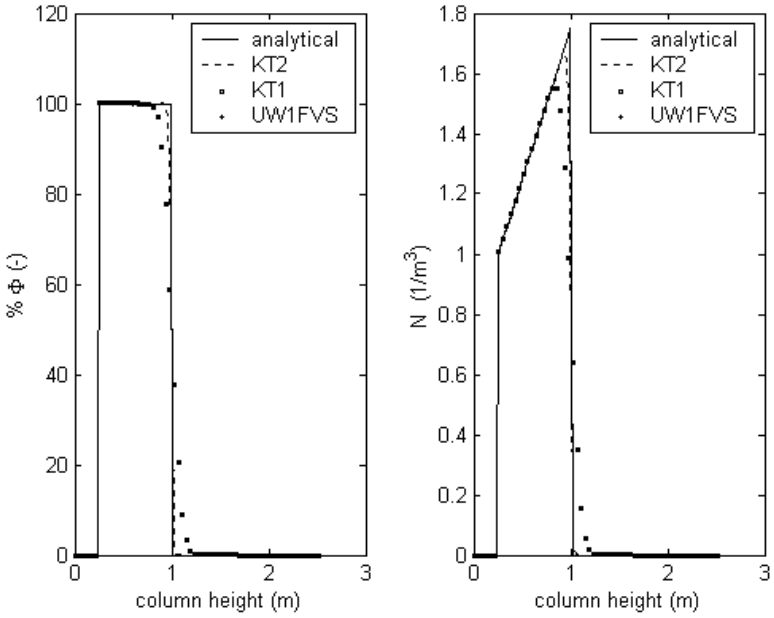

Fig.(10): Comparison between numerical and analytical solutions using the GFP and the spatial discretization schemes for droplet breakage with grid dimension: 300×30, t = 120s, Δt =0.05s, and Q_d=1.111×10^{-4}m^3/s.

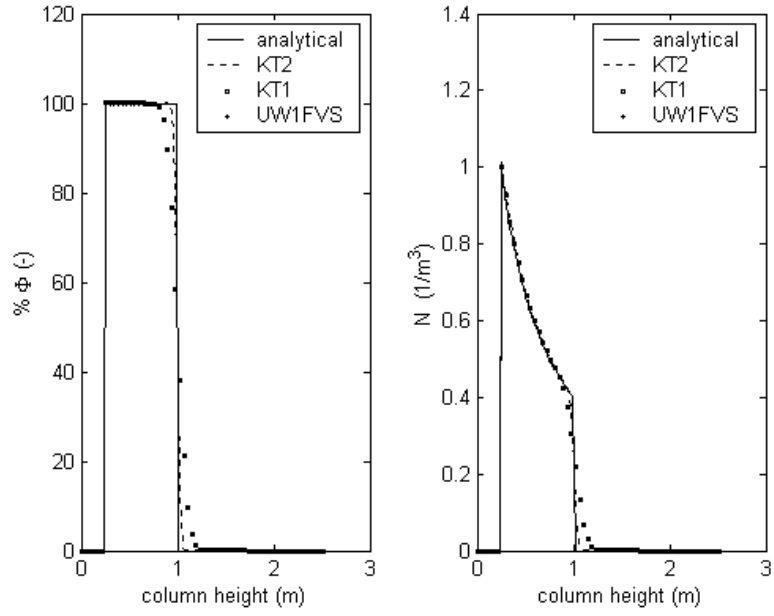

Fig.(11): Comparison between numerical and analytical solutions using the GFP and the spatial discretization schemes for droplet coalescence with grid dimensions:300×30, t = 120s, Δt =0.05s, Q_d=1.111×10^{-4}m^3/s.

Fig.(12) shows the convergence of the GFP technique at fixed spatial grid using the KT2 scheme for spatial discretization. It is clear that the GFP technique is converging on consecutive grids: 70×25 and 70×70 for various droplets interaction mechanism along the column.
Table 2 sheds more light on the quantitative convergence characteristics of the internal and external discretization schemes as well as the CPU time requirements. The convergence test is based on the mean droplet diameter $\overline{d30}$ with respect to diameter and column height. Since no analytical solution is available, we used a reference solution on grid whose dimension is 300×60 at a steady state. It is clear that the discretization in both dimensions is converging with small systematic errors, where the KT2 scheme is the most accurate one. It is also interesting to note that the CPU time requirements for the second order scheme KT2 using 500 integration steps is almost the same as that of the first order schemes: KT1 and UW1FVS with the gain of higher accuracy.

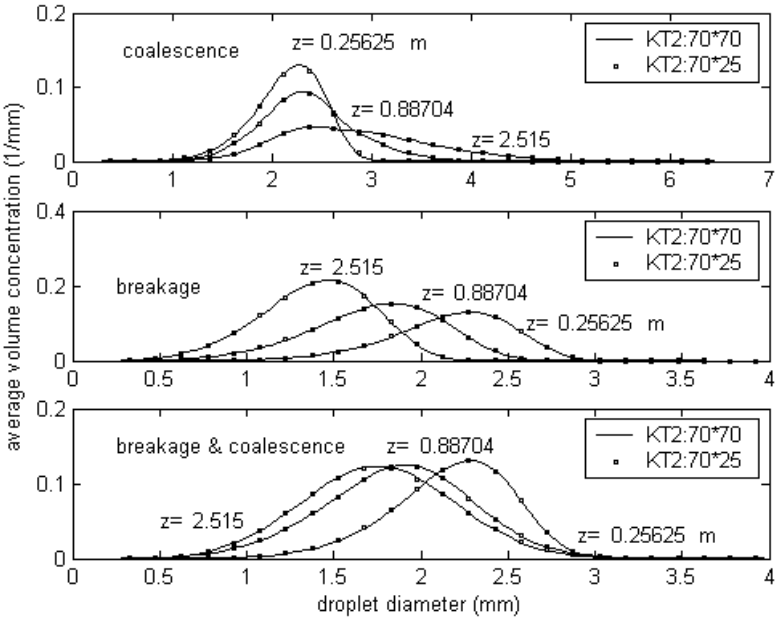

Fig.(12): Steady state convergence of the average volume distributions along the column using the GFP and the KT2 spatial schemes for droplet breakage and coalescence with $\Delta t = 2$ s, $Q_c = 0.28 \times 10^{-4} m^3/s$, $Q_d = 1.11 \times 10^{-4} m^3/s$.

7. Experimental validation

In order to get more trust in the present population balance model and its discrete counterparts, we compare its predictions to some of the available experimental work in the published literature. Modes (2000) studied the steady state hydrodynamics of a laboratory scale RDC column, where his

Table2: The steady state convergence of the GFP and the spatial discretization schemes for case 4.

	Systematic error			CPU* time (s)		
$L \times M_x$	UW1FVS	KT1	KT2	UW1FVS	KT1	KT2
50×15	0.00611	0.00062	0.00091	5	5	6
100×30	0.00171	0.00038	0.00016	28	29	31
150×45	0.00065	0.00032	0.00013	148	156	159

* CPU time measured under Compaq Visual FORTRAN 6.6 on a 750 MHz Pentium III PC

experimentally correlated droplet transport functions, the breakage frequency, and the daughter droplet distribution are used for model validation. These were determined based on single droplet experiments

carried out in a column segment having five compartments of total height 0.15 m. The droplet rise velocity and the breakage probability functions are determined using digital image processing, while the axial dispersion coefficient of the dispersed phase is determined using residence time analysis for a monodispersion of droplets of specified diameters (Modes et al., 1999).
Due to the relative high interfacial tension of the used chemical system (water-toluene), the low values of dispersed phase hold-up, and in the absence of mass transfer, the droplet coalescence could be safely neglected. Additionally, Modes (2000) recommended the use of Vignes (1965) velocity law to estimate the terminal droplet velocity multiplied by ($1-\phi$) to take into account the droplet swarm effect (see Eq.(12)). This author correlated the slowing factor, K_v, and the axial dispersion coefficient, D_d, with the energy input and the droplet diameter as follows:

$$K_v(d,N^*) = 1 - 1.037\left(N^{*3}D_R^5\right)^{0.12} - 0.62\left(\frac{d}{D_s - D_R}\right)^{0.44} \tag{46}$$

$$\frac{D_d}{U_d H} = 0.0138 + 8.26\times10^{-7}\left(\frac{N^* D_R}{U_d}\right)^{3.3} \tag{47}$$

where N^* is the rotor speed (s^{-1}), D_R, and D_s are the rotor and stator diameters respectively.
The droplet breakage frequency in terms of the breakage probability, P_r, is given by:

$$\Gamma(d,\phi) = P_r(d,N^*)\frac{U_d(d,\phi)}{H_c} \tag{48}$$

where

$$\frac{P_r}{1-P_r} = 6.04\times10^{-4}\left(\frac{\rho_c^{0.8}\mu_c^{0.2}dD_R^{1.6}\left(\omega_R^{1.8} - \omega_{R,crit}^{1.8}\right)}{\sigma_{cd}}\right)^{1.595} \tag{49}$$

while $\omega_{R,crit}$ is the critical rotor speed below which the breakage probability falls to zero (Modes, 2000) and H_c is the RDC compartment height.
The daughter droplet distribution (based on number) is assumed to follow the beta distribution, which is given by:

$$\beta_n(d \mid d') = 3\vartheta(\vartheta-1)\left[1-\left(\frac{d}{d'}\right)^3\right]^{(\vartheta-2)}\frac{d^2}{d'^3} \tag{50}$$

where ϑ is the mean number of daughter droplets produced upon breakage of mother droplet of diameter d'. It is experimentally correlated and found dependent on the energy dissipation and having a value ≥ 2.
In all the numerical simulations presented in this section the inlet feed distribution is based on the measured values and for the convergence tests we find the log normal distribution fits will the experimental data. The integration is carried out until steady state with a time step Δt=2 s. The UW1FVS discrete model with uniform grid having a dimension of 70×20 is used for spatial discretization, where doubling of the grid size shows no principal differences in the predicted results. The minimum droplet diameter is chosen to lie below the critical droplet diameter, and the maximum droplet size is estimated based on the feed droplet distribution.
Fig.(13) compares the predicted mean droplet diameter, *d32*, and the dispersed phase hold-up at three rotor speeds, 250, 300 and 350 rpm. The predicted and experimental values of the mean droplet diameter seems to be in good agreement with the experimental data, however, the predicted hold-up values are not as good as the predicted *d32*. This is because the errors in the volume distribution seem to cancel when the *d32* is calculated since it involves the ratio of droplet volume to its surface area. Nevertheless, the model follows correctly the experimental trend where the hold-up increases as the rotor speed increases indicating an increase in the droplet breakage.

Fig.(14) shows the predicted and experimental droplet volume densities at rotor speed 300 rpm at different measuring points along the column. The model predicts fairly well the volume distribution along the column; however, the error increases as the droplet is shifted to the left indicating the breakage of the droplets as they ascend the column.
In Fig.(15), the effect of different droplet terminal velocity laws on the predicted mean droplet diameter and the dispersed phase hold-up is examined. Again, it seems that the error cancellation when calculating the mean droplet diameter makes it less sensitive to the type of the velocity law than the dispersed phase hold-up. Anyhow, more experimental hold-up data is needed to select the right terminal velocity law that describes well the chemical system under investigation. Note that the sensitivity analysis of the model predictions with respect to certain parameters such as, K_v, D_d, Γ, and ϑ is not considered in this work since this issue is analyzed by Modes (2000). He found that the greatest model sensitivity is with respect to the droplet-slowing factor, K_v. It should also be pointed out that the model predicts the flooding behavior of the column when an excessive entrainment of the dispersed phase is observed at the bottom of the column. However, further flooding analysis could be found in Gourdon and Casamatta (1994) and will not be detailed here.

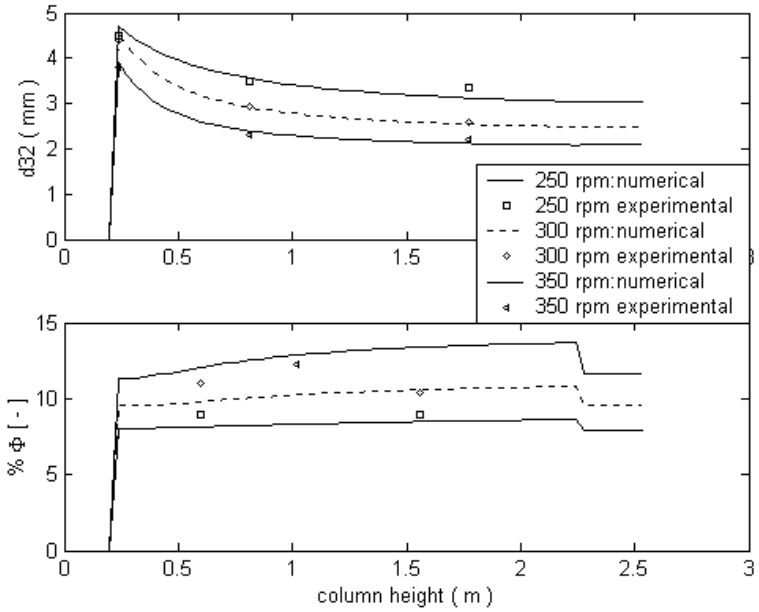

Fig.(13):Steady state comparison between the experimental data and the model prediction with two energy inputs using grid dimension: 70×20, Q_c=2.78×10^{-5} , and Q_d=3.33×10^{-5} m^3/s. The experimental data is from Modes (2000).

8. LLECMOD program

The basic feature of this program described in chapter 6 and by Attarakih, Bart and Faqir (2003c) is to provide the simulation of the hydrodynamics of LLECs based on the population balance approach for both transient and steady state through an interactive windows input dialogs. The LLECMOD (Liquid-Liquid Extraction Column Module) is not restricted to a certain type of liquid-liquid extraction column since it is built in the most general form that allows the user to input the various droplet interaction functions. These functions include droplet terminal velocity taking into account the swarm effect and the slowing factor due to column geometry, the breakage frequency and daughter droplet distribution, the coalescence frequency and the axial dispersion coefficients. Fig.(16) shows the main input dialog for the LLECMOD program.

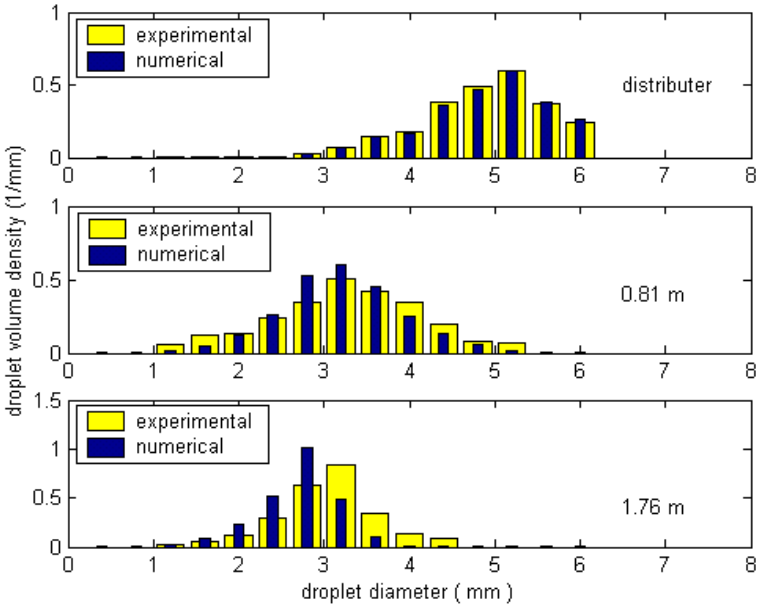

Fig.(14):Steady state comparison between experimental data and the model prediction at 300 rpm using grid dimension: 70×20, Q_c=1.39×10^{-5} and Q_d=3.33×10^{-5} m^3/s. The experimental data is from Modes (2000).

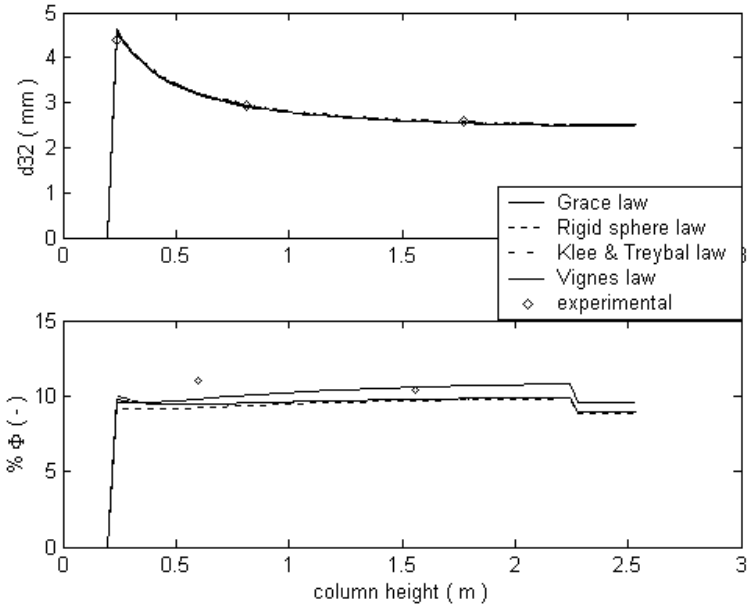

Fig.(15): The effect of the different velocity models (Grace et al., 1976, Klee and Treybal, 1956, Vigness, 1965) on the steady state *d32* and the total column hold-up with grid dimensions:70×20, Q_c=2.78×10^{-5} and Q_d=3.33×10^{-5} m^3/s. The experimental data is from Modes (2000).

8.1 Grids generation

The grid structure depends on the column geometry as well as the minimum and maximum droplet diameters prevailing in the column. The program provides two types of grids for both column height and droplet diameter. For droplet diameter, geometric and uniform droplet discretizations are available. For

the column height, the nonuniform grid structure is constructed by a combination of uniform grids to produce relatively fine structure around the dispersed and continuous phases inlets where permanent discontinuities appear (see Fig.(16)).

8.2 The dispersed and continuous phases chemical components

The physical properties required for the evaluation of droplet transport and interactions (breakage and coalescence) are loaded from a simple database containing ten and three chemical components for the dispersed and continuous phases respectively. However, the user could add the physical properties for any new chemical component by editing the files: LLECMOD\CompData.

8.3 The inlet feed distribution

The inlet feed distribution could be supplied by the user in either two ways: First by representing the data in tabulated form where the first column is the characteristic droplet diameter in mm and the second column is the feed population density (mm^{-1}) corresponding to the given droplet diameter in the first column. The second form of the feed input is in the form of three frequently used distributions to fit the liquid-liquid distributors or droplet distributions in agitated columns: the normal, lognormal and Weibull distributions.

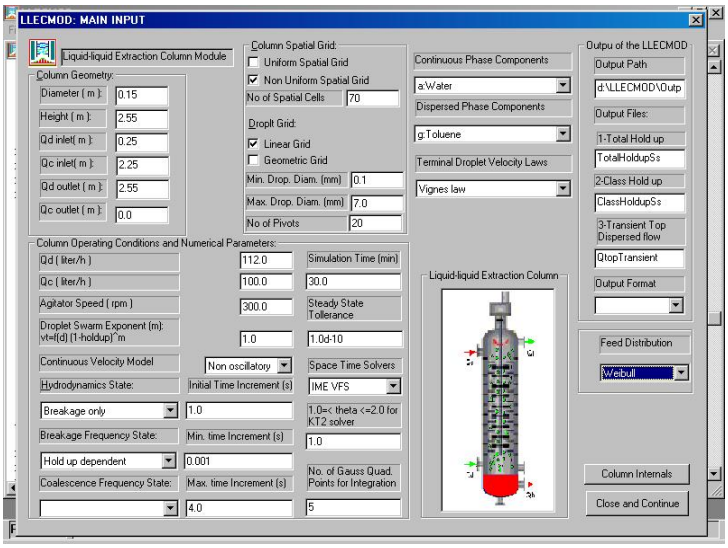

Fig.(16): The main input dialog of the LLECMOD showing the input of case study of section 7.

8.4 The terminal droplet velocity

The LLECMOD has four terminal droplet velocity laws that could be easily chosen by the user. These velocity laws are: Klee and Treybal (1956), Vignes (1965), Grace, Wairegi, and Nguyen (1976) and the rigid sphere law (Wesswlingh & Bollen, 1999). If the user does not choose any of these laws, the LLECMOD automatically chooses by default the suitable velocity law based on the selection chart detailed in the book of Godfrey and Slater (1994). Moreover, if the user has a specific velocity law he could add it simply to the user input module in a standard FORTRAN95 language.

8.5 The continuous phase velocity models

The continuous phase velocity models are required to calculate the dispersed phase velocity. The first velocity model corresponds to the interface level control by manipulating the outlet continuous flow rate at the bottom of the column. The velocity model corresponding to this scheme shows an oscillatory behaviour in the dispersed phase hold-up as reported both experimentally (Hufnagl et al., 1991;

Gerstlauer, 1999) and theoretically (Weinstein et al., 1998; Attarakih, Bart & Faqir, 2004b). The second velocity model assumes that the continuous phase is at a steady state and hence it is not applicable for transient simulations, while the third velocity model is based on the control scheme that manipulates the inlet continuous flow rate (Attarakih, Bart & Faqir, 2004b) (see chapter 5). The advantage of this scheme is found to eliminate the oscillation in the response of the hold-up in the column as shown in Fig.(17).

8.6 The axial dispersion coefficients

The axial dispersion coefficients, D_c and D_d for the dispersed and continuous phases respectively are defined in the user input module as FORTRAN95 functions. These coefficients are allowed only to vary with the column height in the present version of LLECMOD. The dependency on droplet diameter or velocity will be taken into account in the future versions.

8.7 The breakage frequency and daughter droplet distribution

The breakage frequency function $\Gamma(d,U_d, \phi(z,t))$ could be easily defined in the user input module. All the physical properties are declared internally and they need not to be redeclared in this function. The daughter droplet distribution must be based on number rather than volume as a requirement of the GFP technique. For the case that the breakage frequency is independent of the dispersed phase hold-up or the dispersed phase velocity we call it separable; that is, $\Gamma=\Gamma(d)$. In this case we choose from the input menu: *Breakage frequency state/Hold-up independent*, which is the default. On the other hand, if $\Gamma=\Gamma(d, \phi(z,t))$, we choose: *Breakage frequency state/Hold-up dependent*.

8.8 The coalescence frequency

The coalescence frequency function $\omega(d,d', \phi(z,t))$ is defined in the user input module. For the case that the coalescence frequency is independent from the dispersed phase hold-up it is called separable; that is, $\omega=\omega(d,d')$. In this case, the *coalescence frequency state/Hold-up independent* is chosen from the input menu, which is the default choice. On the other hand, if $\omega = \omega(d, d', \phi(z,t))$ the *coalescence frequency state/Hold-up dependent* is chosen.

8.9 The droplet phase space-time solvers

The LLECMOD provides three droplet phase space-time solvers to discretize droplet diameter, column height and time: IME FVS, IME KT1 and IME KT2 as described in sections 4 and 5. The user could choose from the drop list menu provided by the input dialog the suitable solver with IME FVS as the default one. The minimum and maximum time steps, the final simulation time, the steady state tolerance, and the TVD (total variation diminishing) parameter θ for IME KT2 solver could also be chosen by the user from the input dialog.

8.10 The LLECMOD output

The output from the LLECMOD is of two types: the first one is graphical output consisting of the most important simulation results. These are the inlet feed distribution, the relative droplet velocity taking into account the slowing factor K_v, the hold-up along the column, the mean droplet diameter (*d32*) along the column, and the droplet volume distribution at selected positions along the column. The second output is written to three output files: the total hold-up and the mean droplet diameter of the dispersed phase along the column, the droplet volume distribution along the column, and the transient top flow rate. Moreover, in the directory LLECMOD\Output\Plot the user could find a MATLAB file written using MATLAB version 6.1 to plot the two dimensional droplet distribution and the other aforementioned outputs.

9. Conclusions

- The comprehensive literature review of the available numerical techniques for solving the PBE showed that the zero order methods that are inherently consistent with respect to specific droplet integral properties posses the simplicity, robustness, and accuracy for solving the general PBEs. Among these methods the fixed-pivot technique of Kumar and Ramkrishna (1996a) is the most candidate for this task. So, in this work the fixed-pivot technique is generalized to solve the general PBE for continuous flow systems showing both internal and external coordinates dependency.
- In addition to this the moving-pivot technique proposed by Kumar and Ramkrishna (1996b) is also extended to the general continuous flow systems showing spatial dependency and is applied in particular to droplet breakage in a CST.

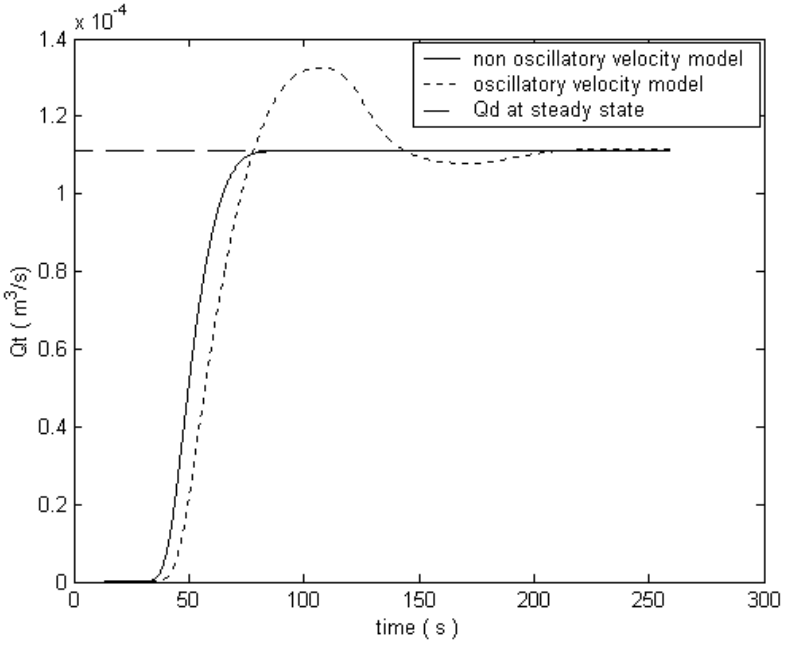

Fig.(17): Comparison between the oscillatory and non oscillatory velocity models using KT2 scheme for droplet breakage and coalescence of case 8 with Δt = .1 s, $Q_c = 0.28 \times 10^{-4} m^3/s$, $Q_d = 1.11 \times 10^{-4} m^3/s$ using uniform droplet diameter and nonuniform spatial grids of dimension 150×30.

- An approximate optimal moving grid technique based on minimizing the total FDE is developed for droplet breakage in batch systems where the sharply increasing number density is successfully tracked out. The redistribution algorithm, on which this technique is based, is consistent with discretized PBEs by preserving any two integral properties of the distribution.
- An optimal fixed grid that minimizes the time-averaged total finite domain error is also developed for continuous droplet breakage. This optimal grid represents a systematic approach for the determination of the minimum and maximum droplet volumes instead of the trial and error procedures that are usually used.
- A general mathematical approach is utilized to discretize the general PBE for droplet breakage describing the hydrodynamics of interacting liquid-liquid dispersions in a continuously stirred tank. The discretization approach presents itself to be computationally efficient since the resulting set of ODEs is free from the evaluation of any double integrals. Moreover, the careful treatment of the breakage matrix makes it possible to decouple the time dependent variables from the repeated evaluation of the single integrals appearing in the discrete equations. The resulting set of discrete equations is forced to be internally consistent with respect to any two integral properties associated with the number density by introducing a set of auxiliary functions that are uniquely determined.

- The external coordinate discretization is carried out using simplified upwind and central differencing schemes where the latter having the advantage of being free of any approximate Riemann solvers. The combined internal and external discretization schemes are found very efficient in solving extremely difficult cases in CSTs and LLECs including droplet breakage and coalescence. The discrete models are validated using different cases of which several analytical solutions are derived. In all these case studies the discretization schemes were able to predict the analytical solutions and found convergent to solutions on fine grids where the analytical solutions are not available. The second order central differencing scheme (KT2) is found the most accurate to capture the moving profiles along the column; however, the three differencing schemes have almost the same accuracy for steady state simulations when sharp profiles are not likely to appear. Moreover, the CPU time requirement for the second order scheme was found comparable to the first order ones with a remarkable high accuracy.
- The transient behavior of the dispersed phase hold-up is found dependent on the type of the continuous phase velocity model. In this work, we introduced a continuous phase velocity model that is non oscillatory based on the idea of Hufnagl, McIntyre and Blass (1991), and hence it is superior to the oscillatory model derived by Casamatta (1981).
- The LLECMOD program is developed based on the population balance approach to model the hydrodynamics of interacting liquid-liquid dispersions taking into account droplet transport as well as breakage and coalescence in the most general way. The user-friendly input dialogs and the user functions input module make the program very general and simple to use.

References

Alatiqi, I., Aly, G., Mjalli, F., & Mumford, C. J. (1995). Mathematical modeling and steady-state analysis of a Scheibel extraction column. *Can. J. Chem. Engng.*, **73,** 523-533.

Al Khani, S. D., Gourdon, C., & Casamatta, G. (1988). Simulation of hydrodynamics and mass transfer of disks and rings pulsed column. *Ind. Engng. Chem. Res.*, **27,** 329-333.

Al Khani, S. D., Gourdon, C., & Casamatta, G. (1989). Dynamic and steady-state simulation of hydrodynamics and mass transfer in liquid-liquid extraction column. *Chem. Engng. Sci.*, **44,** 1295-1305.

Alopaeus, V., Koskinen, J., Keskinen, K. I., & Majander, J. (2002). Simulation of the population balances for liquid-liquid systems in a nonideal stirred tank: Part 2- parameter fitting and the use of multiblock model for dense dispersions. *Chem. Engng. Sci.*, **57,** 1815-1825.

Attarakih, M. M., Bart & Faqir, N. M. (2002). An approximate optimal moving grid technique for the solution of discretized population balances in batch systems. *European Symposium on Computer Aided Engineering-12*, Editors:Grievink, J. and Schijndel, J. Elsevier, Amsterdam, 2002, pp.823-828.

Attarakih, M. M., Bart, H. J., & Faqir, N. M. (2003a). Optimal moving and fixed grids for the solution of discretized population balances in batch and continuous systems: droplet breakage. *Chem. Engng. Sci.*, **58,** 1251-1269.

Attarakih, M. M., Bart, H.-J., & Faqir, N. M. (2003b). Solution of the population balance equation for liquid-liquid extraction columns using a generalized fixed-pivot and central difference schemes. Kraslawski, A. & Turunen, I. (Ed.), *European symposium on computer aided process engineering-13*, Computer-aided chemical engineering 14 (pp. 557-562). Elsevier, Amsterdam.

Attarakih, M. M., Bart, H.-J., & Faqir, N. M. (2003c). LLECMOD: a windows-based program for hydrodynamics simulation of liquid-liquid extraction columns. submitted to the *Comp. Chem. Engng. Journal*.

Attarakih, M. M., Bart, H. J., & Faqir, N. M. (2004a). Solution of the droplet breakage equation for interacting liquid-liquid dispersions: a conservative discretization approach. *Chem. Engng. Sci.*, **59**, 2547-2565.

Attarakih, M. M., Bart, H.-J. & Faqir, N. M. (2004b). Numerical solution of the spatially distributed population balance equation describing the hydrodynamics of interacting liquid-liquid dispersions. *Chem. Engng. Sci.* **59**, 2567-2592.

Bart, H.-J. (2003). Reactive extraction in stirred columns: A review. *Chem. Engng. Tech.*, **26,** 723-731.

Bennett, M. K. , & Rohani, S. (2001). Solution of population balance equations with a new combined Lax-Wendroff/Crank-Nicholson method. *Chem. Engng. Sci.*, **56,** 6623-6633.

Biggs, C. A. , & Lant, P. A. (2002). Modelling activated sludge flocculation using population balances. *Powder Tech.*, **14,** 201-211.

Cabassud, M., Gourdon, C., & Casamatta, G. (1990). Single drop break-up in a Kühni column. *Chem. Engng. J.*, **44,** 27-41.

Campos, F. B. , & Lage, P. L. C. (2003). A numerical method for solving the transient multidimensional population balance equation using Euler-Lagrange formulation. *Chem. Engng. Sci.*, **58,** 2725-2744.

Casamatta, G., (1981): Comportement de la population des gouttes dans une colonne d'extraction: Transport, rupture, coalescence, transfer de matiere, Dissertation, Institut National Polytechnique De Toulouse.

Casamatta, G. , & Vogelpohl, A. (1985). Modelling of fluid dynamics and mass transfer in extraction columns. *Ger. Chem. Engng.*, **8,** 96-103.

Cauwenberg, V., Degreve, J., & Slater, M. J. (1997). The interaction of solute transfer, contaminants and drop break-up in rotating disc contactors: Part I. Correlation of drop breakage probabilities. *Can. J. Chem. Engng.*, **75,** 1046-1055.

Chang, S.-C., Wang, X.-Y., and Chow, C.-Y. (1999). The space-time conservation element and solution element method: A new high-resolution and genuinely multidimensional paradigm for solving conservation laws. *J. Com. Phys.*, **156**, 89-136.

Chatzi, E. , & Lee, J. M. (1987). Analysis of interactions for liquid-liquid dispersions in agitated vessels. *Ind. Engng. Chem. Res.*, **26,** 2263-2267.

Colella, D., Vinci, D., Bagatin, R., & Masi, M. (1999). A study on coalescence and breakage mechanisms in three different bubble columns. *Chem. Engng. Sci.*, **54,** 4767-4777.

Coulaloglou, C. A. , & Tavlarides, L. L. (1977). Description of interaction processes in agitated liquid-liquid dispersions. *Chem. Engng. Sci.*, **32,** 1289-1297.

Desnoyer, C., Masbernat, O., & Gourdon, C. (2003). Experimental study of drop size distribution at high phase ratio in liquid-liquid dispersions. *Chem. Engng. Sci.*, **58,** 1353-1363.

Diemer, R. B. , & Olson, J. H. (2002a). A moment methodology for coagulation and breakage problems: Part 1- analytical solution of the steady-state population balance. *Chem. Engng. Sci.*, **57,** 2193-2209.

Diemer, R. B. , & Olson, J. H. (2002b). A moment methodology for the coagulation and breakage problems: Part 2-moment models and distribution reconstruction. *Chem. Engng. Sci.*, **57,** 2211-2228.

Gelbard, F. , & Seinfeld, J. H. (1978). Numerical solution of the dynamic equation for particulate systems. *J. Comput. Phys.*, **28,** 357-375.

Gelbard, F., Tambour, Y., & Seinfeld, J. H. (1980). Sectional representation of simulating aerosol dynamics. *J. Colloid & Interface Sci.*, **76,** 541-556.

Gerstlauer, A., (1999): Herleitung und Reduktion populationsdynamischer Modelle am Beispiel der Fluessig-Fluessig-Extraktion. Fortschritt-Berichte VDI Reihe, 3, 612.

Godfrey, J. C. , & Slater, M. J. (1991). Slip velocity relationships for liquid-liquid extraction columns. *Trans. Inst. Chem. Engng.*, **69,** 130-141.

Goodson, M. , & Kraft, M., (2003): Stochastic simulation of coalescence and breakage processes: a practical study. Preprint No. 9, pp. 1-30. Cambridge center for computational chemical engineering, Cambridge.

Gourdon, C. , & Casamatta, G. (1994). Population balance based modeling of solvent extraction columns. *Liquid-liquid extraction equipment***,** pp. 136-226, John Wiley, New York

Grace, J. R., Wairegi, T., & Nguyen, T. H. (1976). Shapes and velocities of single drops and bubbles moving freely through immiscible liquids. *Trans. Inst. Chem. Engng.*, **54**, 167-173.

Guimaraes, M. M., Cruz-Pinto, J. J. C., Regueiras, P. F. R., & Madureira, C. M. N. (1992). The simulation of interacting liquid-liquid dispersions- A new algorithm and its potentiality. Sekine T.(Ed.), *Solvent extraction 1990*, Part B, p. 1241-1246, Elsevier, Amsterdam .

Hartland, S. , & Jeelani, S. A. K, (1994): Gravity settlers. *Liquid-liquid extraction equipment*, Godfrey J. C. & Slater M. J., (Eds.), John Wiley, New York

Hill, P. J. , & Ng, K. M. (1995). New discretization procedure for the breakage equation. *AIChE J.*, **41,** 1204-1216.

Hill, P. J. , & Ng, K. M. (1996). New discretization procedure for the agglomeration equation. *AIChE J.*, **42,** 727-741.

Hill, P. J. , & Ng, K. M. (1997). Simulation of solids processes accounting for particle -size distribution. *AIChE J.*, **43,** 715-726.

Hounslow, M. J. (1990). A discretized population balance for continuous systems at a steady state. *AIChE J.*, **36,** 106-116.

Hounslow, M. J., Marshall, V. R., & Ryall, R. L. (1988). A discretized population balance for nucleation, growth, and aggregation. *AIChE J.*, **34,** 1821-1832.

Hufnagl, H., McIntyre, M., & Blass, E. (1991). Dynamic behaviour and simulation of a liquid-liquid extraction column. *Chem. Eng Tech.*, **14,** 301-306.

Hulburt, H., & Katz, S. (1964). Some problems in particle technology. A statistical mechanical formulation. *Chem. Engng. Sci.*, **19**, 555-574.

Karlsen, K. H., Lie, K.-A., Natvig, J. R., Nordhaug, H. F., & Dahle, H. K. (2001). Operator splitting methods for systems of convective-diffusion equations: nonlinear error mechanisms and correction strategies. *J. Comput. Phys.*, **173,** 636-663.

Kentish, S. E., Stevens, G. W., & Pratt, H. R. C. (1998). Estimation of coalescence and breakage rate constants within a Kühni column. *Ind. Engng. Chem. Res.*, **37,** 1099-1106.

Klee, A. J. , & Treybal, R. E. (1956). Rate of rise or fall of liquid drops. *AIChE J.*, **2,** 444-447.

Koren, B., (1993): A robust upwind discretization method for advection, diffusion and source terms. *Numerical methods for advection-diffusion problems*, Vreugdenhil C. B. & Koren B. (Eds.), (pp. 117-138), Vieweg & Sohn, Braunschweig.

Kostoglou, M. , & Karabelas, A. J. (1994). Evaluation of zero order methods for simulating particle coagulation. *J. Colloid Interface Sci.*, **163,** 420-431.

Kronberger, T., Ortner, A., Zulehner, W., & Bart, H.-J. (1994). Numerical determination of drop size distribution in extraction columns. Fasano A. (Ed.), *7th European Conference on Mathematics in Industry,* p. 247-254, B. G. Teubner Stuttgart.

Kronberger, T., (1995): Numerische Simulation von Tropfenpopulationen in Extraktionskolonnen, Dissertation, Johannes Kepler Universitat Linz, Linz 1995.

Kronberger, T., Ortner, A., Zulehner, W., & Bart, H. (1995). Numerical simulation of extraction columns using a drop population model. *Comput. Chem. Engng.*, **19,** S639-S644.

Kumar, S. , & Ramkrishna, D. (1996a). On the solution of population balance equations by discretization-I. A fixed-pivot technique. *Chem. Engng. Sci.*, **51,** 1311-1332.

Kumar, S. , & Ramkrishna, D. (1996b). On the solution of population balance equations by discretization-II. A moving pivot technique. *Chem. Engng. Sci.*, **51,** 1333-1342.

Kumar, S. , & Ramkrishna, D. (1997). On the solution of population balance equations by discretization-III. Nucleation, growth and aggregation of particles. *Chem. Engng. Sci.*, **52,** 4659-4679.

Kurganov, A. , & Tadmor, E. (2000). New high-resolution central schemes for nonlinear conservation laws and convective diffusion equations. *J.Comput. Phys.*, **160,** 241-282.

Lee, G., Yoon, E. S., Lim, Y. I., Le Lann, J. M., Meyer, X. M., & Joulia, X. (2001). Adaptive mesh method for the simulation of crystallization processes including agglomeration and breakage: the potassium sulfate system. *Ind. Engng. Chem. Res.*, **40,** 6228-6235.

Lim, Y. I., Le Lann, J. M., Meyer, X. M., Joulia, X., Lee, G., & Yoon, E. S. (2002). On the solution of population balance equations (PBE) with accurate front tracking methods in practical crystallization processes. *Chem. Engng. Sci.*, **57,** 3715-3732.

Liou, J.-J., Srienc, F., & Fredrickson, A. G. (1997). Solutions of population balance models based on a successive generations approach. *Chem. Engng. Sci.*, **52,** 1529-1540.

Lister, J. D., Smit, D. J., & Hounslow, M. J. (1995). Adjustable discretized population balance for growth and aggregation. *AIChE J.*, **41,** 591-603.

Liu, Y. , & Cameron, T. (2001). A new wavelet-based method for the solution of the population balance equation. *Chem. Engng. Sci.*, **56,** 5283-5294.

Mahoney, A. W. , & Ramkrishna, D. (2002). Efficient solution of population balances equations with discontinuities by finite elements. *Chem. Engng. Sci.*, **57,** 1107-1119.

Mignard, D., Amin, L., & Ni, X.-D. (2003). Population balance modelling of droplets in an oscillatory baffled reactor- using direct measurements of breakage rates constants. *J. Chem. Technol. Biotechnol.*, **78,** 364-369.

Milot, J. F., Duhamet, J., Gourdon, C., & Casamatta, G. (1990). Simulation of a pneumatically pulsed liquid-liquid extraction column. *Chem. Engng. J.*, **45,** 111-122.

Modes, G., (2000): Grundsatzliche Studie zur Populationsdynamik einer Extraktionskolonne auf Basis von Einzeltropfenuntersuchungen, Dissertation, Shaker Verlag.

Modes, G., Bart, H.-J., Rodrigue-Perancho, D., & Broder, D. (1999). Simulation of the fluid dynamics of solvent extraction columns from single droplet parameters. *Chem. Engng. Tech.*, **22,** 231-236.

Mohanty, S. (2000). Modeling of liquid-liquid extraction column: A review. *Rev. Chem. Engng.*, **16,** 199-248.

Motz, S., Mitrovic, A., & Gilles, E.-D. (2002). Comparison of numerical methods for the simulation of dispersed phase systems. *Chem. Engng. Sci.*, **57,** 4329-4344.

Nicmanis, M. , & Hounslow, M. J. (1998). Finite-element methods for steady-state population balance equations. *AIChE J.*, **44,** 2258-2272.

Puel, F., Fevotte, G., & Klein, J. P. (2003). Simulation and analysis of industrial crystallization processes through multidimensional population balance equations. Part 1: a resolution algorithm based on the method of classes. *Chem. Engng. Sci.*, **58,** 3715-3727.

Qian, Y. , & Wang, J. (1992). Modelling of mass transfer in extraction columns with drop forward-mixing and coalescence-redispersion. *Can. J. Chem. Engng.*, **70,** 88-96.

Ramkrishna, D. (1985). The status of population balances. *Rev. Chem. Engng.*, **5,** 49-95.

Ramkrishna, D. (2000). *Population balances: Theory and applications to particulate systems in engineering*. San Diego: Academic Press.

Randolph, A. D. , & Larson, M. A. (1988). *Theory of particulate process*. 2nd Ed. San Diego: Academic Press.

Ribeiro, L. M., Regueiras, P. F. R., Guimaraes, M. M. L., Madureira, C. M. C., & Cruz-Pintu, J. J. C. (1995). The dynamic behavior of liquid-liquid agitated dispersions-I. The hydrodynamics. *Comput. Chem. Engng.*, **19,** 333-343.

Ribeiro, L. M., Regueiras, P. F. R., Guimaraes, M. M. L., Madureira, C. M. N., & Cruz-Pinto, J. J. C. (1997). The dynamic behavior of liquid-liquid agitated dispersions II. Coupled hydrodynamics and mass transfer. *Comput. Chem. Engng.*, **21,** 543-558.

Sastry, K. V. S. , & Gaschignard, P. (1981). Discretization procedure for the coalescence equation of particulate process. *Ind. Engng. Chem. Fundam.*, **20,** 355-361.

Schmidt, S., Simon, M., & Bart, H-J. (2003). Tropfenpopulationsmodellierung-Einfluss von Stoffsystem und technischen Geometrien. *Chemie Ingenieur Technik*, **75**, 62-67.

Song, M., Steif, A., & Weinspach, P.-M. (1997). A very effective method to solve the population balance equation with particle size growth. *Comput. Chem. Engng.*, **52,** 3493-3498.

Steiner, L., Bamelli, M., & Hartland, S. (1999). Simulation of hydrodynamic performance of stirred extraction column. *AIChE J.*, **45,** 257-267.

Toro, E. F. (1999). *Riemann solvers and numerical methods for fluid dynamics*. 2nd ed. Berlin: Springer.

Toutain, J., Lann, J. M. L., Gourdon, C., & Joulia, X. (1998). Maxwell-Stefan approach coupled drop population model for the dynamic simulation of liquid-liquid extraction pulsed column. *Comput. Chem. Engng.*, **22,** S379-S386.

Tsouris, C., Kirou, V. I., & Tavlarides, L. L. (1994). Drop size distribution and holdup profiles in a multistage extraction column. *AIChE J.*, **40,** 407-418.

Valentas, K. J. , & Amundson, A. R. (1966). Breakage and coalescence in dispersed phase systems. *Ind. Engng. Chem. Fundam.*, **5,** 533-542.

Vanni, M. (1999). Discretization procedure for the breakage equation. *AIChE J.*, **45,** 916-919.

Vanni, M. (2000). Approximate population balances equations for aggregation-breakage processes. *J.Coll. Int. Sci.*, **221,** 143-160.

van Peborgh Gooch, J. R. , & Hounslow, M. J. (1996). Monte Carlo simulation of size-enlargement mechanics in crystallization. *AIChE J.*, **42,** 1864-1874.

Verkoeijen, D., Pauw, G. A., Meesters, G. M. H., & Scarlett, B. (2002). Population balances for particulate processes- a volume approach. *Chem. Engng. Sci.*, **57,** 2287-2303.

Vignes, A. (1965). Hydrodynamique des dispersions. *Genie Chimique*, **93,** 129-142.

Weinstein, O., Semiat, R., & Lewin, D. R. (1998). Modeling, simulation and control of liquid-liquid extraction columns. *Chem. Engng. Sci.*, **53,** 325-339.

Wesselingh, J. A. , & Bollen, A. M. (1999). Single particles, bubbles and drops: Their velocities and mass transfer coefficients. *Trans. Inst. Chem. Engng.*, **77,** 89-96.

Wilburn, N. P. (1964). Mathematical determination of concentration profiles in two-phase continuous countercurrent extractors. *Ind. Eng. Chem. Fundam.*, **3,** 189-195.

Wulkow, M., Gerstlauer, A., & Nieken, U. (2001). Modeling and simulation of crystallization process using parsival. *Chem. Engng. Sci.*, **56,** 2575-2588.

Zamponi, G., Stichlmair, J., Gerstlauer, A., & Gilles, E.-D. (1996). Simulation of the transient behaviour of a stirred liquid/liquid extraction column. *Comput. Chem. Engng.*, **20**, S963-S968.

Zhang, S. H., Yu, S. C., Zhou, Y. C., & Su, Y. F. (1985). A model for liquid-liquid extraction column performance- The influence of drop size distribution on extraction efficiency. *Can. J. Chem. Engng.*, **63,** 212-226.

Zimmermann, A., Joulia, X., Gourdon, C., & Gorak, A. (1995). Maxwell-Stefan approach in extractor design. *Chem. Engng. J.*, **57,** 229-236.

CHAPTER 1

An Approximate Optimal Moving Grid Technique for the Solution of Discretized Population Balances in Batch Systems

1.1 Introduction

The population balance equation (PBE) for a well-stirred batch vessel could be written as (Ramkrishna, 2000):

$$\frac{\partial n(v,t)}{\partial t}+\frac{\partial[\dot{v}n(v,t)]}{\partial v}=\rho\{n(v,t),v,t\} \tag{1}$$

where *n(v,t)* is the average number of droplets per unit volume of the vessel at time *t*. The first term on the left hand side denotes the rate of accumulation of droplets of size *v*, and the second term is the convective flux along the droplet volume coordinate. The term on the right hand side is the net rate of droplets generation by coalescence and breakage.

Despite the importance of Eq.(1) it rarely has an analytical solution. So, in general numerical solutions are sought where several methods are proposed in the literature. Kumar and Ramkrishna (1996a) critically reviewed the available methods where they concluded that the methods conserving both total number and volume of droplets are not only computationally efficient but are also accurate. These authors made great achievement in the discretization of the PBE by introducing a general framework of discretization. Their method preserves any two moments of the population, and converts the PBE into set of discrete partial differential equations. The developed methods are called the fixed and moving pivot techniques, where the latter is used in the present work due to its generality and accuracy.

Nevertheless, this discretization is by no means exact, and it is inherently associated with the so-called finite domain error (FDE) resulting from trying to use a finite droplet volume to approximate the infinite one. As so far, only Sovova and Prochazka (1981) tried to investigate rigorously the effect of the FDE on the accuracy of the solution of the DPBEs. They studied droplet breakage and coalescence in batch vessels at steady state and tried to estimate the FDE by extrapolating both ends of the droplet distribution. The main drawback of this technique is the general uncertainties associated with extrapolation and its lack of general relations to predict the time dependent FDE.

The objective of this work is to develop an approximate optimal moving grid technique for batch systems, based on the minimization of the total FDE. The proposed technique has the ability to conserve any two moments of the distribution. A general equation is also derived for the total FDE by approximate discretization of the general PBE.

1.2 The discretized PBE using the moving pivot technique

In the moving pivot technique, the droplet volume is discretized according to the partition (grid) $V_M \equiv \{v_{\min}, v_2, ... v_M, v_{\max}\}$ and the *i*th interval is denoted by $I_i = [v_i, v_{i+1})$. Kumar and Ramkrishna (1996b) derived the DPBEs, which conserve the total number and droplet volume for droplet breakage in batch vessel:

$$\frac{dN_i(t)}{dt}=\lambda_i N_i(t)+\sum_{k=i+1}^{M}\pi_{0,i,k}\Gamma_k N_k(t), \qquad i=1,2, ...M \tag{2}$$

$$\frac{dx_i(t)}{dt} = \eta_i + \frac{1}{N_i(t)} \sum_{k=i+1}^{M} (\pi_{1,i,k} - x_i \pi_{0,i,k}) \Gamma_k N_k(t), \qquad i = 1, 2, \ .....M \tag{3}$$

where x_i is the representative size of the population in the interval I_i and it is called the pivot, N_i is the total number of droplets associated with this pivot, $\eta_i = (\pi_{1,i,i} - x_i \pi_{0,i,i}) \Gamma_i$, $\lambda_i = (\pi_{0,i,i} - 1) \Gamma_i$, $\pi_{0,i,k}$ and $\pi_{1,i,k}$ are given by Kumar and Ramkrishna (1996b) and Γ_i is the breakage frequency.

1.3 The Finite Domain Error

In discretizing an equation defined over an infinite domain an inherent error is incurred due to the failure of taking into account the portion of the function lying outside the domain of discretization. This error is termed the total FDE and is represented by (Sovova and Prochazka, 1981):

$$\varepsilon_0(t) = \int_0^{v_{\min}} n(v,t) dv + \int_{v_{\max}}^{\infty} n(v,t) dv \tag{4}$$

Note that for a given number of intervals, M, and interval width, Δv, an optimal minimum droplet volume, v_{min}, exists and could be found by differentiating Eq.(4) with respect to v_{min} and set the result equal to zero:

$$n(v^*_{\min}, t) - \frac{dv_{\max}}{dv_{\min}} n(v^*_{\max}, t) = 0 \tag{5}$$

According to Eq.(5), the optimal minimum droplet volume must decrease as function of time to account for the increasing number density at the lower size range. This suggests the use of optimal moving grid for droplet breakage, which moves from the upper to the lower size ranges as function of time. Consequently, Eqs.(2) , (3) and (5) must be solved simultaneously at each instant of time to find such an optimal moving grid. Unfortunately, the solution is iterative by solving Eq.(5) at each integration step, and might mask the benefits gained by using the optimal moving grid. To compensate for this drawback, an approximate optimal moving grid technique is derived in the following section.

1.4 An approximate optimal moving grid technique

The total finite domain error, as defined above, will be close to the minimum value when both residuals are equal, which leads to an approximate optimal minimum droplet volume and hence optimal moving grid. This optimal moving grid should keep the number of intervals constant during grid movement, and hence redistribution of the population between the old and the newly formed grids is essential. This should be performed by conserving any two moments of the population in order to be consistent with Eqs.(2) and (3).

Now consider a typical geometric grid ($v_i(t)=\sigma^{i-1} v_{min}(t)$) at two instants of time: t and $t+\Delta t$ where the optimal minimum droplet volume moves from $v^*_{\min}(t)$ to $v^*_{\min}(t+\Delta t)$. Let $\gamma_i^{<i>}(t)$ be the fraction of droplets at the pivot $x_i(t)$ to be assigned to the pivot $x_i(t+\Delta t)$ and $\gamma_{i+1}^{<i>}(t)$ be the fraction of droplets at the pivot $x_i(t)$ to be assigned to the pivot $x_{i+1}(t+\Delta t)$. These fractions are found such that both number and volume of these droplets are conserved after redistribution. Accordingly, the discrete lower and upper residuals at this instant of time are given by:

$$FDE_0^L(t+\Delta t) = \gamma_1^{<0>} N_0(t) \tag{6}$$

$$FDE_0^U(t+\Delta t) = \sum_{i=M+1}^{\infty} \gamma_i^{<i-1>} N_{i-1}(t) + \gamma_i^{<i>} N_i(t) \tag{7}$$

where only the $(M+1)$th term in the summation above has a significant value for sufficiently large M or geometric factor σ.

The optimality condition implied by Eq.(5) could be approximately satisfied by forcing both sides of Eqs. (6) and (7) to be equal, which after some algebraic manipulation yields:

$$\frac{v^*_{\min}(t+\Delta t)}{v^*_{\min}(t)} = \frac{\frac{1}{\sigma-1}N_M(t)+\frac{1}{\sigma}N_0(t)}{\frac{\sigma+1}{\sigma}N_0(t)+\frac{1}{\sigma-1}N_M(t)-N_{M+1}(t)} \tag{8}$$

1.5 Estimation of the lower and upper residuals

To estimate the lower residual, $N_0(t)$, it could be assumed that the first interval will only receive broken droplets from higher ones or from droplets within the interval itself with no droplets are lost through breakage from this interval (Laso et al., 1987; Hill and Ng, 1995). Consequently, an unsteady state number balance on this interval yields:

$$\frac{\mathrm{d}N_0(t)}{\mathrm{d}t} = \vartheta(v^*_{\min}(t))\Gamma_0 N_0(t)+\sum_{k=1}^{M}\pi_{0,0,k}\Gamma_k N_k(t) \tag{9}$$

Since the width of the interval [v_{min}, $v^*_{\min}(t)$] is very small due to the geometric grid used in discretization, the pivot $x_0(t)$ is fixed at the middle of this interval. Similar arguments for the I_{M+1} interval leads to the following equation:

$$\frac{dN_{M+1}(t)}{dt} = \lambda_{M+1}N_{M+1}(t) \tag{10}$$

and the $(M+1)th$ pivot could be derived from Eq.(3). So Eqs.(6) and (7) along with Eqs.(9) and (10) define completely the lower and upper residuals at any instant of time for specified grid parameters σ and M.

1.6 Numerical results and discussion

By using a geometric grid, it should be mentioned that when the last interval is completely passed due to the grid movement, the new and the old interval boundaries completely coincide except for the first boundary. This suggests that the number densities could be updated only when $v^*_{\min}(t)$ is less than or equal to $v_M(t)$ to exclude any numerical inaccuracies due to population redistribution. This strategy is adopted in the present solution algorithm using uniform daughter droplet distribution and linear breakage frequency over a relatively long period of time, $t=100$ (arbitrary time units) to illustrate the steepness of the number density. The solution algorithm is implemented using an exponential initial condition and a number of intervals, $M=15$, and $\sigma=2.0$. The analytical solution is given by by Ziff and McGrady (1985) for binary breakage. We start by comparing the exact and numerical FDE as well as the optimal minimum droplet volumes. Fig.(1-a) shows these results, and it can be seen an excellent agreement between the numerical and exact FDE is obtained. As expected the optimal fixed FDE increases with time due to the failure to account for the increase in number density in the small size range as droplet breakage proceeds. This is actually equivalent to a loss of number of droplets from the system. To compensate for this, we let the grid move in an optimal manner as shown in Fig.(1-b), where the exact minimum droplet volume is depicted along with that predicted using the optimal moving grid algorithm. First the agreement between the optimal piecewise minimum droplet volume and the exact one is also excellent even when the grid moves so fast. Second the great influence of the optimal grid movement on the reduction of the total FDE is obvious when compared to the fixed grid (Fig.(1-a)). Fig.(2-a) shows the exact and numerical average number densities at the final time of simulation where, excellent agreement is perceptible. Also, one could see how the optimal moving grid leaves the approximately empty intervals (large sizes) to accommodate the increasing number densities in the small size range as expected.
Fig.(2-b) shows the clear discrepancies between the discrete zero moment of the distribution using fixed and optimal moving grids respectively.

As expected for a long time of droplet breakage, the number density becomes increasingly sharp. Failure to include the small size range of the population will induce appreciable errors in the total number density as a result of increasing the total FDE. The mean droplet volume is also over predicted, however to a small extent, when fixed grid is used because large number but small volume of droplets are lost at long times of breakage due to the increase in the total FDE. It should be mentioned that as the number of intervals decreases the sum of the residuals becomes the main source of the discretization error (relative to the integration error). Under these circumstances minimizations of these residuals (FDE) is the only way to reduce the discretization error if coarse grid is to be maintained.

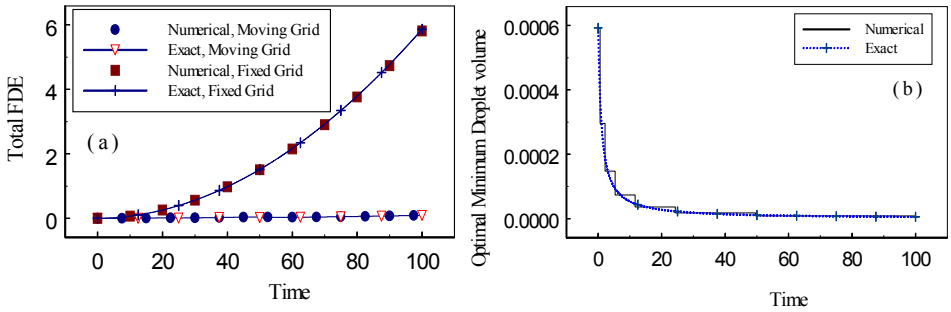

Fig.(1): a-The effect of optimal grid movement on the finite domain error. b– Exact and numerical optimal minimum droplet volumes using geometric grid with factor $\sigma = 2.0$ and $M = 15$.

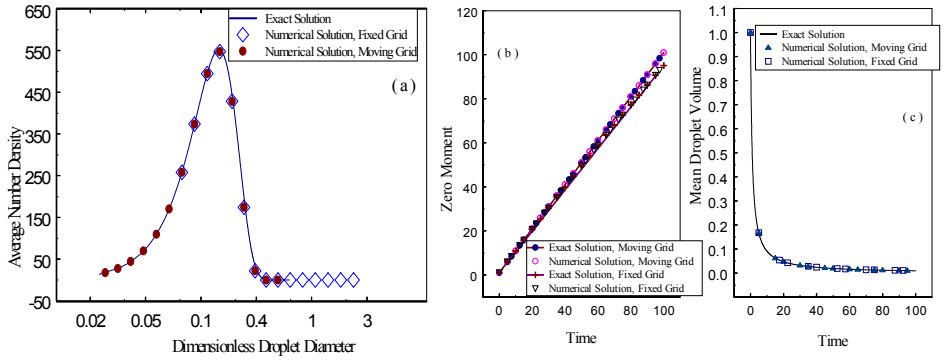

Fig.(2): The effect of the optimal grid movement on: a- The average number density. b- The zero moment and c- The mean droplet volume using geometric grid with factor $\sigma = 2.0$ and $M = 15$.

1.7 Conclusions

An optimal moving grid technique is developed for the solution of the DPBEs for droplet breakage in batch systems base on the minimization of the total FDE. The redistribution algorithm, on which this technique is based, is consistent with DPBEs by preserving any two moments of the distribution. Moreover, ordinary differential equations are derived to estimate the total FDE of the droplet distribution, which shows excellent agreement with the analytical solution studied in this work.

Nomenclature

FDE_0^L , FDE_0^U	lower and upper residuals based on zero moments of the distribution
M	total number of intervals used in droplet volume discretization
$N_i(t)$	total number of droplets in the ith interval, at time t
$n(v,t)dv$	number of droplets in size range v to $v+dv$, at time t per unit volume
v, v'	droplet volumes
$v_{min.}$, $v_{max.}$	minimum and maximum droplet volumes
$v^*_{\min}$, $v^*_{\max.}$	optimal minimum and maximum droplet volumes
$\dot{v}$	droplet growth rate
$x_i(t)$	characteristic volume of the droplet population in the ith interval
t	time

Greek Symbols

$\Gamma(v)$	droplets breakage frequency
$\gamma_i^{<i>}$, $\gamma_i^{<i-1>}$	fractions of droplet assigned to the ith pivot
Δt	time increment
ε_0(t)	total finite domain error based on zero moment of the distribution
η_i	the ith eigenvalue of the pivot equations.
λ_i	the ith eigenvalue of the number density equations
σ	geometric grid factor
$\vartheta(v')$	number of droplets produced when droplet of volume, v', is broken

References

Hill, P. J. and Ng, K. M., 1995, New discretization procedure for the breakage equation. AIChE J., **41,** 1204-1216.

Kumar, S. and Ramkrishna, D., 1996a, On the solution of population balance equations by discretization-I. A fixed pivot technique. Chem. Engng. Sci., **51,** 1311-1332.

Kumar, S. and Ramkrishna, D., 1996b, On the solution of population balance equations by discretization-II. A moving pivot technique. Chem. Engng. Sci., **51,** 1333-1342.

Laso, M., Steiner, L. and Hartland, S., 1987, Dynamic simulation of liquid-liquid agitated dispersions-I. Derivation of a simplified model. Chem. Engng. Sci., **42,** 2429-2436.

Ramkrishna, D., 2000, Population Balances. San Diego: Academic Press.

Sovova, H. and Prochazka, J., 1981, Breakage and coalescence of drops in a batch stirred vessel-I Comparison of continuous and discrete models. Chem. Engng. Sci., **36,** 163-171.

Ziff, R. M. and McGrady, 1985, The kinetics of cluster fragmentation and depolymerisation. J. Phys. A: Math. Gen., **18**, 3027-3037

CHAPTER 2

Optimal Moving and Fixed Grids for the Solution of Discretized Population Balances in Batch and Continuous Systems: Droplet Breakage

2.1 Introduction

In general, the population balance equation (PBE) is a statement of continuity for particulate systems. It represents the net rate of number of particles that are formed by breakage, coalescence, and growth. It is for the sake of mathematical lucidity we define a particle state space continuum that spreads through the internal and external coordinates (Ramkrishna , 1985). By internal coordinates it is meant the variables that describe those quantities associated with the particle, while the term external coordinates is used to denote the position of the particles centre of mass. The population of particles is considered to be large enough so that the random fluctuations in the particle behavior could be averaged out (Mickley, Sherwood & Reed, 1990; Milton & Arnold, 1990; Ramkrishna, 2000). The population of particles in the particle state space continuum is described by a number density function *n(v,r,t)*, where *v* and *r* are the internal and external particle coordinates respectively and *t* is time.
The PBE for a steady and uncompressible flow into a well-stirred vessel could be written as (Barone, Furth & Loynaz, 1980; Lister, Smit & Hounslow, 1995; Ribeiro et al., 1995; Ramkrishna, 2000):

$$\frac{\partial n(v,t)}{\partial t}+\frac{\partial[\dot{v}n(v,t)]}{\partial v}=\frac{1}{\tau}\left(n^{feed}(v,t)-n(v,t)\right)+\rho[\{n(v,t)\};v,t] \tag{1}$$

where the first term on the left hand side denotes the rate of accumulation of droplet of size *v*, the second term is the convective flux along the droplet internal coordinate with a growth velocity $\dot{v}$. The first term on the right hand side is the net bulk flow into the vessel and the second term is the net rate of droplet generation by coalescence and breakage and is given by (Valentas & Amundson, 1966; Valentas, Bilois & Amundson, 1966;Kumar, Kumar & Gandhi, 1993; Kumar & Ramkrishna, 1996a; Podgorska & Baldyga, 2001):

$$\begin{aligned}\rho[\{n(v,t)\};v,t]=-\Gamma(v)n(v,t)-\int_0^{\infty}\omega(v,v')n(v,t)n(v',t)dv'+\int_v^{\infty}\beta(v\,|\,v')\Gamma(v')n(v',t)dv'\\ +\tfrac{1}{2}\int_0^{v}\omega(v-v',v')n(v',t)n(v-v',t)dv'\end{aligned} \tag{2}$$

where: $\Gamma(v)$ and $\omega(v,v')$ are the breakage and coalescence frequencies respectively, and $\beta(v\,|\,v')dv$ is the number of droplets having volume in the range *v* to *v+dv* formed upon breakage of droplet of volume *v´*.
The first two terms represent droplet loss due to breakage and coalescence and the last two terms represent droplet formation due to breakage and coalescence respectively. Note that the source term, $\rho[\{n(v,t)\};v,t]$, is a functional, rather than a simple function of *v* and *t*, but is a function of a whole function *n(v,t)*. Moreover, the function, $\beta(v\,|\,v')$, (sometimes called the daughter droplet distribution) must satisfy the constraints of volume conservation and the average number of daughter droplets produced in a breakage event (Ziff, 1991; Ramkrishna, 2000).
Eqs. (1) and (2) comprise an integro-partial differential equation, which despite its importance rarely has an analytical solution. However, few cases with assumed functional forms of breakage rate, daughter droplet distribution, coalescence kernel functions exist, where most of these solutions are for the batch

stirred vessel. (Blatz & Tobolsky, 1945; Scott, 1968; Bajpai & Ramkrishna, 1976; Vigil & Ziff, 1989; Ziff & McGrady, 1985, McGrady & Ziff ,1988, Ziff, 1991).

In general numerical solutions for Eq. (1) are sought where several methods are proposed in the literature. These methods could be divided into two broad classes (Kostoglou & Karabelas, 1994): zero order methods, where the internal coordinate is represented by a piecewise constant function and a higher order methods in which higher order polynomials are used. Kostoglou and Karabelas (1994) evaluated the zero order methods that are used to solve the coalescence equation in batch vessels and they came to a conclusion that methods conserving droplet number and volume are the most advantageous. Kumar and Ramkrishna (1996a) critically reviewed both methods where they concluded that zero order methods, containing no double integrals, and conserving both numbers and volumes are not only computationally efficient but also are accurate.

To Hounslow, Ryall and Marshal (1988) and Hounslow (1990) goes the credit as they took care of preserving both droplet number and volume for coalescence and growth in batch and continuous vessels at steady state using the zero order method to discretize the PBE. Lister, Smit and Hounslow (1995) introduced a discretized PBE for coalescence and growth with a adjustable geometric internal coordinate discretization and thus had overcome the flaw of the fixed geometric internal coordinate of Hounslow, Ryall and Marshall (1988). Hill & Ng (1995) have followed Hounslow, Ryall and Marshall (1988) in developing a discretized PBE that conserve both number and volume. However, the disadvantage of this method is that it is problem dependent, that is; the discretization coefficients should be derived for each set of breakage functions.

The great achievement made in the discretization of the PBE for batch systems is due to Kumar and Ramkrishna (1996a, b, 1997) where they introduced a general framework of discretization using the zero order approach. Their method deems internal consistency of any two pre-chosen moments of the population such as number and volume. By internal consistency it is meant that for any two pre-chosen moments of the distribution, there exist two ways to obtain them. The first one is by discretizing the continuous PBE, and the second one is by deriving these moments from the discrete population balance equations (DPBE). The internal consistency is enforced by redistribution of the total property for a droplet between two adjacent representative sizes called the pivots. This concept converts the PBE into set of discrete partial differential equations (with no double integrals) and is called the fixed pivot technique.

The fixed pivot technique has a disadvantage by being inappropriate for predicting steeply changing number densities when coarse grids are used. To preserve the desirable coarseness of the grid, and hence keeping the number of equations as small as possible, it is required to change the position of the pivots in the subsequent intervals to follow these sharp changes in number density. The moving pivot technique of Kumar and Ramkrishna (1996b) comes to accomplish this task. Due to the generality and accuracy of this technique it will be used in the present work to discretize Eqs.(1) and (2).

Nevertheless, the discretization of the source term given by Eq.(2) is by no means exact, and it is inherently associated with the so-called finite domain error (FDE) (Gelbard & Seinfeld, 1978; Sovova & Prochazka, 1981; Hounslow, 1990; Nicmanis & Hounslow, 1998). This is an inevitable result of trying to use a finite internal droplet coordinate to approximate the infinite one. As so far, only Sovova and Prochazka (1981) tried to investigate rigorously the effect of the FDE on the accuracy of the DPBE when zero order methods are used. They studied droplet breakage and coalescence in batch vessels at steady state and tried to estimate the FDE by extrapolating both ends of the droplet distribution. The main drawback of this technique is the general uncertainties associated with extrapolation and its lack of general relations to predict the time dependent FDE. Moreover, since the evolution of the droplet size distribution in batch and continuous systems is a dynamic phenomenon, it is desirable to find out how to minimize the increasing FDE with time. Discretization of the internal droplet coordinate (droplet volume) requires specification of minimum and maximum droplet volumes. This discretization results in contiguous intervals compromising a grid that covers the specified range.

The objective of this work is to develop an approximate optimal moving gird technique and a time-averaged optimal fixed grid for batch and continuous systems respectively, based on the minimization of the total FDE. The proposed optimal moving grid for droplet breakage in a batch vessel has the advantage of being internally consistent by conserving any two integral properties of the distribution. General equations are also derived for the FDE by approximate discretization of the general PBE. The possibility of solving the resulting DPBEs sequentially in time is also shown. The developed optimal grids are tested using various analytical solutions available in the literature.

2.2 Discretization of the PBE for continuous systems using the moving pivot technique

In practical applications often of primary interest are some integral properties of the population rather than the entire population itself. For example in modeling of liquid-liquid dispersion systems, the mean droplet size and the hold up are of primary interest (Garg & Pratt, 1984; Eid, Gourdon & Casamatta, 1991; Alopaeus, Koskinen & Keskinen, 1999). However, in this discretization technique it is intended to correctly predict the changes in the required integral properties by exactly preserving the changes of the properties of the single droplets from which the integral ones evolve. This is because the prediction of the number density itself is computationally expensive and contains information more than that is usually required.

To proceed further, let the internal coordinate represents the droplet volume and be discretized according to the partition (grid) $V_M \equiv \{v_0, v_1, ... v_{M+1}\}$, where $v_0=0$, $v_1=v_{min}$, and $v_M = v_{max}$. Let the ith interval be denoted by $I_i = [v_i, v_{i+1})$ and the number density function is represented by (Kumar & Ramkrishna, 1996a):

$$n(v,t) = \sum_i N_i \delta(v - x_i) \tag{3}$$

where δ is the Dirac delta function, x_i is the characteristic or representative size of the population in the interval I_i where it is called the pivot and N_i is the discrete number density. The pivots simply concentrate the population in any interval at a single point where their positions are allowed to change, such that the required integral properties are preserved. The positions of these pivots, as we shall see later, are functions of both time and the coalescence and breakage functions. The pivots are dynamic quantities that follow the changes in the number density according to the following relation when the droplets volume is preserved (Kumar & Ramkrishna, 1996b):

$$x_i(t) = \frac{\int_{v_i}^{v_{i+1}} vn(v,t)dv}{\int_{v_i}^{v_{i+1}} n(v,t)dv}, \qquad v_i \le x_i < v_{i+1} \tag{4}$$

This definition of the pivot is consistent with the mean value theorem of integrals such that it moves in the interval as the number density changes. It remains close to v_i for decreasing number density and close to v_{i+1} or to the middle of the interval for increasing and uniform number densities respectively.

The coefficients N_i resemble the number density function in the interval I_i and are considered functions of time only. These functions represents the total number of droplets in the ith interval and are related to the continuous number density by:

$$N_i(t) = \int_{v_i}^{v_{i+1}} n(v,t)dv \tag{5}$$

In the present work, we will focus on the case of pure breakage in batch and continuous vessels since the coalescence and growth for batch and continuous systems are well studied (Hounslow, Ryall & Marshal, 1988; Hounslow, 1990; Lister, Smit & Hounslow, 1995; Kumar & Ramkrishna, 1996b; Ramkrishna, 2000).

To derive an internally consistent set of DPBE with respect to total number and droplet volume, we follow Kumar and Ramkrishna (1996b), where Eqs.(1) and (2) could be discretized by integrating both sides with respect to v from v_i to v_{i+1} which results in:

$$\frac{dN_i(t)}{dt} = \lambda_i^c N_i(t) + \sum_{k=i+1}^{M} \pi_{0,i,k} \Gamma_k N_k(t) + \frac{N_i^{feed}}{\tau}, \qquad i = 1, 2, \; .....M-1 \tag{6}$$

where:

$$\Gamma_k = \Gamma(x_k(t)) \tag{7}$$

$$\pi_{0,i,k} = \int_{v_i}^{u_i} \beta(v \mid x_k) dv, \qquad \begin{cases} u_i = x_i, & k = i \\ u_i = v_{i+1}, & k > i \end{cases} \tag{8}$$

$$\lambda_i^c = \Gamma_i(\pi_{0,i,i} - 1) - \frac{1}{\tau} \tag{9}$$

Eq.(6) conserves the total number of droplet in the *i*th interval and is internally consistent with respect to the zero moment of the distribution. To conserve the total droplet volume (mass) in each interval, Eqs.(1) and (2) are written in terms of the volume distribution ($p=vn(v)$) and integrated with respect to v from v_i to v_{i+1}, where after some algebraic manipulation one could obtain:

$$\frac{dx_i(t)}{dt} = \eta_i + \frac{1}{N_i(t)} \sum_{k=i+1}^{M} (\pi_{1,i,k} - x_i \pi_{0,i,k}) \Gamma_k N_k(t), \qquad i = 1, 2, \ .....M-1 \tag{10}$$

where:

$$\eta_i = (\pi_{1,i,i} - x_i \pi_{0,i,i}) \Gamma_i + \frac{x_i^{feed} - x_i}{\tau} \left(\frac{N_i^{feed}}{N_i} \right) \tag{11}$$

$$\pi_{1,i,k} = \int_{v_i}^{u_i} v \beta(v \mid x_k) dv, \quad \begin{cases} u_i = x_i, & k = i \\ u_i = v_{i+1}, & k > i \end{cases} \tag{12}$$

It should be noted that Eq.(10) becomes independent of the feed droplet distribution, N^{feed}, as well as the vessel residence time τ in case of sufficiently fine discretization ($x_i^{feed} \approx x_i$), which is a desirable result. This is really the same equation for batch vessels derived by Kumar and Ramkrishna (1996b) when $N_i^{feed} \to 0$. Eqs.(6) and (10) comprise a system of ordinary differential equations describing the evolution of the discrete number density through estimating the total number and volume of droplets in the *i*th interval with the desired accuracy. To completely specify this system, the following two sets of initial conditions are stipulated:

$$\begin{aligned} &N_i(0) = N_i^0, \\ &x_i(0) = x_i^0, \qquad i = 1, \ 2, ...M-1 \end{aligned} \tag{13}$$

2.3 Error of discretization

In discretizing an equation defined over an infinite domain an inherent error is incurred due to the failure of taking into account the portion of the function lying outside the domain of discretization. This type of error is termed finite domain error (FDE) (Gelbard & Seinfeld, 1978; Hounslow, 1990), and as a result it causes a nonzero lower and upper residuals below and above the discrete limits of integration. These lower (FDE^L) and upper (FDE^U) residuals represent cumulative number densities that are given by (Sovova & Prochazka, 1981):

$$FDE_0^L(v_{\min}, t) = \int_0^{v_{\min}} n(v,t) dv \tag{14}$$

$$FDE_0^U(v_{\max},t)=\int_{v_{\max}}^{\infty} n(v,t)dv \tag{15}$$

where the subscript zero is used to refer to the residuals of the zero moment of the distribution. This choice is actually suitable for characterizing the FDE since in droplet breakage a large number of droplets having a small volume is produced as breakage proceeds. So, these lower and upper residuals could be related to the total number of droplets for the continuous distribution as follows:

$$N^c(t)=FDE_0^L(v_{\min},t)+\sum_{i=1}^{M-1}\int_{v_i}^{v_{i+1}} n(n,t)dv+FDE_0^U(v_{\max},t) \tag{16}$$

The discrepancy between the continuous number of droplets, $N^c(t)$, at any instant of time and its discrete counterpart, $N^d(v_{min}, v_{max}, t)$, could be interpreted by defining the so called error of discretization. The error of discretization, ε_0, is defined as the difference of sums between the continuous and discrete number of droplets for the intervals $(0,\infty)$ and $[v_{min}, v_{max}]$ respectively:

$$\varepsilon_0(t)=N^c(t)-\sum_{i=1}^{M-1}N_i(t) \tag{17}$$

By combining the last two equations the error of discretization becomes:

$$\varepsilon_0(t)=FDE_0^L(v_{\min},t)+FDE_0^U(v_{\max},t) \tag{18}$$

This result shows that the discretization error in the number of droplets is solely due to the total finite domain error comprising of the sum of both the lower and upper residuals defined by Eqs.(14) and (15). This means that even for an exact number of droplets, and by excluding the integration error induced by discretization, the total finite domain error will never be zero as long as a finite domain is considered. Moreover, for a given number of intervals, M, and interval width, Δv, the total finite domain error at any instant of time is a function only of v_{min}. Since the lower residual decreases as v_{min} decreases and the upper residual increases at the same time, then there exist due to these opposing effects an optimal minimum droplet volume that minimizes the sum of both residuals. This means as far as discrete distribution is considered, a choice of v_{min}, below the optimal value will increase the discretization error in opposite to the general intuition that decreasing v_{min} will improve the solution. Actually, Hounslow (1990) showed that when a value of minimum droplet volume is chosen below the optimal one, an artifact oscillation in N_i is observed in the few first number of intervals.

To find the optimal minimum droplet volume that minimizes the total finite domain error it is sufficient to differentiate Eq.(18) with respect to v_{min} at given M and Δv. By using the definition of the residuals (Eqs.(14) and (15)) and making use of Leibnitz formula (Mickley, Sherwood & Reed , 1990) one could obtain:

$$n(v_{\min}^*,t)-\frac{dv_{\max}}{dv_{\min}}n(v_{\max}^*,t)=0 \tag{19}$$

and the discrete counterpart of Eq. (19) is:

$$\frac{\overline{N}_0^*(t)+\overline{N}_1^*(t)}{2}-\frac{dv_{\max}}{dv_{\min}}\left(\frac{\overline{N}_{M-1}^*(t)+\overline{N}_M^*(t)}{2}\right)=0 \tag{20}$$

where the number densities $n(v_{\min}^*,t)$ and $n(v_{\max}^*,t)$ are approximated by the arithmetic of their average discrete values at the adjacent intervals I_0, I_1 and I_{M-1}, I_M respectively (Marchal et al., 1988). Note that the maximum droplet volume must be a continuous function of v_{min} in order to satisfy the conditions implied by Eqs.(22) and (23). As will be shown later a geometric grid with adjustable geometric factor, $\sigma>1$, will be a suitable choice for the discretization of the droplet internal coordinate (v):

$$v_{\max} = \sigma^{M-1} v_{\min} \tag{21}$$

It should be noted that the discretization parameters are: the total number of intervals, *M*, the optimal minimum droplet volume, $v^*_{\min}$, and the interval width controlled by the geometric factor σ.

Since the continuous and discrete number densities appearing in Eqs.(19) and (20) respectively are functions of time, it follows that the optimal minimum droplet volume, $v^*_{\min}$ is also function of time. This means that as breakage proceeds to produce smaller number of droplets, the optimal minimum droplet volume must decrease to account for the increasing number density at the lower size range. At the same time, and due to the conservation of droplet volume, the number density function decreases for large droplets leading to empty classes at the upper size range. This suggests the use of optimal moving grid for droplet breakage in batch vessels, which moves from the upper size range to the lower size range as function of time. To find such an optimal moving grid, Eqs.(6) (for batch), (10), and (20) must be solved simultaneously at each instant of time leading to a differential algebraic system of equations (DAE). Unfortunately, the solution is iterative by starting with an initial guess for the minimum droplet volume at given number of intervals, *M*, and geometric factor σ followed by solving the system of ODEs (6) and (10). If Eq.(20) is not satisfied, then an improved guess must be used until convergence at each instant of time is achieved. This algorithm seems to be time consuming since it involves solving *2M* ODEs per iteration at each instant of time and might mask the benefits gained by using the optimal moving grid. To compensate for this drawback, an approximate optimal moving grid technique is derived in the following section.

2.4 An approximate optimal moving grid technique for batch systems

We return back to the definitions of the lower and upper residuals given by Eqs.(14) and (15) and the definition of the total finite domain error given by Eq.(18). Since the lower residual decreases as minimum droplet volume increases, and the upper residual increases at the same time, it follows that the total finite domain error will be close to the minimum value when both residuals are equal (Sovova & Prochazka, 1981). Using this principle, it is possible to force these residuals to be equal at each instant of time and hence producing a minimum droplet volume profile that is close to the exact optimal one. Since the optimal moving grid should keep the number of intervals, and hence the number of DPBE associated with it constant during grid movement, the redistribution of the population between the old and the newly formed grid must conserve any two chosen integral properties of the population. However, we will restrict our attention to the total number and volume in this work (zero and first moment of the population). Now consider the geometric grid shown in Fig.(1) at two instants of time: *t* and *t+Δt* where the minimum droplet volume moves from $v^*_{\min}(t)$ to $v^*_{\min}(t+\Delta t)$. Let $\gamma_i^{<i>}(t)$ be the fraction of droplets at the pivot $x_i(t)$ to be assigned to the pivot $x_i(t+\Delta t)$ and $\gamma_{i+1}^{<i>}(t)$ be the fraction of droplets at the pivot $x_i(t)$ to be assigned to the pivot $x_{i+1}(t+\Delta t)$. To conserve both number and volume of these droplets at the *i*th pivot after redistribution, the following two constraints are set up (refer to Fig.1b) (Kumar & Ramkrishna, 1997):

$$\gamma_i^{<i>} + \gamma_{i+1}^{<i>} = 1 \tag{22}$$

$$x_i(t+\Delta t)\gamma_i^{<i>} + x_{i+1}(t+\Delta t)\gamma_{i+1}^{<i>} = x_i(t) \tag{23}$$

Solving these equations for $\gamma_i^{<i>}(t)$ results in:

$$\gamma_i^{<i>:} = \frac{x_{i+1}(t+\Delta t) - x_i(t)}{x_{i+1}(t+\Delta t) - x_i(t+\Delta t)} \tag{24}$$

Similar equations could be written for the droplet population at the (*i-1*)th pivot where $\gamma_i^{<i-1>}(t)$ is the fraction of droplet at the $x_{i-1}(t)$ pivot assigned to the $x_i(t+\Delta t)$ pivot, and $\gamma_{i-1}^{<i-1>}(t)$ is the fraction of droplets at the $x_{i-1}(t)$ pivot assigned to the $x_{i-1}(t+\Delta t)$. Solving these equations yields an expression for $\gamma_i^{<i-1>}(t)$:

$$\gamma_i^{<i-1>:} = \frac{x_{i-1}(t) - x_{i-1}(t+\Delta t)}{x_i(t+\Delta t) - x_{i-1}(t+\Delta t)} \tag{25}$$

Now by referring to Fig.(1-b), we could obtain the net discrete density of droplet population at the instant $t+\Delta t$ at the new grid from that at the old one at time t using Eqs.(24) and (25):

$$N_i(t+\Delta t) = \gamma_i^{<i-1>} N_{i-1}(t) + \gamma_i^{<i>} N_i(t), \qquad i = 1,\ 2,\ \ldots\ldots\ M \tag{26}$$

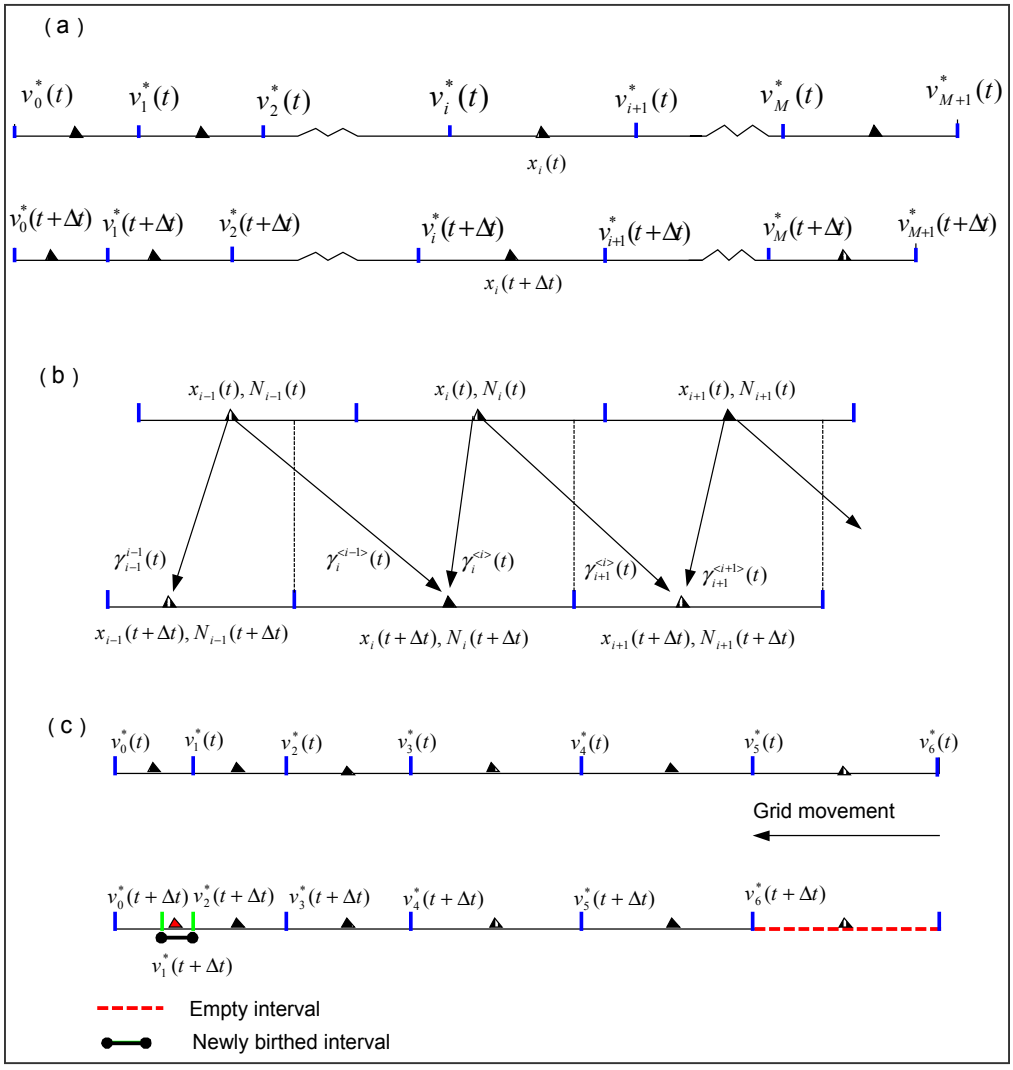

Fig.(1): Typical moving geometric grid.

When i=1, the last equation becomes function of $N_0(t)$ which is not defined by any of the system of Eqs.(6). It is interesting to note that by definition, $N_0(t)$, is the lower residual defined by Eq.(14), and

hence its estimation becomes an inevitable necessity for both $N_1(t+\Delta t)$ and the FDE_0^L. The estimation of $N_0(t)$ from the discrete number density will follow in the next section.
Now we shall turn our attention to force both residuals to be equal at any instant of time $t+\Delta t$ utilizing the redistribution concept above. At the time instant $t+\Delta t$ the discrete lower residual of the distribution is found from Eq.(26):

$$FDE_0^L(t+\Delta t) = \gamma_0^{<0>} N_0(t) \tag{27}$$

and similarly the discrete upper residual is given by:

$$FDE_0^U(t+\Delta t) = \sum_{i=M}^{\infty} \gamma_i^{<i-1>} N_{i-1}(t) + \gamma_i^{<i>} N_i(t) \tag{28}$$

It could be shown that only the Mth term in the summation above has a significant value since the population contained in the interval $[V_{M+1}, \infty)$ is approximately negligible for sufficiently large M or geometric factor σ. This is because during droplets breakage the final intervals (numbering is started from the small size to large size) become gradually empty as breakage progresses. Actually, after sufficient time the last interval becomes completely empty and the zero interval is occupied by the newly birthed population of droplets. Moreover, if the initial minimum and maximum droplets sizes are chosen to be optimal according to Eq.(19), then the higher terms in Eq.(28) will be insignificant for sufficiently large M or σ. This is actually is equivalent to neglecting droplet breakage from the $(M+1)$th intervals and the higher ones.
The necessary condition for optimality stated by Eq.(19) or (20) is approximately satisfied if both residuals are equal at each instant of time. To accomplish this, we force both sides of Eqs.(27) and (28) to be equal, which after some algebraic manipulation yields:

$$\frac{v_{\min}^*(t+\Delta t)}{v_{\min}^*(t)} = \frac{\frac{1}{\sigma-1} N_{M-1}(t) + \frac{1}{\sigma} N_0(t)}{\frac{\sigma+1}{\sigma} N_0(t) + \frac{1}{\sigma-1} N_{M-1}(t) - N_M(t)} \tag{29}$$

with $v_{\min}^*(0)$ found from the initial number density and Eq.(19). Eq.(29) specifies the path that must be followed by the grid in order to keep the total *FDE* approximately minimum based on the zero moment of the distribution.
Since the interval boundaries are now functions of time, then the population contained in it changes also with time. It follows that the discretization of the left hand side of Eq.(1) for a batch system will be different from that used in the case of a fixed grid. This could be shown by multiplying both sides of Eq. (1) by dv and integrating over the size range $[v_i(t), v_{i+1}(t)]$:

$$\frac{\partial}{\partial t} \int_{v_i(t)}^{v_{i+1}(t)} n(v,t)\,dv = \lambda_i^c N_i(t) + \sum_{k=i+1}^{M} \pi_{0,i,k} \Gamma_k N_k(t) \tag{30}$$

By expanding the left hand side using the Leibnitz formula (Mickley, Sherwood & Reed 1990), and noting that the right hand side involves integration with respect to volume only, one could obtain:

$$\int_{v_i(t)}^{v_{i+1}(t)} \frac{\partial n(v,t)}{\partial t} dv + n(v_{i+1}(t),t) \frac{dv_{i+1}(t)}{dt} - n(v_i(t),t) \frac{dv_i(t)}{dt} = \lambda_i^c N_i(t) + \sum_{k=i+1}^{M} \pi_{0,i,k} \Gamma_k N_k(t) \tag{31}$$

Note that the entire grid boundaries move at the same velocity, that is;

$$\frac{dv_i(t)}{dt} = \frac{dv_{i+1}(t)}{dt} = \frac{dv(t)}{dt} \tag{32}$$

Using the above relation, Eq.(31) after some algebraic manipulation simplifies to:

$$\int_{v_i(t)}^{v_{i+1}(t)} \left[\frac{\partial n(v,t)}{\partial t} + \frac{dv}{dt} \frac{\partial n(v,t)}{\partial v} \right] dv = \lambda_i^c N_i(t) + \sum_{k=i+1}^{M} \pi_{0,i,k} \Gamma_k N_k(t) \tag{33}$$

The term in the brackets on the left hand side is merely the total derivative of the number density, which describes the change in the number density of size *v* as noticed by an observer moving with a velocity the same as that of the grid. Using this fact Eq.(33) simplifies to:

$$\frac{\mathrm{d}N_i(t)}{\mathrm{d}t} = \lambda_i^b N_i(t) + \sum_{k=i+1}^{M} \pi_{0,i,k} \Gamma_k N_k(t), \quad i = 1, 2, \ldots\ldots M-1 \tag{34}$$

where λ_i^b is found from λ_i^c by setting $\tau \to \infty$.

Similarly, the equations of the pivots are still given by Eq. (10) with $\eta_i^b = \lim_{\tau \to \infty} \eta_i^c$, where the change in the position of the pivot in any size range is now with respect to the moving grid.

The set of Eqs.(10), (24), (25), (26), (29), (34), and the initial conditions specified by Eq.(13) comprise a differential algebraic system of equations that could be solved sequentially in time.

The notation will be greatly simplified if these equations are written in a compact matrix form as follows:

$$\frac{\mathrm{d}\boldsymbol{N}}{\mathrm{d}t} = \boldsymbol{A}\boldsymbol{N} \tag{35}$$

$$\frac{\mathrm{d}\boldsymbol{x}}{\mathrm{d}t} = \boldsymbol{F}(\boldsymbol{x}, \boldsymbol{N}) \tag{36}$$

$$\boldsymbol{N}(t + \Delta t) = \boldsymbol{\gamma}(t)\boldsymbol{N}(t) + \boldsymbol{N}_0^T(t)\boldsymbol{\gamma}_0(t) \tag{37}$$

$$\boldsymbol{N}(0) = [\ N_1(0) \quad N_2(0)\ \ldots\ N_{M-1}(0) \quad N_M(0)]^T \tag{38}$$

$$\boldsymbol{x}(0) = [\ x_1(0) \quad x_2(0)\ \ldots\ x_{M-1}(0) \quad x_M(0)]^T \tag{39}$$

Where $\boldsymbol{A}$ and $\boldsymbol{F}$ are $M \times M$ upper triangular matrices whose elements are given by:

$$A_{i,k} = \begin{cases} \lambda_i^b, & k = i \\ \pi_{0,i,k} \Gamma_k, & k > i \end{cases} \tag{40}$$

$$F_{i,k} = \begin{cases} \eta_i^b, & k = i \\ \dfrac{(\pi_{1,i,k} - x_i \pi_{0,i,k}) \Gamma_k N_k(t)}{N_i(t)}, & k > i \end{cases} \tag{41}$$

and $\boldsymbol{\gamma}$ is an $M \times M$ bidiagonal matrix whose elements are given by:

$$\gamma_{i,k} = \begin{cases} \gamma_i^{<i>}, & k = i \\ \gamma_i^{<i-1>}, & k = i-1, k \neq 0 \end{cases} \tag{42}$$

γ_0 and $\boldsymbol{N_0}$ are $M \times 1$ vectors whose elements are:

$$\boldsymbol{\gamma_0} = [\ \gamma_1^0 \quad 0\ \ldots\ 0 \quad 0)]^T \tag{43}$$

$$\boldsymbol{N_0} = [\, N_0 \quad 0 \ldots \quad 0 \quad 0)]^{\,T} \tag{47}$$

In the above system of equations, the only undetermined variables are $N_0(t)$ and $N_M(t)$ and their corresponding pivots (x_0 and x_M) which will be considered in the next section.

2.5 Estimation of the lower and upper residuals

It should be clear that in the derivation of the DPBE, the droplets having volume less than v_{min} have zero breakage frequency. This corresponds to the case of limited breakage, where physically stable minimum droplet volume exists below which no further breakage occurs (Valentas, Bilois & Amundson, 1966; Tsouris & Tavlarides, 1994; Hill & Ng, 1995; Aopaeus, Koskinen & Keskinen, 1999). As the breakage proceeds the optimal minimum droplet volume $v^*_{\min}(t)$ will move toward v_{min} until both droplet volumes coincide. For the case of full breakage all the droplets have a nonzero breakage frequency and hence $v_{min} \to 0$. The discrete droplet population density in the intervals $(0,\ v^*_{\min}(t)\,]$ and $[v_{min},\ v^*_{\min}(t)\,]$, for the case of full and limited breakage respectively, represents the lower residual or strictly speaking $N_0(t)$. To estimate this population density, Sovova and Prochazka (1981) used a two point linear extrapolation to estimate the steady state lower residuals in batch vessel where both breakage and coalescence mechanisms were active. Their extrapolation technique is usually useful for non-steep number densities and might lead to significant erroneous predictions for very steep number densities for which the approximate optimal moving grid technique is developed. Instead of extrapolation, which has considerable numerical uncertainties (Mickley, Sherwood & Reed, 1990), a natural approximate extension of the discrete equations to include either of the intervals $(0,\ v^*_{\min}(t)\,]$ and $[v_{min},\ v^*_{\min}(t)\,]$ will be used. It could be assumed that either of the aforementioned intervals will only receive broken droplets from higher ones or from droplets within the intervals themselves, and no droplet will be lost through breakage from these intervals (Laso, Steiner & Hartland, 1987; Hill & Ng, 1995). As a consequence of this assumption an unsteady state number balance on these intervals will produce the required differential equation describing the change of $N_0(t)$ with time:

$$\frac{\mathrm{d}N_0(t)}{\mathrm{d}t} = \vartheta(v^*_{\min}(t))\Gamma_0 N_0(t) + \sum_{k=1}^{M} \pi_{0,0,k}\Gamma_k N_k(t) \tag{45}$$

Here $\vartheta(v^*_{\min})$ is the average number of droplets produced due to the breakage of droplet of volume $v^*_{\min}(t)$.

Since the width of the intervals $(0,\ v^*_{\min}(t)\,]$ or $[v_{min},\ v^*_{\min}(t)\,]$ is very small due to the geometric grid used in discretization, the pivot $x_0(t)$ is fixed at the middle of these intervals without introducing appreciable errors. This is in general always correct when fine grids are used, where it is possible for the fixed pivots to replace the moving ones, that is; the moments of the population could be predicted without appreciable errors (Ramkrishna, 2000).

To estimate the discrete population density $N_M(t)$, we shall follow the same reasoning used to obtain $N_0(t)$. There are only droplets vanishing from the I_M interval to the lower ones, and formation of droplets by breakage within the Mth interval itself is permitted (Laso, Steiner & Hartland, 1987; Hill & Ng, 1995). An unsteady state number balance on the I_M interval results in:

$$\frac{dN_M(t)}{dt} = \lambda^b_M N_M(t) \tag{46}$$

Using similar argument, the Mth pivot follows from Eq.(10):

$$\frac{dx_M(t)}{dt} = \eta_M \tag{47}$$

Eqs.(27) and (28) along with Eqs.(45) through (47) define completely the lower and upper residuals at any instant of time for specified grid parameters σ and M.

2.6 Sequential solution of the number density and pivot equations

The system of equations for the discrete number density and the pivots given by Eqs.(35) and (36) could be solved sequentially in time. The sequential solution starts by first integrating the number density equations over the time interval $t\in[t,\ t+\Delta t]$ followed by the integration of the pivot equations. This method of solution is allowed only if the pivots change slowly when compared to the variation of the number densities over sufficiently small interval of time, and hence making the matrices $\boldsymbol{A}$ and $\boldsymbol{F}$ approximately time independent. This is actually valid if the value of the ratio of each time constant of the pivot and number density equations is a large number. Actually, the time constants of Eqs.(6) and (10) are the reciprocal of the eigenvalues of their matrices $\boldsymbol{A}$ and $\boldsymbol{F}$. Since these matrices are both upper triangular, it can be simply shown that their eigenvalues are given by their diagonal elements (Gerald & Wheatly, 1994). The time constants of the present systems are $\left|\lambda_i^b\right|^{-1}$ and $\left|\eta_i\right|^{-1}$ *(i=1, 2, ... M)* for number density and pivots respectively. Accordingly, the condition stated above for the possibility of sequential solution could be written mathematically as:

$$\frac{\left|\eta_i\right|^{-1}}{\left|\lambda_i^b\right|^{-1}} >> 1 \tag{48}$$

This condition could be satisfied for sufficiently fine grids by using an optimal moving geometric grid. This grid becomes gradually fine as the breakage progresses in time by moving to the left to accommodate the evolving population in the small size range. By applying the mean value theorem of integrals to the system of Eqs.(9) and (11) it is easy to show that:

$$\lim_{\Delta v_i \to 0} \frac{\left|\eta_i\right|^{-1}}{\left|\lambda_i^b\right|^{-1}} \to \infty \tag{49}$$

This insures the validity of the method of sequential solution in time proposed above. Actually, the system of equations given by Eq.(35) has an explicit solution that is given by:

$$\boldsymbol{N}(t) = \boldsymbol{R}\boldsymbol{D}\boldsymbol{R}^{-1}\boldsymbol{N}(0) \tag{50}$$

where $\boldsymbol{D}$ is an $M\times M$ diagonal matrix given by: $\boldsymbol{D} = diag(e^{\lambda_i^b t})$, $i = 1, 2, \ldots M$, and $\boldsymbol{R}$ is an $M\times M$ matrix whose columns are the eigenvectors of **A**.

2.7 The geometric grid

The use of geometric grid in the discretization of the PBEs is extensively used in the literature and its many advantages are found elsewhere (Bleck, 1970; Laso, Steiner & Hartland, 1987; Hounslow, Ryall & Marshal, 1988; Lister, Smit & Hounslow, 1995; Hill & Ng, 1995; Ramkrishna, 2000). However, it is worthwhile to mention two distinctive advantages of the geometric grid that are utilized in this work. The first one is that the geometric grid becomes fine as the entire grid moves to the left and thus allowing steep number density to be correctly tracked out. The second advantage, and the most important, is that when the last grid boundary coincide exactly with v_{max} due to the grid movement, the new and the old interval boundaries completely coincide except for the first boundary ($v_1(t+\Delta t) = v_{\min}^*(t)$) (see Fig.(1-c)). This means that the old and the new population densities have the same intervals to occupy, resulting in an exact match between them ($\boldsymbol{N}(t+\Delta t) = \boldsymbol{N}(t)$) but only for the first interval ($N_1(t+\Delta t) = \gamma_1^{<0>} N_0(t)$). This suggests that the number densities could be updated only when $v_{M+1}^*(t+\Delta t)$ is less than or equal to $v_{\max} = v_M^*(t)$ to exclude any numerical inaccuracies due to population redistribution. However, if the equality is not exactly satisfied, the new pivots are set equal to the old ones since for sufficiently small

time step $v^*_{M+1}(t+\Delta t)$ is not greatly different from $v^*_M(t)$. At the same time, the pivot of the newly birthed interval is set at the middle since the width of this interval is very small thanks to the geometric grid. It follows then the stepwise redistribution of the discrete population density will result in an approximate optimal piecewise constant minimum droplet volume profile as a function of time. In fact this strategy is adopted in the following solution algorithm.

2.8 Solution algorithm

The solution algorithm using the optimal moving grid could be summarized as follows:

1- Specify σ, M, Δt, t_f and the initial condition $n(v,0)$.
2- Set $t_0 = 0$
3- Calculate the discrete initial conditions $\boldsymbol{N}(0)$ and $\boldsymbol{x}(0)$ using Eqs.(5) and (4) and $n(v,0)$.
4- Calculate the initial optimal droplet volume, $v^*_{\min}(0)$, using Eq.(19) and $n(v,0)$.
5- Calculate $\boldsymbol{N}(t_0+\Delta t)$ using Eq.(50) and $\boldsymbol{x}(t_0+\Delta t)$ using Eq.(36) sequentially in time.
6- Calculate $N_0(t_0+\Delta t)$ using Eq.(45)
7- Calculate the optimal droplet volume, $v^*_{\min}(t_0+\Delta t)$, using Eq.(29) and $v^*_{M+1}(t_0+\Delta t) = \sigma^M v^*_{\min.}(t_0+\Delta t)$.
8- If $v^*_{M+1}(t_0+\Delta t) \le v^*_M(t_0)$ then:
   - Calculate $v^*_i(t_0+\Delta t) = \sigma^{i-1} v^*_{\min.}(t_0+\Delta t)$ for $i=1, 2, \ldots M+1$
   - Calculate $x_i(t_0+\Delta t) = (v^*_i(t_0+\Delta t) + v^*_{i+1}(t_0+\Delta t))/2$, $i=0,1$ and $x_i(t_0+\Delta t) = x_{i-1}(t_0),\ i = 2,3,\ldots M$
   - Update the $\boldsymbol{\gamma}$ matrix using Eqs.(24) and (25).
   - Redistribute the number density according to Eq.(37).
   - Set $t_0 = \Delta t$, and $t_0 = t_0 + \Delta t$
9- Else,
   - Got to 10
10- Go to step 5 until $t_0 \ge t_f$.

Note that in step 8 if the equality is exactly satisfied, then $\boldsymbol{N}(t_0+\Delta t) = \boldsymbol{N}(t_0)$ except for the first interval where $N_1(t+\Delta t) = \gamma_1^{<0>} N_0(t)$.

2.9 Optimal fixed grid for droplet breakage in continuous systems

Unfortunately, the optimal moving grid technique developed in this work could not be applied in a straightforward manner to droplet breakage in continuous systems. The reason for this is the existence of two types of population densities in this type of systems. The first is the fixed droplet size distribution of the feed, $n^{feed}(v,t)$, and the second is that of droplets in the vessel itself $n(v,t)$. Since the droplet size distribution in the vessel moves continuously to the small size range with time, and the inlet feed size distribution is usually constant, the optimal maximum droplet size is fixed by that of the feed. Moreover, the optimal minimum droplet size in the vessel must be less than or equal to that of the feed. This leads to different grid widths for the droplet distribution in the vessel and in the feed where it becomes increasingly fine for the former and remains fixed for the latter. Mathematical inconsistencies are expected to occur due to integrating the terms involving $n(v,t)$ using a moving grid, while the feed term is integrated using the same grid at t=0. This is because the discrete number density, $N_i(t)$, is dependent on the size of the interval which is a function of time when a moving grid is used.

However, since droplet breakage in continuous systems is not expected to proceed to a very small size range as in the case of batch systems due to the fixed residence time of the vessel, an optimal fixed grid would be sufficient to minimize the total time-averaged FDE.

In the development of the moving grid technique for batch systems, we sought to minimize a total finite domain error based on the number density, FDE_0. However, there is still a finite domain error induced by excluding droplet volumes due to the failure of extending the domain of the internal coordinate to 0 and

∞. This is actually the total FDE based on the volume or the first moment of the distribution, and could be defined by an analogy to the zero FDE (Eq.(18)):

$$\varepsilon_1 = FDE_1^L(v_{\min},t) + FDE_1^U(v_{\min},t) \tag{51}$$

where FDE_1^L and FDE_1^U are defined based on the first moment of the distribution by equations similar to Eqs.(14) and (15).

Since droplet breakage in batch systems leads to a population density that is skewed to the left, small volume of droplets are lost due to the failure of extending the droplet volume to infinity. However, for continuous systems the zero and first moments of the feed do affect the zero and first moments of the distribution in the vessel. Hence, where the feed distribution is constant as stated above, appreciable errors would result due to the exclusion of numbers and volumes from the domain. This marked influence of the feed density function on the moments of the distribution lends itself to consider both finite domain errors based on the zero and first moments in seeking an optimal grid for discretization. In other words, we seek a grid that minimizes the time-averaged of the sum of the FDE based on both zero and first moments of the distribution. This total FDE is found by adding Eqs.(18) and (51) and the result could be related to the continuous zero and first moments of the distribution by analogy to Eq.(16):

$$M_0^d(v_{\min.}^*(0),t) + M_1^d(v_{\min.}^*(0),t) = M_0^c(t) + M_1^c(t) - [\varepsilon_0(v_{\min.}^*(0),t) + \varepsilon_1(v_{\min.}^*(0),t)] \tag{52}$$

Note that minimizing the total FDE (the term in square brackets) is equivalent to maximizing the sum of the left hand side at any instant of time since the continuous zero and first moments of the distribution are functions of time only. Since the proposed optimal grid is fixed as mentioned above, it is recommended to maximize the time-averaged of the left hand side of Eq.(52). The initial minimum droplet volume, $v_{\min.}^*(0)$, could be obtained from the initial condition or from the feed droplet size distribution. Since $v_{\min.}^*(0)$ is dependent on the interval width or σ for geometric grid, it is then ($M_0^d + M_1^d$) is dependent only on the interval width or geometric factor σ at specified *M*. Thus, an optimal fixed grid is sought by finding the interval width or geometric factor that maximizes the time-averaged of ($M_0^d + M_1^d$). In this work, we will restrict our attention to a geometric grid and thus, the problem at hand could be posed as a constrained one dimensional nonlinear optimization problem as follows:

$$\underset{\sigma}{\text{maximize}} \left(\frac{\int_0^{t_f} [M_0^d(\sigma,t) + M_1^d(\sigma,t)]}{t_f} dt \right) \tag{53}$$

subject to:

$$\boldsymbol{N}(t) = \boldsymbol{R}\boldsymbol{D}\boldsymbol{R}^{-1}[\boldsymbol{N}(0) + \boldsymbol{A}^{-1}\boldsymbol{N}^{feed}] - \boldsymbol{A}^{-1}\boldsymbol{N}^{feed},$$

$$\frac{\mathrm{d}\boldsymbol{x}}{\mathrm{d}t} = \boldsymbol{F}(\boldsymbol{x},\boldsymbol{N}),$$

$$M_0^d(\sigma,t) + M_1^d(\sigma,t) = \boldsymbol{N}^T(t)\boldsymbol{N}(t) + \boldsymbol{x}^T(t)\boldsymbol{N}(t),$$

$1 < \sigma \le \sigma_{\max.}$ for all $t \in [0, t_f]$.

where $\boldsymbol{N}^{feed}$ is an $M \times 1$ vector.

The above formulation minimizing the time-averaged total FDE has a distinctive feature by being dependent only on the chosen preserved properties of the distribution, which are already calculable from the solution of the DPBE themselves. The final time appearing in the system of Eqs.(53) is really the time

at which the continuous system approaches steady state, which is a finite value and normally could be taken about 5τ for linear systems (>99% of final steady state is achieved).

2.10 Numerical results

Although both the optimal moving and the fixed grids constructed in this work for minimizing the total FDE are general and applicable for any set of breakage functions, it is desirable to check thoroughly the numerical results by comparison with analytical solutions whenever it is possible. Two functional forms for both the daughter droplets distribution, $\beta(v \mid v')$, and breakage rate, $\Gamma(v)$, are used:

1- Uniform daughter droplet distribution, where it assumes an equal chance to form a daughter droplet of any smaller size when a mother droplet breaks up, and hence it is independent of daughter droplet volume (cases 1 and 2).
2- Parabolic daughter droplet distribution, where it assumes a more or less likely chance to form two daughter droplets of different sizes upon breakage of mother droplet (case 3).

The breakage rate function is assumed to have a general form:

$$\Gamma(v) = kv^m \tag{54}$$

where k and m are positive parameters.
For the sake of comparison, available analytical solutions for droplet breakage in batch systems are presented in Table 2. Moreover, expressions are derived for the optimal minimum droplet volume, the continuous zero and first moments of the analytical distribution, and the total finite domain error. These are presented in Tables 3 and 4.
For the solution of droplet breakage in continuous systems, the problem of finding general analytical solutions becomes more difficult. However, two specific cases are presented in this work depending on the feed droplet distribution. In the first case McGrady and Ziff (1988) solved analytically the continuous PBE where a monodisperse feed droplet distribution is assumed. In the second case Nicmanis and Hounslow (1998) presented the steady state solution of the continuous PBE with an exponential feed droplet distribution. However, for the dynamic solution, we extend the method of moments presented in the work of Vigil and Ziff (1989) for batch systems to continuous systems. Unfortunately, only the analytical zero and first moment of the distribution are obtained. In the following two sections, we first compare the numerical and the available analytical solutions for droplet breakage in batch systems, and finally the comparison is made for the continuous ones.

2.10.1 Droplet breakage in batch systems

In Table 2 we present three case studies to illustrate how the optimal moving grid works for the solution of droplet breakage in batch systems. In the first two cases a uniform daughter droplet distribution is assumed, while the exponent m in Eq.(54) is taken as 1 and 2 respectively. The initial droplet size distribution is exponential and the two cases along with their analytical solutions are shown in Table 2. The third case represents a more general parabolic daughter droplet distribution, however the analytical solution, to the best of the authors' knowledge, is not available. Nevertheless, the solutions using the fixed and optimal moving grid techniques will be compared. The comparison between the analytical and numerical results will be made on the bases of average number densities due to the sensitivity of the discrete number density to the interval width. Consequently, the average numerical and analytical discrete number densities are defined as:

$$\overline{N}_i^{num.} = \frac{N_i^{num.}(t)}{\Delta v_i(t)} \tag{55a}$$

$$\overline{N}_i^{anal.} = \frac{N_i^{anal.}(t)}{\Delta v_i(t)} \tag{55b}$$

Note that the interval width is a function of time for an optimal moving grid and is time-invariant for the fixed one. Using the zero and first moments of the distribution the mean droplet volume is compared with the analytical solution using the following relation:

$$\bar{v}(t) = \frac{M_1^d(t)}{M_0^d(t)} \tag{56}$$

Moreover, since wide differences in the average number density values are encountered as breakage progresses with time, a semi-log plot will be suitable for comparison. In this work the number rather than the volume density is used to avoid damping the numerical errors, if any, where it actually occurs when a small droplet volume multiplies the number density particularly in the small size range. In all the case studies that follow arbitrary time units are used. Furthermore, all the simulation runs are carried out using the MATLAB software.

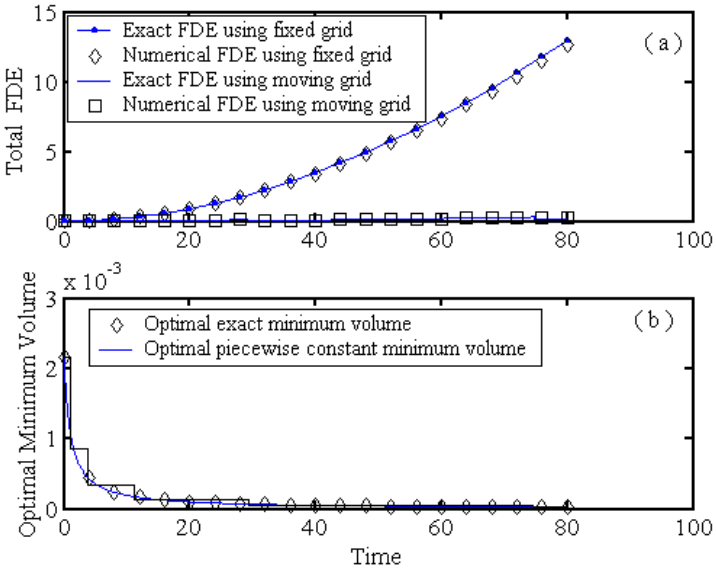

Fig.(2): a-The effect of the optimal grid movement on the total finite domain error. b- The approximate and exact optimal minimum droplet volume profiles for droplet breakage in a batch vessel using a geometric grid with factor σ = 2.5, M = 10, binary breakage, $\Gamma=v$, $\beta(v|v')=1/v'$, and exponential initial condition.

2.10.1.1 Case 1: Breakage with uniform daughter droplet distribution and $\Gamma(v) = v$

In this case (see Table 2) the simulation is carried out over a relatively long period of time, t_f=80, to illustrate the steepness of the number density due to long time breakage. The solution algorithm is implemented for a number of intervals, M=10, and σ=2.5 to stress the use of a desirable relatively coarse geometric grid. We start this case by comparing the exact and numerical FDE as well as the optimal minimum droplet volumes. Fig.(2-a) shows these results, and it can be seen an excellent agreement between the numerical and exact FDE is obtained. As expected the optimal fixed FDE increases with time due to the failure to account for the increase in number density in the small size range as droplet breakage proceeds. This is actually equivalent to a loss of number of droplets from the system. To compensate for this, we let the grid move in an optimal manner as shown in Fig.(2-b), where the exact minimum droplet volume (see Table 3) is depicted along with that predicted using the optimal moving grid technique. First the agreement between the optimal piecewise minimum droplet volume and the exact one is also good even when the grid moves so fast. Actually, the approximate profile is expected to approach the exact one as the number of pivots increases. The exact solution is obtained by inserting the analytical solution from Table 2 into Eq.(19). Second the great influence of the optimal grid movement on the reduction of the total FDE is obvious when compared to the fixed grid (Fig.(2-a)). The exact solution is obtained by combining the analytical solution from Table 2 with Eq.(18).
Fig.(3) shows the exact and numerical average number densities at the final time of simulation where, excellent agreement is perceptible. Also, one could see how the optimal moving grid leaves the

approximately empty intervals (large sizes) to accommodate the increasing number densities in the small size range as expected.

Fig.(4) depicts the sum of square errors (SSE), based on the difference between the exact and numerical solutions, as a function of time at different levels of discretization. The fixed and approximately optimal moving grids are compared such that the total FDE is negligible by extending the minimum and maximum droplet volumes to sufficiently small and large values (see Table 1). First grids of 10 pivots are used where it is clear that the fixed grid could cover the same domain spanned by the moving one only by having a geometric factor $\sigma = 6.28$.

This relatively large geometric factor increases the error of integration with respect to v due to the large intervals width and hence the SSE increases as the distribution becomes sharp (after long breakage time). If the geometric factor is to be kept constant at $\sigma = 2.5$ for the fixed as well as the moving grids, then we need approximately 20 pivots for the fixed grid to have approximately the same SSE as the moving one.

This will increase the computational time by about 40% when compared to case a (only 10 pivots) as is clear by referring to Table 1. This increase in the computational time is clearly due to the increase in the size of the system of ordinary differential equations (from 10 to 20). Similarly, if 15 pivots are used for both the fixed and moving grids the same trend is observed with the reduction of the SSE due to the small width of the intervals ($\sigma = 2$), and hence the integration error with respect to v.

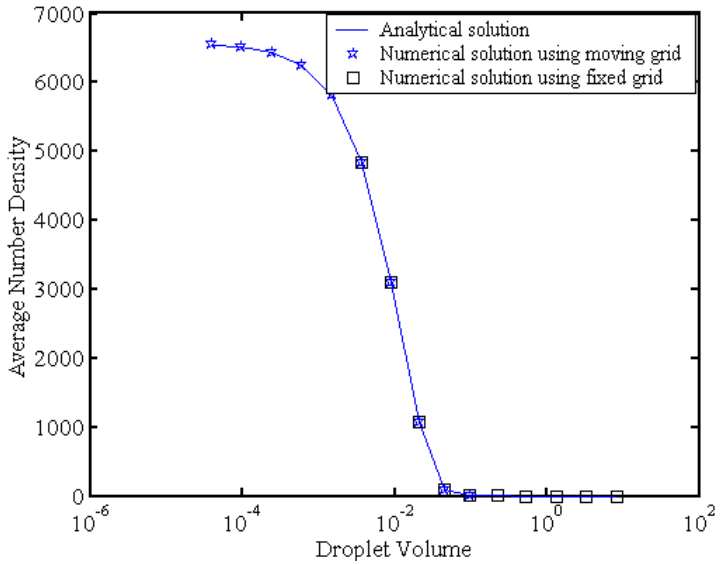

Fig.(3): The effect of the optimal grid movement on the average number density for droplet breakage in a batch vessel using a geometric grid with factor $\sigma = 2.5$, $M = 10$, binary breakage, $\Gamma = v$, $\beta(v|v') = 1/v'$, exponential initial condition, and $t = 80$.

In this case the fixed grid requires approximately 32 pivots to cover the same domain spanned by the moving grid ($M = 15$) with relative increase in the CPU time about 100% (see Table 1). However, by referring to Table 1, the relative increase in the computational time in the case of the moving grid technique due to the redistribution algorithm is only about 3.6% in both cases. This clearly shows the effectiveness of the approximate optimal moving grid technique particularly for long time breakage.

Fig.(5) shows the optimal moving and fixed grids and their corresponding pivots at the end of the simulation time. It is clear that the positions of the moving and fixed pivots are approximately the same for the case of moving grids. This is because as the grid moves it becomes finer, and hence the moving pivots approaches the fixed ones, which agrees with the condition implied by Eq. (49). However, in the case of the fixed grids with the same number of pivots, the fixed pivots are completely different from the moving ones particularly in the small size range due to the fixed width of the intervals as droplet breakage proceeds. This suggests that the solution of the PBE using the fixed pivot technique could be improved by using the present optimal moving grid.

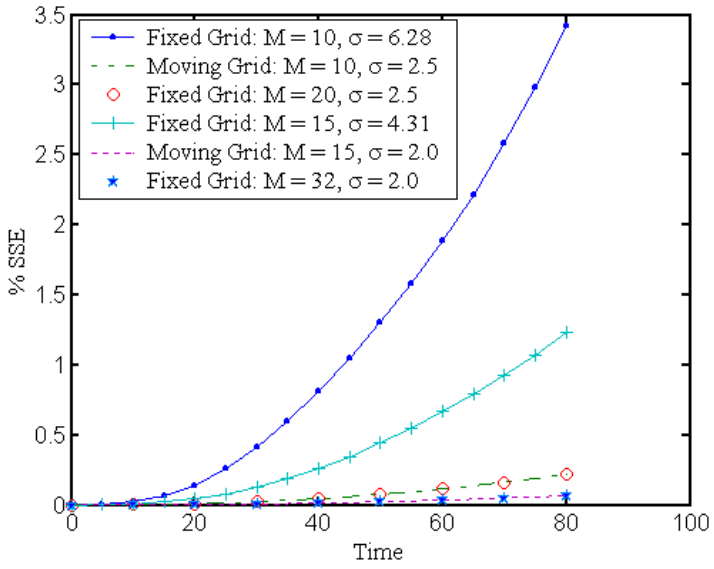

Fig.(4): The effect of the approximate optimal and fixed grids on the SSE using different levels of discretization for droplet breakage in a batch vessel with binary breakage, $\Gamma=v$, $\beta(v|v')=1/v'$, and exponential initial condition.

2.10.1.2 Case 2: Breakage with uniform daughter droplet distribution and $\Gamma(v) = v^2$

In this case, the rate of droplet breakage is proportional to the square of its volume. A close look at the time constants given by $\left|\lambda_i^b\right|^{-1}$ (i=1, 2,...M) indicates that droplets with volume less than one will show slower dynamics when compared with that having the same volume in case 1. On the contrary, droplets having volume greater than one will show faster dynamics when compared with that in case 1. Since the number density becomes skewed to the left as droplet breakage proceeds, slow dynamics will be dominant at long times. Due to this we have increased the simulation time to t=100.

Table 1: The CPU time requirements of the moving and fixed grids for droplet breakage in a batch vessel.

Case	$V_{min.}$	V_{M+1}	M	σ	% Increase in the CPU time relative to case A	% Time averaged relative error in:	
						M_0	$\bar{V}$
A1: Fixed Grid	2.16×10^{-7}	20.6	10	6.3	———	0.3000	0.0000
B1: Moving Grid	$v^*_{min.}(t)$	$v^*_{M+1}(t)$	10	2.5	3.59*	0.0976	0.0000
C1: Fixed Grid	2.16×10^{-7}	20.6	20	2.5	39.88*	0.0976	0.0000
A2: Fixed Grid	5.92×10^{-9}	19.4	15	4.3	———	0.1900	0.0000
B2: Moving Grid	$v^*_{min.}(t)$	$v^*_{M+1}(t)$	15	2.0	3.59*	0.0614	0.0000
C2: Fixed Grid	5.92×10^{-9}	19.4	32	2.0	99.35*	0.0604	0.0000

* The CPU times are estimated under MATLAB 6.1 environment using a PC Pentium III 750 MHz processor.

Fig.(6-a) shows how the optimal moving grid keeps the total FDE almost constant during the droplet breakage time. Moreover, the magnitude of the total FDE is considerably less than that in case 1 because of the non sharply increasing number density with time at the small size range (see Fig.(7)). As in case 1,

it is clear from Fig.(6-b) that the optimal moving grid technique produces an optimal piecewise constant minimum droplet volume that is in a good agreement with the exact one given in Table 3.

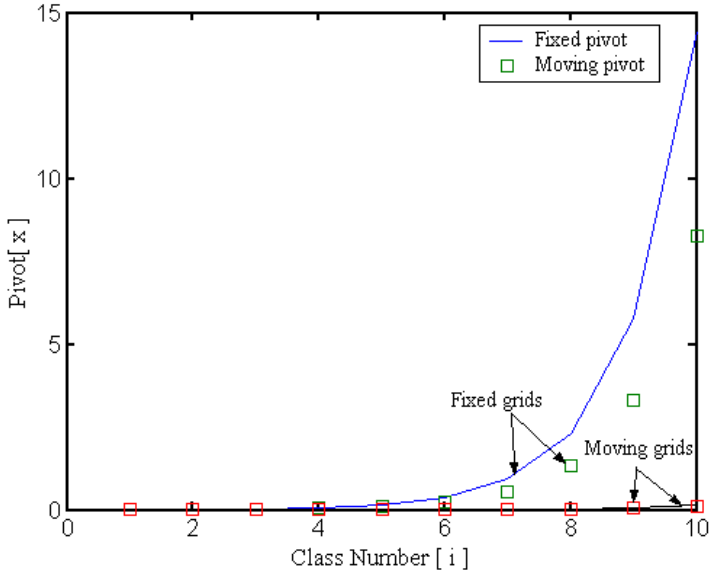

Fig.(5): The effect of the approximate optimal and fixed grids on the fixed and moving pivots at t=80 using a geometric grid with factor σ = 2.5, M = 10 for droplet breakage in a batch vessel with binary breakage, $\Gamma=v$, $\beta(v|v')=1/v'$, and exponential initial condition.

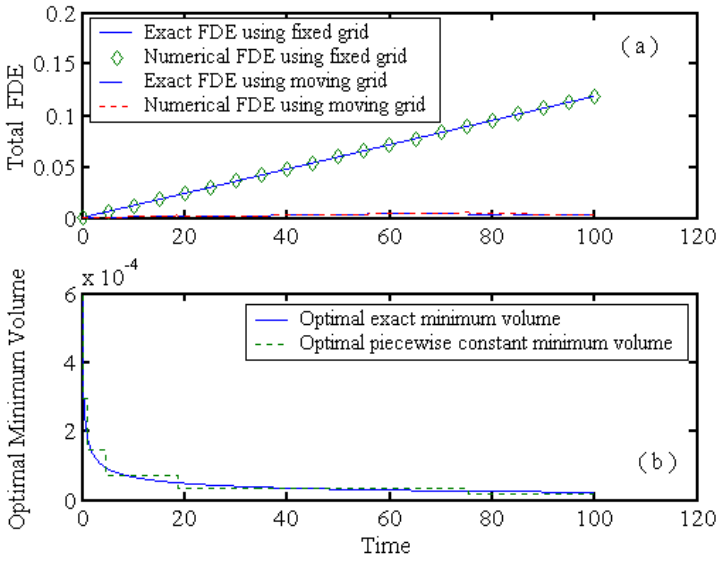

Fig.(6): a-The effect of the optimal grid movement on the total finite domain error. b- The approximate and exact optimal minimum droplet volume profiles for droplet breakage in a batch vessel using a geometric grid with factor σ = 2, M = 15, binary breakage, $\Gamma=v^2$, $\beta(v|v')=1/v'$, and exponential initial condition.

Fig.(7) shows the expected average number density for the analytical (see Table 2) and numerical solutions at the end of the simulation time. Due to the slow and fast dynamics in the small and large size ranges respectively; a sharp transition in the number density between these size ranges is encountered. Again it is evident how the approximate optimal moving grid leaves the almost empty intervals at the large size range to occupy the newly birthed population in the small size range.

Fig.(8) shows the behavior of the SSE as a function of time for this case using fixed and approximate optimal moving grids. The SSE using a fixed grid could only be reduced to that of the moving one (M=15) only by increasing the number of pivots to 25 with the same geometric grid factor σ = 2.0. This is will be at the expense of the computational time as is mentioned in case 1. In this case the value of the SSE is greater than that of case 1 due to the increasing sharpness of the number density at the transition region from the large to the small size range.

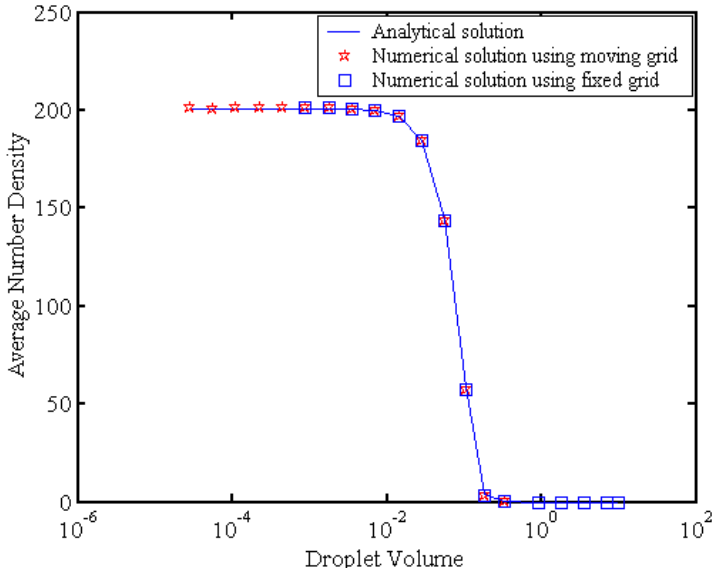

Fig.(7): The effect of the optimal grid movement on the average number density for droplet breakage in a batch vessel using a geometric grid with factor σ = 2, M = 15, binary breakage, $\Gamma=v^2$, $\beta(v|v')=1/v'$, and exponential initial condition.

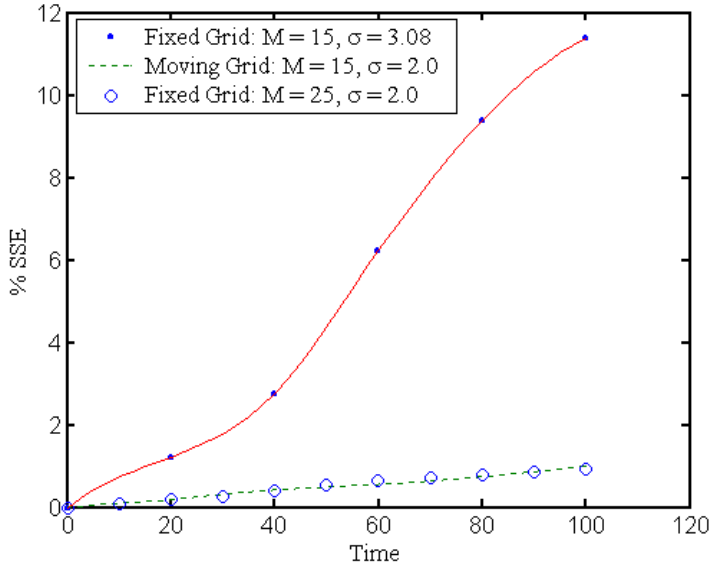

Fig.(8): The effect of the approximate optimal and fixed grids on the SSE using different levels of discretization for droplet breakage in a batch vessel with binary breakage, $\Gamma=v^2$, $\beta(v|v')=1/v'$, and exponential initial condition.

2.10.1.3 Case 3: Breakage with parabolic daughter droplet distribution and $\Gamma(v) = v$

In this case, where parabolic daughter droplet distribution is assumed (Hill & Ng, 1995), we have added one different aspect being $\beta(v \mid v')$ is no longer independent of the daughter droplet volume. Since the analytical solution is not available, comparisons are made between the fixed and optimal moving grid techniques. Fig.(9-a) shows how the optimal moving grid reduces the total FDE and keeps it almost constant. The optimal piecewise constant minimum droplet volume is shown in Fig.(9-b) as is expected. The average number densities for both fixed and moving grids are depicted in Fig.(10) at the final simulation time. It is evident how the optimal moving grid follows the sharp part of the distribution while leaving the almost empty size intervals. All the desirable advantages achieved in cases 1 and 2 are retained in this case, which consolidate one's faith in the optimal moving grid technique.

Table 2: Available analytical solution for droplet breakage in batch systems.

Case	$\beta(v \mid v')$	$\Gamma(v)$	$n(v,0)$	Analytical solution, $n(v,t)$	Reference
1	$\frac{2}{v'}$	v	e^{-v}	$(1+t)^2 e^{-v(1+t)}$	(Ziff and McGrady, 1985)
2	$\frac{2}{v'}$	v^2	e^{-v}	$[1+2t(1+v)]e^{-(tv^2+v)}$	Ziff, and McGrady, (1985)
3	$\frac{24(v^2 - vv') + 6v'^2}{v'^3}$	v	e^{-v}	Not available	(Hill and Ng, 1995)

2.10.2 Droplet breakage in continuous systems

In this section optimal geometric factors (and hence optimal grids) are found for a given number of intervals by solving the constrained nonlinear optimization problem given by Eq. (53). The breakage functions considered are linear breakage rate (k=1, m=1) and uniform daughter droplet distribution for the two cases studied where zero initial conditions are assumed in the vessel. All the numerical simulations are conducted using MATLAB software.

Table 3: Analytical optimal minimum droplet volume, continuous zero and first moments, mean droplet volume, and the total finite domain error for droplet breakage in batch systems

Case	$v^*_{\min.}(t)$	$M_0^c(t)$	$M_1^c(t)$	$\bar{v}^c(t)$	$\varepsilon_0(t)$
1	$\frac{(M-1)\ln(\sigma)}{(1+t)(\sigma^{M-1}-1)}$	$1+t$	1	$\frac{1}{1+t}$	$(1+t)\times$ $\left(1+e^{-(1+t)v_{\max.}} - e^{-(1+t)v_{\min..}}\right)$
2	$\frac{1+2t(1+v^*_{\min.})}{1+2t(1+v^*_{\max.})} -$ $\sigma^{M-1}\frac{e^{-(v^*_{\max.}+v^{*\,2}_{\max.}t)}}{e^{-(v^*_{\min..}+v^{*\,2}_{\min..}t)}} = 0$	$1+\sqrt{\pi t}\,e^{(\frac{1}{4t})}\times$ $\left[1-erf\left(\frac{1}{2\sqrt{t}}\right)\right]$	1	$\frac{1}{M_0^c(t)}$	$(1+e^{-(v_{\max.}+v^2_{\max}t)})+$ $\sqrt{\pi}e^{(\frac{1}{4t})}\times\left[\begin{array}{l}1+erf\left(\frac{2tv_{\min.}+1}{2\sqrt{t}}\right)\\ -erf\left(\frac{2tv_{\max.}+1}{2\sqrt{t}}\right)-erf\left(\frac{1}{2\sqrt{t}}\right)\end{array}\right]$
3	N.a.*	N.a.	1	N.a.	N.a.

* Not available.

2.10.2.1 Case 1: Exponential feed droplet distribution

In this case the initial condition is assumed zero and the feed distribution is exponential. Table 4 shows the derived analytical solutions for the zero and first moments of the distribution, as well as the mean droplet volume for this special case. The optimization problem (Eq. (53)) is solved using three different levels of discretization (M=15, 20, 25) to see their effect on the optimal geometric factor σ. The simulation time is chosen large enough (15τ) to insure that true final steady state is reached.

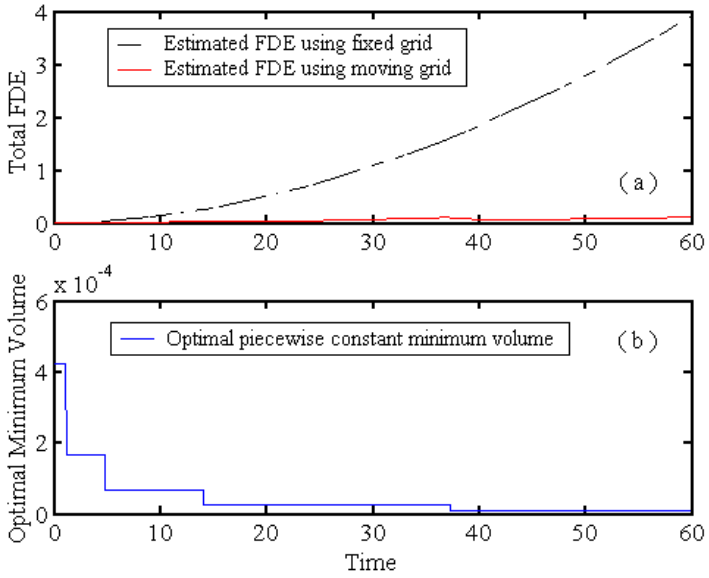

Fig.(9): a-The effect of the optimal grid movement on the total finite domain error. b- The approximate optimal minimum droplet volume profiles for droplet breakage in a batch vessel using a geometric grid with factor σ = 2.5, M = 12, binary breakage, $\Gamma=v$, $\beta(v|v')$=*parabolic,* and exponential initial condition.

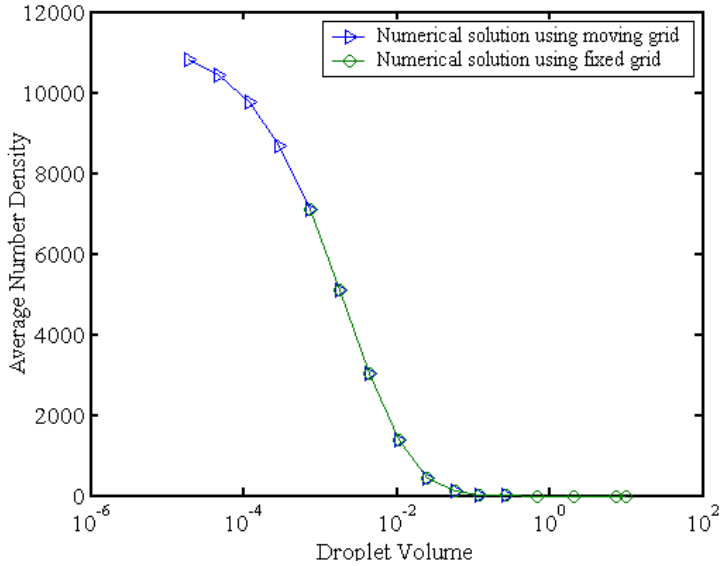

Fig.(10): The effect of the optimal grid movement on the average number density for droplet breakage in a batch vessel using a geometric grid with factor σ = 2.5, M = 12, binary breakage, $\Gamma=v$, $\beta(v|v')$=*parabolic,* and exponential initial condition.

The initial optimal fixed grid used in the simulation is constructed using the feed droplet distribution and the optimal condition given by Eq. (19). The resulting geometric grid has the property of being expanding in both directions as σ increases to cover the lower and upper size ranges. This type of grid results in a monotone increasing function represented by the sum: ($M_0^d + M_1^d$), since the number and volume densities increases monotonically as a result of simultaneous decrease and increase of v_{min} and v_{max} respectively. So, the optimal values of σ are the minimum ones which make the time-averaged ($M_0^d + M_1^d$) constants to a prescribed accuracy.

The numerical results are shown in Figs.(11) and (12). Fig.(11-a) shows the total zero and first moments of the distribution as function of the geometric factor at steady state. This Figure shows three distinctive features: the first is the sharp decrease in the steady state sum of the moments ($M_0^d + M_1^d$) when the geometric factor is reduced below the optimal value, which is indeed equivalent to increasing the minimum droplet volume above the optimal one. This is equivalent to a sharp increase in the total FDE as it is evident from Eq. (52). This increase in the FDE is caused by the sharp increase in $v^*_{\min.}(0)$ as a result of decreasing σ according to Eq. (19).

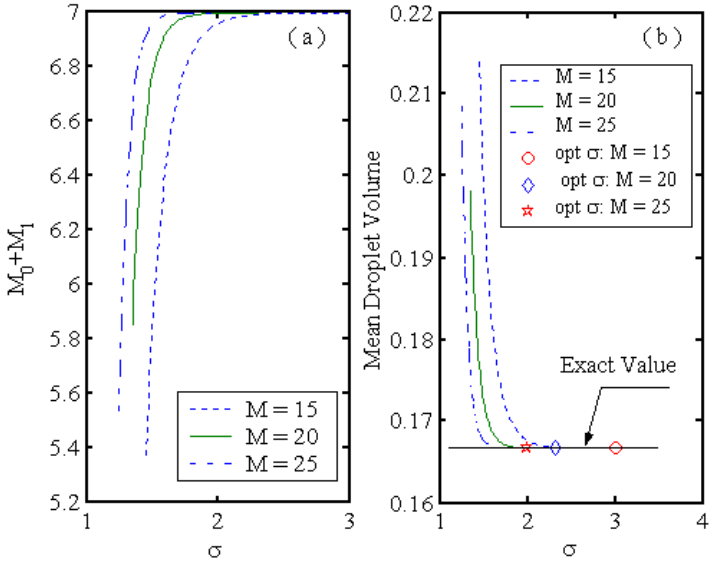

Fig.(11): Effect of the optimal geometric grid factor on: a-The steady state sum of zero and first moments of the distribution. b- The mean droplet volume for droplet breakage in a continuous vessel with $\Gamma=v$ and $\beta(v|v')=1/v'$, binary breakage, $\tau = 5$, and exponential feed distribution.

The second feature is that the optimal geometric factor decreases as the number of intervals increases (Fig.(11-b)), which is expected since small geometric factor requires large number of intervals to cover the required discretized domain. The third feature is that all the steady state values of ($M_0^d + M_1^d$) are monotonically increasing where they become approximately identical and are slowly varying as the geometric factor is increased. This is again is attributed to the behavior of $v^*_{\min.}(0)$, where it decreases sharply as σ increases resulting in negligible lower and upper residuals.

Fig.(11-b) shows the significant effect of the choice of the geometric factor on the mean droplet volume of the distribution. It is clear how the optimal values of σ result in an excellent predictions of the mean droplet volume. It is also evident that a small error in choosing σ below the optimal value will lead to significant error in the mean droplet volume due to the significant loss of droplet volumes and numbers from both boundaries.

Fig.(12) shows the average number density at steady state as predicted using three fixed grids with optimal geometric factors. The results show how the numerical solution is very close to the exact one at steady state at the three levels of discretization using optimal geometric grid factors. Fig.(13) shows an excellent agreement between the analytical and numerical mean droplet volumes even in the presence of the jump occurring at t=0 due to the zero initial condition. Despite the small error involved in the

predicted number densities at low level of discretization (M=15), the numerical mean droplet volume is still in good agreement with the analytical one. This is natural since the present discretization technique preserves both total number and volume of the distribution.

2.10.2.2 Case 2: Monodisperse feed droplet distribution

In this case zero initial and monodisperse feed droplet distributions are used. The monodisperse feed distribution is mathematically represented by the Dirac delta function:

$$n^{feed}(v) = \delta(v - x_f) \tag{57}$$

McGrady and Ziff (1988) presented the analytical solution of a slight modified form of Eq. (1) for this case of droplet breakage in a continuous vessel. Table 4 shows the derived mean droplet volume, zero and first moments of the distribution.

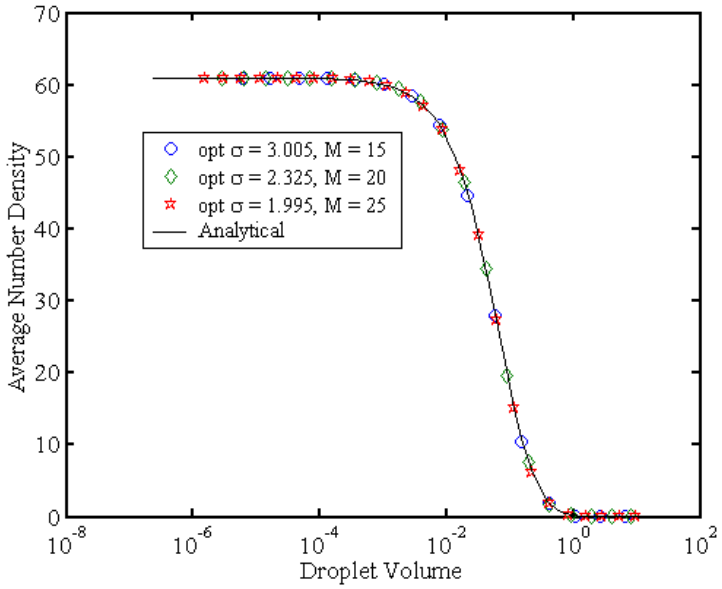

Fig.(12): Effect of the optimal geometric grid factor on the steady state number density for droplet breakage in a continuous vessel with Γ=v and $\beta(v|v')$=1/v', binary breakage, τ = 5, and exponential feed distribution.

The discontinuous nature of the Dirac delta function imposes another difficulty when Eq. (57) is discretized. This function is approximated using the rectangular pulse function of unit area (Rice and Do, 1995; David et al., 1996):

$$N^{feed}(v - x_i) = \begin{cases} \dfrac{1}{\Delta v_f}, & v_f \le v < v_{f+1} \\ 0, & i \ne f \end{cases} \tag{58}$$

where f is the index of the interval containing the feed droplet volume, x_f.
However, still another difficulty is imposed by Eq. (58) since the geometric grid which, is relatively coarse in the upper size range, makes the approximation above inaccurate. Introducing a linear grid to just encompass the interval containing the feed droplet size, x_f, alleviates this problem. The accuracy of the approximation is improved by making the linear grid as fine as required.
The system of Eqs. (53) is solved with (x_f =2.0 as the maximum droplet volume) using three different levels of discretization to see how they affect the optimal gird geometric factor σ.

Table 4: Mean droplet volume, zero and first moments of the distribution for droplet breakage in continuous systems.

Case	$\beta(v \mid v')$	$\Gamma(v)$	$n^{feed}(v)$	$\bar{v}\ (t)$	$M_0(t)$	$M_1(t)$
1	$\frac{2}{v'}$	kv	e^{-v}	$\frac{M_1(t)}{M_0(t)}$	$c_2\tau\left(1-e^{-\frac{t}{\tau}}\right)+\left(M_0(0)+c_1 t\right)e^{-\frac{t}{\tau}}$ $c_1 = k\left(M_1(0)-M_1^{feed}\right)$ $c_2\tau = M_0^{feed}+kM_1^{feed}$	$M_1^{feed}+$ $\left(M_1(0)-M_1^{feed}\right)e^{-\frac{t}{\tau}}$
2	$\frac{2}{v'}$	kv	$\delta(v-x_f)$	$\frac{M_1(t)}{M_0(t)}$	$c_2\tau\left(1-e^{-\frac{t}{\tau}}\right)+\left(M_0(0)+c_1 t\right)e^{-\frac{t}{\tau}}$ $c_1 = k\left(M_1(0)-\tau M_1^{feed}\right)$ $c_2 = M_0^{feed}+k\tau M_1^{feed}$	$\tau M_1^{feed}+\left(M_1(0)-\tau M_1^{feed}\right)e^{-\frac{t}{\tau}}$

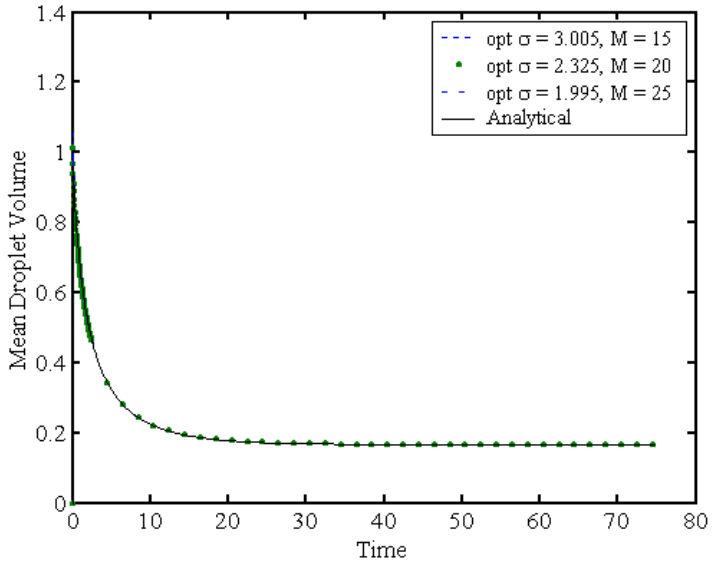

Fig.(13): Effect of the optimal geometric grid factor on the mean droplet volume for droplet breakage in a continuous vessel with $\Gamma=v$ and $\beta(v|v')=1/v'$, binary breakage, $\tau = 5$, and exponential feed distribution.

The simulation results are shown in Figs.(14), (15), and (16). In Fig.(14-a) the steady state ($M_0^d + M_1^d$) are plotted against the grid geometric factor, where as in case 1, sharp increase in the total FDE results for those slightly below the optimal values. However, it is clear that above certain values of σ the steady state ($M_0^d + M_1^d$) becomes constant for the three levels of discretization used. This simply means that the upper residual of the distribution has a constant zero value, and hence the lower residual controls the total FDE. This result is not surprising, since the upper value of the droplet volume is bounded by the size of the monodisperse feed, x_f. Since the number density vanishes for all $v>x_f$, it follows then that the upper residual of the distribution is always zero provided that $v_{max} \geq x_f$. In this case, the optimal values of σ are the minimum ones which make the time-averaged ($M_0^d + M_1^d$) constants to a prescribed accuracy and are shown in Fig.(14-b). This case actually isolates the effect of the lower distribution residual and shows clearly that it is the dominant part contributing to the total FDE as long as pure droplet breakage is considered. As in case 1, the sensitivity of the total FDE to the changes of σ and its subsequence effect on the steady state mean droplet volume is evident from Fig.(14-b).

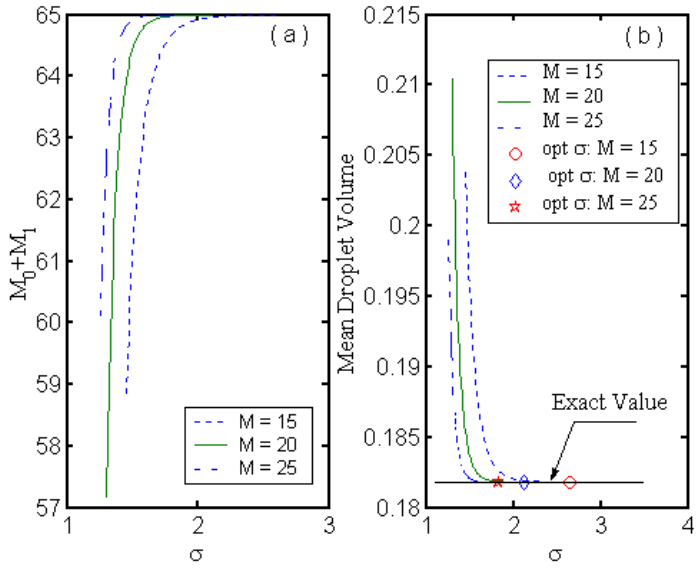

Fig.(14): Effect of the optimal geometric grid factor on: a- The steady state sum of zero and first moments of the distribution. b- The mean droplet volume for droplet breakage in a continuous vessel with $\Gamma=v$, $\beta(v|v')=1/v'$, binary breakage, $\tau = 5$, and monodispersed feed distribution.

This means that the moving pivot technique converges at a rate that is inversely proportional to the square of the number of pivots ($\propto 1/M^2$). The magnitude of the *SysErr* for the case of the monodisperse feed distribution is smaller than that of the exponential one due to the effect of the total FDE. In the case of the monodisperse feed, $v_{max} = x_f$ and hence the upper residual is zero resulting in a bounded domain from the upper size range. This bounded domain makes the size of the intervals smaller than the case of the unbounded one for the exponential feed distribution and hence reduces the *SysErr*. This is actually reflected by comparing the values of the optimal geometric grid factors for both cases (σ = 2.645 for monodisperse and σ = 3.005 for exponential feed distributions when M = 15).

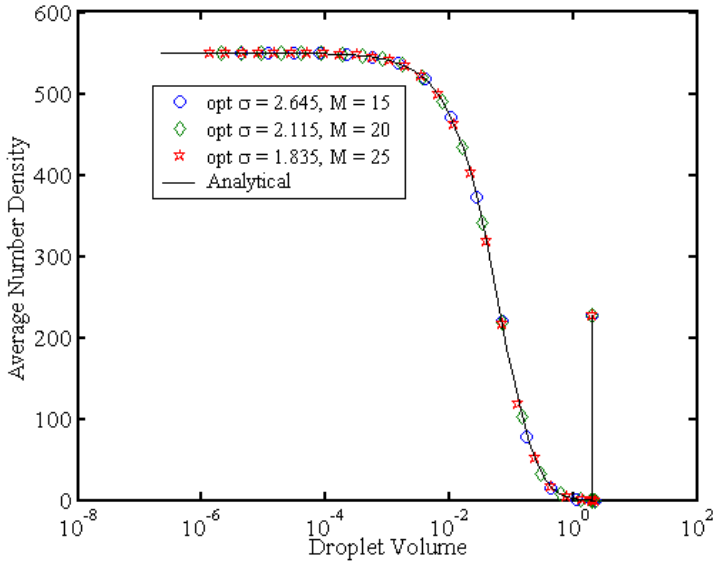

Fig.(15): Effect of the optimal geometric grid factor on the steady state number density for droplet breakage in a continuous vessel with $\Gamma=v$ and $\beta(v|v')=1/v'$, binary breakage, $\tau = 5$, and monodispersed feed distribution.

Fig.(15) shows the average number density at steady state as it is predicted along with the analytical solution using the optimal geometric grid factors shown in Fig.(14-b). It is obvious that the agreement between the analytical and the numerical solutions is excellent. It is also worthwhile to see how the discontinuity in the number density is correctly predicted by using a fine linear grid around it. Fig.(16) shows how the predicted mean droplet volume is very close to the analytical one during the simulation time at different optimal geometric grid factors. To get more insight into the convergence characteristics of the numerical solutions presented in Figs.(12), (13), (15), and (16), it is helpful to define the systematic error (*SysErr*) as the absolute difference between the exact and the numerical mean droplet volumes:

$$SysErr = \left| \overline{v}_{exac.} - \overline{v}_{num.} \right| \tag{59}$$

This is in fact is a suitable choice since it involves both the conserved total number and volume of the droplet distribution. Fig.(17) shows the *SysErr* for both cases plotted on a log-log scale versus the number of pivots (intervals). The numerical solutions for both cases (monodisperse and exponential feed distributions) converge at the same rate due to the similar form of the distributions as it is evident from Figs. 12 and 15 where the slopes of both lines are equal to 2.2.

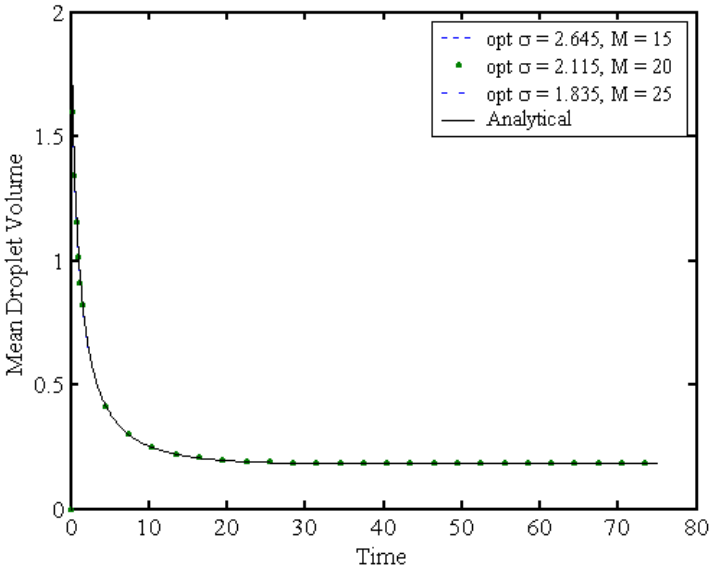

Fig.(16): Effect of the optimal geometric grid factor on the mean droplet volume for droplet breakage in a continuous vessel with $\Gamma=v$ and $\beta(v|v')=1/v'$, binary breakage, τ = 5, and monodispersed feed distribution.

2.11 Conclusions

- The moving pivot technique proposed by Kumar and Ramkrishna (1996b) is extended to continuous flow systems.
- The slow movement of the pivots for sufficiently fine grid makes possible the sequential solution of the number density and the pivot equations in time.
- Ordinary differential equations are derived to estimate the lower and upper residuals of the droplet distribution, which show excellent agreement with the analytical solutions studied in this work.
- An approximate optimal moving grid technique is developed for droplet breakage in batch systems where the sharply increasing number density is successfully tracked out. The redistribution algorithm, on which this technique is based, is consistent with DPBEs by preserving any two integral properties of the distribution.
- An optimal fixed grid that minimizes the time-averaged total finite domain error is also developed for continuous droplet breakage. This optimal grid represents a systematic

approach for the determination of the minimum and maximum droplet volumes instead of the trial and error procedures that are usually used. The numerical results show that the lower residual of the distribution is dominant and makes the total finite domain error sensitive to small changes in the grid geometric factor.

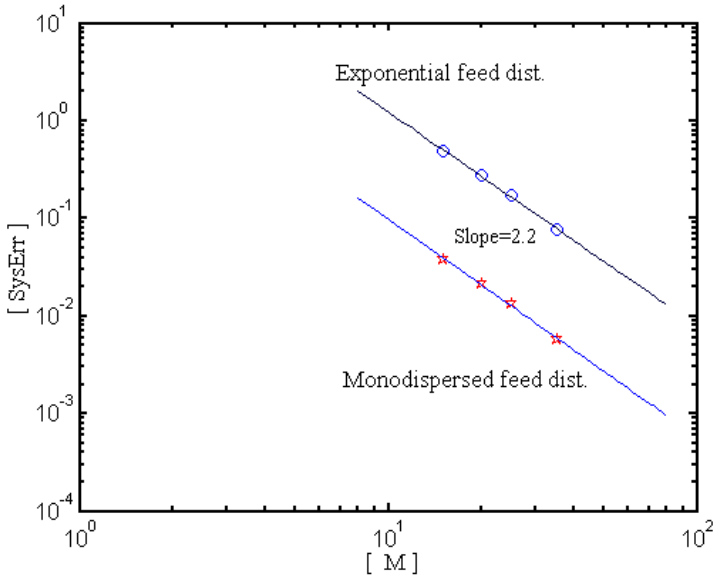

Fig.(17): The convergence characteristics of the moving pivot technique for droplet breakage in a continuous vessel with $\Gamma=v$ and $\beta(v|v')=1/v'$, binary breakage, and $\tau = 5$.

Nomenclature

$\boldsymbol{A}$	matrix for the number density equations as defined by Eq.(40)
$\boldsymbol{D}$	diagonal matrix whose elements are given by: $e^{\lambda_i^b t}$
FDE_0^L	lower residual based on the zero moment of the distribution as defined by Eq.(14)
FDE_1^L	lower residual based on the 1st moment of the distribution.
FDE_0^U	upper residual based on the zero moment of the distribution as defined by Eq.(15)
FDE_1^U	upper residual based on the 1st moment of the distribution.
$\boldsymbol{F}$	matrix for the pivot equations as defined by Eq.(41)
I_i	ith interval: $I_i=[v_i, v_{i+1})$
M	total number of intervals used in droplet volume discretization
M_0^c	zero moment of the continuous distribution
M_0^d	zero moment of the discrete distribution
M_1^c	first moment of the continuous distribution
M_1^d	first moment of the discrete distribution
$\boldsymbol{N(t)}$	vector whose ith component is the total number of droplets in the ith interval, at time t
$N_i(t)$	total number of droplets in the ith interval, at time t
N^{feed}	vector whose ith component is the total number of droplets in the ith interval for the feed
$\overline{N}_i(t)$	average discrete number density in the ith interval at time t.
$\overline{N}_i^{anal.}$	average discrete analytical number density in the ith interval defined by Eq.(55a)
$\overline{N}_i^{num.}$	average discrete numerical number density in the ith interval defined by Eq.(55b)
$n(v,t)dv$	number of droplets in size range v to $v+dv$, at time t
$\boldsymbol{R}$	matrix whose columns are the eigenvectors of the matrix $\boldsymbol{A}$
v, v'	droplet volumes
$v_{min.}, v_{max.}$	minimum and maximum droplet volumes
$v^*_{\min}, v^*_{\max.}$	optimal minimum and maximum droplet volumes
$\overline{v}$	mean droplet volume
$\dot{v}$	droplet growth rate
$x_i(t)$	characteristic volume of the droplet population in the ith interval as defined by Eq.(4)
SSE	sum of square of errors
t	time
t_0	initial simulation time
t_f	final simulation time

Greek Symbols

$\beta(v \mid v')dv$	fractional number of droplets formed in the size range v to $v+dv$ formed upon breakage of droplet of volume v'
$\Gamma(v)$	number of droplets in the size range v to $v+dv$ disappearing per unit time by breakage
$\gamma_i^{<i>}$	fraction of droplets at the pivot $x_i(t)$ that is assigned to the pivot $x_i\ (t+\Delta t)$ in the ith interval
$\Delta v(t)$	width of the ith interval, v_{i+1}-v_i, at time t
δ	Dirac delta function
ε_0(t)	total finite domain error based on zero moment of the distribution as defined by Eq.(18) (error of discretization)
ε_1(t)	total finite domain error based on 1st moment of the distribution as defined by Eq.(51) (error of discretization)
η_i	the ith eigenvalue of the matrix $\boldsymbol{F}$ as defined by Eq.(11)

λ_i^b	the *i*th eigenvalue of the matrix ***A*** for batch droplet breakage
λ_i^c	the *i*th eigenvalue of the matrix ***A*** as defined by Eq.(9) for continuous droplet breakage
$\pi_{0,i,k}$	as defined by Eq.(8)
$\pi_{1,i,k}$	as defined by Eq.(12)
σ	geometric grid factor
τ	vessel residence time
$\omega(v,v')$	coalescence frequency between two droplets of volumes v and v`
$\vartheta(v')$	average number of droplets produced when mother droplet of volume, v', is broken

References

Alopaeus, V., Koskinen, J. , & Keskinen, K. I. (1999). Simulation of population balances for liquid-liquid systems in a nonideal stirred tank. Part1 description and qualitative validation of model. *Chem. Engng. Sci.*, **54,** 5887-5899.

Bajpai, R. K., & Ramkrishna, D. (1976). A coalescence redispersion model for drop-size distribution in an agitated vessel. *Chem. Engng. Sci.*, **31,** 913-920.

Barone, J. P., Furth, W., & Loynaz, S. (1980). Simplified derivation of the general population balance equation for a seeded, continuous flow crystallizer. *Can. J. Chem. Engng.*, **58,** 137-138.

Blatz, P. J., & Tobolsky, A. V. (1945). Note on the kinetics of systems manifesting simultaneous polymerization-depolymerization phenomena. *J. Phys. Chem.*, **49,** 77-80.

Bleck, R. (1970). A fast, approximate method for integrating the stochastic coalescence equation. *J. Geophys. Res.*, **75,** 5165-5171.

David, R., Villermaux, J., Marchal, P. & Klein, J. P. (1991). Crystallization and precipitation engineering-IV. Kinetic model of adipic acid crystallization. *Chem. Engng. Sci.*, **46,** 1129-1136.

Eid, K., Gourdon, C., & Casamatta, G. (1991). Drop breakage in a pulsed sieve-plate column. *Chem. Engng. Sci.*, **46,** 1595-1608.

Garg, M. O., & Pratt, H. R. C. (1984). Measurement and modeling of droplet coalescence and breakage in a pulsed plate extraction column. *AIChE J.*, **30,** 432-441.

Gelbard, F., & Seinfeld, J. H. (1978). Numerical solution of the dynamic equation for particulate systems. *J. Comput. Phys.*, **28,** 357-375.

Gerald, C. F., & Wheatly, P. O. (1994). *Applied numerical analysis*. 5 ed. New York: Addison-Wesley Pub. Co.

Hill, P. J., & Ng, K. M. (1995). New discretization procedure for the breakage equation. *AIChE J.*, **41,** 1204-1216.

Hounslow, M. J. (1990). A discretized population balance for continuous systems at steady state. *AIChE J.*, **36,** 106-116.

Hounslow, M. J., Ryall , R. L. & Marshall, V. R., (1988). A discretized population balance for nucleation, growth, and aggregation. *AIChE J.*, **34,** 1821-1832.

Kostoglou, M., & Karabelas, A. J. (1994). Evaluation of zero order methods for simulating particle coagulation. *J. Colloid Interface Sci.*, **163,** 420-431.

Kumar, S., & Ramkrishna, D. (1996a). On the solution of population balance equations by discretization-I. A fixed pivot technique. *Chem. Engng. Sci.*, **51,** 1311-1332.

Kumar, S., & Ramkrishna, D. (1996b). On the solution of population balance equations by discretization-II. A moving pivot technique. *Chem. Engng. Sci.*, **51,** 1333-1342.

Kumar, S., & Ramkrishna, D. (1997). On the solution of population balance equations by discretization-III. Nucleation, growth and aggregation of particles. *Chem. Engng. Sci.*, **52,** 4659-4679.

Kumar, S., Kumar, R., & Gandhi, K. S. (1993). A new model for coalescence efficiency of drops in stirred dispersions. *Chem. Engng. Sci.*, **48,** 2025-2038.

Laso, M., Steiner, L., & Hartland, S. (1987). Dynamic simulation of liquid-liquid agitated dispersions-I. Derivation of a simplified model. *Chem. Engng. Sci.*, **42,** 2429-2436.

Lister, J. D., Smit, D. J., & Hounslow, M. J. (1995). Adjustable discretized population balance for growth and aggregation. *AIChE J.*, **41,** 591-603.

Marchal, P., David, R., Klein, J. P., & Villermaux, J. (1988). Crystallization and precipitation engineering-I. An efficient method for solving population balance in crystallization with agglomeration. *Chem. Engng. Sci.*, **43,** 59-67.

McGrady, E. D., & Ziff, R. M. (1988). Analytical solutions to fragmentation equation with flow. *AIChE J.*, **34,** 2073-2076.

Mickley, H. S., Sherwood, T. S., & Reed, C. E. (1990). *Applied Mathematics in Chemical Engineering*. New Delhi: McGraw-Hill Pub. Co.

Milton, J. S., & Arnold, J. C. (1990). *Introduction to probability and statistics*. Second Edition, New York: McGraw-Hill Pub. Co.

Nicmanis, M. , & Hounslow, M. J. (1998). Finite-element methods for steady-state population balance equations. *AIChE J.*, **44,** 2258-2272.

Podgorska, W., & Baldyga, J. (2001). Scale-up effects on the drop size distribution of liquid-liquid dispersions in agitated vessels. *Chem. Engng. Sci.*, **56,** 741-746.

Hill, P. J., & Ng, K. M. (1995). New discretization procedure for the breakage equation. *AIChE J.*, **41,** 1204-1216.

Ramkrishna, D. (1985). The status of population balances. *Rev. Chem. Engng.*, **3,** 49-95.

Ramkrishna, D. (2000). *Population Balances*. San Diego: Academic Press.

Ribeiro, L. M., Regueiras, P. F. R., Guimaraes, M. M. L., Madureira, C. M. C., & Cruz-Pintu, J. J. C. (1995). The dynamic behavior of liquid-liquid agitated dispersions-I. The hydrodynamics. *Computers Chem. Engng.*, **19,** 333-344.

Rice, G. R., & Do, D. D. (1995). *Applied mathematics and modeling for chemical engineers*. New York: John Wiley and Sons, Inc.

Scott, W. T. (1968). Analytical studies in cloud droplet coalescence I. *J. Atmos. Sci.*, **25,** 54-65.

Sovova, H., & Prochazka, J. (1981). Breakage and coalescence of drops in a batch stirred vessel-I Comparison of continuous and discrete models. *Chem. Engng. Sci.*, **36,** 163-171.

Tsouris, C., & Tavlarides, L. L. (1994). Breakage and coalescence models for drops in turbulent dispersions. *AIChE J.*, **40,** 395-406.

Valentas, K. J., & Amundson, A. R. (1966 a). Breakage and coalescence in dispersed phase systems. *Ind. Engng. Chem. Fundam.*, **5,** 533-542.

Valentas, K. J., Bilois, O., & Amundson, A. R. (1966 b). Analysis of breakage in dispersed phase systems. *Ind. Engng. Chem. Fundam.*, **5,** 271-279.

Vigil, R. D., & Ziff, R. M. (1989). On the stability of coagulation-fragmentation population balances. *J. Colloid Interface Sci.*, **133,** 257-264.

Ziff, R. M. (1991). New solutions to the fragmentation equation. *J. Phys. A: Math. Gen*., **24**, 2821-2828

Ziff, R. M. & McGrady, E. D. (1985). The kinetics of cluster fragmentation and depolymerisation. *J. Phys. A: Math. Gen*., **18**, 3027-3037

CHAPTER 2

Optimal Moving and Fixed Grids for the Solution of Discretized Population Balances in Batch and Continuous Systems: Droplet Breakage

2.1 Introduction

In general, the population balance equation (PBE) is a statement of continuity for particulate systems. It represents the net rate of number of particles that are formed by breakage, coalescence, and growth. It is for the sake of mathematical lucidity we define a particle state space continuum that spreads through the internal and external coordinates (Ramkrishna , 1985). By internal coordinates it is meant the variables that describe those quantities associated with the particle, while the term external coordinates is used to denote the position of the particles centre of mass. The population of particles is considered to be large enough so that the random fluctuations in the particle behavior could be averaged out (Mickley, Sherwood & Reed, 1990; Milton & Arnold, 1990; Ramkrishna, 2000). The population of particles in the particle state space continuum is described by a number density function *n(v,r,t)*, where *v* and *r* are the internal and external particle coordinates respectively and *t* is time.
The PBE for a steady and uncompressible flow into a well-stirred vessel could be written as (Barone, Furth & Loynaz, 1980; Lister, Smit & Hounslow, 1995; Ribeiro et al., 1995; Ramkrishna, 2000):

$$\frac{\partial n(v,t)}{\partial t}+\frac{\partial[\dot{v}n(v,t)]}{\partial v}=\frac{1}{\tau}\left(n^{feed}(v,t)-n(v,t)\right)+\rho[\{n(v,t)\};v,t] \tag{1}$$

where the first term on the left hand side denotes the rate of accumulation of droplet of size *v*, the second term is the convective flux along the droplet internal coordinate with a growth velocity $\dot{v}$. The first term on the right hand side is the net bulk flow into the vessel and the second term is the net rate of droplet generation by coalescence and breakage and is given by (Valentas & Amundson, 1966; Valentas, Bilois & Amundson, 1966;Kumar, Kumar & Gandhi, 1993; Kumar & Ramkrishna, 1996a; Podgorska & Baldyga, 2001):

$$\begin{aligned}\rho[\{n(v,t)\};v,t]=-\Gamma(v)n(v,t)-\int_0^\infty\omega(v,v')n(v,t)n(v',t)dv'+\int_v^\infty\beta(v\,|\,v')\Gamma(v')n(v',t)dv'\\+\tfrac{1}{2}\int_0^v\omega(v-v',v')n(v',t)n(v-v',t)dv'\end{aligned} \tag{2}$$

where: $\Gamma(v)$ and $\omega(v,v')$ are the breakage and coalescence frequencies respectively, and $\beta(v\,|\,v')dv$ is the number of droplets having volume in the range *v* to *v+dv* formed upon breakage of droplet of volume *v´*.
The first two terms represent droplet loss due to breakage and coalescence and the last two terms represent droplet formation due to breakage and coalescence respectively. Note that the source term, $\rho[\{n(v,t)\};v,t]$, is a functional, rather than a simple function of *v* and *t*, but is a function of a whole function *n(v,t)*. Moreover, the function, $\beta(v\,|\,v')$, (sometimes called the daughter droplet distribution) must satisfy the constraints of volume conservation and the average number of daughter droplets produced in a breakage event (Ziff, 1991; Ramkrishna, 2000).
Eqs. (1) and (2) comprise an integro-partial differential equation, which despite its importance rarely has an analytical solution. However, few cases with assumed functional forms of breakage rate, daughter droplet distribution, coalescence kernel functions exist, where most of these solutions are for the batch

stirred vessel. (Blatz & Tobolsky, 1945; Scott, 1968; Bajpai & Ramkrishna, 1976; Vigil & Ziff, 1989; Ziff & McGrady, 1985, McGrady & Ziff ,1988, Ziff, 1991).

In general numerical solutions for Eq. (1) are sought where several methods are proposed in the literature. These methods could be divided into two broad classes (Kostoglou & Karabelas, 1994): zero order methods, where the internal coordinate is represented by a piecewise constant function and a higher order methods in which higher order polynomials are used. Kostoglou and Karabelas (1994) evaluated the zero order methods that are used to solve the coalescence equation in batch vessels and they came to a conclusion that methods conserving droplet number and volume are the most advantageous. Kumar and Ramkrishna (1996a) critically reviewed both methods where they concluded that zero order methods, containing no double integrals, and conserving both numbers and volumes are not only computationally efficient but also are accurate.

To Hounslow, Ryall and Marshal (1988) and Hounslow (1990) goes the credit as they took care of preserving both droplet number and volume for coalescence and growth in batch and continuous vessels at steady state using the zero order method to discretize the PBE. Lister, Smit and Hounslow (1995) introduced a discretized PBE for coalescence and growth with a adjustable geometric internal coordinate discretization and thus had overcome the flaw of the fixed geometric internal coordinate of Hounslow, Ryall and Marshall (1988). Hill & Ng (1995) have followed Hounslow, Ryall and Marshall (1988) in developing a discretized PBE that conserve both number and volume. However, the disadvantage of this method is that it is problem dependent, that is; the discretization coefficients should be derived for each set of breakage functions.

The great achievement made in the discretization of the PBE for batch systems is due to Kumar and Ramkrishna (1996a, b, 1997) where they introduced a general framework of discretization using the zero order approach. Their method deems internal consistency of any two pre-chosen moments of the population such as number and volume. By internal consistency it is meant that for any two pre-chosen moments of the distribution, there exist two ways to obtain them. The first one is by discretizing the continuous PBE, and the second one is by deriving these moments from the discrete population balance equations (DPBE). The internal consistency is enforced by redistribution of the total property for a droplet between two adjacent representative sizes called the pivots. This concept converts the PBE into set of discrete partial differential equations (with no double integrals) and is called the fixed pivot technique.

The fixed pivot technique has a disadvantage by being inappropriate for predicting steeply changing number densities when coarse grids are used. To preserve the desirable coarseness of the grid, and hence keeping the number of equations as small as possible, it is required to change the position of the pivots in the subsequent intervals to follow these sharp changes in number density. The moving pivot technique of Kumar and Ramkrishna (1996b) comes to accomplish this task. Due to the generality and accuracy of this technique it will be used in the present work to discretize Eqs.(1) and (2).

Nevertheless, the discretization of the source term given by Eq.(2) is by no means exact, and it is inherently associated with the so-called finite domain error (FDE) (Gelbard & Seinfeld, 1978; Sovova & Prochazka, 1981; Hounslow, 1990; Nicmanis & Hounslow, 1998). This is an inevitable result of trying to use a finite internal droplet coordinate to approximate the infinite one. As so far, only Sovova and Prochazka (1981) tried to investigate rigorously the effect of the FDE on the accuracy of the DPBE when zero order methods are used. They studied droplet breakage and coalescence in batch vessels at steady state and tried to estimate the FDE by extrapolating both ends of the droplet distribution. The main drawback of this technique is the general uncertainties associated with extrapolation and its lack of general relations to predict the time dependent FDE. Moreover, since the evolution of the droplet size distribution in batch and continuous systems is a dynamic phenomenon, it is desirable to find out how to minimize the increasing FDE with time. Discretization of the internal droplet coordinate (droplet volume) requires specification of minimum and maximum droplet volumes. This discretization results in contiguous intervals compromising a grid that covers the specified range.

The objective of this work is to develop an approximate optimal moving gird technique and a time-averaged optimal fixed grid for batch and continuous systems respectively, based on the minimization of the total FDE. The proposed optimal moving grid for droplet breakage in a batch vessel has the advantage of being internally consistent by conserving any two integral properties of the distribution. General equations are also derived for the FDE by approximate discretization of the general PBE. The possibility of solving the resulting DPBEs sequentially in time is also shown. The developed optimal grids are tested using various analytical solutions available in the literature.

2.2 Discretization of the PBE for continuous systems using the moving pivot technique

In practical applications often of primary interest are some integral properties of the population rather than the entire population itself. For example in modeling of liquid-liquid dispersion systems, the mean droplet size and the hold up are of primary interest (Garg & Pratt, 1984; Eid, Gourdon & Casamatta, 1991; Alopaeus, Koskinen & Keskinen, 1999). However, in this discretization technique it is intended to correctly predict the changes in the required integral properties by exactly preserving the changes of the properties of the single droplets from which the integral ones evolve. This is because the prediction of the number density itself is computationally expensive and contains information more than that is usually required.

To proceed further, let the internal coordinate represents the droplet volume and be discretized according to the partition (grid) $V_M \equiv \{v_0, v_1, ... v_{M+1}\}$, where $v_0=0$, $v_1=v_{min}$, and $v_M = v_{max}$. Let the ith interval be denoted by $I_i = [v_i, v_{i+1})$ and the number density function is represented by (Kumar & Ramkrishna, 1996a):

$$n(v,t) = \sum_i N_i \delta(v - x_i) \tag{3}$$

where δ is the Dirac delta function, x_i is the characteristic or representative size of the population in the interval I_i where it is called the pivot and N_i is the discrete number density. The pivots simply concentrate the population in any interval at a single point where their positions are allowed to change, such that the required integral properties are preserved. The positions of these pivots, as we shall see later, are functions of both time and the coalescence and breakage functions. The pivots are dynamic quantities that follow the changes in the number density according to the following relation when the droplets volume is preserved (Kumar & Ramkrishna, 1996b):

$$x_i(t) = \frac{\int_{v_i}^{v_{i+1}} vn(v,t)dv}{\int_{v_i}^{v_{i+1}} n(v,t)dv}, \qquad v_i \le x_i < v_{i+1} \tag{4}$$

This definition of the pivot is consistent with the mean value theorem of integrals such that it moves in the interval as the number density changes. It remains close to v_i for decreasing number density and close to v_{i+1} or to the middle of the interval for increasing and uniform number densities respectively.

The coefficients N_i resemble the number density function in the interval I_i and are considered functions of time only. These functions represents the total number of droplets in the ith interval and are related to the continuous number density by:

$$N_i(t) = \int_{v_i}^{v_{i+1}} n(v,t)dv \tag{5}$$

In the present work, we will focus on the case of pure breakage in batch and continuous vessels since the coalescence and growth for batch and continuous systems are well studied (Hounslow, Ryall & Marshal, 1988; Hounslow, 1990; Lister, Smit & Hounslow, 1995; Kumar & Ramkrishna, 1996b; Ramkrishna, 2000).

To derive an internally consistent set of DPBE with respect to total number and droplet volume, we follow Kumar and Ramkrishna (1996b), where Eqs.(1) and (2) could be discretized by integrating both sides with respect to v from v_i to v_{i+1} which results in:

$$\frac{dN_i(t)}{dt} = \lambda_i^c N_i(t) + \sum_{k=i+1}^{M} \pi_{0,i,k} \Gamma_k N_k(t) + \frac{N_i^{feed}}{\tau}, \qquad i = 1, 2, \; .....M-1 \tag{6}$$

where:

$$\Gamma_k = \Gamma(x_k(t)) \tag{7}$$

$$\pi_{0,i,k} = \int_{v_i}^{u_i} \beta(v \mid x_k) dv, \qquad \begin{cases} u_i = x_i, & k = i \\ u_i = v_{i+1}, & k > i \end{cases} \tag{8}$$

$$\lambda_i^c = \Gamma_i(\pi_{0,i,i} - 1) - \frac{1}{\tau} \tag{9}$$

Eq.(6) conserves the total number of droplet in the *i*th interval and is internally consistent with respect to the zero moment of the distribution. To conserve the total droplet volume (mass) in each interval, Eqs.(1) and (2) are written in terms of the volume distribution ($p=vn(v)$) and integrated with respect to v from v_i to v_{i+1}, where after some algebraic manipulation one could obtain:

$$\frac{dx_i(t)}{dt} = \eta_i + \frac{1}{N_i(t)} \sum_{k=i+1}^{M} (\pi_{1,i,k} - x_i \pi_{0,i,k}) \Gamma_k N_k(t), \qquad i = 1, 2, \ .....M-1 \tag{10}$$

where:

$$\eta_i = (\pi_{1,i,i} - x_i \pi_{0,i,i}) \Gamma_i + \frac{x_i^{feed} - x_i}{\tau} \left(\frac{N_i^{feed}}{N_i} \right) \tag{11}$$

$$\pi_{1,i,k} = \int_{v_i}^{u_i} v \beta(v \mid x_k) dv, \quad \begin{cases} u_i = x_i, & k = i \\ u_i = v_{i+1}, & k > i \end{cases} \tag{12}$$

It should be noted that Eq.(10) becomes independent of the feed droplet distribution, N^{feed}, as well as the vessel residence time τ in case of sufficiently fine discretization ($x_i^{feed} \approx x_i$), which is a desirable result. This is really the same equation for batch vessels derived by Kumar and Ramkrishna (1996b) when $N_i^{feed} \to 0$. Eqs.(6) and (10) comprise a system of ordinary differential equations describing the evolution of the discrete number density through estimating the total number and volume of droplets in the *i*th interval with the desired accuracy. To completely specify this system, the following two sets of initial conditions are stipulated:

$$\begin{aligned} &N_i(0) = N_i^0, \\ &x_i(0) = x_i^0, \qquad i = 1, \ 2, ...M-1 \end{aligned} \tag{13}$$

2.3 Error of discretization

In discretizing an equation defined over an infinite domain an inherent error is incurred due to the failure of taking into account the portion of the function lying outside the domain of discretization. This type of error is termed finite domain error (FDE) (Gelbard & Seinfeld, 1978; Hounslow, 1990), and as a result it causes a nonzero lower and upper residuals below and above the discrete limits of integration. These lower (FDE^L) and upper (FDE^U) residuals represent cumulative number densities that are given by (Sovova & Prochazka, 1981):

$$FDE_0^L(v_{\min}, t) = \int_0^{v_{\min}} n(v,t) dv \tag{14}$$

$$FDE_0^U(v_{\max},t)=\int_{v_{\max}}^{\infty} n(v,t)dv \tag{15}$$

where the subscript zero is used to refer to the residuals of the zero moment of the distribution. This choice is actually suitable for characterizing the FDE since in droplet breakage a large number of droplets having a small volume is produced as breakage proceeds. So, these lower and upper residuals could be related to the total number of droplets for the continuous distribution as follows:

$$N^c(t)=FDE_0^L(v_{\min},t)+\sum_{i=1}^{M-1}\int_{v_i}^{v_{i+1}} n(n,t)dv+FDE_0^U(v_{\max},t) \tag{16}$$

The discrepancy between the continuous number of droplets, $N^c(t)$, at any instant of time and its discrete counterpart, $N^d(v_{min}, v_{max}, t)$, could be interpreted by defining the so called error of discretization. The error of discretization, ε_0, is defined as the difference of sums between the continuous and discrete number of droplets for the intervals $(0,\infty)$ and $[v_{min}, v_{max}]$ respectively:

$$\varepsilon_0(t)=N^c(t)-\sum_{i=1}^{M-1}N_i(t) \tag{17}$$

By combining the last two equations the error of discretization becomes:

$$\varepsilon_0(t)=FDE_0^L(v_{\min},t)+FDE_0^U(v_{\max},t) \tag{18}$$

This result shows that the discretization error in the number of droplets is solely due to the total finite domain error comprising of the sum of both the lower and upper residuals defined by Eqs.(14) and (15). This means that even for an exact number of droplets, and by excluding the integration error induced by discretization, the total finite domain error will never be zero as long as a finite domain is considered. Moreover, for a given number of intervals, M, and interval width, Δv, the total finite domain error at any instant of time is a function only of v_{min}. Since the lower residual decreases as v_{min} decreases and the upper residual increases at the same time, then there exist due to these opposing effects an optimal minimum droplet volume that minimizes the sum of both residuals. This means as far as discrete distribution is considered, a choice of v_{min}, below the optimal value will increase the discretization error in opposite to the general intuition that decreasing v_{min} will improve the solution. Actually, Hounslow (1990) showed that when a value of minimum droplet volume is chosen below the optimal one, an artifact oscillation in N_i is observed in the few first number of intervals.

To find the optimal minimum droplet volume that minimizes the total finite domain error it is sufficient to differentiate Eq.(18) with respect to v_{min} at given M and Δv. By using the definition of the residuals (Eqs.(14) and (15)) and making use of Leibnitz formula (Mickley, Sherwood & Reed , 1990) one could obtain:

$$n(v_{\min}^*,t)-\frac{dv_{\max}}{dv_{\min}}n(v_{\max}^*,t)=0 \tag{19}$$

and the discrete counterpart of Eq. (19) is:

$$\frac{\overline{N}_0^*(t)+\overline{N}_1^*(t)}{2}-\frac{dv_{\max}}{dv_{\min}}\left(\frac{\overline{N}_{M-1}^*(t)+\overline{N}_M^*(t)}{2}\right)=0 \tag{20}$$

where the number densities $n(v_{\min}^*,t)$ and $n(v_{\max}^*,t)$ are approximated by the arithmetic of their average discrete values at the adjacent intervals I_0, I_1 and I_{M-1}, I_M respectively (Marchal et al., 1988). Note that the maximum droplet volume must be a continuous function of v_{min} in order to satisfy the conditions implied by Eqs.(22) and (23). As will be shown later a geometric grid with adjustable geometric factor, $\sigma>1$, will be a suitable choice for the discretization of the droplet internal coordinate (v):

$$v_{\max} = \sigma^{M-1} v_{\min} \tag{21}$$

It should be noted that the discretization parameters are: the total number of intervals, *M*, the optimal minimum droplet volume, $v^*_{\min}$, and the interval width controlled by the geometric factor σ.

Since the continuous and discrete number densities appearing in Eqs.(19) and (20) respectively are functions of time, it follows that the optimal minimum droplet volume, $v^*_{\min}$ is also function of time. This means that as breakage proceeds to produce smaller number of droplets, the optimal minimum droplet volume must decrease to account for the increasing number density at the lower size range. At the same time, and due to the conservation of droplet volume, the number density function decreases for large droplets leading to empty classes at the upper size range. This suggests the use of optimal moving grid for droplet breakage in batch vessels, which moves from the upper size range to the lower size range as function of time. To find such an optimal moving grid, Eqs.(6) (for batch), (10), and (20) must be solved simultaneously at each instant of time leading to a differential algebraic system of equations (DAE). Unfortunately, the solution is iterative by starting with an initial guess for the minimum droplet volume at given number of intervals, *M*, and geometric factor σ followed by solving the system of ODEs (6) and (10). If Eq.(20) is not satisfied, then an improved guess must be used until convergence at each instant of time is achieved. This algorithm seems to be time consuming since it involves solving *2M* ODEs per iteration at each instant of time and might mask the benefits gained by using the optimal moving grid. To compensate for this drawback, an approximate optimal moving grid technique is derived in the following section.

2.4 An approximate optimal moving grid technique for batch systems

We return back to the definitions of the lower and upper residuals given by Eqs.(14) and (15) and the definition of the total finite domain error given by Eq.(18). Since the lower residual decreases as minimum droplet volume decreases, and the upper residual increases at the same time, it follows that the total finite domain error will be close to the minimum value when both residuals are equal (Sovova & Prochazka, 1981). Using this principle, it is possible to force these residuals to be equal at each instant of time and hence producing a minimum droplet volume profile that is close to the exact optimal one. Since the optimal moving grid should keep the number of intervals, and hence the number of DPBE associated with it constant during grid movement, the redistribution of the population between the old and the newly formed grid must conserve any two chosen integral properties of the population. However, we will restrict our attention to the total number and volume in this work (zero and first moment of the population). Now consider the geometric grid shown in Fig.(1) at two instants of time: *t* and *t+Δt* where the minimum droplet volume moves from $v^*_{\min}(t)$ to $v^*_{\min}(t+\Delta t)$. Let $\gamma_i^{<i>}(t)$ be the fraction of droplets at the pivot $x_i(t)$ to be assigned to the pivot $x_i(t+\Delta t)$ and $\gamma_{i+1}^{<i>}(t)$ be the fraction of droplets at the pivot $x_i(t)$ to be assigned to the pivot $x_{i+1}(t+\Delta t)$. To conserve both number and volume of these droplets at the *i*th pivot after redistribution, the following two constraints are set up (refer to Fig.1b) (Kumar & Ramkrishna, 1997):

$$\gamma_i^{<i>} + \gamma_{i+1}^{<i>} = 1 \tag{22}$$

$$x_i(t+\Delta t)\gamma_i^{<i>} + x_{i+1}(t+\Delta t)\gamma_{i+1}^{<i>} = x_i(t) \tag{23}$$

Solving these equations for $\gamma_i^{<i>}(t)$ results in:

$$\gamma_i^{<i>:} = \frac{x_{i+1}(t+\Delta t) - x_i(t)}{x_{i+1}(t+\Delta t) - x_i(t+\Delta t)} \tag{24}$$

Similar equations could be written for the droplet population at the (*i-1*)th pivot where $\gamma_i^{<i-1>}(t)$ is the fraction of droplet at the $x_{i-1}(t)$ pivot assigned to the $x_i(t+\Delta t)$ pivot, and $\gamma_{i-1}^{<i-1>}(t)$ is the fraction of droplets at the $x_{i-1}(t)$ pivot assigned to the $x_{i-1}(t+\Delta t)$. Solving these equations yields an expression for $\gamma_i^{<i-1>}(t)$:

$$\gamma_i^{<i-1>:} = \frac{x_{i-1}(t) - x_{i-1}(t+\Delta t)}{x_i(t+\Delta t) - x_{i-1}(t+\Delta t)} \tag{25}$$

Now by referring to Fig.(1-b), we could obtain the net discrete density of droplet population at the instant $t+\Delta t$ at the new grid from that at the old one at time t using Eqs.(24) and (25):

$$N_i(t+\Delta t) = \gamma_i^{<i-1>} N_{i-1}(t) + \gamma_i^{<i>} N_i(t), \qquad i = 1,\ 2,\ \ldots\ldots\ M \tag{26}$$

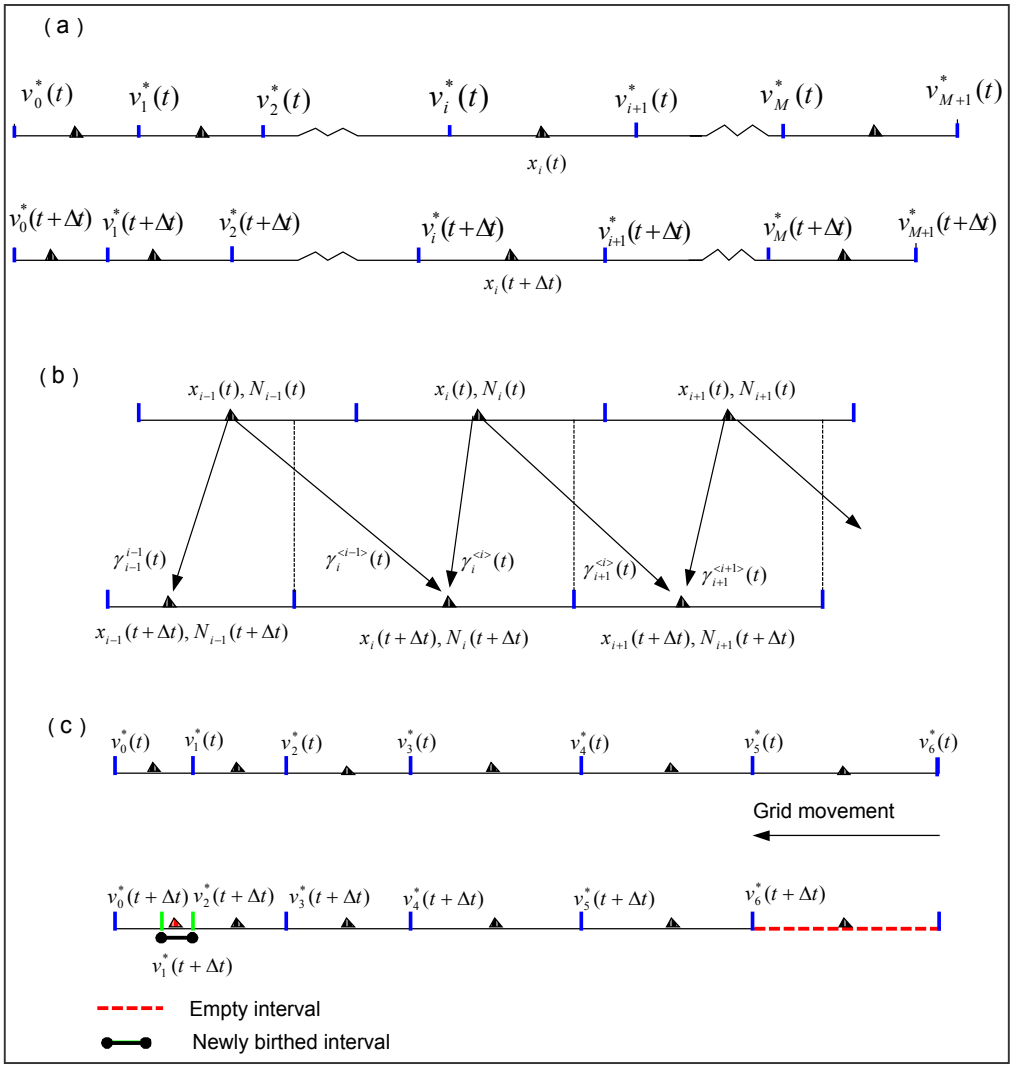

Fig.(1): Typical moving geometric grid.

When i=1, the last equation becomes function of $N_0(t)$ which is not defined by any of the system of Eqs.(6). It is interesting to note that by definition, $N_0(t)$, is the lower residual defined by Eq.(14), and

hence its estimation becomes an inevitable necessity for both $N_1(t+\Delta t)$ and the FDE_0^L. The estimation of $N_0(t)$ from the discrete number density will follow in the next section.
Now we shall turn our attention to force both residuals to be equal at any instant of time $t+\Delta t$ utilizing the redistribution concept above. At the time instant $t+\Delta t$ the discrete lower residual of the distribution is found from Eq.(26):

$$FDE_0^L(t+\Delta t) = \gamma_0^{<0>} N_0(t) \tag{27}$$

and similarly the discrete upper residual is given by:

$$FDE_0^U(t+\Delta t) = \sum_{i=M}^{\infty} \gamma_i^{<i-1>} N_{i-1}(t) + \gamma_i^{<i>} N_i(t) \tag{28}$$

It could be shown that only the Mth term in the summation above has a significant value since the population contained in the interval $[V_{M+1}, \infty)$ is approximately negligible for sufficiently large M or geometric factor σ. This is because during droplets breakage the final intervals (numbering is started from the small size to large size) become gradually empty as breakage progresses. Actually, after sufficient time the last interval becomes completely empty and the zero interval is occupied by the newly birthed population of droplets. Moreover, if the initial minimum and maximum droplets sizes are chosen to be optimal according to Eq.(19), then the higher terms in Eq.(28) will be insignificant for sufficiently large M or σ. This is actually is equivalent to neglecting droplet breakage from the $(M+1)$th intervals and the higher ones.
The necessary condition for optimality stated by Eq.(19) or (20) is approximately satisfied if both residuals are equal at each instant of time. To accomplish this, we force both sides of Eqs.(27) and (28) to be equal, which after some algebraic manipulation yields:

$$\frac{v_{\min}^*(t+\Delta t)}{v_{\min}^*(t)} = \frac{\frac{1}{\sigma-1} N_{M-1}(t) + \frac{1}{\sigma} N_0(t)}{\frac{\sigma+1}{\sigma} N_0(t) + \frac{1}{\sigma-1} N_{M-1}(t) - N_M(t)} \tag{29}$$

with $v_{\min}^*(0)$ found from the initial number density and Eq.(19). Eq.(29) specifies the path that must be followed by the grid in order to keep the total *FDE* approximately minimum based on the zero moment of the distribution.
Since the interval boundaries are now functions of time, then the population contained in it changes also with time. It follows that the discretization of the left hand side of Eq.(1) for a batch system will be different from that used in the case of a fixed grid. This could be shown by multiplying both sides of Eq. (1) by dv and integrating over the size range $[v_i(t), v_{i+1}(t)]$:

$$\frac{\partial}{\partial t} \int_{v_i(t)}^{v_{i+1}(t)} n(v,t)dv = \lambda_i^c N_i(t) + \sum_{k=i+1}^{M} \pi_{0,i,k} \Gamma_k N_k(t) \tag{30}$$

By expanding the left hand side using the Leibnitz formula (Mickley, Sherwood & Reed 1990), and noting that the left hand side involves integration with respect to volume only, one could obtain:

$$\int_{v_i(t)}^{v_{i+1}(t)} \frac{\partial n(v,t)}{\partial t} dv + n(v_{i+1}(t),t) \frac{dv_{i+1}(t)}{dt} - n(v_i(t),t) \frac{dv_i(t)}{dt} = \lambda_i^c N_i(t) + \sum_{k=i+1}^{M} \pi_{0,i,k} \Gamma_k N_k(t) \tag{31}$$

Note that the entire grid boundaries move at the same velocity, that is;

$$\frac{dv_i(t)}{dt} = \frac{dv_{i+1}(t)}{dt} = \frac{dv(t)}{dt} \tag{32}$$

Using the above relation, Eq.(31) after some algebraic manipulation simplifies to:

$$\int_{v_i(t)}^{v_{i+1}(t)} \left[\frac{\partial n(v,t)}{\partial t} + \frac{dv}{dt} \frac{\partial n(v,t)}{\partial v} \right] dv = \lambda_i^c N_i(t) + \sum_{k=i+1}^{M} \pi_{0,i,k} \Gamma_k N_k(t) \tag{33}$$

The term in the brackets on the left hand side is merely the total derivative of the number density, which describes the change in the number density of size *v* as noticed by an observer moving with a velocity the same as that of the grid. Using this fact Eq.(33) simplifies to:

$$\frac{\mathrm{d}N_i(t)}{\mathrm{d}t} = \lambda_i^b N_i(t) + \sum_{k=i+1}^{M} \pi_{0,i,k} \Gamma_k N_k(t), \quad i = 1, 2, \ldots\ldots M-1 \tag{34}$$

where λ_i^b is found from λ_i^c by setting $\tau \to \infty$.

Similarly, the equations of the pivots are still given by Eq. (10) with $\eta_i^b = \lim_{\tau \to \infty} \eta_i^c$, where the change in the position of the pivot in any size range is now with respect to the moving grid.

The set of Eqs.(10), (24), (25), (26), (29), (34), and the initial conditions specified by Eq.(13) comprise a differential algebraic system of equations that could be solved sequentially in time.

The notation will be greatly simplified if these equations are written in a compact matrix form as follows:

$$\frac{\mathrm{d}\boldsymbol{N}}{\mathrm{d}t} = \boldsymbol{A}\boldsymbol{N} \tag{35}$$

$$\frac{\mathrm{d}\boldsymbol{x}}{\mathrm{d}t} = \boldsymbol{F}(\boldsymbol{x}, \boldsymbol{N}) \tag{36}$$

$$\boldsymbol{N}(t + \Delta t) = \boldsymbol{\gamma}(t)\boldsymbol{N}(t) + \boldsymbol{N}_0^T(t)\boldsymbol{\gamma}_0(t) \tag{37}$$

$$\boldsymbol{N}(0) = [\ N_1(0) \quad N_2(0)\ \ldots\ N_{M-1}(0) \quad N_M(0)]^T \tag{38}$$

$$\boldsymbol{x}(0) = [\ x_1(0) \quad x_2(0)\ \ldots\ x_{M-1}(0) \quad x_M(0)]^T \tag{39}$$

Where $\boldsymbol{A}$ and $\boldsymbol{F}$ are $M \times M$ upper triangular matrices whose elements are given by:

$$A_{i,k} = \begin{cases} \lambda_i^b, & k = i \\ \pi_{0,i,k} \Gamma_k, & k > i \end{cases} \tag{40}$$

$$F_{i,k} = \begin{cases} \eta_i^b, & k = i \\ \dfrac{(\pi_{1,i,k} - x_i \pi_{0,i,k}) \Gamma_k N_k(t)}{N_i(t)}, & k > i \end{cases} \tag{41}$$

and $\boldsymbol{\gamma}$ is an $M \times M$ bidiagonal matrix whose elements are given by:

$$\gamma_{i,k} = \begin{cases} \gamma_i^{<i>}, & k = i \\ \gamma_{\mathrm{i}}^{<\mathrm{i-1}>}, & k = i-1, k \neq 0 \end{cases} \tag{42}$$

γ_0 and $\boldsymbol{N_0}$ are $M \times 1$ vectors whose elements are:

$$\boldsymbol{\gamma_0} = [\ \gamma_1^0 \quad 0\ \ldots\ 0 \quad 0)]^T \tag{43}$$

$$\boldsymbol{N_0} = [\, N_0 \quad 0 \;....\quad 0 \quad 0)]^{\,T} \tag{47}$$

In the above system of equations, the only undetermined variables are $N_0(t)$ and $N_M(t)$ and their corresponding pivots (x_0 and x_M) which will be considered in the next section.

2.5 Estimation of the lower and upper residuals

It should be clear that in the derivation of the DPBE, the droplets having volume less than v_{min} have zero breakage frequency. This corresponds to the case of limited breakage, where physically stable minimum droplet volume exists below which no further breakage occurs (Valentas, Bilois & Amundson, 1966; Tsouris & Tavlarides, 1994; Hill & Ng, 1995; Aopaeus, Koskinen & Keskinen, 1999). As the breakage proceeds the optimal minimum droplet volume $v^*_{\min}(t)$ will move toward v_{min} until both droplet volumes coincide. For the case of full breakage all the droplets have a nonzero breakage frequency and hence $v_{min} \to 0$. The discrete droplet population density in the intervals $(0,\ v^*_{\min}(t)\,]$ and $[v_{min},\ v^*_{\min}(t)\,]$, for the case of full and limited breakage respectively, represents the lower residual or strictly speaking $N_0(t)$. To estimate this population density, Sovova and Prochazka (1981) used a two point linear extrapolation to estimate the steady state lower residuals in batch vessel where both breakage and coalescence mechanisms were active. Their extrapolation technique is usually useful for non-steep number densities and might lead to significant erroneous predictions for very steep number densities for which the approximate optimal moving grid technique is developed. Instead of extrapolation, which has considerable numerical uncertainties (Mickley, Sherwood & Reed, 1990), a natural approximate extension of the discrete equations to include either of the intervals $(0,\ v^*_{\min}(t)\,]$ and $[v_{min},\ v^*_{\min}(t)\,]$ will be used. It could be assumed that either of the aforementioned intervals will only receive broken droplets from higher ones or from droplets within the intervals themselves, and no droplet will be lost through breakage from these intervals (Laso, Steiner & Hartland, 1987; Hill & Ng, 1995). As a consequence of this assumption an unsteady state number balance on these intervals will produce the required differential equation describing the change of $N_0(t)$ with time:

$$\frac{\mathrm{d}N_0(t)}{\mathrm{d}t} = \vartheta(v^*_{\min}(t))\Gamma_0 N_0(t) + \sum_{k=1}^{M} \pi_{0,0,k}\Gamma_k N_k(t) \tag{45}$$

Here $\vartheta(v^*_{\min})$ is the average number of droplets produced due to the breakage of droplet of volume $v^*_{\min}(t)$.

Since the width of the intervals $(0,\ v^*_{\min}(t)\,]$ or $[v_{min},\ v^*_{\min}(t)\,]$ is very small due to the geometric grid used in discretization, the pivot $x_0(t)$ is fixed at the middle of these intervals without introducing appreciable errors. This is in general always correct when fine grids are used, where it is possible for the fixed pivots to replace the moving ones, that is; the moments of the population could be predicted without appreciable errors (Ramkrishna, 2000).

To estimate the discrete population density $N_M(t)$, we shall follow the same reasoning used to obtain $N_0(t)$. There are only droplets vanishing from the I_M interval to the lower ones, and formation of droplets by breakage within the Mth interval itself is permitted (Laso, Steiner & Hartland, 1987; Hill & Ng, 1995). An unsteady state number balance on the I_M interval results in:

$$\frac{dN_M(t)}{dt} = \lambda^b_M N_M(t) \tag{46}$$

Using similar argument, the Mth pivot follows from Eq.(10):

$$\frac{dx_M(t)}{dt} = \eta_M \tag{47}$$

Eqs.(27) and (28) along with Eqs.(45) through (47) define completely the lower and upper residuals at any instant of time for specified grid parameters σ and M.

2.6 Sequential solution of the number density and pivot equations

The system of equations for the discrete number density and the pivots given by Eqs.(35) and (36) could be solved sequentially in time. The sequential solution starts by first integrating the number density equations over the time interval $t\in[t,\ t+\Delta t]$ followed by the integration of the pivot equations. This method of solution is allowed only if the pivots change slowly when compared to the variation of the number densities over sufficiently small interval of time, and hence making the matrices $\boldsymbol{A}$ and $\boldsymbol{F}$ approximately time independent. This is actually valid if the value of the ratio of each time constant of the pivot and number density equations is a large number. Actually, the time constants of Eqs.(6) and (10) are the reciprocal of the eigenvalues of their matrices $\boldsymbol{A}$ and $\boldsymbol{F}$. Since these matrices are both upper triangular, it can be simply shown that their eigenvalues are given by their diagonal elements (Gerald & Wheatly, 1994). The time constants of the present systems are $\left|\lambda_i^b\right|^{-1}$ and $\left|\eta_i\right|^{-1}$ *(i=1, 2, ... M)* for number density and pivots respectively. Accordingly, the condition stated above for the possibility of sequential solution could be written mathematically as:

$$\frac{\left|\eta_i\right|^{-1}}{\left|\lambda_i^b\right|^{-1}} >> 1 \tag{48}$$

This condition could be satisfied for sufficiently fine grids by using an optimal moving geometric grid. This grid becomes gradually fine as the breakage progresses in time by moving to the left to accommodate the evolving population in the small size range. By applying the mean value theorem of integrals to the system of Eqs.(9) and (11) it is easy to show that:

$$\lim_{\Delta v_i \to 0} \frac{\left|\eta_i\right|^{-1}}{\left|\lambda_i^b\right|^{-1}} \to \infty \tag{49}$$

This insures the validity of the method of sequential solution in time proposed above. Actually, the system of equations given by Eq.(35) has an explicit solution that is given by:

$$\boldsymbol{N}(t) = \boldsymbol{R}\boldsymbol{D}\boldsymbol{R}^{-1}\boldsymbol{N}(0) \tag{50}$$

where $\boldsymbol{D}$ is an $M\times M$ diagonal matrix given by: $\boldsymbol{D} = diag(e^{\lambda_i^b t})$, $i = 1, 2, \ldots M$, and $\boldsymbol{R}$ is an $M\times M$ matrix whose columns are the eigenvectors of **A**.

2.7 The geometric grid

The use of geometric grid in the discretization of the PBEs is extensively used in the literature and its many advantages are found elsewhere (Bleck, 1970; Laso, Steiner & Hartland, 1987; Hounslow, Ryall & Marshal, 1988; Lister, Smit & Hounslow, 1995; Hill & Ng, 1995; Ramkrishna, 2000). However, it is worthwhile to mention two distinctive advantages of the geometric grid that are utilized in this work. The first one is that the geometric grid becomes fine as the entire grid moves to the left and thus allowing steep number density to be correctly tracked out. The second advantage, and the most important, is that when the last grid boundary coincide exactly with v_{max} due to the grid movement, the new and the old interval boundaries completely coincide except for the first boundary ($v_1(t+\Delta t) = v^*_{\min}(t)$) (see Fig.(1-c)). This means that the old and the new population densities have the same intervals to occupy, resulting in an exact match between them ($\boldsymbol{N}(t+\Delta t) = \boldsymbol{N}(t)$) but only for the first interval ($N_1(t+\Delta t) = \gamma_1^{<0>} N_0(t)$). This suggests that the number densities could be updated only when $v^*_{M+1}(t+\Delta t)$ is less than or equal to $v_{\max} = v^*_M(t)$ to exclude any numerical inaccuracies due to population redistribution. However, if the equality is not exactly satisfied, the new pivots are set equal to the old ones since for sufficiently small

time step $v^*_{M+1}(t+\Delta t)$ is not greatly different from $v^*_M(t)$. At the same time, the pivot of the newly birthed interval is set at the middle since the width of this interval is very small thanks to the geometric grid. It follows then the stepwise redistribution of the discrete population density will result in an approximate optimal piecewise constant minimum droplet volume profile as a function of time. In fact this strategy is adopted in the following solution algorithm.

2.8 Solution algorithm

The solution algorithm using the optimal moving grid could be summarized as follows:

1- Specify σ, M, Δt, t_f and the initial condition $n(v,0)$.
2- Set $t_0 = 0$
3- Calculate the discrete initial conditions $\boldsymbol{N}(0)$ and $\boldsymbol{x}(0)$ using Eqs.(5) and (4) and $n(v,0)$.
4- Calculate the initial optimal droplet volume, $v^*_{\min}(0)$, using Eq.(19) and $n(v,0)$.
5- Calculate $\boldsymbol{N}(t_0+\Delta t)$ using Eq.(50) and $\boldsymbol{x}(t_0+\Delta t)$ using Eq.(36) sequentially in time.
6- Calculate $N_0(t_0+\Delta t)$ using Eq.(45)
7- Calculate the optimal droplet volume, $v^*_{\min}(t_0+\Delta t)$, using Eq.(29) and $v^*_{M+1}(t_0+\Delta t) = \sigma^M v^*_{\min.}(t_0+\Delta t)$.
8- If $v^*_{M+1}(t_0+\Delta t) \le v^*_M(t_0)$ then:
   - Calculate $v^*_i(t_0+\Delta t) = \sigma^{i-1} v^*_{\min.}(t_0+\Delta t)$ for $i=1, 2, \ldots M+1$
   - Calculate $x_i(t_0+\Delta t) = (v^*_i(t_0+\Delta t) + v^*_{i+1}(t_0+\Delta t))/2$, $i=0,1$ and $x_i(t_0+\Delta t) = x_{i-1}(t_0),\ i = 2,3,\ldots M$
   - Update the $\boldsymbol{\gamma}$ matrix using Eqs.(24) and (25).
   - Redistribute the number density according to Eq.(37).
   - Set $t_0 = \Delta t$, and $t_0 = t_0 + \Delta t$
9- Else,
   - Got to 10
10- Go to step 5 until $t_0 \ge t_f$.

Note that in step 8 if the equality is exactly satisfied, then $\boldsymbol{N}(t_0+\Delta t) = \boldsymbol{N}(t_0)$ except for the first interval where $N_1(t+\Delta t) = \gamma_1^{<0>} N_0(t)$.

2.9 Optimal fixed grid for droplet breakage in continuous systems

Unfortunately, the optimal moving grid technique developed in this work could not be applied in a straightforward manner to droplet breakage in continuous systems. The reason for this is the existence of two types of population densities in this type of systems. The first is the fixed droplet size distribution of the feed, $n^{feed}(v,t)$, and the second is that of droplets in the vessel itself $n(v,t)$. Since the droplet size distribution in the vessel moves continuously to the small size range with time, and the inlet feed size distribution is usually constant, the optimal maximum droplet size is fixed by that of the feed. Moreover, the optimal minimum droplet size in the vessel must be less than or equal to that of the feed. This leads to different grid widths for the droplet distribution in the vessel and in the feed where it becomes increasingly fine for the former and remains fixed for the latter. Mathematical inconsistencies are expected to occur due to integrating the terms involving $n(v,t)$ using a moving grid, while the feed term is integrated using the same grid at t=0. This is because the discrete number density, $N_i(t)$, is dependent on the size of the interval which is a function of time when a moving grid is used.

However, since droplet breakage in continuous systems is not expected to proceed to a very small size range as in the case of batch systems due to the fixed residence time of the vessel, an optimal fixed grid would be sufficient to minimize the total time-averaged FDE.

In the development of the moving grid technique for batch systems, we sought to minimize a total finite domain error based on the number density, FDE_0. However, there is still a finite domain error induced by excluding droplet volumes due to the failure of extending the domain of the internal coordinate to 0 and

∞. This is actually the total FDE based on the volume or the first moment of the distribution, and could be defined by an analogy to the zero FDE (Eq.(18)):

$$\varepsilon_1 = FDE_1^L(v_{\min},t) + FDE_1^U(v_{\min},t) \tag{51}$$

where FDE_1^L and FDE_1^U are defined based on the first moment of the distribution by equations similar to Eqs.(14) and (15).

Since droplet breakage in batch systems leads to a population density that is skewed to the left, small volume of droplets are lost due to the failure of extending the droplet volume to infinity. However, for continuous systems the zero and first moments of the feed do affect the zero and first moments of the distribution in the vessel. Hence, where the feed distribution is constant as stated above, appreciable errors would result due to the exclusion of numbers and volumes from the domain. This marked influence of the feed density function on the moments of the distribution lends itself to consider both finite domain errors based on the zero and first moments in seeking an optimal grid for discretization. In other words, we seek a grid that minimizes the time-averaged of the sum of the FDE based on both zero and first moments of the distribution. This total FDE is found by adding Eqs.(18) and (51) and the result could be related to the continuous zero and first moments of the distribution by analogy to Eq.(16):

$$M_0^d(v_{\min.}^*(0),t) + M_1^d(v_{\min.}^*(0),t) = M_0^c(t) + M_1^c(t) - [\varepsilon_0(v_{\min.}^*(0),t) + \varepsilon_1(v_{\min.}^*(0),t)] \tag{52}$$

Note that minimizing the total FDE (the term in square brackets) is equivalent to maximizing the sum of the left hand side at any instant of time since the continuous zero and first moments of the distribution are functions of time only. Since the proposed optimal grid is fixed as mentioned above, it is recommended to maximize the time-averaged of the left hand side of Eq.(52). The initial minimum droplet volume, $v_{\min.}^*(0)$, could be obtained from the initial condition or from the feed droplet size distribution. Since $v_{\min.}^*(0)$ is dependent on the interval width or σ for geometric grid, it is then ($M_0^d + M_1^d$) is dependent only on the interval width or geometric factor σ at specified *M*. Thus, an optimal fixed grid is sought by finding the interval width or geometric factor that maximizes the time-averaged of ($M_0^d + M_1^d$). In this work, we will restrict our attention to a geometric grid and thus, the problem at hand could be posed as a constrained one dimensional nonlinear optimization problem as follows:

$$\underset{\sigma}{\text{maximize}} \left(\frac{\int_0^{t_f} [M_0^d(\sigma,t) + M_1^d(\sigma,t)]}{t_f} dt \right) \tag{53}$$

subject to:

$$\boldsymbol{N}(t) = \boldsymbol{R}\boldsymbol{D}\boldsymbol{R}^{-1}[\boldsymbol{N}(0) + \boldsymbol{A}^{-1}\boldsymbol{N}^{feed}] - \boldsymbol{A}^{-1}\boldsymbol{N}^{feed},$$

$$\frac{\mathrm{d}\boldsymbol{x}}{\mathrm{d}t} = \boldsymbol{F}(\boldsymbol{x},\boldsymbol{N}),$$

$$M_0^d(\sigma,t) + M_1^d(\sigma,t) = \boldsymbol{N}^T(t)\boldsymbol{N}(t) + \boldsymbol{x}^T(t)\boldsymbol{N}(t),$$

$1 < \sigma \le \sigma_{\max.}$ for all $t \in [0, t_f]$.

where $\boldsymbol{N}^{feed}$ is an $M \times 1$ vector.

The above formulation minimizing the time-averaged total FDE has a distinctive feature by being dependent only on the chosen preserved properties of the distribution, which are already calculable from the solution of the DPBE themselves. The final time appearing in the system of Eqs.(53) is really the time

at which the continuous system approaches steady state, which is a finite value and normally could be taken about 5τ for linear systems (>99% of final steady state is achieved).

2.10 Numerical results

Although both the optimal moving and the fixed grids constructed in this work for minimizing the total FDE are general and applicable for any set of breakage functions, it is desirable to check thoroughly the numerical results by comparison with analytical solutions whenever it is possible. Two functional forms for both the daughter droplets distribution, $\beta(v \mid v')$, and breakage rate, $\Gamma(v)$, are used:

1- Uniform daughter droplet distribution, where it assumes an equal chance to form a daughter droplet of any smaller size when a mother droplet breaks up, and hence it is independent of daughter droplet volume (cases 1 and 2).
2- Parabolic daughter droplet distribution, where it assumes a more or less likely chance to form two daughter droplets of different sizes upon breakage of mother droplet (case 3).

The breakage rate function is assumed to have a general form:

$$\Gamma(v) = kv^m \tag{54}$$

where k and m are positive parameters.
For the sake of comparison, available analytical solutions for droplet breakage in batch systems are presented in Table 2. Moreover, expressions are derived for the optimal minimum droplet volume, the continuous zero and first moments of the analytical distribution, and the total finite domain error. These are presented in Tables 3 and 4.
For the solution of droplet breakage in continuous systems, the problem of finding general analytical solutions becomes more difficult. However, two specific cases are presented in this work depending on the feed droplet distribution. In the first case McGrady and Ziff (1988) solved analytically the continuous PBE where a monodisperse feed droplet distribution is assumed. In the second case Nicmanis and Hounslow (1998) presented the steady state solution of the continuous PBE with an exponential feed droplet distribution. However, for the dynamic solution, we extend the method of moments presented in the work of Vigil and Ziff (1989) for batch systems to continuous systems. Unfortunately, only the analytical zero and first moment of the distribution are obtained. In the following two sections, we first compare the numerical and the available analytical solutions for droplet breakage in batch systems, and finally the comparison is made for the continuous ones.

2.10.1 Droplet breakage in batch systems

In Table 2 we present three case studies to illustrate how the optimal moving grid works for the solution of droplet breakage in batch systems. In the first two cases a uniform daughter droplet distribution is assumed, while the exponent m in Eq.(54) is taken as 1 and 2 respectively. The initial droplet size distribution is exponential and the two cases along with their analytical solutions are shown in Table 2. The third case represents a more general parabolic daughter droplet distribution, however the analytical solution, to the best of the authors' knowledge, is not available. Nevertheless, the solutions using the fixed and optimal moving grid techniques will be compared. The comparison between the analytical and numerical results will be made on the bases of average number densities due to the sensitivity of the discrete number density to the interval width. Consequently, the average numerical and analytical discrete number densities are defined as:

$$\overline{N}_i^{num.} = \frac{N_i^{num.}(t)}{\Delta v_i(t)} \tag{55a}$$

$$\overline{N}_i^{anal.} = \frac{N_i^{anal.}(t)}{\Delta v_i(t)} \tag{55b}$$

Note that the interval width is a function of time for an optimal moving grid and is time-invariant for the fixed one. Using the zero and first moments of the distribution the mean droplet volume is compared with the analytical solution using the following relation:

$$\bar{v}(t) = \frac{M_1^d(t)}{M_0^d(t)} \tag{56}$$

Moreover, since wide differences in the average number density values are encountered as breakage progresses with time, a semi-log plot will be suitable for comparison. In this work the number rather than the volume density is used to avoid damping the numerical errors, if any, where it actually occurs when a small droplet volume multiplies the number density particularly in the small size range. In all the case studies that follow arbitrary time units are used. Furthermore, all the simulation runs are carried out using the MATLAB software.

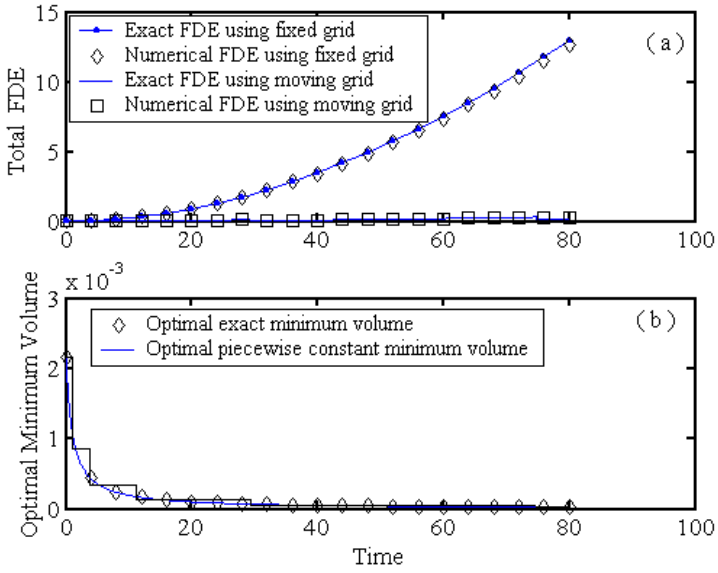

Fig.(2): a-The effect of the optimal grid movement on the total finite domain error. b- The approximate and exact optimal minimum droplet volume profiles for droplet breakage in a batch vessel using a geometric grid with factor σ = 2.5, M = 10, binary breakage, $\Gamma=v$, $\beta(v|v')=1/v'$, and exponential initial condition.

2.10.1.1 Case 1: Breakage with uniform daughter droplet distribution and $\Gamma(v) = v$

In this case (see Table 2) the simulation is carried out over a relatively long period of time, t_f=80, to illustrate the steepness of the number density due to long time breakage. The solution algorithm is implemented for a number of intervals, M=10, and σ=2.5 to stress the use of a desirable relatively coarse geometric grid. We start this case by comparing the exact and numerical FDE as well as the optimal minimum droplet volumes. Fig.(2-a) shows these results, and it can be seen an excellent agreement between the numerical and exact FDE is obtained. As expected the optimal fixed FDE increases with time due to the failure to account for the increase in number density in the small size range as droplet breakage proceeds. This is actually equivalent to a loss of number of droplets from the system. To compensate for this, we let the grid move in an optimal manner as shown in Fig.(2-b), where the exact minimum droplet volume (see Table 3) is depicted along with that predicted using the optimal moving grid technique. First the agreement between the optimal piecewise minimum droplet volume and the exact one is also good even when the grid moves so fast. Actually, the approximate profile is expected to approach the exact one as the number of pivots increases. The exact solution is obtained by inserting the analytical solution from Table 2 into Eq.(19). Second the great influence of the optimal grid movement on the reduction of the total FDE is obvious when compared to the fixed grid (Fig.(2-a)). The exact solution is obtained by combining the analytical solution from Table 2 with Eq.(18).
Fig.(3) shows the exact and numerical average number densities at the final time of simulation where, excellent agreement is perceptible. Also, one could see how the optimal moving grid leaves the

approximately empty intervals (large sizes) to accommodate the increasing number densities in the small size range as expected.
Fig.(4) depicts the sum of square errors (SSE), based on the difference between the exact and numerical solutions, as a function of time at different levels of discretization. The fixed and approximately optimal moving grids are compared such that the total FDE is negligible by extending the minimum and maximum droplet volumes to sufficiently small and large values (see Table 1). First grids of 10 pivots are used where it is clear that the fixed grid could cover the same domain spanned by the moving one only by having a geometric factor $\sigma = 6.28$.
This relatively large geometric factor increases the error of integration with respect to v due to the large intervals width and hence the SSE increases as the distribution becomes sharp (after long breakage time). If the geometric factor is to be kept constant at $\sigma = 2.5$ for the fixed as well as the moving grids, then we need approximately 20 pivots for the fixed grid to have approximately the same SSE as the moving one.
This will increase the computational time by about 40% when compared to case a (only 10 pivots) as is clear by referring to Table 1. This increase in the computational time is clearly due to the increase in the size of the system of ordinary differential equations (from 10 to 20). Similarly, if 15 pivots are used for both the fixed and moving grids the same trend is observed with the reduction of the SSE due to the small width of the intervals ($\sigma = 2$), and hence the integration error with respect to v.

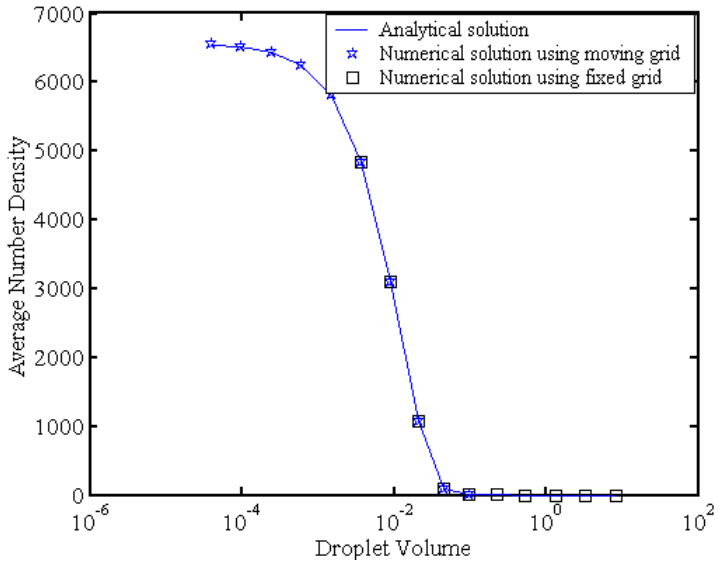

Fig.(3): The effect of the optimal grid movement on the average number density for droplet breakage in a batch vessel using a geometric grid with factor $\sigma = 2.5$, $M = 10$, binary breakage, $\Gamma = v$, $\beta(v|v') = 1/v'$, exponential initial condition, and $t = 80$.

In this case the fixed grid requires approximately 32 pivots to cover the same domain spanned by the moving grid ($M = 15$) with relative increase in the CPU time about 100% (see Table 1). However, by referring to Table 1, the relative increase in the computational time in the case of the moving grid technique due to the redistribution algorithm is only about 3.6% in both cases. This clearly shows the effectiveness of the approximate optimal moving grid technique particularly for long time breakage.
Fig.(5) shows the optimal moving and fixed grids and their corresponding pivots at the end of the simulation time. It is clear that the positions of the moving and fixed pivots are approximately the same for the case of moving grids. This is because as the grid moves it becomes finer, and hence the moving pivots approaches the fixed ones, which agrees with the condition implied by Eq. (49). However, in the case of the fixed grids with the same number of pivots, the fixed pivots are completely different from the moving ones particularly in the small size range due to the fixed width of the intervals as droplet breakage proceeds. This suggests that the solution of the PBE using the fixed pivot technique could be improved by using the present optimal moving grid.

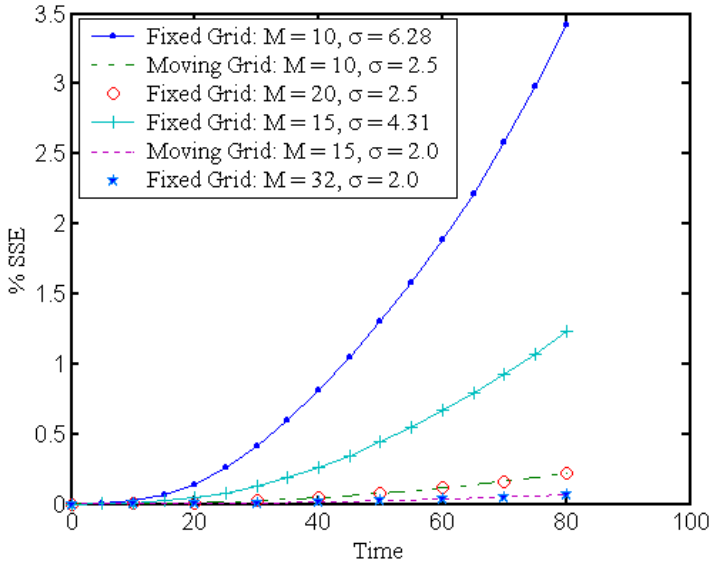

Fig.(4): The effect of the approximate optimal and fixed grids on the SSE using different levels of discretization for droplet breakage in a batch vessel with binary breakage, $\Gamma=v$, $\beta(v|v')=1/v'$, and exponential initial condition.

2.10.1.2 Case 2: Breakage with uniform daughter droplet distribution and $\Gamma(v) = v^2$

In this case, the rate of droplet breakage is proportional to the square of its volume. A close look at the time constants given by $\left|\lambda_i^b\right|^{-1}$ (i=1, 2,...M) indicates that droplets with volume less than one will show slower dynamics when compared with that having the same volume in case 1. On the contrary, droplets having volume greater than one will show faster dynamics when compared with that in case 1. Since the number density becomes skewed to the left as droplet breakage proceeds, slow dynamics will be dominant at long times. Due to this we have increased the simulation time to t=100.

Table 1: The CPU time requirements of the moving and fixed grids for droplet breakage in a batch vessel.

Case	$V_{min.}$	V_{M+1}	M	σ	% Increase in the CPU time relative to case A	% Time averaged relative error in:	
						M_0	$\bar{V}$
A1: Fixed Grid	2.16×10^{-7}	20.6	10	6.3	———	0.3000	0.0000
B1: Moving Grid	$v^*_{min.}(t)$	$v^*_{M+1}(t)$	10	2.5	3.59*	0.0976	0.0000
C1: Fixed Grid	2.16×10^{-7}	20.6	20	2.5	39.88*	0.0976	0.0000
A2: Fixed Grid	5.92×10^{-9}	19.4	15	4.3	———	0.1900	0.0000
B2: Moving Grid	$v^*_{min.}(t)$	$v^*_{M+1}(t)$	15	2.0	3.59*	0.0614	0.0000
C2: Fixed Grid	5.92×10^{-9}	19.4	32	2.0	99.35*	0.0604	0.0000

* The CPU times are estimated under MATLAB 6.1 environment using a PC Pentium III 750 MHz processor.

Fig.(6-a) shows how the optimal moving grid keeps the total FDE almost constant during the droplet breakage time. Moreover, the magnitude of the total FDE is considerably less than that in case 1 because of the non sharply increasing number density with time at the small size range (see Fig.(7)). As in case 1,

it is clear from Fig.(6-b) that the optimal moving grid technique produces an optimal piecewise constant minimum droplet volume that is in a good agreement with the exact one given in Table 3.

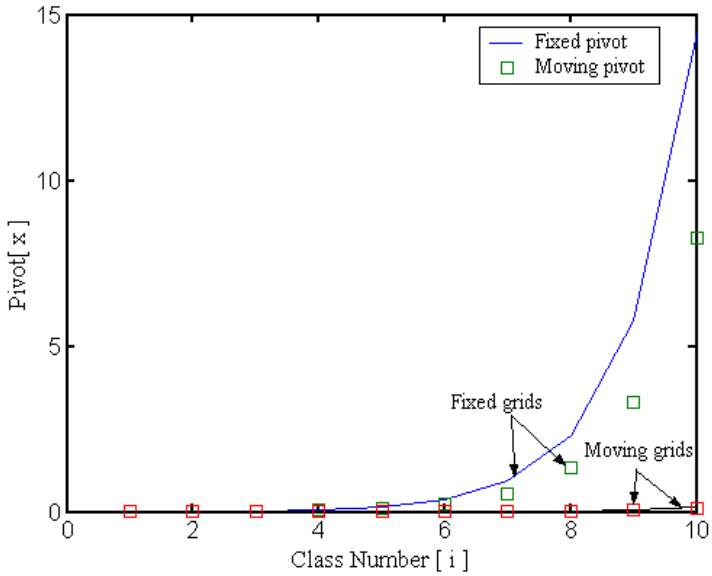

Fig.(5): The effect of the approximate optimal and fixed grids on the fixed and moving pivots at t=80 using a geometric grid with factor σ = 2.5, M = 10 for droplet breakage in a batch vessel with binary breakage, $\Gamma=v$, $\beta(v|v')=1/v'$, and exponential initial condition.

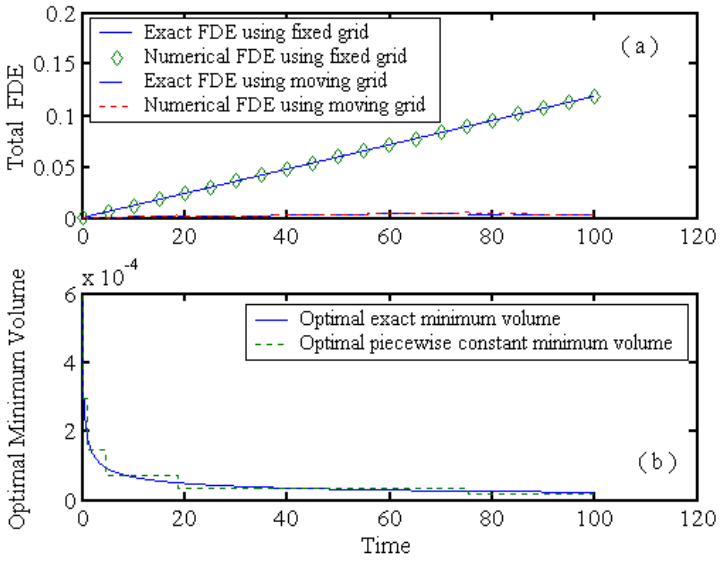

Fig.(6): a-The effect of the optimal grid movement on the total finite domain error. b- The approximate and exact optimal minimum droplet volume profiles for droplet breakage in a batch vessel using a geometric grid with factor σ = 2, M = 15, binary breakage, $\Gamma=v^2$, $\beta(v|v')=1/v'$, and exponential initial condition.

Fig.(7) shows the expected average number density for the analytical (see Table 2) and numerical solutions at the end of the simulation time. Due to the slow and fast dynamics in the small and large size ranges respectively; a sharp transition in the number density between these size ranges is encountered. Again it is evident how the approximate optimal moving grid leaves the almost empty intervals at the large size range to occupy the newly birthed population in the small size range.

Fig.(8) shows the behavior of the SSE as a function of time for this case using fixed and approximate optimal moving grids. The SSE using a fixed grid could only be reduced to that of the moving one (M=15) only by increasing the number of pivots to 25 with the same geometric grid factor σ = 2.0. This is will be at the expense of the computational time as is mentioned in case 1. In this case the value of the SSE is greater than that of case 1 due to the increasing sharpness of the number density at the transition region from the large to the small size range.

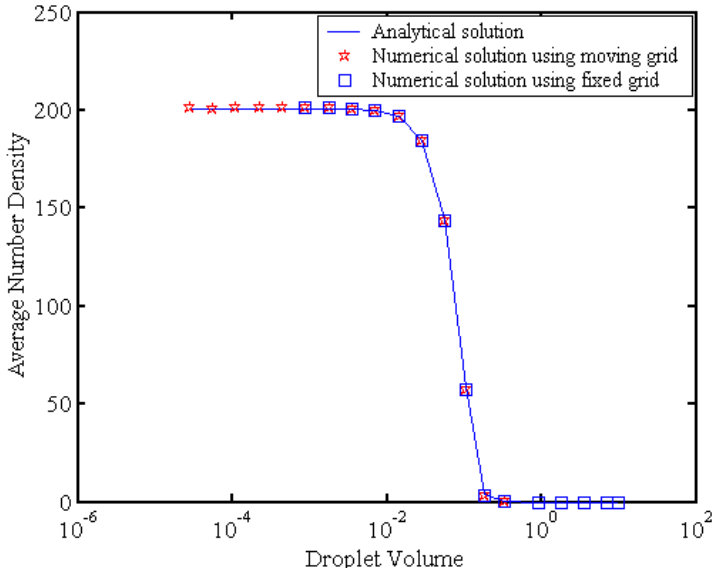

Fig.(7): The effect of the optimal grid movement on the average number density for droplet breakage in a batch vessel using a geometric grid with factor σ = 2, M = 15, binary breakage, $\Gamma=v^2$, $\beta(v|v')=1/v'$, and exponential initial condition.

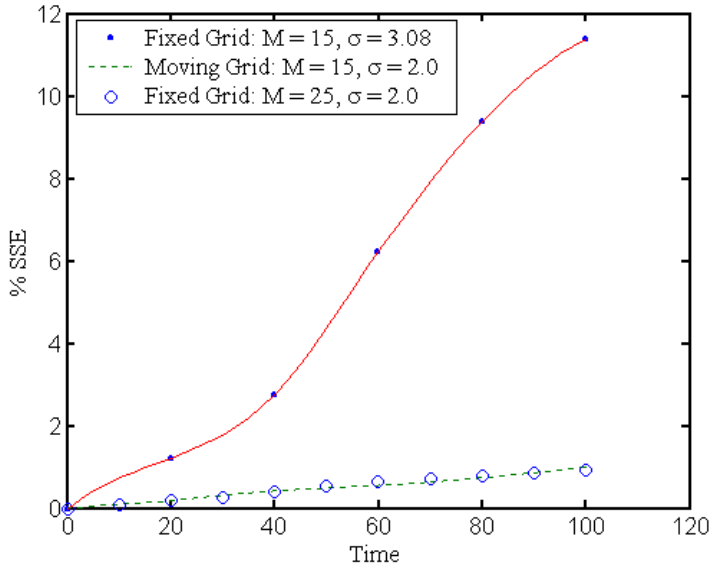

Fig.(8): The effect of the approximate optimal and fixed grids on the SSE using different levels of discretization for droplet breakage in a batch vessel with binary breakage, $\Gamma=v^2$, $\beta(v|v')=1/v'$, and exponential initial condition.

2.10.1.3 Case 3: Breakage with parabolic daughter droplet distribution and $\Gamma(v) = v$

In this case, where parabolic daughter droplet distribution is assumed (Hill & Ng, 1995), we have added one different aspect being $\beta(v \mid v')$ is no longer independent of the daughter droplet volume. Since the analytical solution is not available, comparisons are made between the fixed and optimal moving grid techniques. Fig.(9-a) shows how the optimal moving grid reduces the total FDE and keeps it almost constant. The optimal piecewise constant minimum droplet volume is shown in Fig.(9-b) as is expected. The average number densities for both fixed and moving grids are depicted in Fig.(10) at the final simulation time. It is evident how the optimal moving grid follows the sharp part of the distribution while leaving the almost empty size intervals. All the desirable advantages achieved in cases 1 and 2 are retained in this case, which consolidate one's faith in the optimal moving grid technique.

Table 2: Available analytical solution for droplet breakage in batch systems.

Case	$\beta(v \mid v')$	$\Gamma(v)$	$n(v,0)$	Analytical solution, $n(v,t)$	Reference
1	$\frac{2}{v'}$	v	e^{-v}	$(1+t)^2 e^{-v(1+t)}$	(Ziff and McGrady, 1985)
2	$\frac{2}{v'}$	v^2	e^{-v}	$[1+2t(1+v)]e^{-(tv^2+v)}$	Ziff, and McGrady, (1985)
3	$\frac{24(v^2 - vv') + 6v'^2}{v'^3}$	v	e^{-v}	Not available	(Hill and Ng, 1995)

2.10.2 Droplet breakage in continuous systems

In this section optimal geometric factors (and hence optimal grids) are found for a given number of intervals by solving the constrained nonlinear optimization problem given by Eq. (53). The breakage functions considered are linear breakage rate (k=1, m=1) and uniform daughter droplet distribution for the two cases studied where zero initial conditions are assumed in the vessel. All the numerical simulations are conducted using MATLAB software.

Table 3: Analytical optimal minimum droplet volume, continuous zero and first moments, mean droplet volume, and the total finite domain error for droplet breakage in batch systems

Case	$v^*_{\min.}(t)$	$M_0^c(t)$	$M_1^c(t)$	$\bar{v}^c(t)$	$\varepsilon_0(t)$
1	$\frac{(M-1)\ln(\sigma)}{(1+t)(\sigma^{M-1}-1)}$	$1+t$	1	$\frac{1}{1+t}$	$(1+t)\times$ $\left(1+e^{-(1+t)v_{\max.}} - e^{-(1+t)v_{\min..}}\right)$
2	$\frac{1+2t(1+v^*_{\min.})}{1+2t(1+v^*_{\max.})} -$ $\sigma^{M-1}\frac{e^{-(v^*_{\max.}+v^{*\,2}_{\max.}t)}}{e^{-(v^*_{\min..}+v^{*\,2}_{\min..}t)}} = 0$	$1+\sqrt{\pi t}e^{(\frac{1}{4t})}\times$ $\left[1-erf\left(\frac{1}{2\sqrt{t}}\right)\right]$	1	$\frac{1}{M_0^c(t)}$	$(1+e^{-(v_{\max.}+v^2_{\max}t)})+$ $\sqrt{\pi}e^{(\frac{1}{4t})}\times\left[\begin{array}{l}1+erf\left(\frac{2tv_{\min.}+1}{2\sqrt{t}}\right)\\ -erf\left(\frac{2tv_{\max.}+1}{2\sqrt{t}}\right)-erf\left(\frac{1}{2\sqrt{t}}\right)\end{array}\right]$
3	N.a.*	N.a.	1	N.a.	N.a.

* Not available.

2.10.2.1 Case 1: Exponential feed droplet distribution

In this case the initial condition is assumed zero and the feed distribution is exponential. Table 4 shows the derived analytical solutions for the zero and first moments of the distribution, as well as the mean droplet volume for this special case. The optimization problem (Eq. (53)) is solved using three different levels of discretization (M=15, 20, 25) to see their effect on the optimal geometric factor σ. The simulation time is chosen large enough (15τ) to insure that true final steady state is reached.

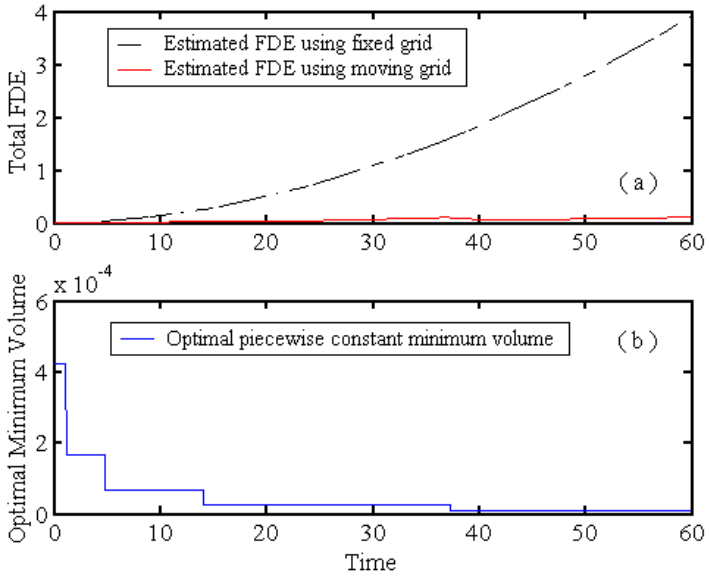

Fig.(9): a-The effect of the optimal grid movement on the total finite domain error. b- The approximate optimal minimum droplet volume profiles for droplet breakage in a batch vessel using a geometric grid with factor σ = 2.5, M = 12, binary breakage, $\Gamma=v$, $\beta(v|v')$=*parabolic,* and exponential initial condition.

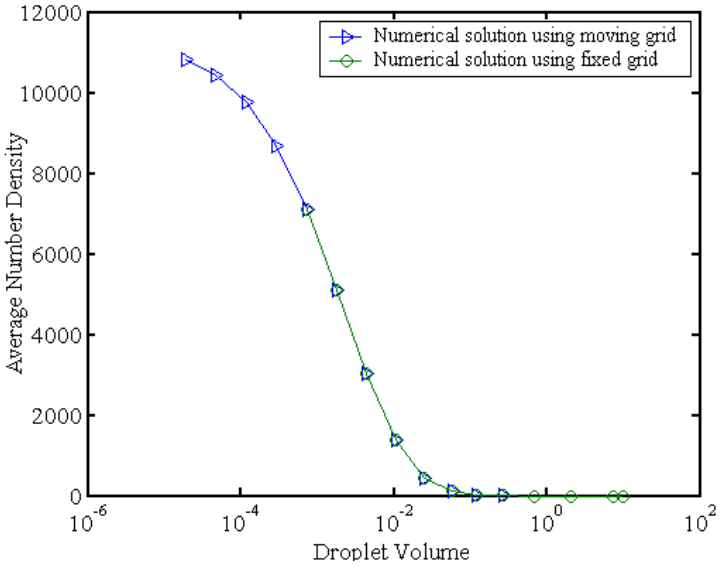

Fig.(10): The effect of the optimal grid movement on the average number density for droplet breakage in a batch vessel using a geometric grid with factor σ = 2.5, M = 12, binary breakage, $\Gamma=v$, $\beta(v|v')$=*parabolic,* and exponential initial condition.

The initial optimal fixed grid used in the simulation is constructed using the feed droplet distribution and the optimal condition given by Eq. (19). The resulting geometric grid has the property of being expanding in both directions as σ increases to cover the lower and upper size ranges. This type of grid results in a monotone increasing function represented by the sum: $(M_0^d + M_1^d)$, since the number and volume densities increases monotonically as a result of simultaneous decrease and increase of v_{min} and v_{max} respectively. So, the optimal values of σ are the minimum ones which make the time-averaged $(M_0^d + M_1^d)$ constants to a prescribed accuracy.

The numerical results are shown in Figs.(11) and (12). Fig.(11-a) shows the total zero and first moments of the distribution as function of the geometric factor at steady state. This Figure shows three distinctive features: the first is the sharp decrease in the steady state sum of the moments $(M_0^d + M_1^d)$ when the geometric factor is reduced below the optimal value, which is indeed equivalent to increasing the minimum droplet volume above the optimal one. This is equivalent to a sharp increase in the total FDE as it is evident from Eq. (52). This increase in the FDE is caused by the sharp increase in $v^*_{\min.}(0)$ as a result of decreasing σ according to Eq. (19).

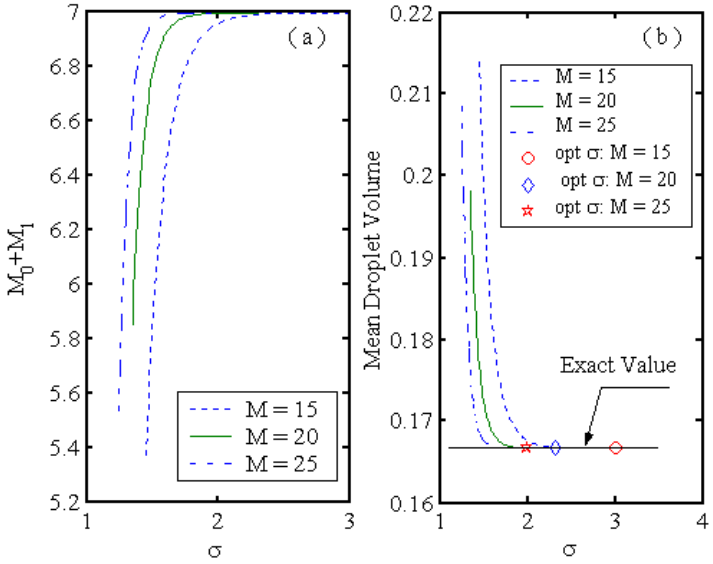

Fig.(11): Effect of the optimal geometric grid factor on: a-The steady state sum of zero and first moments of the distribution. b- The mean droplet volume for droplet breakage in a continuous vessel with $\Gamma=v$ and $\beta(v|v')=1/v'$, binary breakage, $\tau = 5$, and exponential feed distribution.

The second feature is that the optimal geometric factor decreases as the number of intervals increases (Fig.(11-b)), which is expected since small geometric factor requires large number of intervals to cover the required discretized domain. The third feature is that all the steady state values of $(M_0^d + M_1^d)$ are monotonically increasing where they become approximately identical and are slowly varying as the geometric factor is increased. This is again is attributed to the behavior of $v^*_{\min.}(0)$, where it decreases sharply as σ increases resulting in negligible lower and upper residuals.

Fig.(11-b) shows the significant effect of the choice of the geometric factor on the mean droplet volume of the distribution. It is clear how the optimal values of σ result in an excellent predictions of the mean droplet volume. It is also evident that a small error in choosing σ below the optimal value will lead to significant error in the mean droplet volume due to the significant loss of droplet volumes and numbers from both boundaries.

Fig.(12) shows the average number density at steady state as predicted using three fixed grids with optimal geometric factors. The results show how the numerical solution is very close to the exact one at steady state at the three levels of discretization using optimal geometric grid factors. Fig.(13) shows an excellent agreement between the analytical and numerical mean droplet volumes even in the presence of the jump occurring at t=0 due to the zero initial condition. Despite the small error involved in the

predicted number densities at low level of discretization (M=15), the numerical mean droplet volume is still in good agreement with the analytical one. This is natural since the present discretization technique preserves both total number and volume of the distribution.

2.10.2.2 Case 2: Monodisperse feed droplet distribution

In this case zero initial and monodisperse feed droplet distributions are used. The monodisperse feed distribution is mathematically represented by the Dirac delta function:

$$n^{feed}(v) = \delta(v - x_f) \tag{57}$$

McGrady and Ziff (1988) presented the analytical solution of a slight modified form of Eq. (1) for this case of droplet breakage in a continuous vessel. Table 4 shows the derived mean droplet volume, zero and first moments of the distribution.

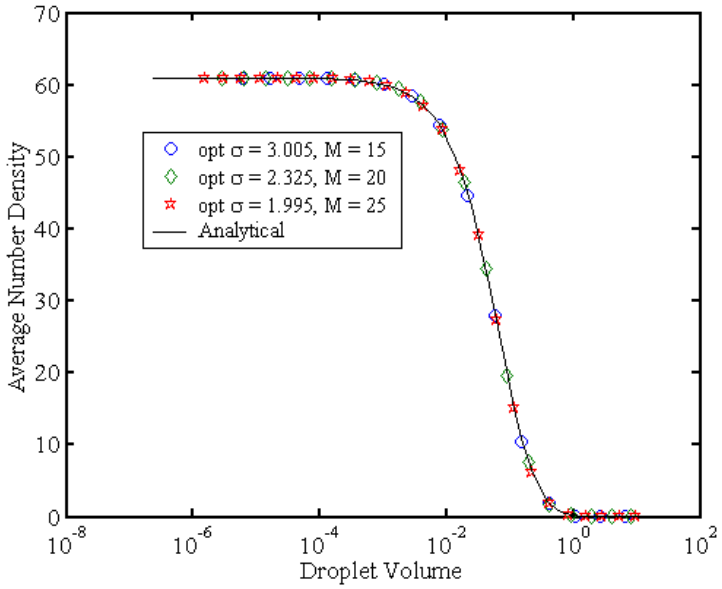

Fig.(12): Effect of the optimal geometric grid factor on the steady state number density for droplet breakage in a continuous vessel with $\Gamma = v$ and $\beta(v|v') = 1/v'$, binary breakage, τ = 5, and exponential feed distribution.

The discontinuous nature of the Dirac delta function imposes another difficulty when Eq. (57) is discretized. This function is approximated using the rectangular pulse function of unit area (Rice and Do, 1995; David et al., 1996):

$$N^{feed}(v - x_i) = \begin{cases} \dfrac{1}{\Delta v_f}, & v_f \le v < v_{f+1} \\ 0, & i \ne f \end{cases} \tag{58}$$

where f is the index of the interval containing the feed droplet volume, x_f.
However, still another difficulty is imposed by Eq. (58) since the geometric grid which, is relatively coarse in the upper size range, makes the approximation above inaccurate. Introducing a linear grid to just encompass the interval containing the feed droplet size, x_f, alleviates this problem. The accuracy of the approximation is improved by making the linear grid as fine as required.
The system of Eqs. (53) is solved with (x_f =2.0 as the maximum droplet volume) using three different levels of discretization to see how they affect the optimal gird geometric factor σ.

Table 4: Mean droplet volume, zero and first moments of the distribution for droplet breakage in continuous systems.

Case	$\beta(v \mid v')$	$\Gamma(v)$	$n^{feed}(v)$	$\bar{v}\ (t)$	$M_0(t)$	$M_1(t)$
1	$\frac{2}{v'}$	kv	e^{-v}	$\frac{M_1(t)}{M_0(t)}$	$c_2\tau\left(1-e^{-\frac{t}{\tau}}\right)+\left(M_0(0)+c_1 t\right)e^{-\frac{t}{\tau}}$ $c_1 = k\left(M_1(0)-M_1^{feed}\right)$ $c_2\tau = M_0^{feed}+kM_1^{feed}$	$M_1^{feed}+$ $\left(M_1(0)-M_1^{feed}\right)e^{-\frac{t}{\tau}}$
2	$\frac{2}{v'}$	kv	$\delta(v-x_f)$	$\frac{M_1(t)}{M_0(t)}$	$c_2\tau\left(1-e^{-\frac{t}{\tau}}\right)+\left(M_0(0)+c_1 t\right)e^{-\frac{t}{\tau}}$ $c_1 = k\left(M_1(0)-\tau M_1^{feed}\right)$ $c_2 = M_0^{feed}+k\tau M_1^{feed}$	$\tau M_1^{feed}+\left(M_1(0)-\tau M_1^{feed}\right)e^{-\frac{t}{\tau}}$

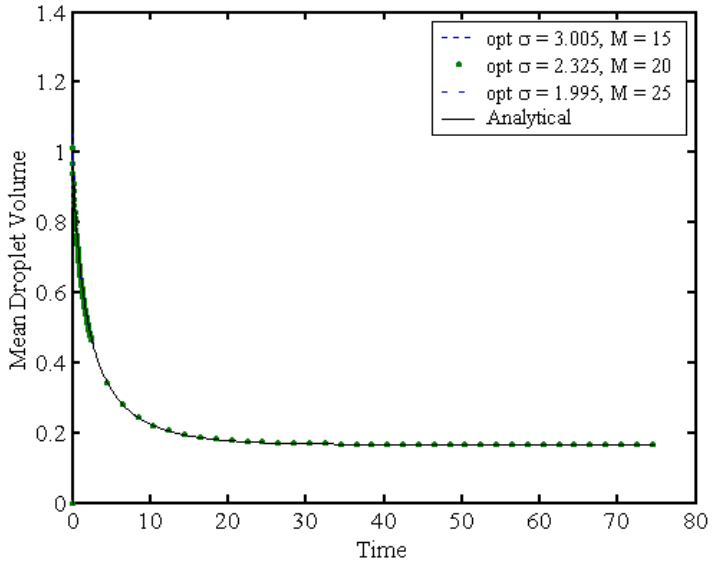

Fig.(13): Effect of the optimal geometric grid factor on the mean droplet volume for droplet breakage in a continuous vessel with $\Gamma=v$ and $\beta(v|v')=1/v'$, binary breakage, $\tau = 5$, and exponential feed distribution.

The simulation results are shown in Figs.(14), (15), and (16). In Fig.(14-a) the steady state ($M_0^d + M_1^d$) are plotted against the grid geometric factor, where as in case 1, sharp increase in the total FDE results for those slightly below the optimal values. However, it is clear that above certain values of σ the steady state ($M_0^d + M_1^d$) becomes constant for the three levels of discretization used. This simply means that the upper residual of the distribution has a constant zero value, and hence the lower residual controls the total FDE. This result is not surprising, since the upper value of the droplet volume is bounded by the size of the monodisperse feed, x_f. Since the number density vanishes for all $v>x_f$, it follows then that the upper residual of the distribution is always zero provided that $v_{max} \geq x_f$. In this case, the optimal values of σ are the minimum ones which make the time-averaged ($M_0^d + M_1^d$) constants to a prescribed accuracy and are shown in Fig.(14-b). This case actually isolates the effect of the lower distribution residual and shows clearly that it is the dominant part contributing to the total FDE as long as pure droplet breakage is considered. As in case 1, the sensitivity of the total FDE to the changes of σ and its subsequence effect on the steady state mean droplet volume is evident from Fig.(14-b).

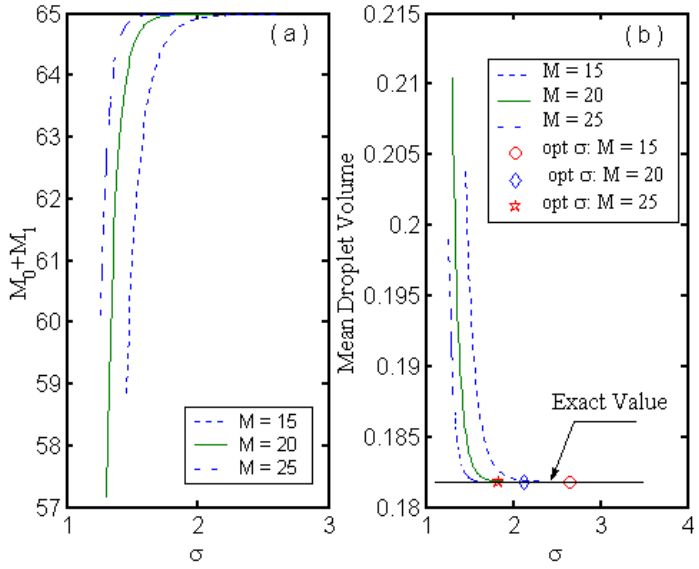

Fig.(14): Effect of the optimal geometric grid factor on: a- The steady state sum of zero and first moments of the distribution. b- The mean droplet volume for droplet breakage in a continuous vessel with $\Gamma=v$, $\beta(v|v')=1/v'$, binary breakage, $\tau = 5$, and monodispersed feed distribution.

This means that the moving pivot technique converges at a rate that is inversely proportional to the square of the number of pivots ($\propto 1/M^2$). The magnitude of the *SysErr* for the case of the monodisperse feed distribution is smaller than that of the exponential one due to the effect of the total FDE. In the case of the monodisperse feed, $v_{max} = x_f$ and hence the upper residual is zero resulting in a bounded domain from the upper size range. This bounded domain makes the size of the intervals smaller than the case of the unbounded one for the exponential feed distribution and hence reduces the *SysErr*. This is actually reflected by comparing the values of the optimal geometric grid factors for both cases (σ = 2.645 for monodisperse and σ = 3.005 for exponential feed distributions when M = 15).

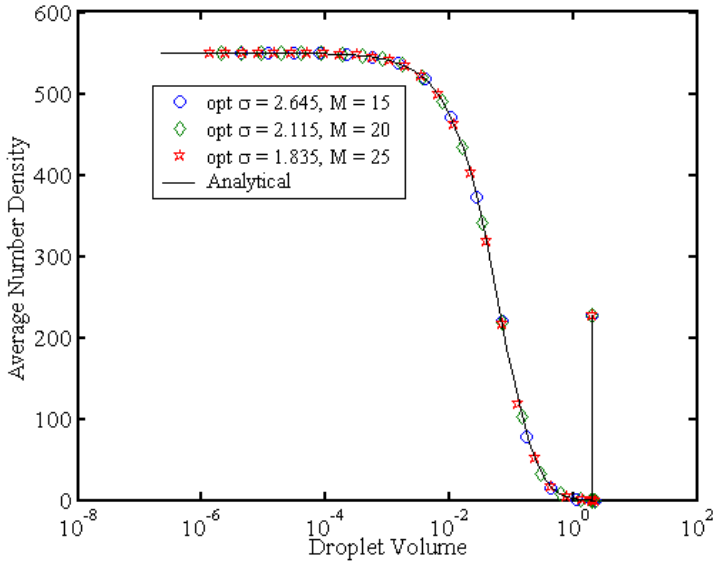

Fig.(15): Effect of the optimal geometric grid factor on the steady state number density for droplet breakage in a continuous vessel with $\Gamma=v$ and $\beta(v|v')=1/v'$, binary breakage, $\tau = 5$, and monodispersed feed distribution.

Fig.(15) shows the average number density at steady state as it is predicted along with the analytical solution using the optimal geometric grid factors shown in Fig.(14-b). It is obvious that the agreement between the analytical and the numerical solutions is excellent. It is also worthwhile to see how the discontinuity in the number density is correctly predicted by using a fine linear grid around it. Fig.(16) shows how the predicted mean droplet volume is very close to the analytical one during the simulation time at different optimal geometric grid factors. To get more insight into the convergence characteristics of the numerical solutions presented in Figs.(12), (13), (15), and (16), it is helpful to define the systematic error (*SysErr*) as the absolute difference between the exact and the numerical mean droplet volumes:

$$SysErr = \left| \overline{v}_{exac.} - \overline{v}_{num.} \right| \tag{59}$$

This is in fact is a suitable choice since it involves both the conserved total number and volume of the droplet distribution. Fig.(17) shows the *SysErr* for both cases plotted on a log-log scale versus the number of pivots (intervals). The numerical solutions for both cases (monodisperse and exponential feed distributions) converge at the same rate due to the similar form of the distributions as it is evident from Figs. 12 and 15 where the slopes of both lines are equal to 2.2.

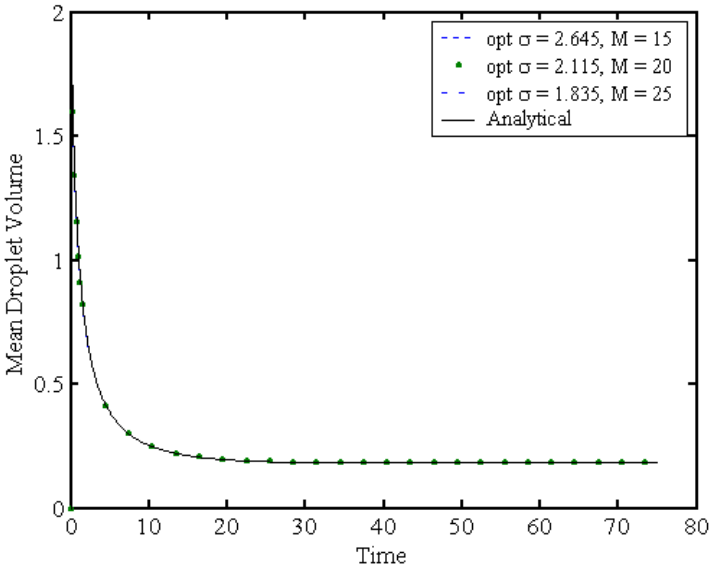

Fig.(16): Effect of the optimal geometric grid factor on the mean droplet volume for droplet breakage in a continuous vessel with $\Gamma=v$ and $\beta(v|v')=1/v'$, binary breakage, τ = 5, and monodispersed feed distribution.

2.11 Conclusions

- The moving pivot technique proposed by Kumar and Ramkrishna (1996b) is extended to continuous flow systems.
- The slow movement of the pivots for sufficiently fine grid makes possible the sequential solution of the number density and the pivot equations in time.
- Ordinary differential equations are derived to estimate the lower and upper residuals of the droplet distribution, which show excellent agreement with the analytical solutions studied in this work.
- An approximate optimal moving grid technique is developed for droplet breakage in batch systems where the sharply increasing number density is successfully tracked out. The redistribution algorithm, on which this technique is based, is consistent with DPBEs by preserving any two integral properties of the distribution.
- An optimal fixed grid that minimizes the time-averaged total finite domain error is also developed for continuous droplet breakage. This optimal grid represents a systematic

approach for the determination of the minimum and maximum droplet volumes instead of the trial and error procedures that are usually used. The numerical results show that the lower residual of the distribution is dominant and makes the total finite domain error sensitive to small changes in the grid geometric factor.

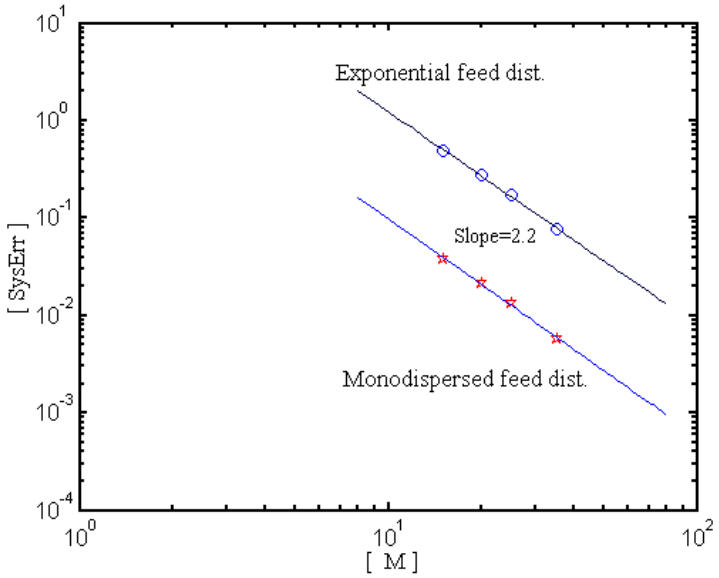

Fig.(17): The convergence characteristics of the moving pivot technique for droplet breakage in a continuous vessel with $\Gamma=v$ and $\beta(v|v')=1/v'$, binary breakage, and $\tau = 5$.

Nomenclature

$\boldsymbol{A}$	matrix for the number density equations as defined by Eq.(40)
$\boldsymbol{D}$	diagonal matrix whose elements are given by: $e^{\lambda_i^b t}$
FDE_0^L	lower residual based on the zero moment of the distribution as defined by Eq.(14)
FDE_1^L	lower residual based on the 1st moment of the distribution.
FDE_0^U	upper residual based on the zero moment of the distribution as defined by Eq.(15)
FDE_1^U	upper residual based on the 1st moment of the distribution.
$\boldsymbol{F}$	matrix for the pivot equations as defined by Eq.(41)
I_i	ith interval: $I_i=[v_i, v_{i+1})$
M	total number of intervals used in droplet volume discretization
M_0^c	zero moment of the continuous distribution
M_0^d	zero moment of the discrete distribution
M_1^c	first moment of the continuous distribution
M_1^d	first moment of the discrete distribution
$\boldsymbol{N(t)}$	vector whose ith component is the total number of droplets in the ith interval, at time t
$N_i(t)$	total number of droplets in the ith interval, at time t
N^{feed}	vector whose ith component is the total number of droplets in the ith interval for the feed
$\overline{N}_i(t)$	average discrete number density in the ith interval at time t.
$\overline{N}_i^{anal.}$	average discrete analytical number density in the ith interval defined by Eq.(55a)
$\overline{N}_i^{num.}$	average discrete numerical number density in the ith interval defined by Eq.(55b)
$n(v,t)dv$	number of droplets in size range v to $v+dv$, at time t
$\boldsymbol{R}$	matrix whose columns are the eigenvectors of the matrix $\boldsymbol{A}$
v, v'	droplet volumes
$v_{min.}, v_{max.}$	minimum and maximum droplet volumes
$v_{\min}^*, v_{\max.}^*$	optimal minimum and maximum droplet volumes
$\overline{v}$	mean droplet volume
$\dot{v}$	droplet growth rate
$x_i(t)$	characteristic volume of the droplet population in the ith interval as defined by Eq.(4)
SSE	sum of square of errors
t	time
t_0	initial simulation time
t_f	final simulation time

Greek Symbols

$\beta(v \mid v')dv$	fractional number of droplets formed in the size range v to $v+dv$ formed upon breakage of droplet of volume v'
$\Gamma(v)$	number of droplets in the size range v to $v+dv$ disappearing per unit time by breakage
$\gamma_i^{<i>}$	fraction of droplets at the pivot $x_i(t)$ that is assigned to the pivot x_i $(t+\Delta t)$ in the ith interval
$\Delta v(t)$	width of the ith interval, v_{i+1}-v_i, at time t
δ	Dirac delta function
ε_0(t)	total finite domain error based on zero moment of the distribution as defined by Eq.(18) (error of discretization)
ε_1(t)	total finite domain error based on 1st moment of the distribution as defined by Eq.(51) (error of discretization)
η_i	the ith eigenvalue of the matrix $\boldsymbol{F}$ as defined by Eq.(11)

λ_i^b	the *i*th eigenvalue of the matrix ***A*** for batch droplet breakage
λ_i^c	the *i*th eigenvalue of the matrix ***A*** as defined by Eq.(9) for continuous droplet breakage
$\pi_{0,i,k}$	as defined by Eq.(8)
$\pi_{1,i,k}$	as defined by Eq.(12)
σ	geometric grid factor
τ	vessel residence time
$\omega(v,v')$	coalescence frequency between two droplets of volumes v and v`
$\vartheta(v')$	average number of droplets produced when mother droplet of volume, v', is broken

References

Alopaeus, V., Koskinen, J. , & Keskinen, K. I. (1999). Simulation of population balances for liquid-liquid systems in a nonideal stirred tank. Part1 description and qualitative validation of model. *Chem. Engng. Sci.*, **54,** 5887-5899.

Bajpai, R. K., & Ramkrishna, D. (1976). A coalescence redispersion model for drop-size distribution in an agitated vessel. *Chem. Engng. Sci.*, **31,** 913-920.

Barone, J. P., Furth, W., & Loynaz, S. (1980). Simplified derivation of the general population balance equation for a seeded, continuous flow crystallizer. *Can. J. Chem. Engng.*, **58,** 137-138.

Blatz, P. J., & Tobolsky, A. V. (1945). Note on the kinetics of systems manifesting simultaneous polymerization-depolymerization phenomena. *J. Phys. Chem.*, **49,** 77-80.

Bleck, R. (1970). A fast, approximate method for integrating the stochastic coalescence equation. *J. Geophys. Res.*, **75,** 5165-5171.

David, R., Villermaux, J., Marchal, P. & Klein, J. P. (1991). Crystallization and precipitation engineering-IV. Kinetic model of adipic acid crystallization. *Chem. Engng. Sci.*, **46,** 1129-1136.

Eid, K., Gourdon, C., & Casamatta, G. (1991). Drop breakage in a pulsed sieve-plate column. *Chem. Engng. Sci.*, **46,** 1595-1608.

Garg, M. O., & Pratt, H. R. C. (1984). Measurement and modeling of droplet coalescence and breakage in a pulsed plate extraction column. *AIChE J.*, **30,** 432-441.

Gelbard, F., & Seinfeld, J. H. (1978). Numerical solution of the dynamic equation for particulate systems. *J. Comput. Phys.*, **28,** 357-375.

Gerald, C. F., & Wheatly, P. O. (1994). *Applied numerical analysis*. 5 ed. New York: Addison-Wesley Pub. Co.

Hill, P. J., & Ng, K. M. (1995). New discretization procedure for the breakage equation. *AIChE J.*, **41,** 1204-1216.

Hounslow, M. J. (1990). A discretized population balance for continuous systems at steady state. *AIChE J.*, **36,** 106-116.

Hounslow, M. J., Ryall , R. L. & Marshall, V. R., (1988). A discretized population balance for nucleation, growth, and aggregation. *AIChE J.*, **34,** 1821-1832.

Kostoglou, M., & Karabelas, A. J. (1994). Evaluation of zero order methods for simulating particle coagulation. *J. Colloid Interface Sci.*, **163,** 420-431.

Kumar, S., & Ramkrishna, D. (1996a). On the solution of population balance equations by discretization-I. A fixed pivot technique. *Chem. Engng. Sci.*, **51,** 1311-1332.

Kumar, S., & Ramkrishna, D. (1996b). On the solution of population balance equations by discretization-II. A moving pivot technique. *Chem. Engng. Sci.*, **51,** 1333-1342.

Kumar, S., & Ramkrishna, D. (1997). On the solution of population balance equations by discretization-III. Nucleation, growth and aggregation of particles. *Chem. Engng. Sci.*, **52,** 4659-4679.

Kumar, S., Kumar, R., & Gandhi, K. S. (1993). A new model for coalescence efficiency of drops in stirred dispersions. *Chem. Engng. Sci.*, **48,** 2025-2038.

Laso, M., Steiner, L., & Hartland, S. (1987). Dynamic simulation of liquid-liquid agitated dispersions-I. Derivation of a simplified model. *Chem. Engng. Sci.*, **42,** 2429-2436.

Lister, J. D., Smit, D. J., & Hounslow, M. J. (1995). Adjustable discretized population balance for growth and aggregation. *AIChE J.*, **41,** 591-603.

Marchal, P., David, R., Klein, J. P., & Villermaux, J. (1988). Crystallization and precipitation engineering-I. An efficient method for solving population balance in crystallization with agglomeration. *Chem. Engng. Sci.*, **43,** 59-67.

McGrady, E. D., & Ziff, R. M. (1988). Analytical solutions to fragmentation equation with flow. *AIChE J.*, **34,** 2073-2076.

Mickley, H. S., Sherwood, T. S., & Reed, C. E. (1990). *Applied Mathematics in Chemical Engineering*. New Delhi: McGraw-Hill Pub. Co.

Milton, J. S., & Arnold, J. C. (1990). *Introduction to probability and statistics*. Second Edition, New York: McGraw-Hill Pub. Co.

Nicmanis, M. , & Hounslow, M. J. (1998). Finite-element methods for steady-state population balance equations. *AIChE J.*, **44,** 2258-2272.

Podgorska, W., & Baldyga, J. (2001). Scale-up effects on the drop size distribution of liquid-liquid dispersions in agitated vessels. *Chem. Engng. Sci.*, **56,** 741-746.

Hill, P. J., & Ng, K. M. (1995). New discretization procedure for the breakage equation. *AIChE J.*, **41,** 1204-1216.

Ramkrishna, D. (1985). The status of population balances. *Rev. Chem. Engng.*, **3,** 49-95.

Ramkrishna, D. (2000). *Population Balances*. San Diego: Academic Press.

Ribeiro, L. M., Regueiras, P. F. R., Guimaraes, M. M. L., Madureira, C. M. C., & Cruz-Pintu, J. J. C. (1995). The dynamic behavior of liquid-liquid agitated dispersions-I. The hydrodynamics. *Computers Chem. Engng.*, **19,** 333-344.

Rice, G. R., & Do, D. D. (1995). *Applied mathematics and modeling for chemical engineers*. New York: John Wiley and Sons, Inc.

Scott, W. T. (1968). Analytical studies in cloud droplet coalescence I. *J. Atmos. Sci.*, **25,** 54-65.

Sovova, H., & Prochazka, J. (1981). Breakage and coalescence of drops in a batch stirred vessel-I Comparison of continuous and discrete models. *Chem. Engng. Sci.*, **36,** 163-171.

Tsouris, C., & Tavlarides, L. L. (1994). Breakage and coalescence models for drops in turbulent dispersions. *AIChE J.*, **40,** 395-406.

Valentas, K. J., & Amundson, A. R. (1966 a). Breakage and coalescence in dispersed phase systems. *Ind. Engng. Chem. Fundam.*, **5,** 533-542.

Valentas, K. J., Bilois, O., & Amundson, A. R. (1966 b). Analysis of breakage in dispersed phase systems. *Ind. Engng. Chem. Fundam.*, **5,** 271-279.

Vigil, R. D., & Ziff, R. M. (1989). On the stability of coagulation-fragmentation population balances. *J. Colloid Interface Sci.*, **133,** 257-264.

Ziff, R. M. (1991). New solutions to the fragmentation equation. *J. Phys. A: Math. Gen*., **24**, 2821-2828

Ziff, R. M. & McGrady, E. D. (1985). The kinetics of cluster fragmentation and depolymerisation. *J. Phys. A: Math. Gen*., **18**, 3027-3037

CHAPTER 3

Solution of the Droplet Breakage Equation for Interacting Liquid-Liquid Dispersions: A Conservative Discretization Approach

3.1 Introduction

The population balance approach is now being successfully used to model the complex behavior of the dispersed phase in many of the chemical processes taking place in liquid systems. In these systems the population of droplets are considered to lose their identity due to many stochastic events and hence the internal properties (coordinates) of these droplets (such as size, concentration, age, … etc.) are subject to inevitable changes during a given residence time period. These changes are due to the entry and exit events (for continuous flow systems), droplet breakage resulting from the interaction of a single liquid droplet and the turbulent continuous phase as well as the interaction of the continuous phase and any two droplets through coalescence. After a sufficiently long period of time, equilibria is reached between these events that result in a steady state distribution with respect to certain internal droplet coordinates such as size or concentration. Among these distributions is the droplet size distribution, which is very important in determining the total interfacial area that should be made available to mass and heat fluxes calculations. A conservation law that is able to describe such a complex behavior and hence the evolution of the droplet size distribution of the dispersed phase is the population balance equation (PBE). This PBE could be written for a continuous flow system as follows (Randolph and Larson, 1988; Ramkrishna, 2000):

$$\frac{\partial n(z,t)}{\partial t} + \nabla \bullet \left(\frac{dz_i}{dt} \cdot n(z,t) \right) = \frac{1}{\tau} \left(n^{feed}(z,t) - n(z,t) \right) + \rho[\{n(z,t)\}; z, t] \tag{1}$$

where $n(z,t)$ is the average number of droplets per unit volume of the droplet phase space at location z and the time instant t. The independent variable, z, is a vector of the droplet internal coordinates (z_i) such as droplet size, concentration, …etc. and its external coordinates (spatial location). In the differential phase space z to $z+dz$, the first term on the left hand side of Eq. (1) represents the accumulation rate of the number of droplets, while the second term is the convective rate along the droplet internal coordinates. The first term on the right hand side represents the net rate of the number of droplets per unit volume crossing the boundary of the continuous flow system in a specified residence time, τ. While the second term on the right hand side represents the net rate of number of droplet generation ρdz per unit volume due to droplet breakage and coalescence.

Despite the importance of Eq. (1), it rarely has an analytical solution due to the relatively complex form of the source term, ρ, which has integral terms as we will show below. However, a few analytical solutions exist for a simple set of breakage and feed distribution functions where the convection term is neglected (McGrady & Ziff ,1988; Nicmanis & Hounslow, 1998). In general for realistic modeling of the breakage and coalescence phenomena it is not possible to find a general analytical solution, and hence a numerical approximation is sought.

Accordingly, the underlying idea of this work is to present a general, detailed and conservative (by conserving any two integral properties associated with the number distribution) discretization approach to solve numerically the PBE for droplet breakage describing the hydrodynamics in a perfectly mixed continuous flow vessel. However, the generality of the approach does not restrict it to this type of process and it could be easily coupled with a suitable discretization approach such as the fixed-pivot technique of Kumar and Ramkrishna (1996a) for droplet coalescence. Special attention will be paid to the dynamic evolution of the droplet size distribution and it will be validated analytically by presenting two analytical

dynamic solutions of the problem in hand through converting the integro-partial differential equation (IPDE) into an ODE with respect to the droplet size. Moreover, various combinations of the experimentally validated breakage functions from the published literature are used to assess the present approach.

This chapter is organized as follows: We start by simplifying Eq. (1) to match our objectives stated in this work followed by a review of the previous work that is interrelated to the present discretization approach. The subdomain method (Rice & Do, 1995) will be then introduced to project the IPDE into a system of ODEs where we will show that these discrete equations are internally consistent (Ramkrishna, 2000) only with respect to one integral property associated with the number distribution. The internal consistency will be extended to include any two integral properties of the number distribution using the approach of Kumar and Ramkrishna (1996a) and the present approach with certain emphases on the concept of the intrinsic discretization error. The present discretization approach will then be validated through introducing two analytical solutions of Eq. (1) followed by two realistic case studies to assess the reliability of the approach. The convergence and the performance of the approach and the conclusions drawn from the numerical simulations will be presented at the end of the paper.

3.2 The PBE for droplet breakage

In the present work we confine ourselves only to the hydrodynamic behavior of completely mixed continuous flow systems and the droplet convective rate is neglected (in the absence of mass transfer). Moreover, among the aforementioned stochastic events the droplet coalescence could be neglected at low concentration of the dispersed phase (lean dispersions) and hence droplet breakage is said to be dominant (Shah and Ramkrishna, 1973). These assumptions simplify Eq. (1) to:

$$\frac{\partial n(v,t)}{\partial t} = \frac{1}{\tau}\left(n^{feed}(v,t) - n(v,t)\right) - \Gamma(v)n(v,t) + \int_{v}^{v_{\max}} \Gamma(v')\beta_n(v \mid v')n(v',t)dv' \tag{2}$$

where v is the droplet volume, Γ is the breakage frequency and β_n is the number distribution of the daughter droplets resulting from the breakage of a mother droplet of volume v'. This distribution should satisfy the following two constraints (Ziff, 1991; Ramkrishna, 2000):

$$\int_0^{v'} \beta_n(v \mid v')dv = \vartheta(v') \tag{3}$$

$$\int_0^{v'} v\beta_n(v \mid v')dv = v' \tag{4}$$

where the first constraint conserves the average number of daughter droplets and the second one conserves exactly the volume upon the breakage of a mother droplet of volume v'. Normally, the droplet internal coordinate is chosen as the droplet diameter instead of volume as appears in Eq. (2). However, it is simpler to discretize the PBE in terms of droplet volume rather than diameter and then the discrete ODEs will be projected onto the droplet diameter coordinate.

The initial condition for the PBE equation, Eq. (2), is given by some initial distribution of the dispersed phase droplets $n_0(v)$ such that:

$$n(v,0) = n_0(v) \tag{5}$$

The boundary or the regulatory conditions for Eq.(2) could be obtained by considering the minimum and maximum droplet sizes prevailing in the interacting liquid-liquid dispersion at a given turbulent energy dissipation and physicochemical properties. The maximum droplet size is needed such that negligible distribution of the droplets above this size exists. This could be estimated in terms of droplet diameter from the following correlation (Tsouris & Tavlarides, 1994):

$$d_{\max} = c_m\left(\frac{D_R}{We^{0.6}}\right)\left(1 + 2.5\phi\frac{\mu_d + 0.4\mu_c}{\mu_d + \mu_c}\right)^{1.2} \tag{6}$$

where c_m is a constant whose accepted value is 0.125, We is the Weber number, ϕ is the dispersed phase hold up in the vessel, and μ_c and μ_d are the viscosities of the continuous and the dispersed phases respectively. Actually, this correlation predicts the maximum droplet diameter that is prevailing in the turbulent dispersion inside the vessel. So, if larger droplet diameter than that predicted using Eq. (5) is fed into the vessel, then the following boundary condition takes it into account:

$$n(v > \max(v_{\max}, v_{\max}^{feed}), t) = 0 \tag{7}$$

The minimum droplet size could be estimated if the assumption of a local dynamic equilibrium between breakage and coalescence is established. Accordingly, the droplets having diameter larger than d_{max} will break up and that smaller than d_{min} will coalesce. Based on this, Liu and Li (1999) derived an expression for the estimation of the minimum droplet diameter:

$$d_{\min} = \left(\frac{\gamma^{1.38} B^{0.46}}{0.0272 \mu_c \rho_c^{0.84} \varepsilon^{0.89}} \right)^{\frac{1}{3.11}} \tag{8}$$

where B is the London-van der Waals constant and ε is the energy dissipation. Since the coalescence is assumed to be negligible in this work, it is expected that d_{min} will be smaller than that predicted using Eq.(8). Moreover, if the minimum droplet diameter of the droplets fed to the vessel is less than that estimated from Eq.(8), then we could apply the following boundary condition at the small size range:

$$n(v < \min(v_{\min}, v_{\min}^{feed}), t) = 0 \tag{9}$$

Anyhow, the above relations will be very useful for initial estimations but the actual values of d_{min} and d_{max} will be estimated in the next sections based on the minimization of the total finite domain error (FDE) (Attarakih , Bart & Faqir, 2003a).

3.3 Previous Work

Many discretization techniques are proposed in the literature to approximate the PBE given by Eq.(2). These approximate methods could be categorized into two broad classes: zero and high order methods. In the first category the droplet internal coordinate (size) is divided into many intervals (classes) and the population in each interval is considered to behave like a concentrated single droplet (Nambiar et al., 1992; Hill & Ng, 1995; Kronberger, 1995; Kaumar & Ramkrishna, 1996a, b; Ramkrishna, 2000; Vanni, 1999, 2000). The second category approximates the size distribution function within each interval by a higher order polynomial (usually cubic) at certain nodal points at which the exact solution is approximated based either on the orthogonal collocation or the Galarkin methods. Although these methods are more accurate, they are expensive from the computational point of view and sometimes suffer from stability problems particularly when convection along the droplet internal coordinate is considered (Nicmanis & Hounslow, 1998; Mahoney & Ramkrishna, 2002). Several comprehensive reviews concerning the discretization techniques for the approximation of the PBE are available (Ramkrishna, 1985; Kostoglou & Karabelas, 1994; Kumar & Ramkrishna, 1996a; Vanni, 2000). The zero order methods could be further classified into three groups: the first two groups are classified according to the work of Kumar and Ramkrishna (1996a) depending on the way of closing the resulting set of equations due to discretization. The first class of this group is due to Gelbard et al. (1980) where they applied the mean value theorem of integrals on the number density function. The resulting discrete equations are a set of ODEs with many double integrals appearing inside the summations. These double integrals are considered to be computationally expensive especially when real time dependent breakage functions are encountered. The original work of these authors is only recently extended to droplet breakage by Vanni (2000). Beside the inefficiency due to the evaluation of the double integrals in each interval, the approach suffers from its conservation only of one integral property associated with the number distribution making it less accurate as pointed out by Gelbard et al. (1980), Kumar and Ramkrishna (1996a), and Vanni (2000). Kronberger et al. (1995) used the Galerkin method with a set of zero order polynomials as the test and trial functions. Although the method is computationally attractive for a few time independent breakage and coalescence functions, it places a heavy computational load for

such real time dependent functions. Moreover, the method is only consistent with respect to the conservation of the total droplet volume and the evaluation of the double integrals may encounter singularity problems as pointed out by Kronberger (1995) and Mahoney and Ramkrishna (2002). Through applying the mean value theorem of integrals on the breakage/coalescence frequency, the second class of methods is laid down by Kumar and Ramkrishna (1996a) to obtain a closed set of ODEs. The resulting method is free of evaluation of the double integrals in each interval. This approach is called the fixed-pivot technique and has the advantage of being flexible to conserve any two integral properties associated with the number distribution. Vanni (2000) showed that this technique offers a robust and versatile solver for the PBE by applying it successfully to 11 case studies. Attarakih et al. (2003b) has generalized the fixed-pivot technique to solve numerically the PBE describing the hydrodynamics in differential liquid-liquid contactors. The present authors exploited the special structure of this technique to decouple the time dependent variables from the breakage and coalescence frequency functions by introducing the idea of breakage and coalescence matrices. This makes it possible to generate these matrices off-line and only once a time thus reducing dramatically the computational time particularly when the sparse structure of the coalescence matrix is taken into consideration.

Within the same framework, Kumar and Ramkrishna (1996b) developed a more accurate approach than the fixed-pivot technique, which they called the moving-pivot technique. The technique has the advantage of conserving any two specific integral properties by simultaneously solving, for example, the number and the volume (mass) balances. These equations are coupled through the representative droplets volumes, which are allowed to move to satisfy both balances. The technique was tested only for droplet coalescence in a batch vessel and the numerical results showed a superior performance when compared to the fixed-pivot technique. However, it is only recently that the moving-pivot technique for droplet breakage was tested and extended to continuous flow systems by Attarakih, Bart and Faqir (2002, 2003a,b). In spite of its remarkable accuracy the technique has a drawback of being computationally expensive due to the continuous change of the droplet representative sizes and hence calls for repeated evaluations of the breakage and coalescence functions. Ribeiro et al. (1995) introduced a simple first order finite difference scheme for the discretization of the PBE in a continuous flow vessel. The algorithm introduced could be considered as a special case of the Galerkin method described above where the rectangular rule of integration is used to evaluate the resulting integrals. The resulting discrete set of equations could not be considered consistent with respect to any of the droplet distribution integral properties and so it is expected to converge slowly toward these properties.

The third group of the zero order methods represents an attempt to obtain a set of discrete ODEs from the continuous PBE by forcing these equations to conserve total droplet volume (mass) and number simultaneously. Hounslow, Ryall, and Marshall (1988) presented a zero discretization approach to discretize the PBE for droplet coalescence and growth by considering all the possible events leading to birth and death of the droplets (particles) in each interval. The discrete population balance appears to correctly conserve the total number of the droplets but not the total droplets volume. To circumvent this problem, the authors introduced a volume correction factor that appears fortunately independent of coalescence frequency function. The major drawback of this approach is in its fixed geometric grid structure and thus making it not amenable to grid refinement. Moreover, Hounslow's approach is not extendable to droplet breakage due to its dependence on the specific nature of the coalescence PBE. Lister, Smit, and Hounslow (1995) generalized Hounslow's approach to accommodate a variable geometric factor and hence increased its accuracy and flexibility. Hill and Ng (1995) followed Hounslow's approach to discretize the PBE for droplet breakage by trying to conserve the total droplet number and volume. The major flaw of this approach is its dependence on the form of the breakage frequency and on the type of the grid structure and hence making it impossible to be automated. Vanni (1999) tried to resolve this problem by introducing two correction factors to the discrete set of the PBEs to account for the errors resulting from the intra-interval interactions caused by the overlap of the birth and death events in the same interval or size range (Hill & Ng, 1995; Kumar & Ramkrishna, 1996a). These factors are determined in such a way to conserve the total droplet volume and to correct the death term due to the intra-interval problem. The approach was shown to be less accurate than that of Hill and Ng (1995) by comparing its performance using two simple case studies with known analytical solutions. Vanni (2000) had also showed that the combination of this approach for droplet breakage and Lister, Smit, and Hounslow (1995) approach for droplet coalescence is less accurate than the approach of Kumar and Ramkrishna (1996a). The approach is considered numerically inefficient when compared to the fixed pivot technique due to the double integrals appearing in the discretized PBE. Moreover, the approach does not guarantee that the zero moment of the distribution obtained from the discrete set of equations is the same as that obtained from the continuous PBE and hence it is considered internally inconsistent. What we mean by the internal consistency is the following: *the discretized PBE is considered to be*

internally consistent if any integral property associated with the population density derived from it is exactly the same as that derived from its continuous counterpart (Ramkrishna, 2000). This specific internal consistency with respect to a certain number of integral properties is shown to improve the accuracy of the predicted droplet distribution and its associated total properties (Hill & Ng, 1995; Kumar & Ramkrishna, 1996a; Attarakih, Bart & Faqir, 2003a).
The forgoing brief review of the relevant discretization methods elucidates the practical importance of the zero order methods conserving any two integral properties associated with the droplet distribution and at the same time are independent of the grid structure. In the following section we will present a rigorous mathematical background for the zero order methods of discretization based on the subdomain method (Rice & Do, 1995). This is because all the aforementioned zero-order methods suffer from the lack of a general derivation approach except that introduced by Kronberger (1995).

3.4 Discretization of the PBE using the subdomain method

The method of weighted residuals has been extensively used in solving the boundary value problems and as a particular case the PBE (Gelbard & Seinfeld, 1978; Kronberger et al., 1995; Nicmanis & Hounslow, 1998; Mahoney & Ramkrishna, 2002). Most of these applications of the weighted residuals use either the Galerkin or the orthogonal collocation methods on finite elements using higher order polynomials of degree three which will not be considered in this work. Since we are concerned with the zero order methods in this chapter, the subdomain method as a variation on the theme of weighted residuals will be used. The choice of this method, with the Dirac delta function and the unit step function as the trial and test functions respectively, has a decisive role in eliminating the appearance of the computationally expensive double integrals in the discrete set of the resulting ODEs. However, before we proceed to describe the subdomain method, we have to generalize the PBE given by Eq.(2) to accommodate any quantity of interest, u_m, that is associated with the droplet distribution *n(v,t)* such as droplet volume, for example. This generalization could be done by multiplying both sides of Eq.(2) by u_m and making the necessary transformation to get (Kumar & Ramkrishna, 1996b):

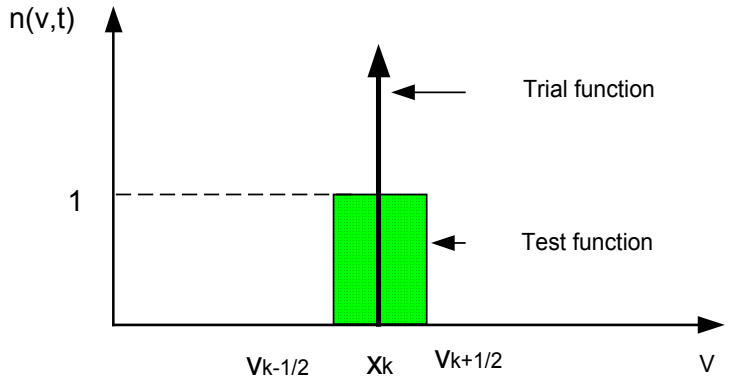

Fig. (1): The subdomain method: trial and test functions.

$$\frac{\partial F(v,t)}{\partial t}=\frac{1}{\tau}\left(F^{feed}(v,t)-F(v,t)\right)-\Gamma(v)F(v,t)+\int_{v}^{v_{\max}}\Gamma(v')\left[\frac{u_m(v)}{u_m(v')}\right]\beta_n(v\,|\,v')F(v',t)dv' \tag{10}$$

where *F(v,t)* is defined as:

$$F(v,t)=u_m(v)n(v,t) \tag{11}$$

To project the IPDE given by Eq.(10) into a finite set of ODEs, we discretize the droplet internal coordinate, *v*, according to the following discrete set : $\{v_{i-1/2}\,|\,i=1,\ ....\ M_x+1\}$ with $v_{\min}=v_{1/2}<v_{3/2}<...<v_{M_x+1/2}=v_{\max}$. Let the *k*th subdomain be defined as $V_k=[v_{k-1/2},v_{k+1/2}),\ k=1,...M_x$

and the population of the *k*th subdomain be concentrated at the middle of this subdomain such that $x_k = \left(v_{k-1/2} + v_{k+1/2}\right)/2$ (see Fig. (1)).

Then the droplet size distribution is expanded using a point wise sampling of the distribution at the middle of the *k*th subdomain (also called the pivot) according to the following relation (this is called the trial function):

$$F^a(v,t) = \sum_{k=1}^{M_x} F_k(t)\delta(v - x_k) \tag{12}$$

where δ refers to the Dirac delta function and the set of the unknown coefficients, $F_k(t)$, refer to the total quantity of droplets in the *k*th subdomain and are given by:

$$F_i(t) = \int_{v_{i-1/2}}^{v_{i+1/2}} u_m(v)n(v,t)dv = u_m(x_i)N_i(t) \tag{13}$$

To proceed further, we choose the test function for the method of weighted residuals as a unit step function in the *k*th subdomain (see Fig.(1)) such that:

$$w_k = \begin{cases} 1, \ if \ v_{k-1/2} \le v < v_{k+1/2} \\ 0, \ otherwise \end{cases} \tag{14}$$

Now let us define the linear breakage operator as (McGrady & Ziff, 1988):

$$B_o\left\{v, F(v,t)\right\} = -\Gamma(v)F(v,t) + \int_v^{v_{\max}} \Gamma(v')\left[\frac{u_m(v)}{u_m(v')}\right]\beta_n(v \mid v')F(v',t)dv' \tag{15}$$

Accordingly Eq.(10) could be rewritten as:

$$L\left\{v, F(v,t)\right\} = \frac{\partial F(v,t)}{\partial t} - \frac{1}{\tau}\left(F^{feed}(v,t) - F(v,t)\right) - B_o(v, F(v,t)) = 0 \tag{16}$$

where we defined $L\{v,F(v,t)\}$ as some differential operator. The right hand side of Eq.(16) will never be satisfied by substituting $F^a(v,t)$ from Eq.(12) into Eq.(16) since the trial function is only approximation to the exact solution $n(v,t)$. This approximation will result in a nonzero residual that has to be minimized over the whole domain of interest: $v \in [v_{min}, v_{max}]$ since the distribution function $n(v,t)$ and so $F(v,t)$ is assumed to vanish for all v outside the interval $[v_{min}, v_{max}]$ according to the boundary conditions given by Eqs.(7) and (9). This minimization of the residual is accomplished by multiplying Eq.(16) by the test function, Eq.(14), and integrating the result with respect to v over the interval $[v_{min}, v_{max}]$ as follows:

$$\int_{v_{\min}}^{v_{\max}} w_k(v)L\left\{v, F^a(v,t)\right\}dv = \sum_{i=1}^{M_x}\int_{v_{i-1/2}}^{v_{i+1/2}} w_k(v)L\left\{v, F^a(v,t)\right\}dv = 0 \tag{17}$$

Now, Eq.(17) could be further simplified by substituting Eqs.(14), (15), and (16) into Eq.(17) and after some algebraic manipulation we get:

$$\frac{dF_i(t)}{dt} = \frac{1}{\tau}\left(F_i^{feed}(t) - F_i(t)\right) - \Gamma(x_i)F_i(t) + \sum_{k=i}^{M_x}\Gamma(x_k)F_k(t)\int_{v_{i-1/2}}^{\min(x_k, v_{i+1/2})}\left(\frac{u_m(v)}{u_m(x_k)}\right)\beta_n(v \mid x_k)dv \tag{18}$$

This equation is exactly the same as that obtained by Kumar and Ramkrishna (1996b) and Ramkrishna (2000) using a completely different approach of derivation (the moving pivot technique for example). Since in many practical situations we are interested in targeting our discrete equations toward the calculation of some total (integral) properties associated with the number density, then it could by shown that the above equation is only consistent with respect to conserving only one such total property. This fact will be shown by first calculating the integral property of the quantity, u_m, from the continuous PBE

given by Eq.(10) by integrating its both sides with respect to v over the interval $[v_{min},v_{max}]$ and after some algebraic manipulations one could obtain:

$$\frac{dF(t)}{dt}=\frac{1}{\tau}\left(F^{feed}(t)-F(t)\right)+\int_{v_{\min}}^{v_{\max}}\Gamma(v')F(v',t)dv'\left(\int_0^{v'}\left[\frac{u_m(v)}{u_m(v')}\right]\beta_n(v\mid v')dv-1\right) \tag{19}$$

where :

$$F(t)=\int_{v_{\min}}^{v_{\max}}u_m(v)n(v,t)dv \tag{20}$$

Now the right hand side of Eq.(19) is simplified with the aid of Eq.(12) to:

$$\left(\frac{dF(t)}{dt}\right)_c=\frac{1}{\tau}\left(F^{feed}(t)-F(t)\right)_c+\left(\sum_{i=1}^{M_x}\Gamma(x_i)F(x_i)\left[\sum_{k=1}^{i}\int_{v_{k-1/2}}^{\min(x_i,v_{k+1/2})}\left(\frac{u_m(v)}{u_m(x_i)}\right)\beta_n(v\mid x_i)dv-1\right]\right)_c \tag{21}$$

where the c subscript on both sides indicates that the time change of the integral property that is derived from the continuous PBE to differentiate it from the discrete one (with subscript d). On the other hand, the time change of the integral property as derived from the discrete PBE could be obtained by summing Eq.(18) over i from 1 to M_x:

$$\left(\frac{dF(t)}{dt}\right)_d=\frac{1}{\tau}\left(F^{feed}(t)-F(t)\right)_d+\left(\sum_{i=1}^{M_x}\Gamma(x_i)F(x_i)\left[\sum_{k=1}^{i}\int_{v_{k-1/2}}^{\min(x_i,v_{k+1/2})}\left(\frac{u_m(v)}{u_m(x_i)}\right)\beta_n(v\mid x_i)dv-1\right]\right)_d \tag{22}$$

It is clear that the last two equations are exactly identical and hence the discrete PBE given by Eq.(18) is internally consistent with respect to any single integral property. For example if $u_m(v)$=1, we get a single ODE describing the evolution of the total number concentration, $N(t)$. On the other hand, if $u_m(v)=v$, the term between the squared brackets is zero according to the constraint given by Eq.(4) and hence we end up with the rate of change of the dispersed phase hold up (concentration) due to the in and out flows across the vessel boundaries.

Now, to gain more insight into the problem of integral property conservation, we let u_m=1 in Eq.(18) and we will call the resulting set of discrete equations as the base discrete set. This could be justified since all the other discrete integral properties are derived from these base equations by multiplying it with $u_m(x_i)$. So, the base discrete set of ODEs follows from Eq.(18):

$$\frac{dN_i(t)}{dt}=\frac{1}{\tau}\left(N_i^{feed}(t)-N_i(t)\right)-\Gamma(x_i)N_i(t)+\sum_{k=i}^{M_x}\Gamma(x_k)N_k(t)\int_{v_{i-1/2}}^{\min(x_k,v_{i+1/2})}\beta_n(v\mid x_k)dv \tag{23}$$

As stated previously, this equation is consistent only with respect to the total number concentration according to Eq.(21) and Eq.(22). If the prediction of the other discrete integral properties is demanded, then it could be obtained from this equation by multiplying its both sides by $u_m(x_i)$ and denoting $u_m(x_i)N_i(t)=(F_i(t))_d$ to differentiate it from the continuous integral property: $(F_i(t))_c$ obtainable from Eq. (18):

$$\left(\frac{dF_i(t)}{dt}\right)_d=\frac{1}{\tau}\left(F_i^{feed}(t)-F_i(t)\right)_d-\left(\Gamma(x_i)F_i(t)-\sum_{k=i}^{M_x}\Gamma(x_k)F_k(t)\left(\frac{u_m(x_i)}{u_m(x_k)}\right)\int_{v_{i-1/2}}^{\min(x_k,v_{i+1/2})}\beta_n(v\mid x_k)dv\right)_d \tag{24}$$

and by summing both sides of this equation over i from 1 to M_x we get:

$$\left(\frac{dF(t)}{dt}\right)_d=\frac{1}{\tau}\left(F^{feed}(t)-F(t)\right)_d+\left(\sum_{i=1}^{M_x}\Gamma(x_i)F(x_i)\left[\sum_{k=1}^{i}\left(\frac{u_m(x_k)}{u_m(x_i)}\right)\int_{v_{k-1/2}}^{\min(x_i,v_{k+1/2})}\beta_n(v\mid x_i)dv-1\right]\right)_d \tag{25}$$

It is clear now that Eq.(25) is only identical to Eq.(21) if $\left(F^{feed}(x_i)\right)_d = \int_{v_{i-1/2}}^{v_{i+1/2}} u_m(v) n^{feed}(v) dv$ and $u_m(v)=1$; that is the internal consistency is only recovered for the base set of the discrete equations as expected. Actually, we can only recover the internal consistency with respect to any integral property in the case of very fine grids such that the mean value theorem of integrals is valid according to the following condition so that Eq.(21) and Eq.(25) are approximately identical:

$$\lim_{\Delta v_k \to (\Delta v_i)_s} \left(\int_{v_{k-1/2}}^{\min(x_i, v_{k+1/2})} \left(\frac{u_m(v)}{u_m(x_i)} \right) \beta_n(v \mid x_i) dv \right) \approx \left(\frac{u_m(x_k)}{u_m(x_i)} \right) \int_{v_{k-1/2}}^{\min(x_i, v_{k+1/2})} \beta_n(v \mid x_i) dv \tag{26}$$

Unfortunately, since the daughter droplet distribution becomes sharp and narrow in the small size range (as x_k becomes small), then the integrand on the left hand side of Eq.(26) becomes also sharp and depending on the variation of $u_m(v)$. This makes the approximation stated by Eq.(26) questionable, and hence very fine grid is required to guarantee its correctness (very small $(\Delta v_k)_s$). Since our aim is to make use of the less computationally expensive coarse grid, we have to seek another approach to recover the internal consistency of Eq.(24), at least with respect to some specific integral properties rather than all of them. To do so, we will first briefly introduce the fixed-pivot technique of Kumar and Ramkrishna (1996a) before we lay down our approach for the purpose of comparison since they are closely interrelated.

3.5 The fixed-pivot technique

We start by considering the formation term in the PBE given by Eq.(2) and let us consider a daughter droplet of volume v resulting from the breakage of a mother droplet of volume v'. Since the droplet volume coordinate is discretized into a finite number of subdomains, then it is only allowed for droplet of sizes, x_k, to be represented in the kth subdomain during the transformation from the continuous to the discrete domains. If the resulting daughter droplet volume, v, does not coincide with any of the available representative sizes (pivots) of the subdomains, then the simplest way to do it is to assign it to the nearest representative size. This type of assignment could only preserve one integral property in the discrete form as we have shown in the previous section. The genius idea of the fixed-pivot technique is to redistribute the property of the formed droplet between two adjacent subdomains, V_{k-1} and V_k, at their representative sizes, x_{k-1}, and x_k, provided that $v \in [x_{k-1}, x_k)$ such that any two integral properties are enforced due to the transformation from the continuous to the discrete domains. Kumar and Rmakrishna (1996a) showed that for the conservation of any two properties, $u_1(v)$, and $u_2(v)$, we could set up the following two constraints by assigning the fractions $\gamma_{k-1}^{<k-1>}(v)$ and $\gamma_k^{<k-1>}(v)$ to the droplet populations at x_{k-1} and x_k respectively:

$$\gamma_{k-1}^{<k-1)}(v) u_m(x_{k-1}) + \gamma_k^{<k-1>}(v) u_m(x_k) = u_m(v), \; m = 1, 2 \tag{27}$$

It is obvious from these constraints that droplet population in the kth subdomain receives a net gain of droplet population for every daughter droplet that is formed in the range $[x_{k-1}, x_{k+1}]$. This calls for the modification of the formation term appearing in Eq.(15) such that the discrete linear breakage operator is modified to:

$$\begin{aligned} B_o\left\{x_k, N_k(t)\right\} = & -\Gamma(x_i) N_i(t) + \\ & \int_{x_{i-1}}^{x_i} \gamma_k^{<k-1>}(v) dv \int_v^{v_{\max}} \Gamma(v') \beta_n(v \mid v') n(v', t) dv' + \int_{x_k}^{x_{k+1}} \gamma_k^{<k>}(v) dv \int_v^{v_{\max}} \Gamma(v') \beta_n(v \mid v') n(v', t) dv' \end{aligned} \tag{28}$$

where the fractions the $\gamma_{k-1}^{<k>}(v)$ and $\gamma_k^{<k>}(v)$ are found by solving the linear system given by Eq.(27). Note that the subscript in the previous fractions refer to the representative size while the superscript refers to the representative size range. Proceeding as we have done in the previous section, the final base set of the discrete equations is given by:

$$\frac{dN_i(t)}{dt} = \frac{1}{\tau}\left(N_i^{feed}(t) - N_i(t)\right) - \Gamma(x_i) N_i(t) + \sum_{k=i}^{M_x} \pi_{i,k}^{<m>} \Gamma(x_k) N_k(t) \tag{29}$$

where the breakage matrix elements $\pi_{i,k}^{<k>}$ are given by:

$$\pi_{i,k}^{<m>} = \int_{x_{i-1}}^{x_i} \gamma_i^{<i-1>}(v)\beta_n(v \mid x_k)dv + \int_{x_i}^{\min(x_k, x_{i+1})} \gamma_i^{<i>}(v)\beta_n(v \mid x_k)dv \tag{30}$$

The upper limit of the integration on the second integral is introduced to take into account the fact that the daughter droplet volume, v, cannot exceed its mother droplet volume, x_k. The discrete set of equations given by Eq.(29) is *approximately* internally consistent with respect to any two integral properties as shown by Rmakrishna (2000). However, in their original work Kumar and Rmakrishna (1996a) set the first integral to zero for i=1 since the representative size (pivot) x_0 does not exist. Since x_1 is greater than zero, it follows that any droplet having volume less than x_1 will be lost from the left boundary. This loss becomes significant for large residence time or batch time for continuous and batch systems respectively. This error will be called the intrinsic discretization error (*IDE*) and will be quantified in the next section.

3.6 The IDE of the fixed-pivot technique

It is clear that the fixed-pivot technique could not exactly conserve the prescribed integral properties exactly due to the *IDE*; but instead it conserves one of them approximately. The reason for this approximation is clear if we reconsider the system of linear equations given by Eq.(27) for k=1, and let us concentrate on the conservation of total droplet number concentration and the fractional volume of the dispersed phase (hold up). Since the representative droplet volume x_0 does not exist we have two equations in one unknown; namely $\gamma_1^{<0>}(v) = 1$ and $\gamma_1^{<0>}(v)x_1 = v$. This means that any daughter droplet that is born in the size range $[v_{min}, x_1)$ will be totally assigned to the representative droplet size x_1 indicating that only the total droplet number concentration is exactly conserved. This inherent error associated with the fixed-pivot technique is really unavoidable and it causes a loss of the second integral property from the left boundary if the first integral property is chosen to be exactly conserved, particularly if x_1 is not sufficiently small. Since the dispersed phase hold up, ϕ, should be exactly conserved, we will pay particular attention to this integral quantity, and the other one will be chosen as the total number concentration, $N(t)$. Doing so, we are ready to derive a quantitative measure of this *IDE* through multiplying Eq.(29) by x_i and summing both sides over i=1 to M_x and after some algebraic manipulation it is not difficult to show:

$$\tau \frac{d\phi(t)}{dt} = \left(\phi^{feed}(t) - \phi(t)\right) - \tau \sum_{k=1}^{M_x} \Gamma(x_k) N_k(t) \int_0^{x_1} \left(v - x_1\right) \beta_n(v \mid x_k) dv \tag{31}$$

It is the second term on the right hand side that we termed the *IDE*, and it is clear that it is proportional to the magnitude of the first representative size and will never tend to zero since x_1 is always greater than zero. It is also worthwhile to note that the *IDE* has a cumulative nature and is increasing with time since the set $\{N_i(t) \mid i=1, \ldots i_{max}\}$ is an increasing set of functions, where i_{max} is some index above which discrete population densities are decreasing with time. This maximum index always exists due to the loss and formation terms comprising the linear breakage operator. This is because the subdomains of the upper size range start to loss their population while the small size range subdomains receive a net gain of the droplet population.

Note that at a steady state the *IDE* could be accurately estimated from Eq.(31) according to the following relation:

$$IDE(x_1) = \tau \sum_{k=1}^{M_x} \Gamma(x_k) N_k(t=\infty) \int_0^{x_1} \left|\left(v - x_1\right)\right| \beta_n(v \mid x_k) dv = \left|\phi^{feed} - \phi(t=\infty)\right| \tag{32}$$

Now, the second term on the right hand side of this equation could be identically zero if the total volume concentration is exactly conserved. So, the magnitude of deviation of this term from zero represents an indirect estimation of the *IDE* since the feed hold up, ϕ^{feed} is exactly known.

3.7 The present discretization approach

It should be first emphasized that the recovery of internal consistency (as pointed out in section 4) with respect to certain integral properties is not necessarily corresponding to the same number distribution function. This means that we could estimate for example one integral property from two number distributions that are slightly different. For example, one such integral property is the total number concentration (the zero moment of the distribution) corresponding to the total area under the number density curve. Now, we could generate an infinite number of these number density curves but still having the same total area. By referring to section 4 and particularly to Eq.(21) and Eq.(25) it has been shown that only one degree of freedom exists to make these two equations identical. The question arising at this stage is how we could increase the degrees of freedom to two so that any two integral properties associated with the base set of equations could be achieved? This question might be answered by taking into consideration the aforementioned discussion concerning the non-uniqueness of the number density function (and hence the base set of equations) from which the integral properties are derived. It then appears that it is feasible to solve a modified but slightly different PBE with the property that the base set of equations of this slightly modified PBE is internally consistent with respect to any two integral properties. However, this does not mean that the slightly modified PBE will converge to a completely different or erroneous number distribution. This is because we enforce the slightly modified PBE to be identical to its original counterpart, at least with respect to the desired integral properties. It should also be stressed that the discrete solution generated by the base set of equations of this slightly modified PBE should converge to the solution of its continuous counterpart as the grid is made fine.

To proceed further, we introduce the pair of auxiliary functions: $\eta(v)$ and $\sigma(v)$ to account for the intra-interval problem when the PBE is transformed from the continuous to the discrete domains. So, the proper choice of placing these functions is at the loss and formation terms so that we could obtain the following modified linear breakage operator:

$$B_o\left\{v,F(v,t)\right\} = -\eta(v)\Gamma(v)F(v,t) + \int_v^{v_{\max}} \sigma(v')\Gamma(v')\left[\frac{u_m(v)}{u_m(v')}\right]\beta_n(v\mid v')F(v',t)dv' \tag{33}$$

Now substituting this expression in Eq.(16) and making use of Eq.(14), and Eq.(17) and by setting $u_m(v)$=1, the following modified base set of equations is obtained:

$$\frac{dN_i(t)}{dt} = \frac{1}{\tau}\left(N_i^{feed}(t) - N_i(t)\right) - \eta(x_i)\Gamma(x_i)N_i(t) + \sum_{k=i}^{M_x}\sigma(x_k)\Gamma(x_k)N_k(t)\int_{v_{i-1/2}}^{\min(x_k,v_{i+1/2})}\beta_n(v\mid x_k)dv \tag{34}$$

Before we proceed further to determine the forms of the introduced functions $\eta(x_i)$ and $\sigma(x_i)$ we have to generalize Eq.(34) to handle any discrete property, $u_m(x_i)$ exactly in the same way as we did in obtaining Eq.(24):

$$\begin{aligned}\left(\frac{dF_i(t)}{dt}\right)_d &= \frac{1}{\tau}\left(F_i^{feed}(t) - F_i(t)\right)_d - \\ &\left(\eta(x_i)\Gamma(x_i)F_i(t) - \sum_{k=i}^{M_x}\sigma(x_k)\Gamma(x_k)F_k(t)\left(\frac{u_m(x_i)}{u_m(x_k)}\right)\int_{v_{i-1/2}}^{\min(x_k,v_{i+1/2})}\beta_n(v\mid x_k)dv\right)_d\end{aligned} \tag{35}$$

and by summing both side of this equation over i from 1 to M_x we get:

$$\begin{aligned}\left(\frac{dF(t)}{dt}\right)_d &= \frac{1}{\tau}\left(F^{feed}(t) - F(t)\right)_d + \\ &\left(\sum_{i=1}^{M_x}\Gamma(x_i)F(x_i)\left[\sigma(x_i)\sum_{k=1}^{i}\left(\frac{u_m(x_k)}{u_m(x_i)}\right)\int_{v_{k-1/2}}^{\min(x_i,v_{k+1/2})}\beta_n(v\mid x_i)dv - \eta(x_i)\right]\right)_d\end{aligned} \tag{36}$$

Now we are ready to determine the form of the discrete functions $\eta(x_i)$ and $\sigma(x_i)$ by enforcing internal consistency of Eq.(35) with respect to any two integral properties: $u_1(v)$ and $u_2(v)$ that are associated with the number distribution. This could be simply accomplished by equating the right hand sides of Eq.(21) and Eq.(36) to get the following two set of constraints:

$$\left(F^{feed}(x_i)\right)_d = \int_{v_{i-1/2}}^{v_{i+1/2}} u_m(v) n^{feed}(v) dv \tag{37}$$

$$\sigma(x_i)\sum_{k=1}^{i}\left(\frac{u_m(x_k)}{u_m(x_i)}\right)\int_{v_{k-1/2}}^{\min(x_i,v_{k+1/2})}\beta_n(v\mid x_i)dv - \eta(x_i) = \sum_{k=1}^{i}\int_{v_{k-1/2}}^{\min(x_i,v_{k+1/2})}\left(\frac{u_m(v)}{u_m(x_i)}\right)\beta_n(v\mid x_i)dv - 1,\ m=1,2 \tag{38}$$

The first constraint given by Eq.(37) is imposed due to the droplet transport across the system boundary along with the feed. The second set of constraints is due to the internal inconsistency resulting from the discrepancy between the continuous and discrete nature of the droplet breakage. These constraints form a system of two linear equations in $\eta(x_i)$ and $\sigma(x_i)$ that are linearly independent for all values of $i = 2, \ldots M_x$. However, for i=1 there is only one independent equation as we will show in the next section. The solution of this system of equations could be written in the following form for any two desired integral properties $u_1(v)$ and $u_2(v)$:

$$\sigma(x_i) = \frac{q_2(x_i) - q_1(x_i)}{r_2(x_i) - r_1(x_i)} \tag{39}$$

$$\eta(x_i) = 1 + \left[\sigma(x_i) r_2(x_i) - q_2(x_i)\right] \tag{40}$$

where:

$$r_m(x_i) = \sum_{k=1}^{i}\left(\frac{u_m(x_k)}{u_m(x_i)}\right)\int_{v_{k-1/2}}^{\min(x_i,v_{k+1/2})}\beta_n(v\mid x_i)dv,\ m=1,2 \tag{41}$$

$$q_m(x_i) = \sum_{k=1}^{i}\int_{v_{k-1/2}}^{\min(x_i,v_{k+1/2})}\left(\frac{u_m(v)}{u_m(x_i)}\right)\beta_n(v\mid x_i)dv,\ m=1,2 \tag{42}$$

for i=2,...M_x and $\eta(x_i)= \sigma(x_i)$=1 for i=1.
For a especial case of conserving droplet number and volume concentrations, we can simply set $u_1(v)=1$ and $u_2(v)=v$ in Eqs. (39) through (42) to get the following set of equations:

$$\sigma(x_i) = \frac{\vartheta(x_i) - 1}{\vartheta(x_i) - r_2(x_i)} \tag{43}$$

$$\eta(x_i) = \sigma(x_i) r_2(x_i) \tag{44}$$

$$r_2(x_i) = \sum_{k=1}^{i}\left(\frac{x_k}{x_i}\right)\int_{v_{k-1/2}}^{\min(x_i,v_{k+1/2})}\beta_n(v\mid x_i)dv \tag{45}$$

where $\vartheta(x_i)$ is given by Eq.(3).
Since $\vartheta(x_i) \geq 2$ and $(x_k/x_i) \leq 1$ for k=1,...i, it is then not difficult to show that $\vartheta(x_i) \geq r_2(x_i)$. The equality sign holds only for k=i=1 where the system of equations (41) looses its linear independency, and hence $\eta(x_i)= \sigma(x_i)$=1. This means that the auxiliary functions $\eta(x_i)$ and $\sigma(x_i)$ given by Eqs.(43) and (44) are always positive as required.
It is clear that the modified base set of equations given by Eq.(34) and the two auxiliary functions $\eta(x_i)$ and $\sigma(x_i)$ given by Eqs.(39) and (40) are free from any assumption concerning the droplet breakage functions or the type of grid. This makes these equations cope, in a flexible way, with binary or multiple droplet breakage in a straightforward manner. This approach also allows a combination of different types of grids (e.g. linear, geometric, ...etc.) even for a single problem and does make grid refinement a possible way to improve the numerical accuracy whenever it is required. Moreover, the generality of the conservation of any two desired integral properties makes the approach attractive for directing the calculations toward the targeted dispersed phase quantities that are of practical interest (such as hold up, *d32*, … etc.). In addition, the internal consistency of the approach makes it easy to be coupled with the fixed-pivot technique of Kumar and Ramkrishna (1996a) for droplet coalescence.

It should be noted that the correction factors introduced by Hill and Ng (1995) and Vanni (1999) to the discrete PBE for droplet breakage were an attempt to obtain discrete functions like $\eta(x_i)$ and $\sigma(x_i)$. However, the main concern of the first author is to conserve only the total number and volume concentrations that are only applicable to special limited cases of breakage functions. The second author tried to resolve this problem by introducing a correction factor for the loss term without guarantee to produce an internal consistency with respect to the total droplet concentration.

3.8 The IDE of the present discretization approach

As in the case of the fixed-pivot technique, the present discretization approach could not exactly conserve the prescribed integral properties exactly due to the *IDE*; but instead it conserves one of them approximately. The reason for this approximation is the loss of linear dependency in the first subdomain. For this case we choose, as in the case of the fixed-pivot technique, to conserve the total number concentration, $N(t)$, and leave the total volume concentration, $\phi(t)$, approximately conserved. This could be done by setting $\eta(x_i)= \sigma(x_i)=1$ for $i=1$ and $u_2(v)=v$ and noting that the term between the square brackets is identically zero except for $i=1$ due to the constraints given by Eq.(39) and Eq.(40). So, Eq.(36) simplifies to:

$$\tau \frac{d\phi(t)}{dt} = \left(\phi^{feed}(t) - \phi(t)\right) + \tau x_1 \Gamma(x_1) N(x_1) \left(\vartheta(x_1) - 1\right) \tag{46}$$

As stated previously the second term on the right hand side is the *IDE* and it is clear that it is proportional to the magnitude of the first representative droplet size and will never tend to zero if $\Gamma(x_1)$ and $N(x_1)>0$ since x_1 is always greater than zero.
Note that at a steady state the *IDE* could be accurately estimated from Eq.(46) according to the following relation:

$$IDE(x_1) = \tau x_1 \Gamma(x_1) \left(\vartheta(x_1) - 1\right) N_1(t=\infty) = \left|\phi^{feed} - \phi(t=\infty)\right| \tag{47}$$

From this result, it is worthwhile to note that the magnitude of the *IDE* of the present approach is much smaller than that of the fixed-pivot technique given by Eq.(32) and has not a cumulative nature. This is not surprising since the present discretization approach does not redistribute the resulting droplet volume due to any breakage event between two contiguous subdomains as the fixed-pivot does. So, to this redistribution we attribute the cumulative nature of the *IDE* of the fixed-pivot technique. However, in the present approach the formation and loss terms adjust themselves automatically in each subdomain to conserve the desired integral properties through the aid of the auxiliary functions $\eta(x_i)$ and $\sigma(x_i)$. Moreover, if the representative droplet size, x_1, is chosen to be less than v_{min}, then the *IDE* of the present approach is identically zero due to the regulatory condition given by Eq.(9). So, it could be concluded that the present discretization approach is superior to the fixed-pivot technique at least from the *IDE* point of view.

3.9 The finite domain error (FDE)

Due to the presence of the boundary conditions (regulatory conditions) given by Eq.(7) and Eq.(9), there would be an inevitable underestimation of the integral properties obtained from the number distribution if these boundary conditions are not exactly satisfied. This failure of taking into account the nonzero values of the portions of the distribution below v_{min}, and above v_{max} (if these droplet sizes are not properly chosen) is termed the finite domain error (FDE) (Gelbard & Seinfeld, 1978; Nicmanis & Hounslow, 1998; Attarakih, Bart & Faqir, 2003a). The subsequent erroneous estimation of v_{min}, and v_{max} such that Eq.(7) and Eq.(9) are not approximately satisfied will results in an underestimation of the estimated integral quantities of interest such that the lower and upper FDEs are given by (Attarakih et al., 2003a):

$$FDE = \sum_{m=1}^{2} \int_0^{v_{\min}} u_m(v) n(v,t) dv + \int_{v_{\max}}^{\infty} u_m(v) n(v,t) dv = \sum_{m=1}^{2} FDE_m^L + FDE_m^U \tag{48}$$

Since in an only breakage process the maximum droplet size could not exceed the maximum one imposed by the feed or the initial condition, it follows that d_{max} could be easily chosen, based on the inlet feed distribution and the initial condition, so that $FDE < TOL/2$ (m=1,2), where TOL is some small, real and positive number. So the minimum and maximum droplet diameters are estimated from:

$$FDE(d_{\min}, d_{\max}, M_x) = FDE^L + FDE^U \le TOL \tag{49}$$

where:

$$FDE^L \approx \sum_{m=1}^{2}\sum_{i=1}^{2}\frac{1}{\Delta d_i}u_m(d_i)N_i(z,t) + \sum_{m=1}^{2}\sum_{i}^{2}\frac{1}{\Delta d_i}\left(\int_{d_{i-1/2}}^{d_{i+1/2}} u_m(d)n^{feed}(d)\delta d + \int_{d_{i-1/2}}^{d_{i+1/2}} u_m(d)n^{ic}(d)\delta d\right) \tag{50}$$

$$FDE^U \approx \sum_{m=1}^{2}\sum_{i=M_x-1}^{M_x}\frac{1}{\Delta d_i}u_m(d_i)N_i(z,t) + \sum_{m=1}^{2}\sum_{i=M_x-1}^{M_x}\frac{1}{\Delta d_i}\left(\int_{d_{i-1/2}}^{d_{i+1/2}} u_m(d)n^{feed}(d)\delta d + \int_{d_{i-1/2}}^{d_{i+1/2}} u_m(d)n^{ic}(d)\delta d\right) \tag{51}$$

The detailed derivation of these relations is given by Attarakih, Bart and Faqir (2004).
Since the initial and inlet feed distributions are a priory known, then d_{max} will also be a priory estimated as described above. However, the estimation of d_{min} has an iterative nature by starting first with an initial estimation, solving the complete problem, and we check if the condition implied by Eq.(48) is satisfied. If it is not satisfied, then d_{min}, will be reduced by a small amount and the problem is solved again until Eq.(48) is satisfied. A particular advantage of this approach is that the above condition is checked at each integration step or perhaps at regular time steps. So, once this condition is violated the calculations should be stopped and restarted again with an improved estimation of d_{min} thus reducing the computational time significantly while at the same time achieving an automatic FDE estimation.

3.10 Validation and realization of the present discretization approach

In general, the discretization techniques are called for when the analytical solutions are impossible to obtain. In spite of this, these techniques should be thoroughly tested for their accuracy and rate of convergence to gain some confidence in their performance. In this work, the numerical accuracy and convergence for the present discretization approach and the fixed-pivot technique were tested using two classes of case studies. The first class is merely of theoretical form where analytical solutions are possible, while the second class belongs to real interacting liquid-liquid dispersions without known analytical solutions. The first class is used for the discretization approach validation by comparing the numerical results with the analytical ones. On the other hand, applying the present approach to real physical problems compromises a real challenge to such discretization schemes.

Since droplet diameter is practically used as the droplet internal coordinate, it is desirable to transform the volume coordinate in the final discrete PBEs given by Eq.(29) and Eq.(34) and the other related equations. As stated previously, the transformation of the internal coordinate is easier when the PBE in discrete form rather than in the continuous form by making use of the following identity:

$$\int_{v_{i-1/2}}^{v_{i+1/2}} n(v,t)dv = \int_{d_{i-1/2}}^{d_{i+1/2}} n(d,t)\delta d \tag{52}$$

and hence, $N(x_i) = N(d_i)$. If the transformation of coordinate occurs without integration, then the following relation must be used:

$$n(d,t) = \frac{\partial v}{\partial d}n(v,t) \tag{53}$$

where the droplet volume is given by: $v=k_v d^3$ and $k_v=\pi/6$ if the droplet shape is assumed spherical. The above two relations are sufficient to transform the discrete PBEs from volume to diameter coordinate. For clarity the daughter droplet distribution in Eq.(34) is transformed simply by setting

$\beta_n(d \mid d') = \left(\pi d^2 / 2\right) \beta_n(v(d) \mid v(d'))$. It should be taken into account that the δ symbol appearing in Eq.(52) is a differential operator rather than the Dirac delta function used in this work. It should also be clarified that the integrals appearing in Eq.(30), Eq.(37) and Eq.(45) are estimated numerically using a 5-point Gauss quadrature.

The system of ODEs given by either Eq.(29) or Eq.(34) are integrated using the implicit Euler method with a constant time step. Although the method is of first order accuracy it has two distinct advantages: the first one is its stability that is independent of the size of the time step, and the second is the guarantee that the resulting solution is always positive, which is a requirement imposed by the physical process itself. The algorithm presents itself as an efficient scheme especially when the PBE is extended to model the dispersed phase in multistage or differential flow systems (countercurrent liquid-liquid extraction columns) (Attarakih, Bart & Faqir, 2003b).

3.10.1 Validation of the present discretization approach

In this validation phase we have chosen the following set of functions and parameters for the present breakage problem:

$$n^{feed}(d) = \frac{3d^2 N_0^f}{d_0^3} e^{-\left(\frac{d}{d_0}\right)^3} \tag{54}$$

$$\Gamma(d) = \left(\frac{\pi d^3}{6}\right)^p,\ p = 1,2 \tag{55}$$

$$\beta_n(d \mid d') = 6\frac{d^2}{d'^3} \tag{56}$$

$$n(d,0) = 0 \tag{57}$$

$$d_{k+1/2} = \left(\frac{d_{\max}}{d_{\min}}\right)^{\frac{k}{M_x}} d_{\min},\ k = 0,...,M_x \tag{58}$$

To the best of the authors' knowledge, the PBE given by Eq.(2) has no general analytical solution. However, McGrady and Ziff (1988) proposed an analytical solution for a slightly different form of Eq.(2) and a special case of monodisperse feed distribution. Nicmanis and Hounslow (1998) proposed an analytical solution only for the steady state version of the breakage problem given by Eq.(2) using the conditions stated by Eqs. (54) through (57) with p=1. So, in this work we provide the following analytical solutions of Eq.(2) for the set of functions given by Eqs.(54-57) as a sum of transient and steady state solutions, where the detailed derivation is listed in appendix A:

$$n(d,t) = \frac{3d^2 N_0^f}{d_0^3}\left[n_t(d,t) + n(d,\infty)\right] \tag{59}$$

for p=1 (in Eq.(55)) we have:

$$n_t(d,t) = -\left\{\frac{t^2}{a} + \left(2\tau\left[1 + \frac{t}{\tau_b}\right]\left[\frac{1}{a^2} + \frac{\tau}{a^3}\right] + \frac{1}{a}\right)\right\} e^{-\left(d/d_0\right)^3 - t/\tau_b} \tag{60}$$

$$n(d,\infty) = \left(\frac{1}{a} + \frac{2\tau}{a^2} + \frac{2\tau^3}{a^3}\right) e^{-(d/d_0)^3} \tag{61}$$

and for p = 2 we have:

$$n_t(d,t)=\left\{a\left(\frac{t}{\tau_b}\right)-\left(1+\frac{t}{\tau_b}\right)\left(1+\tau+\tau\left[1+\left(\frac{d}{d_0}\right)^3\right]^2\right)\right\}\frac{e^{-(d/d_0)^3-(t/\tau_b)}}{a^2} \tag{62}$$

$$n(d,\infty)=\left(1+\tau+\tau\left[1+\left(\frac{d}{d_0}\right)^3\right]^2\right)\frac{e^{-(d/d_0)^3}}{a^2} \tag{63}$$

$$\tau_b=\frac{\tau}{1+\tau\left(\frac{d}{d_0}\right)^{3p}},\ p=1,2 \tag{64}$$

$$a=1+\tau\left(\frac{d}{d_0}\right)^{3p},\ p=1,2 \tag{65}$$

It should be noted that Eq.(59) is reduced exactly to that derived by Nicmanis and Hounslow (1998) at steady state. The most important fact that could be drawn from Eq.(64) that the breakage time constants are dependent, as expected, on the breakage frequency. Moreover, the breakage time constant, τ_b, in a perfectly mixed vessel is always less than the vessel time constant, τ. These time constants are dependent only on the droplet diameter and the vessel time constant, thus small droplets exhibit longer breakage times than the larger ones.

All the numerical studies that are presented for these two case studies are based on conserving droplet volume and number; that is $u_1(v)=1$ and $u_2(v)=v$. It should also be clear that the geometric grid given by Eq.(58) is constructed with number of subdomains (or pivots) M_x =50 unless it is stated for some particular cases. The minimum and maximum droplet diameters were chosen so that the total finite domain error is less than 0.1% over the simulation period ($FDE(t)<0.001\ \forall t\in[0,\ t_{final}]$). The magnitude of the time step, Δt, was chosen to trade off between the computational accuracy and the execution time. A value of $\Delta t=1$ s was found satisfactory for all the numerical tests. The droplet distribution is solved for in terms of the droplet volume concentration by multiplying Eq.(29) by $v(d_i)$ for the fixed-pivot technique, while we set $u_m(v)=v$ in Eq.(36) for the present discretization approach and substituting $\varphi_i(t)=v(d_i)N_i(t)$. The droplet volume density is then recovered from the droplet volume concentration using the following relation:

$$P(d_i,t)=\frac{\varphi(d_i,t)}{\sum_{i=1}^{M_x}\varphi(d_i,t)\Delta d_i},\ i=1,....,M_x \tag{66}$$

while the analytical volume density $p(d,t)$ is obtained from Eq.(59) through Eq.(65) using a continuous analog of Eq.(66) with a very fine uniform grid of 1000 intervals. The main advantage of using the volume instead of the number density may be justified by obtaining the dispersed phase hold-up directly by summing the local hold up of each class ($\phi(t)=\sum_{i=1}^{M_x}\varphi(d_i,t)$) (Ribeiro et al., 1995; Alopaeus et al., 2002). The numerical moments of the distribution are calculated, based on the discrete number concentration, $N(d_i,t)$ according to the following relation:

$$M_j(t)=\sum_{i=1}^{M_x}d_i^j N(d_i,t),\ j=0,1,... \tag{67}$$

Similarly, the exact moments are calculated from a continuous analog to the previous equations except when j=0 and 3 where simple explicit forms rare available (Attarakih, Bart & Faqir, 2003a).

To completely define the problem in hand, only the continuous phase is considered to present when the dispersed phase is fed to the vessel which corresponds to zero initial condition ($\varphi_i(0)=0,\ i=1,...,M_x$). The

dispersed feed hold-up is also specified, (ϕ^{feed}=0.4), where this relatively high value of the hold-up seems to contradict the assumption of negligible droplet coalescence. The reason for this value is just only to be consistent with the experimentally validated breakage functions at this value of hold-up (Alopaeus et al., 2002). Anyhow, we think from a numerical point of view that the discretization approach should be applicable for a wide range of the dispersed phase hold-up. The vessel residence time (τ = 100 s) is chosen also to be large enough to allow for a considerable breakage extent. It should also be noted that in all the figures in this work we denoted the present discretization approach by: present approach and the generalized fixed-pivot by GFP.

3.10.1.1 Case 1: $\Gamma(d) = \pi d^3 / 6$

In this case the droplet breakage frequency is considered to be proportional to the droplet volume which corresponds to p=1 in Eq.(55). We start our presentation of the numerical results by shedding some light on the behavior of the intrinsic discretization error (*IDE*) of both the present discretization approach and the generalized fixed-pivot technique (GFP). Fig. (2a) depicts the variation of the *IDE* at steady state based on the relations given by Eq.(32) and Eq.(47) for the GFP and the present discretization approach respectively. First, the present approach has a smaller *IDE* than that of the GFP as is predicted by Eq.(32) and Eq.(47). Second, the variation of the *IDE* as a function of the droplet diameter in the first subdomain (d_1) seems to be linear on a log-log plot, which may be attributed to the power law breakage frequency.
Fig.(3) shows the dynamic evolution of the volume density at different times over a one-time constant period where the changes in the droplet population are evidently sharp. The minimum and maximum droplet diameters were chosen as indicated above to keep the total finite domain error below 0.1% until the steady state is reached (d_{min} = 0.001 and d_{max} = 3.5 mm). Also, the minimum droplet diameter is sufficiently small to make the *IDE* of negligible value particularly for sufficient number of subdomains (*Mx* = 50) as is clear from Fig.(2a). For the sake of clarity, the predicted solution using the GFP is not shown along with the present approach on this figure since the two solutions are almost identical. This is really not surprising, since the two approaches are based on the same framework by conserving any two integral properties associated with the distribution. It is clear also that there is a close match between the analytical solution obtained from Eq.(60) through Eq.(63) and the numerical solution at all times.

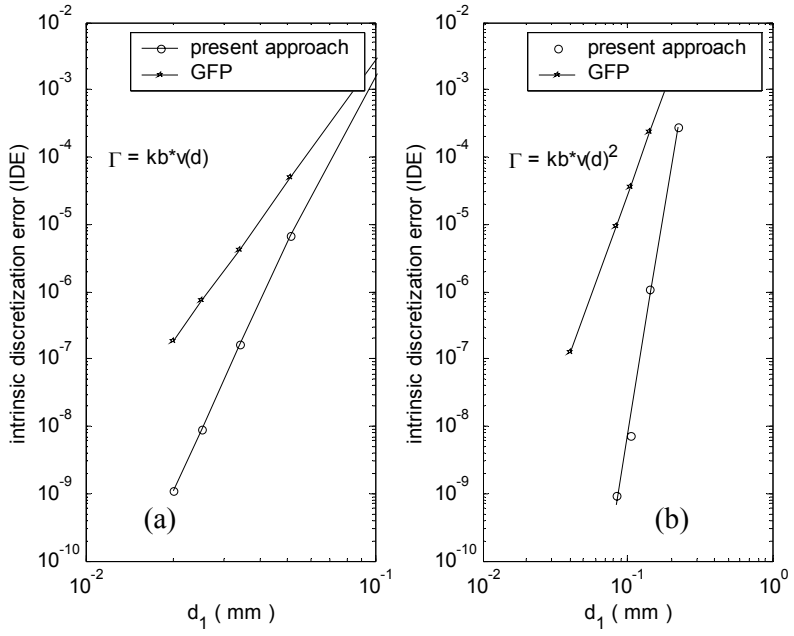

Fig.(2) The steady state intrinsic discretization error (*IDE*) using the present approach and the GFP technique: a- $\Gamma(d) = k_b \left(\pi d^3 / 6\right)$. b- $\Gamma(d) = k_b \left(\pi d^3 / 6\right)^2$ where k_b = 1, τ = 100 s, and the inlet feed distribution is given by Eq.(54) with d_0=1 and N_0^f=1.

Note that the dynamic evolution of the droplet population in the small size range is sharper than that at the large size range due to the differences in the breakage time constants ($[\tau_b]_{small\ \text{droplets}} > [\tau_b]_{large\ \text{droplets}}$) as predicted by Eq.(64). Here it is also worthwhile to mention that due to the geometric grid used in the discretization, numerical errors are likely to appear on the upper tail of the distribution. This error is attributed to the increasing size of the subdomains and hence increasing the integration error with respect to d. This error could be reduced through either increasing the number of subdomins or by refining the grid on the upper size range (Kumar and Ramkrishna, 1996a), where the latter one is adopted here (M_x = 50). The steady state solution for this case is also shown in Fig.(8a) where again the agreement between the numerical and analytical solutions is excellent.

Fig.(4) shows the zero, first, second, and third moments of the predicted (using the present approach) and the analytical solutions as calculated by Eq.(67) over the period, $t \in [10,\ 10\tau]$. This period of time is sufficient to follow the time course of the indicated moments until steady state. Excellent agreement between the predicted and the calculated moments is evident over the complete simulation period.

3.10.1.2 Case 2: $\Gamma(d) = (\pi d^3/6)^2$

In this case the droplet breakage frequency is proportional to the square of the droplet volume. This case is somewhat different from case 1 from the dynamic and steady state point of view. This is clear if we focus again on the breakage time constant given by Eq.(64) with p=2. This time constant indicates that droplets having volume less than one show slower dynamics when they are compared to those having the same volume in case 1. On the other hand, droplets having volume greater than one exhibit faster dynamics as compared with those in case 1. Due to this it is expected to have slow dynamics at the small size range for the droplet breakage as the steady state is approached when compared to case 1. Moreover, due to the fast and slow breakage rates for the small and large sizes respectively, it is expected to have a sharp transition in the droplet distribution through passing from droplets having v>1 to those with v<1, where these facts are clear if we compare both breakage rates (p=1 & 2) as they are depicted in Fig.(5).

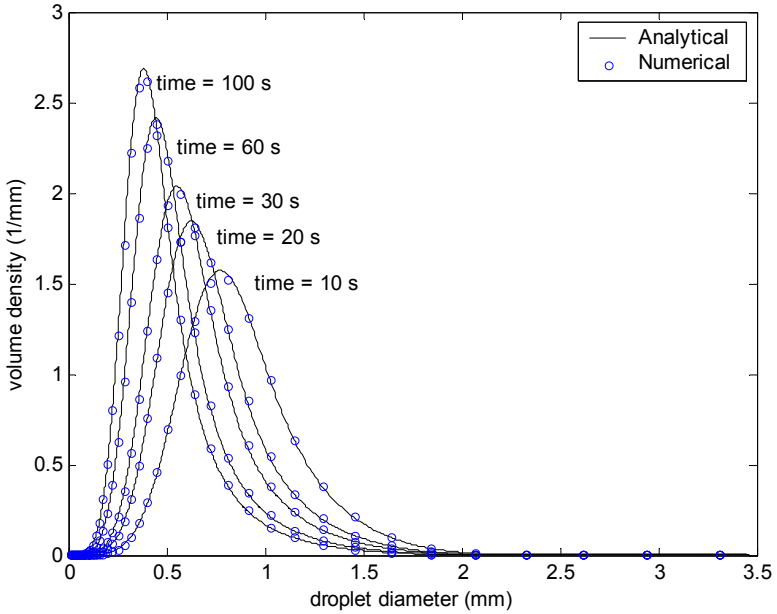

Fig.(3): The dynamic evolution of the droplet volume density: $\Gamma(d) = k_b\left(\pi d^3/6\right)$ with k_b = 1, τ = 100 s, and M_x = 50.

It is clear from this figure that the breakage rate of case 2 is only greater than that of case 1 for droplet diameter greater than 1.5 mm approximately. Fig.(6) shows the predicted and the analytical solutions as obtained from Eq.(62) through Eq.(65) with p=2, where the two solutions are almost identical. The predicted solution using the present approach is obtained under the same conditions used in case 1. The sharp changes in the upper size range are also evident in this figure due to the presence of considerable

differences in the breakage frequencies when passing from large to small size ranges. This is also clear by referring to Fig.(8a) where both cases 1 and 2 are compared at steady sate. The close agreement between the analytical and the predicted solutions are also evident.

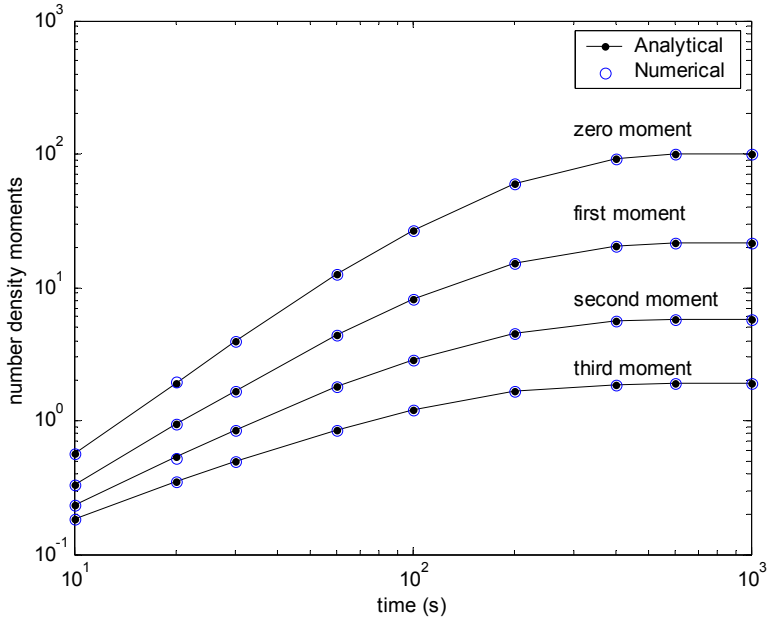

Fig.(4): The dynamic evolution of the number density moments: $\Gamma(d) = k_b\left(\pi d^3/6\right)$ with $k_b = 1$, $\tau = 100$ s, and $M_x = 50$.

Fig.(7) presents the time course of the zero, first, second and third moments of the droplet distribution as calculated using Eq.(67). Again, as in case 1, the good agreement between the predicted moments using the present approach and the analytical ones is clear. Two important features are revealed by Fig.(7) when compared to Fig.(4): the first one is that the steady state is approached faster in case 2 than in case 1 as predicted by the breakage time constants given by Eq.(64) for p=1 and 2 respectively. The second feature is the difference in the magnitude of the zero moments representing the total droplet concentration for the two cases. Again, since the breakage rate for the droplets having diameter d<1.5 mm (refer to Fig.(5) is much smaller in case 2 than that in case 1, and since the droplet distribution is shifted to the left, it is expected that the total number of droplets produced in the second case is much smaller than that in the first one.

3.10.2 Realization of the present discretization approach

In the previous section we have validated theoretically the performance of the present discretization approach. Before the approach is said to be acceptable we would like to realize it through an application to real cases describing the droplet evolution in interacting liquid-liquid dispersions. The most widely used droplet breakage frequency is due to Coulaloglou and Tavlarides (1977). The model is based on the fact that the agitation power dissipated into the continuous phase imparts a distribution of energies and sizes to the turbulent eddies. These eddies interact with the dispersed phase droplets and hence determine the rate at which a given size of droplet will break. However, this droplet breakage occurs when the ratio of turbulent energy to the surface droplet energy exceeds a critical value of Weber number (refer to Eq.(6)). Thus in the turbulent region, the droplet breakage rate is given as:

$$\Gamma(d) = C_1 \frac{\varepsilon^{1/3}}{(1+\phi)d^{2/3}} e^{\left(-C_2 \frac{\sigma(1+\phi)^2}{\rho_d \varepsilon^{3/2} d^{5/3}}\right)} \tag{68}$$

where C_1 and C_2 are empirical constants with typical values: 0.00481 and 0.08 respectively (Bapat & Tavlarides, 1985), and σ is the dispersion interfacial tension.

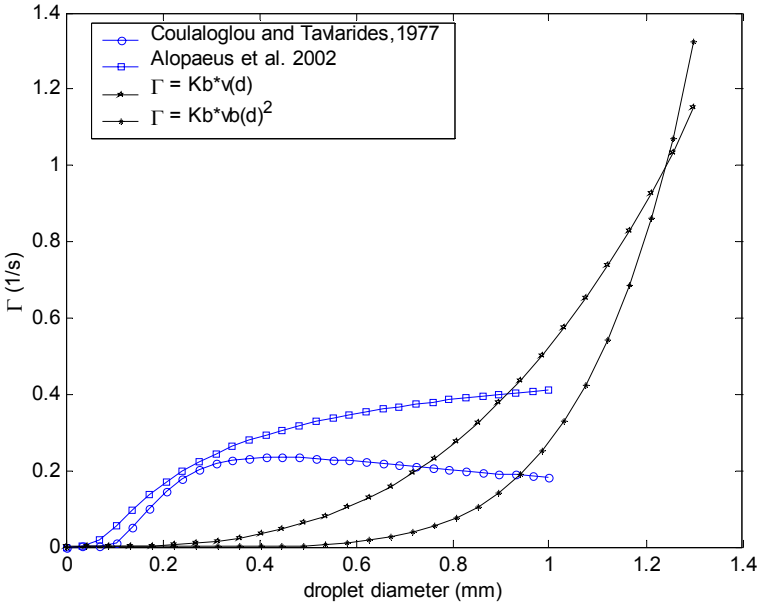

Fig.(5): The behavior of different breakage frequency functions using the physical properties and the energy input specification for cases 3 and 4 and k_b=1 for cases 1 and 2.

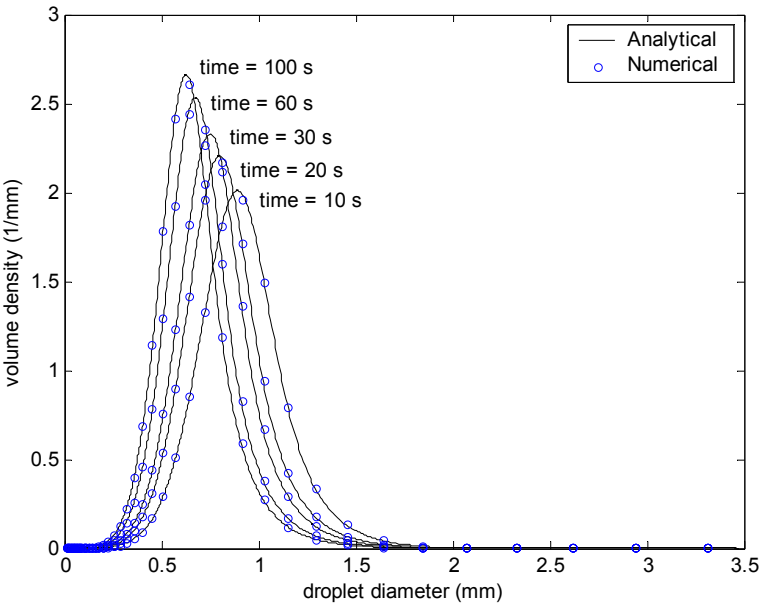

Fig.(6): The dynamic evolution of the droplet volume density: $\Gamma(d) = k_b \left(\pi d^3 / 6\right)^2$ with $k_b = 1$, $\tau = 100$ s, and $M_x = 50$.

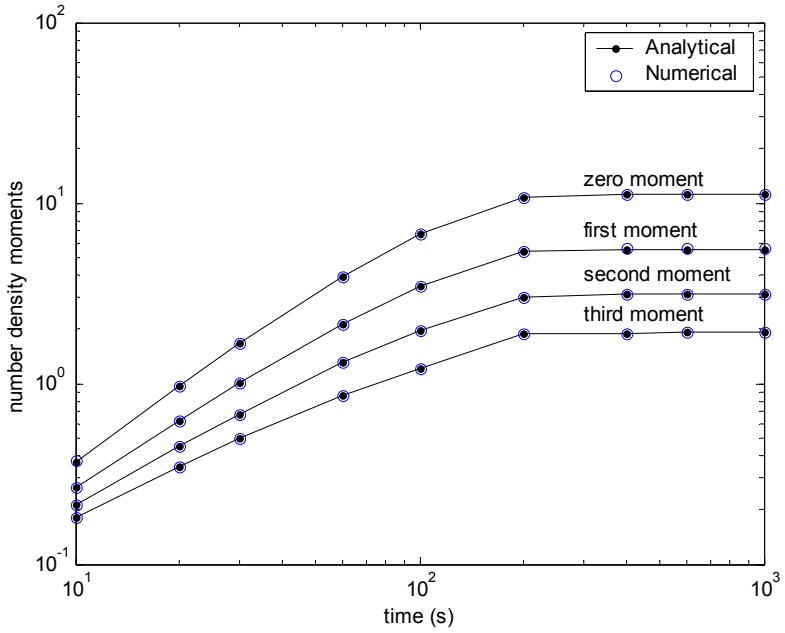

Fig.(7):The dynamic evolution of the number density moments: $\Gamma(d) = k_b\left(\pi d^3/6\right)$ with $k_b = 1$, $\tau = 100$ s, and $M_x = 50$.

The average turbulent energy in the whole vessel could be estimated using the following relation (Alopaeus, Koskinen & Keskinen, 1999):

$$\varepsilon = \frac{N_p D_R^5 N^3}{V} \tag{69}$$

where D_R is the impeller diameter, N is the impeller speed, V is the vessel volume, and N_p is the impeller power number whose value in the turbulent region for most of the impeller types ranges between 0.3 to 6.0 . Recently, Alopaeus et al. (2002) introduced the following droplet breakage frequency that takes into account the droplet surface and viscous energies simultaneously:

$$\Gamma(d) = C_3 \varepsilon^{1/3} erfc\left(\sqrt{C_4 \frac{\sigma}{\rho_c \varepsilon^{2/3} d^{5/3}} + C_5 \frac{\mu_d}{d^{4/3}\varepsilon^{1/3}\sqrt{\rho_c \rho_d}}}\right) \tag{70}$$

where C_3, C_4, and C_5 are empirical constants assuming values: 0.986 $m^{-2/3}$, 0.892×10^{-3}, and 0.2 respectively, and *erfc* is the complementary error function.
To completely describe the breakage process, the daughter droplet distribution resulting from the breakage of a single mother droplet must be specified. Two of the most frequently used distributions are the normal and beta distribution functions (Coulaloglou & Tavlarides, 1977; Tsouris & Tavalrides, 1994):

$$\beta_n(d \mid d') = \frac{3c\vartheta}{\sqrt{2\pi}}\left(\frac{d^2}{d'^3}\right) e^{-\left(\frac{c^2}{2}\left[1-\vartheta\left(\frac{d}{d'}\right)^3\right]^2\right)} \tag{71}$$

where the constant c is chosen to be 3.5 so that a probability of less than 0.1% of the daughter droplets lies outside the range $d \in [0, d']$. The beta distribution function takes the following form:

$$\beta_n(d,d') = \frac{90\vartheta d^2}{d'^3}\left(\frac{d}{d'}\right)^6\left(1-\left[\frac{d}{d'}\right]^3\right)^2 \tag{72}$$

Note that both the above distributions satisfy the constraints given by Eq.(3) and Eq.(4) and hence conserve droplet number and volume exactly.

The inlet feed droplet distribution is chosen as log normal distribution according to Valentas, Bilois and Amundson (1966) with mean droplet diameter 0.3 mm and standard deviation of 0.1, where the feed volume distribution is normalized such that its integral with respect to d yields the inlet dispersed phase hold up (ϕ^{feed}).

In this realization phase a perfectly mixed industrial scale vessel is considered where the vessel specifications and the two phases physical properties are taken from the work of Alopaeus, Koskinen & Keskinen (1999). The vessel specifications are as follows: N_p=5, D_T = 3.0 m, H_T = 3.0 m, D_R = 1.0 m, τ = 100 s, and ϕ^{feed} = 0.4 and the physical properties of the dispersion are: μ_d = 0.0205 kg.m^{-1}. s^{-1}, μ_c = 0.002 kg.m^{-1}. s^{-1}, ρ_d = 923 kg.m^{-3}, ρ_c = 1193 kg.m^{-3}, and σ = 0.002 N.m^{-1}.

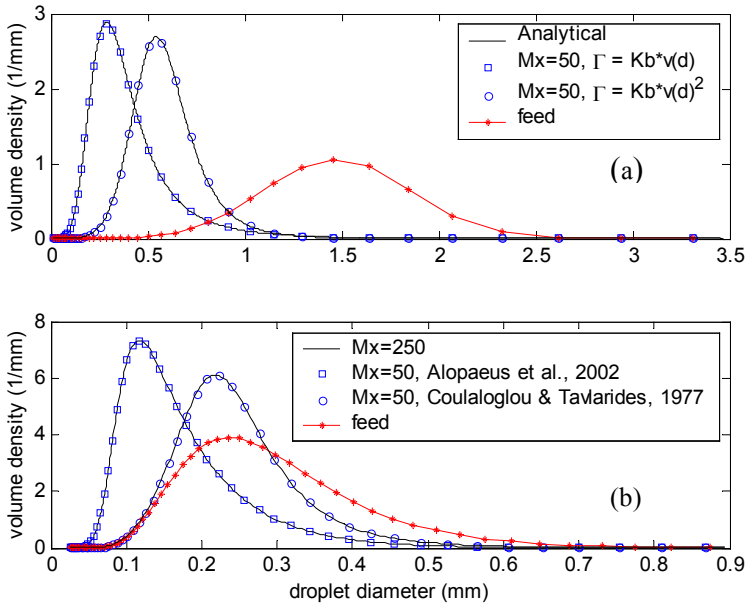

Fig.(8): The steady state droplet volume distribution using the present discretization approach with τ = 100 s : a-cases 1 and 2 with k_b = 1. b- cases 3 and 4.

3.10.2.1 Case 3: Coulaloglou and Tavlarides (1977) breakage frequency

In this case study the breakage frequency of Coulaloglou and Tavlarides (1977) that is given by Eq.(68) is used, while the daughter droplet distribution is chosen as the beta distribution given by Eq.(72) with ϑ = 2 (binary breakage). This breakage frequency is plotted in Fig.(5) showing a maximum value at about 0.5 mm droplet diameter (Tsouris & Tavlarides, 1994). The actual droplet diameter range of the experimentally operated perfectly mixed vessels ranges from 0.1 to 0.6 mm in some cases (Coulaloglou & Tavlarides, 1977) and from 0.1 to 0.4 mm in other cases (Alopaeus et al., 2002). However, in this case study and the other one that will follow a larger droplet diameter is used because of the inlet feed distribution. So, the maximum and minimum droplet diameters are initially estimated using Eq.(6) and Eq.(8) and then refined according to Eq.(51) so that the total FDE is less than 0.1% over the whole simulation period $t \in [0,\ 20\tau]$. Values of d_{min} = 0.025 mm and d_{max} = 0.9 mm are found to satisfy the aforementioned criterion at impeller speed N = 0.5 s^{-1}. These minimum and maximum droplet diameters are used to construct the geometric grid according to Eq.(58). Since analytical solution is not available for this case study, a numerical solution based on Eq.(66) using a very fine grid of 250 subdomins is considered as the base for the numerical comparisons. Fig.(8b) shows the steady state volume droplet distribution using 50 subdomins where this solution seems to be indistinguishable from the base solution

using fine grid of 250 subdomins. Due to the relative decrease in the breakage frequency after approximately d = 0.5 mm (refer to Fig.(5)), the droplet distribution given in Fig.(8b) is not very sharp. Since the droplet volume is exactly conserved during the droplet breakage, we can check the accuracy of the predicted solution by integrating Eq.(10) with respect to v form v_{min} to v_{max} and by setting $u_m(v)=v$ to get an analytical solution for the dispersed phase hold up (Attarakih et al., 2003a):

$$\phi(t) = \phi^{feed}\left(1 - e^{-t/\tau}\right) \tag{73}$$

Eq.(73) assumes zero initial condition and it approaches the inlet feed hold-up asymptotically at steady state. Fig.(9) shows the dynamic response of the dispersed phase hold-up using Eq.(73) and the predicted one using Eq.(66) for M_x = 50, and Δt = 1 s. A very close agreement between the analytical solution and the predicted one using the present approach is evident over all the simulation period elucidating again our confidence in the present discretization approach.

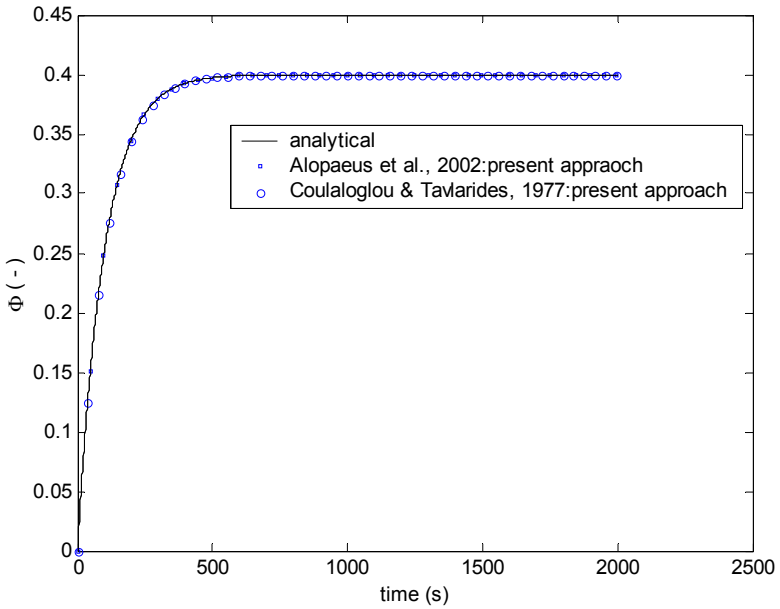

Fig.(9): The dynamic response of the dispersed phase hold-up for cases 3 and 4 with τ = 100 s and ϕ^{feed}=0.4.

3.10.2.2 Case 4: Alopaeus et al. (2002) breakage frequency

In this case we use the same inlet feed and daughter droplet distributions as in case 3 except the droplet breakage frequency, where the model given by Eq.(70) is used. The numerical parameters, the initial condition, and the energy input are also the same as in case 3. Fig.(8b) shows the steady state volume distribution using two levels of discretization: the first one is of 250 subdomains and is considered as the base solution since no analytical one is available. The second level of discretization is of 50 subdomains and it is clear that the two solutions are almost indistinguishable. In this case the volume density is sharper than that of case 3 in the small and in the large size range. This is because the present breakage frequency as is evident from Fig.(5) is higher in magnitude than that given by Coulaloglou and Tavlarides (1977) and it is monotone increasing for all $d \in [d_{min}, d_{max}]$. The transient responses of the dispersed phase hold up as predicted using the present approach and Eq.(73) are also shown in Fig.(9). These solutions are very close to each other even at the beginning of the response where sharp changes in the hold-up are encountered. In this case we also studied the effect of the shape of the daughter droplet distribution on the steady state volume density. Fig.(10a) compares two steady state volume densities with normal and beta daughter droplet distributions given by Eq.(71) and Eq.(72) respectively for binary breakage (ϑ = 2). The normal daughter droplet distribution tends to produce sharper distribution than the beta daughter droplet

distribution. This behavior is attributed to the sharp form of the normal distribution when compared to the beta distribution; however, the difference is not so large.

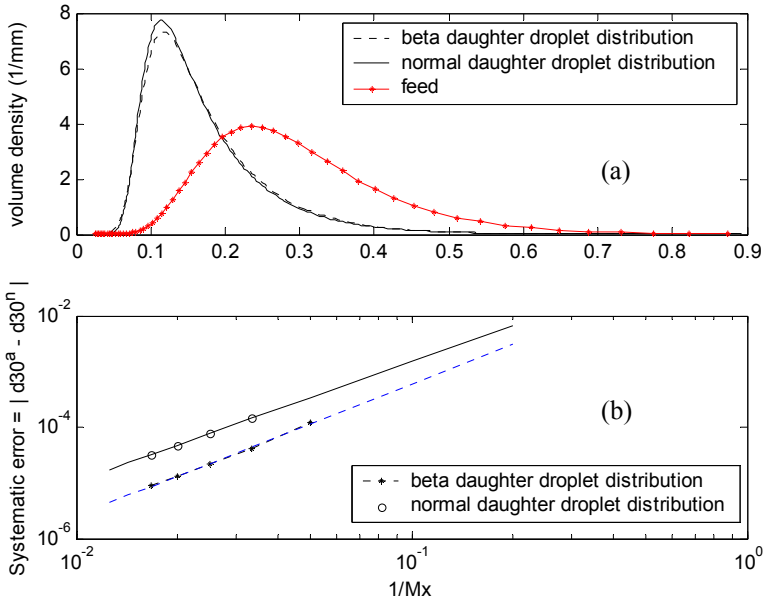

Fig.(10): The effect of daughter droplet distribution on: a-The steady state droplet volume for case 4with $\tau =$ 100 s. b-The systematic error for case 4 with $\tau = 100$ s.

3.10.3 The convergence of the present discretization approach and the GFP

In the previous four case studies we have presented only qualitative comparisons between the analytical (when it is available) and the predicted solutions, and the predicted solution on relatively coarse and fine grids (when the analytical solution is not available). In this section we would like to thoroughly investigate the quantitative convergence characteristics of the present discretization approach and the generalized fixed-pivot technique (GFP) since they belong to the same discretization framework. It seems that the systematic error representing the difference between the analytical and the predicted *d30* at steady state is a suitable measure to study the convergence characteristics (Attarakih, Bart & Faqir, 2003a):

$$SysErr = \left| d30^{a} - d30^{n} \right| = K \left(\frac{1}{M_x} \right)^{\alpha} \tag{74}$$

where K is some constant and α is called the order of convergence and it is expected to depend on the discretization method as well as on the sharpness of the distribution. If the second equality suggested by the above equation is valid, then a straight line is expected if the above relation is plotted on log-log paper with a slope α estimating the order of convergence. It should be emphasized that in cases where analytical solution is not available we will use the representative droplet diameter, *d30,* based on the fine grid of 250 subdomins for cases 3 and 4 above.

We will start our discussion from the last case above (case 4) and we will show the effect of the daughter droplet distribution on the systematic error given by Eq.(74). Fig.(10b) shows the systematic error versus the inverse of the number of subdomains (intervals) on a log-log scale. First it is clear that the plot is linear with an approximate slope of 2, although the magnitude of the slope in the case of beta distribution is a little bit higher. Also the magnitude of the systematic error in this case is lower than that of the normal distribution due to the difference in the sharpness of the two volume density curves (Fig.(10a)).

Fig.(11) shows the convergence characteristics of the present discretization approach and the generalized fixed-pivot (GFP) for the four cases studied above. First, it is clear that all the systematic errors of the four cases produced straight lines when plotted on a log-log scale elucidating the validity of the proposed

relation given by Eq.(74). Second, all these straight lines having slopes of magnitudes ranging between 2 and 2.36, except case 1 which has a slope of magnitude 4. As stated previously, the magnitude of the exponent α in Eq.(74) depends on the sharpness of the distribution where it is expected to be large for smooth and symmetric distributions as it is the case in Fig.(8a) for case 1. Consequently, it could be concluded that the convergence rate of the present discretization approach is approximately proportional to $(1/M_x)^2$. This result agrees well with the convergence rate of the moving pivot technique (Attarakih, Bart & Faqir, 2003a).

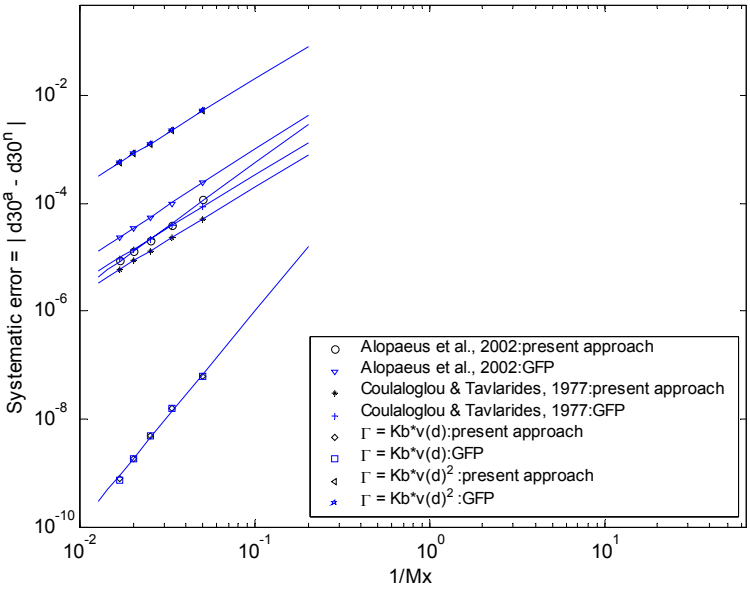

Fig.(11): The convergence characteristics of the present discretization approach and the GFP technique as measured by the systematic error for cases 1, 2, 3, and 4 at steady state with τ = 100 s.

Third, the convergence of the present approach and the generalized fixed-pivot (GFP) are almost the same for cases 1 and 2, while the present approach has a smaller systematic error than the GFP for cases 3 and 4. This improved convergence of the present approach might be attributed to the different behavior of the breakage frequency functions as shown in Fig.(5), where the breakage frequencies of cases 3 and 4 change sharply in the small size range (when compared to cases 1 and 2) resulting in a sharp droplet distribution in this range. So, it might be concluded that the present discretization approach is superior to the GFP when sharp changes are encountered particularly in the small size range. It is also worthwhile to mention here that the magnitude of the systematic error is less than 10^{-3} for the most cases investigated in this work even when only 15 subdomains are used (refer to Fig.(11)). This makes the present approach or the GFP a powerful tool for detailed modeling of the liquid-liquid dispersions by coupling the PBE with computational fluid dynamics (CFD) where complex transport equations are needed.

3.10.4 The CPU time

In this section we compare the execution times for the present discretization approach and the generalized fixed-pivot (GFP) technique using two different aspects: first, the CPU time of generating the breakage matrices for the two approaches, and second the execution time of the integration algorithm. The importance of the breakage matrix is to decouple the time dependent variables ($N_i(t)$, $\Gamma(d_i, \phi(t))$) from the simple integrals appearing in Eq.(30) and Eq.(45) for the GFP technique and the present discretization approach respectively. This allows the breakage matrix to be generated off line and hence the computational time will be considerably reduced. All the runs for the estimation of the CPU time requirements are performed on a PC with Pentium III processor of 700MHz speed performing a single task. To avoid errors due to the small CPU times, these experiments are repeated for each run three times and the results are averaged. Case 3 is chosen as a real breakage problem to estimate the CPU times as is shown in Fig.(12) where the simulation is carried out over a period of time $t \in [0, 8\tau]$ using an integration time step of 1 s and τ =100 s . Fig.(12a) shows the CPU time required to generate the breakage matrices

for the present and the GFP technique as a function of number of subdomains (pivots). All the integrals appearing in Eqs(30) and (45) are performed numerically using a 5-point Gauss quadrature. It is clear that the breakage matrix of the present approach requires shorter computational times than those required by the GFP technique. This is because we only have a single integral in the present discretization approach plus simple algebraic expression given by Eq.(44), while we have two single integrals in the GFP technique. Fig12b shows identical CPU requirements for the present approach and the GFP technique. This is not surprising, since once the breakage matrices are generated, the two approaches becomes exactly identical from the computational point of view. It is also worthwhile to mention here that the CPU time requirement for the generation of the breakage matrices or for integration is proportional to the square of the number of subdomains (pivots).

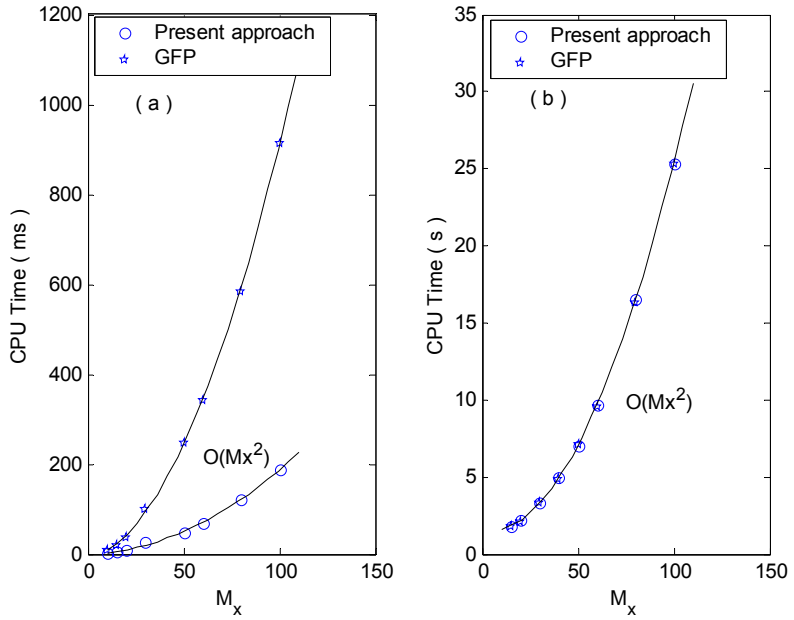

Fig.(12): The CPU time requirements for the present discretization approach and the GFP technique using the problem specification of case 4 for:a-The generation of the breakage matrix. b-The integration algorithm using Δt = 1 s and final simulation time = 800s.

3.11 Conclusions

- A general mathematical approach using the subdomain method is utilized to discretize the general PBE for droplet breakage describing the hydrodynamics of interacting liquid-liquid dispersions in a continuously stirred vessel. The discretization approach presents itself to be computationally efficient since the resulting set of ODEs is free from the evaluation of any double integrals. Moreover, the careful treatment of the breakage matrix makes it possible to decouple the time dependent variables from the repeated evaluation of the single integrals appearing in the discrete equations.
- The resulting set of discrete equations (using the subdomain method) is shown to be only internally consistent with respect to one integral property associated with the number density. Based on any two conserved integral properties internal consistency is enforced by introducing a set of auxiliary functions that are uniquely determined.
- The concept of intrinsic discretization error (*IDE*) is introduced to show that an exact conservation of two integral properties in all the discrete subdomains (intervals) is not possible. It is also shown quantitatively that the present approach enjoys a lower value of *IDE* than that of the generalized fixed-pivot.
- The present discretization approach is validated through comparing its predictions with two analytical solutions of the problem in hand. The numerical results seem to agree well with the analytical solutions for both the volume density and some selected moments. Realization of the

approach is performed using two experimentally validated breakage frequency functions, as well as two daughter droplet distributions. For these cases the predicted dispersed phase hold-up is found to agree to a very good extent with the exact solutions.

- The convergence characteristics of the present approach are found identical to that of the generalized fixed-pivot technique and in some cases they are even better. The order of convergence is found to be approximately proportional to $(1/M_x)^2$ in spite of its dependence on the sharpness of the distribution. The results show that 15-20 subdomains (intervals) are sufficient to produce acceptable predictions when the hydrodynamics of liquid-liquid dispersions are considered.
- The discrete set of equations of the present approach is independent of the grid structure and hence allowing selective grid refinement as well as the coupling of this approach with the fixed-pivot technique for droplet coalescence.

Nomenclature

B	London-van der Waals constant, Jm
B_o	linear droplet breakage operator as defined in Eq.(15)
D_R	impeller diameter, m
D_T	vessel diameter, m
d, $d`$	droplet diameter, m
d_{min}, d_{max}	minimum and maximum droplet diameters, m
d_i	the characteristic droplet diameter in the ith subdomain, m
d_0	parameter in Eqs.(54) and (59) that is set to unity, m
$d30$	representative droplet diameter defined as $\left(\int_{d_{\min}}^{d_{\max}} d^3 n(d,t)\delta d \,/\, \int_{d_{\min}}^{d_{\max}} n(d,t)\delta d\right)^{1/3}$, m
$d30^a$, $d30^n$	analytical and numerical $d30$ respectively
FDE	total finite domain error as defined by Eq.(48)
$FDE_m^L(t)$	lower finite domain error based on the mth integral property
$FDE_m^U(t)$	upper finite domain error based on the mth integral property
$F(t)$, $F_i(t)$	integral properties defined as $\int_{v_{\min}}^{v_{\max}} u_m(v)n(v,t)dv$, $\int_{v_{i-1/2}}^{v_{i+1/2}} u_m(v)n(v,t)dv$
H_T	vessel height, m
IDE	intrinsic discretization error as defined in Eq.(32)
K	empirical constant appearing in Eq.(74)
L	differential operator as defined in Eq.(16)
M_x	total number of subdomains (intervals) used in droplet volume discretization
$M_j(t)$	the jth moment associated with the number density, $n(d,t)$
N	rotor speed, s^{-1}
N_p	power number
$N(t)$	total number of droplets per unit volume of the dispersion at time t, m^{-3}
$N_i(t)$	total number of droplets in the ith subdomain (interval) per unit volume at time t, m^{-3}
N^{feed}	total number of droplets in the inlet feed per unit volume, m^{-3}
N_0^f	parameter in Eqs.(54) and (59) that is set to unity, m^{-3}
$n(v,t)dv$	number of droplets in size range v to $v+dv$ at time t
$n^{feed}(v,t)dv$	number of droplets in the inlet feed in size range v to $v+dv$ at time t
$n^{ic}(v,0)dv$	number of droplets initially present in size range v to $v+dv$ at
$p(d,t)\delta d$	volume of droplets in the size range d to $d+\delta d$ at time t
$SysErr$	systematic error as defined in Eq.(74)
t	time, s
u_m	the mth desired integral property associated with the number droplet distribution
V	vessel volume, m^3
v, v'	droplet volumes, m^3
$v_{min.}$, $v_{max.}$	minimum and maximum droplet volumes, m^3
We	Weber number ($\rho_{disp.} N^2 D_R^3 / \sigma$)
w_k	unit step function in the kth subdomain as defined in Eq.(14)
x_i	characteristic droplet volume in the ith subdomain

Greek Symbols

α	order of convergence as appears in Eq.(74)
$\beta_n(v \mid v')dv$	fractional number of droplets formed in the size range v to $v+dv$ formed upon breakage of droplet of volume v'
ϕ, ϕ^{feed}	the dispersed phase hold up in the vessel and the feed respectively
$\Gamma(v)$	number of droplets in the size range v to $v+dv$ disappearing per unit time by breakage
$\gamma_i^{<i>}$	fraction of droplets from the interval $[x_i, x_{i+1})$ that is assigned to the pivot x_i
$\gamma_i^{<i-1>}$	fraction of droplets from the interval $[x_{i-1}, x_i)$ that is assigned to the pivot x_i

δ	Dirac delta function
ε	average turbulent energy dissipated in the continuous phase, $m^2.s^{-3}$
$\eta(x_i)$	auxiliary function as defined in Eq.(44)
$\pi_{i,k}^{<m>}$	breakage matrix as defined in Eq. (30)
μ_c, μ_d	viscosity of the continuous and dispersed phases respectively, $kg.m^{-1}.s^{-1}$
ρ	the source term describing droplet breakage and coalescence as appears in Eq.(1)
ρ_c, ρ_d	density of the continuous and dispersed phases respectively, $kg.m^{-3}$
σ	interfacial tension, $N.m^{-1}$
$\sigma(x_i)$	auxiliary function as defined in Eq.(43)
τ	vessel time constant, s
$\vartheta(v')$	average number of droplets produced when mother droplet of volume, v', is broken

Appendix A. Analytical solution of the unsteady state breakage equation in a continuous flow vessel (especial case)

We start analytically solving the unsteady state breakage equation by introducing the dimensionless variable $z=v/v_0$ and the new density function $f(z,t)=v_0 n(v,t)/N_0^f$ into Eq.(2):

$$\frac{\partial f(z,t)}{\partial t}=\frac{1}{\tau}\left(f^{feed}(z,t)-f(z,t)\right)-\Gamma(z)f(z,t)+\int_z^{\infty}\Gamma(z')\beta_n(z\mid z')f(z',t)dz' \tag{A1}$$

where:

$$\Gamma(z)=z^p \tag{A2}$$

$$f^{feed}(z)=e^{-z} \tag{A3}$$

$$f(z,0)=0 \tag{A4}$$

Taking the Laplace transform of both sides of Eq.(A1) with respect to t and let $F(z,s)$ be the Laplace transform of $f(z,t)$ one could obtain:

$$\left(a(z)+\tau s\right)F(z,s)=F^{feed}(z,s)+2\tau\int_z^{\infty}(z')^{p-1}F(z',s)dz' \tag{A5}$$

where:

$$a(z)=1+\tau z^p \tag{A6}$$

Following Nicmanis and Hounsloe (1998), Eq.(A5) is an integral equation and could be transformed to a first order linear ODE by differentiating it with respect to z and after some algebraic manipulation we get:

$$\frac{dF(z,s)}{dz}+\frac{(p+2)\tau z^{p-1}}{a(z)+\tau s}F(z,s)=\left(\frac{1}{a(z)+\tau s}\right)\frac{dF^{feed}(z,s)}{dz} \tag{A7}$$

The initial condition for this ODE could be obtained by setting $z = 0$ in Eq.(A5) to get:

$$F_p(0,s)=\left(\frac{2\tau}{1+\tau s}\right)M_{p-1}(s)+\frac{F^{feed}(0,s)}{1+\tau s} \tag{A8}$$

where $M_{p-1}(s)$ is the Laplace transform of the *(p-1)*th moment of the function $F(z,s)$ which could only be obtained for the two special cases when p=1 and 2. This is because the higher order moments (p>2) of the breakage equation (Eq.(A1)) are unclosed according to the following equation:

$$M_m(s)=\frac{\tau}{1+\tau s}\left(\frac{2}{m+1}-1\right)M_{m+p}(s)+\frac{\tau}{1+\tau s}M_m^{feed}(s), m=0,1,.. \tag{A9}$$

So, for p=1, and 2 we have to find expressions for $M_0(s)$ and $M_1(s)$ as required by Eq.(A8). These expressions follow directly from the last equation by setting m=0 when p=1 and m=1 when p=2:

$$M_1(s)=\frac{1}{1+\tau s}M_1^{feed}(s) \tag{A10}$$

$$M_0(s) = \frac{1}{1+\tau s} M_0^{feed}(s) + \frac{\tau}{1+\tau s} M_1(s) \tag{A11}$$

So the initial condition given by Eq.(A8) is now completely defined for p=1 and p=2.
The integration factor for Eq.(A7) could be easily obtained as follows:

$$I(z,s) = \exp\left((p+2)\tau \int_0^z \frac{z'^{p-1}}{a(z)+\tau s} dz' \right) = \left(a(z)+\tau s\right)^{\frac{p+2}{p}} \tag{A12}$$

Now the complete solution of Eq.(A7) using the feed distribution as given by Eq.(A3) could be written with the aid of this integration factor as:

$$F(z,s) = \frac{(1+\tau s) F_p(0,s)}{\left(a(z)+\tau s\right)^{\frac{p+2}{p}}} - \frac{1}{\left(a(z)+\tau s\right)^{\frac{p+2}{p}}} \int_0^z \frac{\left(a(z')+\tau s\right)^{\frac{2}{p}} e^{-z'}}{s} dz' \tag{A13}$$

The integral on the left hand side of this equation could be evaluated depending on the values of p =1 and 2 so one could obtain the following two solutions:

$$F(z,s) = \frac{e^{-z}}{s\left(a(z)+\tau s\right)} + \frac{2\tau e^{-z}}{s}\left(\frac{\tau}{\left(a(z)+\tau s\right)^3} + \frac{1}{\left(a(z)+\tau s\right)^2} \right), \text{ for } p = 1 \tag{A14}$$

$$F(z,s) = \frac{\tau e^{-z}}{\left(a(z)+\tau s\right)^2} + \left(\frac{1+\tau+\tau(1+z)^2}{s\left(a(z)+\tau s\right)^2} \right) e^{-z}, \text{ for } p = 2 \tag{A15}$$

The inversion of Eqs.(A14) and (A15) from the Laplace domain to the time domain is straightforward but it involves a tedious and lengthy algebra. Therefore, we used Mathcad7 software to symbolically perform these operations. We finally got the complete analytical solutions of Eq.(A1) using the following relation for transforming the resulting equations from the droplet volume into diameter coordinates:

$$n(d,t) = \frac{3d^2 N_0^f}{d_0^3} f(z,t) \tag{A16}$$

The complete analytical solution is given by Eqs.(59) through (65) for the two special cases described above.

References

Alopaeus, V., Koskinen, J. , & Keskinen, K. I. (1999). Simulation of population balances for liquid-liquid systems in a nonideal stirred tank. Part1: description and qualitative validation of model. *Chem. Engng. Sci.*, **54,** 5887-5899.

Alopaeus, V., Koskinen, J. , Keskinen, K. I. & Majander, J. (2002). Simulation of population balances for liquid-liquid systems in a nonideal stirred tank. Part2 parameter fitting and the use of the multiblock model for dense dispersion. *Chem. Engng. Sci.*, **57,** 1815-1825.

Attarakih, M. M., Bart, H., J. and Faqir, M. .M. (2002). An approximate optimal moving grid technique for the solution of discretized population balances in batch systems. In J. Grievink, & J. Schijndel van (Eds.), *European symposium on computer aided process engineering-12*, Computer-Aided Chemical Engineering 10 (pp. 823-828). Amsterdam: Elsevier.

Attarakih, M. M., Bart, H.-J., & Faqir, N. M. (2003a). Optimal moving and fixed grids for the solution of discretized population balances in batch and continuous systems: droplet breakage. *Chem. Engng. Sci.*, **58,** 1251-1269.

Attarakih, M. M., Bart, H.-J., & Faqir, N. M. (2003b). Solution of the population balance equation for liquid-liquid extraction columns using a generalized fixed-pivot and central difference schemes. Kraslawski, A. & Turunen, I. (Ed.), *European symposium on computer aided process engineering-13*, Computer-aided chemical engineering 14 (pp. 557-562). Elsevier, Amsterdam.

Attarakih, M. M., Bart, H.-J. & Faqir, N. M. (2004).). Numerical solution of the spatially distributed population balance equation describing the hydrodynamics of interacting liquid-liquid dispersions. *Chem. Engng. Sci.* **59**, 2567-2592.

Bapat, P. M. , & Tavlarides, L. L. (1985). Mass transfer in liquid-liquid CFSTR. *AIChE J.*, **31,** 659-666.

Coulaloglou, C. A. , & Tavlarides, L. L. (1977). Description of interaction processes in agitated liquid-liquid dispersions. *Chem. Engng Sci.*, **32,** 1289-1297.

Gelbard, F., & Seinfeld, J. H. (1978). Numerical solution of the dynamic equation for particulate systems. *J. Comput. Phys.*, **28,** 357-375.

Gelbard, F., Tambour, Y., & Seinfeld, J. H. (1980). Sectional representation of simulating aerosol dynamics. *J. Colloid & Interface Sci.*, **76,** 541-556.

Hill, P. J. , & Ng, K. M. (1995). New discretization procedure for the breakage equation. *AIChE J.*, **41,** 1204-1216.

Hounslow, M. J. (1990). A discretized population balance for continuous systems at steady state. *AIChE J.*, **36,** 106-116.

Hounslow, M. J., Ryall , R. L. & Marshall, V. R., (1988). A discretized population balance for nucleation, growth, and aggregation. *AIChE J.*, **34,** 1821-1832.

Kostoglou, M., & Karabelas, A. J. (1994). Evaluation of zero order methods for simulating particle coagulation. *J. Colloid Interface Sci.*, **163,** 420-431.

Kronberger, T., (1995): Numerische Simulation von Tropfenpopulationen in Extraktionskolonnen, Dissertation, Johannes Kepler Universitat Linz, Linz.

Kronberger, T., Ortner, A., Zulehner, W., & Bart, H. (1995). Numerical simulation of extraction columns using a drop population model. *Computers Chem. Engng.*, **19,** S639-S644.

Kumar, S., & Ramkrishna, D. (1996a). On the solution of population balance equations by discretization-I. A fixed pivot technique. *Chem. Engng. Sci.*, **51,** 1311-1332.

Kumar, S., & Ramkrishna, D. (1996b). On the solution of population balance equations by discretization-II. A moving pivot technique. *Chem. Engng. Sci.*, **51,** 1333-1342.

Lister, J. D., Smit, D. J., & Hounslow, M. J. (1995). Adjustable discretized population balance for growth and aggregation. *AIChE J.*, **41,** 591-603.

Liu, S. , & Li, D. (1999). Drop coalescence in turbulent dispersions. *Chem. Engng. Sci.*, **54,** 5667-5675.

Mahoney, A. W., & Ramkrishna, D. (2002). Efficient solution of population balances equations with discontinuities by finite elements. *Chem. Engng. Sci.*, **57,** 1107-1119.

McGrady, E. D., & Ziff, R. M. (1988). Analytical solutions to fragmentation equation with flow. *AIChE J.*, **34,** 2073-2076.

Nambiar, D. K. R., Kumar, R., Das, T. R., & Gandhi, K. S. (1992). A new model for the breakage frequency of drops in turbulent stirred dispersions. *Chem. Engng Sci.*, **47,** 2989-3002.

Nicmanis, M. , & Hounslow, M. J. (1998). Finite-element methods for steady-state population balance equations. *AIChE J.*, **44,** 2258-2272.

Ramkrishna, D. (1985). The status of population balances. *Rev. Chem. Engng.*, **3,** 49-95.

Ramkrishna, D. (2000). *Population Balances*. San Diego: Academic Press.

Randolph, A. D. , & Larson, M. A. (1988). *Theory of particulate processes*. (2nd ed.). Sandiego: Academic Press, Inc.

Ribeiro, L. M., Regueiras, P. F. R., Guimaraes, M. M. L., Madureira, C. M. C., & Cruz-Pintu, J. J. C. (1995). The dynamic behavior of liquid-liquid agitated dispersions-I. The hydrodynamics. *Computers Chem. Engng.*, **19,** 333-344.

Rice, G. R., & Do, D. D. (1995). *Applied mathematics and modeling for chemical engineers*. New York: Wiley

Shah, B. H. , & Ramkrishna, D. (1973). A population balance model for mass transfer in lean liquid-liquid dispersions. *Chem. Engng. Sci.*, **28,** 389-399.

Tsouris, C., & Tavlarides, L. L. (1994). Breakage and coalescence models for drops in turbulent dispersions. *AIChE J.*, **40,** 395-406.

Valentas, K. J., Bilois, O., & Amundson, A. R. (1966). Analysis of breakage in dispersed phase systems. *Ind. Engng. Chem. Fundam.*, **5,** 271-279.

Vanni, M. (1999). Discretization procedure for the breakage equation. *AIChE J.*, **45,** 916-919.

Vanni, M. (2000). Approximate population balances equations for aggregation-breakage processes. *J.Coll. & Int. Sci.*, **221,** 143-160.

Ziff, R. M. (1991). New solutions to the fragmentation equation. *J. Phys. A: Math. Gen*., **24**, 2821-2828.

Ziff, R. M. & McGrady, E. D. (1985). The kinetics of cluster fragmentation and depolymerisation. *J. Phys. A: Math. Gen*., **18**, 3027-3037.

CHAPTER 4

Solution of the Population Balance Equation for Liquid-Liquid Extraction Columns using a Generalized Fixed-Pivot and Central Difference Schemes

4.1 Introduction

In liquid-liquid extraction columns droplet population balance models are now being used to describe the hydrodynamics of the dispersed phase as well as the mass transfer. For the hydrodynamics this model accounts for droplet breakage, coalescence, axial dispersion, exit, and entry events. The resulting population balance equations are integro-partial differential equations (IPDE) that rarely have an analytical solution. These IPDEs are usually projected into a system of hyperbolic partial differential equations by discretizing the droplet diameter. This is done using the method of weighted residuals with the evaluation of many double integrals especially when the breakage and coalescence functions are not separable (Mahoney and Ramkrishna, 2002). In the present work we generalized the fixed- pivot technique of Kumar and Ramkrishna (Ramkrishna, 2000) to handle any integral property of the population number density for continuous flow systems. This technique has the advantage of being free of double integrals and hence it is considered computationally efficient. The discretization of the spatial variable is usually accomplished by the finite volume method using upwind differencing schemes. Kronberger et al. (1995) used the vector flux splitting based on the sign of the local droplet velocity; while the second order scheme they used is still dependent on the Riemann approximate solvers. In the present work we utilize the recently developed family of central differencing schemes of Kurganove and Tadmor (2000). These schemes are of first and second order accuracy and having the advantage of being free of characteristic decomposition beyond the CFL (Courant, Friedrichs and Lewy) related local speeds. The time discretization is accomplished using a first order implicit approach that is essentially noniterative by careful lagging of the nonlinear terms. The accuracy of the combined algorithm is tested using a simplified analytical solution of the population balance equation (PBE).

4.2 The mathematical model

The PBE describing the behavior of the dispersed phase in a continuous LLEC in terms of the concentration of a general quantity , $p(v)$, could be written as:

$$\frac{\partial p}{\partial t}+\frac{\partial [U_d p]}{\partial z}=\frac{\partial}{\partial z}\left(D_d \frac{\partial p}{\partial z}\right)+\frac{Q_d}{A}\left(\frac{uf^{feed}}{\overline{v}}\right)\delta(z-z_d)+\rho\{p,v\} \tag{1}$$

where $p= u(v)\, N(t) f(v;t,z)\delta v$ is the average quantity associated with droplets having a volume between $v\pm\delta v$ per unit volume of the dispersion at height z and time t. $N(t)$ is the average total number of droplets per unit volume of the dispersion and $f(v;t,z)$ is the average droplet number density function. U_d is the dispersed phase velocity that is determined by coupling the volume balances of the two phases (Kronberger et al., 1995). Note that $f^{feed}(v)$ is the normalized number density of the droplets leaving the distributor with an average volume $\overline{v}$. The last term on the right hand side is the net rate of droplet generation by coalescence and breakage per unit volume and unit time (Ramkrishna, 2000). In order to complete the specification of the problem, initial and boundary conditions are to be defined. The initial

conditions are dependent on the start up situation of the LLEC, however the Danckwert's boundary conditions are utilized for this model by considering the LLEC with an active height *H* to behave like a closed vessel between 0^+ and H^- (Wilburn, 1964).

4.3 Discretization of the PBE with respect to droplet diameter

The droplet volume (and hence diameter) is discretized using the fixed pivot technique. Consequently it is partitioned into M_x grid points according to the structure: $v_i = v_{i\pm1/2}$, $x_i = (v_{i-1/2} + v_{i+1/2})/2$, where x_i is called the fixed *i*th pivot. Let the total quantity associated with the population density in the *i*th interval be defined as: $\varphi_i(t,z) = \int_{v_{i-1/2}}^{v+1/2} u(v)n(v,t,z)\delta v$ where the remarkable significant of this quantity will be utilized in defining the total hold up (when *u*=*v*) of the dispersed phase ($\phi = \sum_{i=1}^{M_x} \varphi_i$). The quantity, *p*, is now expanded using a point wise sampling of the related function at the pivot points: (the dependence of the discrete variables on *t* and *z* will be omitted for sake of simplicity):

$$p(v,t,z) = \sum_{i=1}^{M_x} \varphi_i \delta(v - x_i) \tag{2}$$

The basic idea in the fixed pivot technique is that when a droplet of volume, *v*, is produced by either breakage or coalescence it will never coincide exactly with the *i*th pivot except for linear grid. So, the volume of this droplet will be assigned to the adjacent pivots such that any two moments of order m_1 and m_2 related to the population density are conserved. Following this, Eq.(1) is discretized with respect to droplet volume by integrating its both sides over the *i*th grid boundaries and making use of Eq.(2) and after some algebraic manipulations we get:

$$\frac{\partial \varphi_i}{\partial t} + \frac{\partial [U_d \varphi_i]}{\partial z} = \frac{\partial}{\partial z}\left(D_d \frac{\partial \varphi_i}{\partial z} \right) + \frac{Q_d}{A_c} \varphi_i^{feed} \delta(z - z_d) + \rho\{\boldsymbol{\varphi}, x_i\} \tag{3}$$

The discrete source term will be written in a rather compact form by introducing the idea of the interaction matrices for droplet breakage and coalescence which decouples the working variables vector, $\boldsymbol{\varphi}$, from the grid structure. Consequently, the interaction matrices are generated only once a time even for time dependent frequencies. Now the discretized PBE (3) is projected onto the droplet diameter coordinate using the identity: $\int_{v_{i-1/2}}^{v+1/2} un(v,t,z)\delta v = \int_{d_{i-1/2}}^{d+1/2} un(d,t,z)\delta d$ that leads to the vector function source term:

$$\boldsymbol{\rho}(\varphi) = \begin{pmatrix} \boldsymbol{\varphi}^T \left[\left(\boldsymbol{\omega} \bullet \boldsymbol{\Psi}^{<1>} \right) \boldsymbol{\varphi} \right] \\ \boldsymbol{\varphi}^T \left[\left(\boldsymbol{\omega} \bullet \boldsymbol{\Psi}^{<2>} \right) \boldsymbol{\varphi} \right] \\ \cdots\cdots\cdots\cdots \\ \boldsymbol{\varphi}^T \left[\left(\boldsymbol{\omega} \bullet \boldsymbol{\Psi}^{<M_x>} \right) \boldsymbol{\varphi} \right] \end{pmatrix} - \boldsymbol{\varphi}^T \bullet \left[\boldsymbol{\omega} \left(\boldsymbol{\zeta} \bullet \boldsymbol{\varphi} \right) \right] + A[\boldsymbol{\Gamma} \bullet \boldsymbol{\varphi}] \tag{4}$$

Note that the breakage matrix $\boldsymbol{A}$ is upper triangular with elements that are given by:

$$a_{i,i} = \Gamma_i \left(\vartheta_i \pi_{u,i,i} / u_i - 1 \right),\ a_{i,k} = \vartheta_k \Gamma_k \pi_{u,i,k},\ i \neq k,\ k = i,\ i+1,\ \ldots M_x,\ i = 1,2,..M_x$$

$$\pi_{u,i,k} = \int_{d_{i-1/2}}^{d_{i+1/2}} \beta_u(d \mid d_k^3) \gamma_i^{<i-1>}(m_1, m_2, d)\delta d + \int_{d_{i+1/2}}^{d_{i+3/2}} \beta_u(d \mid d_k^3) \gamma_i^{<i>}(m_1, m_2, d)\delta d \tag{5}$$

where $\gamma_i^{<i-1>}$ and $\gamma_i^{<i>}$ are the fractional volumes during droplet assignment satisfying the conservation of any two moments of order m_1 and m_2 (Ramkrishna, 2000), and $\beta_u(d \mid d_k) = u(d_i)\beta(d \mid d_k)/u(d_k)$ is a modified daughter droplet distribution. The ith coalescence interaction matrix $\boldsymbol{\Psi}^{<i>}$ depends only on the grid structure with nonzero elements: $\Psi_{k,j}^{<i>} = \omega(d_j^3, d_k^3, \phi)\Upsilon_{k,j}^{<i>}$, where ω is the coalescence frequency and,

$$\Upsilon_{j,k}^{<i>} = \begin{cases} [1-\frac{1}{2}\delta_{j,k}][\gamma_i^{<i-1>}(m_1, m_2, d_j^3 + d_k^3)\left[\frac{u(d_j^3 + d_k^3 = d_i^3)}{u(d_j^3)u(d_k^3)}\right], \ if \ d_{i-1}^3 \le d_j^3 + d_k^3 < d_i^3 \\ [1-\frac{1}{2}\delta_{j,k}][\gamma_i^{<i>}(m_1, m_2, d_j^3 + d_k^3)\left[\frac{u(d_j^3 + d_k^3 = d_i^3)}{u(d_j^3)u(d_k^3)}\right], \ if \ d_i^3 \le d_j^3 + d_k^3 < d_{i+1}^3 \end{cases} \tag{6}$$

and $\boldsymbol{\zeta}_k = \dfrac{1}{u_m(x_k)}, \ \ k = 1, 2, ...M_x$

It is worthwhile to note that $\delta_{j,k}$ is the kronecker delta and the symbol, •, appearing in Eq.(4) denotes the element by element product between the two given vectors.

4.4 Discretization of the PBE with respect to space and time

Eq.(3) represent a system of conservation laws that are coupled through the convective and source terms and is dominated by the convective term for typical values of D_d and U_d encountered in LLECs (*Peclet No.*$\approx 1\times10^3 H - 2\times10^3 H$). Since we are interested in the droplet volume balance to determine the column hold up, we let $m_1=0$ and $m_2=1$ corresponding to conserving the zero and the first moments of the number population density. Due the dominance of the convective term it is expected that the hold up profile of each class (φ_i) will move with time along the column height with a steep front. So, accurate front tracking discretization approaches are to be used such as the nonoscillatory first and second order central difference schemes. Let the ith convective flux be denoted as $F_i = U_{d,i}\varphi_i$ and the staggering spatial grid: $z_{l\pm1/2} = z_l \pm \Delta z/2$ and the average cell hold up as $\varphi_{i,l} = \int_{z_{l-1/2}}^{z_{l+1/2}} \varphi_i(t,z)\delta z/\Delta z$. The convective flux then is discretized in conservative form using the Kurganove and Tadmor (2000) central schemes as follows:

$$F_{i,l+1/2} = \frac{F(\varphi_{i,l+1}, \partial\varphi_{i,l+1}/\partial z) + F(\varphi_{i,l}, \partial\varphi_{i,l}/\partial z)}{2} - \frac{S_{i,l+1/2}}{2}\left(\varphi_{i,l+1} - \varphi_{i,l} - \frac{\partial\varphi_{i,l+1}}{\partial z} - \frac{\partial\varphi_{i,l}}{\partial z}\right) \tag{7}$$

where the numerical derivatives appearing in Eq.(7) are reconstructed from the computed cell averages using a minmod-like limiter with adjustable parameter $\theta \in [1,2]$. The local maximum speeds, $S_{i,l+1/2}$, are evaluated component wise without resource to the full evaluation of the Jacobian $\partial\boldsymbol{F}/\partial\boldsymbol{\varphi}$. This is accomplished by lagging the nonlinear term during the implicit time discretization where the numerical flux becomes locally linear $\boldsymbol{F}^{r+1} = \boldsymbol{U}_d^r\boldsymbol{\varphi}^{r+1}$ at the time level $r+1$. Note that the above central differencing scheme is of second order accuracy and could be made first order by setting the spatial derivatives in Eq.(7) to zero. The diffusion term appearing in Eq.(3) is approximated using the difference between two adjacent first order derivatives. The time discretization is accomplished using the implicit Euler method where it is made noniterative by carefully lagging the nonlinear parts in the convective and source terms.

4.5 Numerical results and discussion

Before we apply the numerical approach developed in this work to the full PBE, we would like to gain some trust in its performance by comparing it with some standard although simplified analytical solution. So, we consider a LLEC with a dispersed phase introduced at the location ($z_d>0$) to flow freely upward through a stagnant continuous phase. The dispersed phase velocity, U_d, could be taken as the free rising velocity of a single droplet for low values of hold up (U_t) and the axial dispersion of the dispersed phase

is neglected as well as the droplet breakage and coalescence. The latter assumption should not be considered as an oversimplification of the problem since the authors have tested the performance of the droplet diameter discretization separately (Attarakih et al., 2003). Accordingly the analytical solution for the system of Eqs.(3) using the Laplace transforms could be simplified in terms of dispersed phase hold up to:

$$\phi(t,z) = U_d^{\sup} \int_{d_{\min}}^{d_{\max}} P^{feed}(d)/U_t(d)\, u\left(t - \frac{z - z_d}{U_t(d)}\right) \delta d \tag{8}$$

where u is the unit step function and $U_d^{\sup}$ is the superficial dispersed phase velocity. To completely specify the problem we assume the following for a laboratory scale LLEC: H=2.55 m, z_d=0.25 m, z_c=2.25 m, column diameter = 0.15 m, the feed distribution is exponential in terms of number density ($e^{-\pi d^3/6}$), d_{min} = 0.1 mm, d_{max}=3mm, and the volumetric flow rate of the dispersed phase is 0.1m^3/h. The single droplet terminal velocity is taken: $U_t = 0.036d$, where d is in mm and the droplet diameters as well as the spatial grids are uniformly constructed. The initial condition is taken as zero (no dispersed phase present initially). All the numerical testes are conducted using a PC processor PentiumIII with 750 MGH speed and digital visual FORTRAN version 5.0. The L_1 error ($L_1(t) = \sum_{i=1}^{M_x} \sum_{l=1}^{L} |\varphi_{i,l}^{<exact>}(t) - \varphi_{i,l}^{<num>}(t)|\, \Delta d_l \Delta z_i$) is used to test the accuracy of the numerical solution at a given instant of time. In this work , the first and second order central schemes are denoted by KT1 and KT2 respectively. Fig. 1 shows the convergence characteristics of the present numerical algorithm when compared with the analytical solution given by Eq.(8). First both KT1 and KT2 converge in the senesce of the L_1 error as the number of pivots and spatial cells is increased. Second the L_1 error of the KT2 method is approximately 40% lower than the KT1 method as expected where the minmod parameter, θ is set equal to 2. Fig. 2 compares the analytical and the numerical solutions using both KT1 and KT2 after t=10s. As expected KT1 shows numerical dispersion especially around the steep moving front and hence the front is somewhat smeared. However, the KT2 scheme tries to capture the moving front in a better way with a slight increase in the CPU time. The CPU time is compared for both schemes using 500 time steps of length Δt=0.02s using the implicit Euler method where it is found that KT1 needs 5s while KT2 7s.

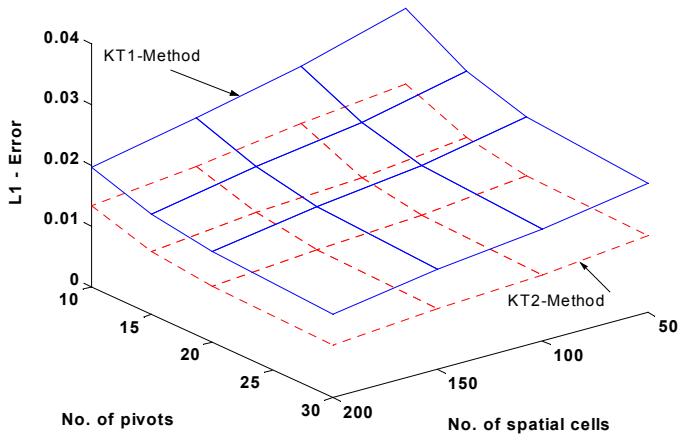

Fig.(1): Convergence of the central differencing schemes, t=10 s: KT1 & KT2.

Next we applied the present numerical approach to simulate the full PBE including droplet breakage and coalescence with the following frequencies: $\Gamma = 1.4\times10^{-3} d^6$, $\omega = (d^3 + d'^3)/100$, $\beta(d \mid d') = 6d^2/d'^3$, grid of 15×100 cells and $U_t = 0.036d(1-\phi)$. Fig. 3 shows the steady state droplet volume distribution calculated using the above specifications and the KT1 and KT2 schemes. It is clear that the droplet breakage is dominant and so as the droplets ascend the column the distribution is shifted to the small size range. This results in a nonuniform dispersed phase hold up along the column. The KT1 and KT2 schemes produced identical results since the steady state profile is not sharp.

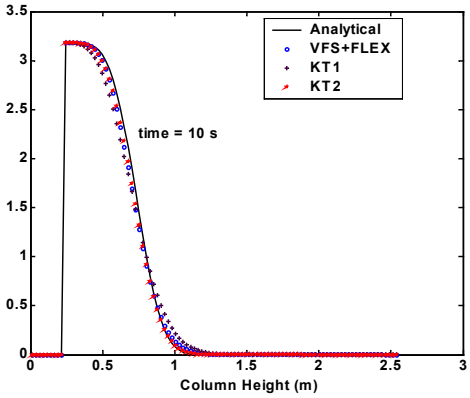

Fig.(2): Comparison between KT1 and KT2 methods.

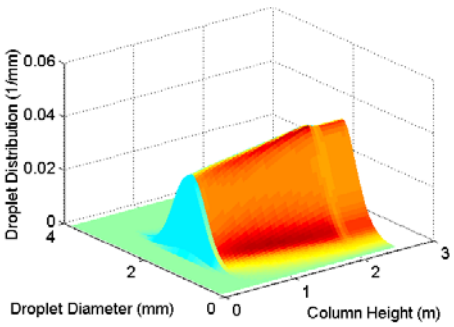

Fig.(3): Steady state droplet volume distribution using KT1 and KT2 methods.

4.6 Conclusions

The PB approach is used to model the complex behavior of the dispersed phase in a general LLEC. The resulting IPDEs are projected into a system of nonlinear and coupled conservation laws by generalizing the fixed pivot technique. These conservation laws were spatially discretized using nonoscillatory central differencing schemes. The implicit time discretization is made noniterative by careful lagging of the nonlinear terms. The extension of the present algorithm to mass transfer is under current development.

Nomenclature

A_c	column cross-sectional area, m^2
$\boldsymbol{A}$	breakage interaction matrix
D_d	dispersed phase dispersion coefficient, $m^2.s^{-1}$
d	droplet diameter, m
d_{min}, d_{max}	minimum and maximum droplet diameters, m
F	the convective flux, $m.s^{-1}$
f	number density function. m^{-1}
H	column height, m
m_1, m_2	order of moments
n	number concentration, m^{-3}
S	local propagation speed, $m.s^{-1}$
t	time, s
U_d	dispersed phase velocity, $m.s^{-1}$
u	single droplet property
U_t	droplet terminal velocity, $m\text{-}s^{-1}$
z	space coordinate
z_d	dispersed phase inlet, m

Greek symbols

φ_i	the ith class hold up
$\boldsymbol{\phi}$	the dispersed phase hold up
ω	coalescence frequency, $m^3.s^{-1}$
$\boldsymbol{\psi}$	the coalescence interaction matrix

References

Attarakih, M. M., Bart, H. J., & Faqir, N. M. (2003a). *Chem. Engng. Sci.*, **58,** 1251-1269.
Kronberger, T., Ortner, A., Zulehner, W., and Bart, H., J., 1995, *Computers Chem. Engng*., **19**, S639.
Kurganov, A., and Tadmor, E., 2000, *J. Comput. Phys*., **160**, 241.
Mahoney, A., W., and Ramkrishna, D., 2002, *Chem. Engng. Sci.*, **57,** 1107.
Ramkrishna, D., 2000, Population Balances, Academic Press, San Diego.
Wilburn, N.,P., 1964, *Ind. and Engng. Chem. Fund*., **3**, 189.

CHAPTER 5

Numerical Solution of the Two-Dimensional Population Balance Equation Describing the Hydrodynamics of Interacting Liquid-Liquid Dispersions

5.1 Introduction

The modeling of the multi-phase flow systems occurring in chemical engineering is now widely accepted based on the population balance concept. Within this framework it appears that Hulburt and Katz (1964) and Valentas and Amundson (1966) were among the first who introduced the PBE into the modeling of chemical engineering processes involving dispersed phase operations. Such processes include unit operations carried out in batch and continuous stirred tanks as well as in differential contacting equipment such as crystallization (Motz, Mitrovic & Gills, 2002), bubble (Campos & Lage, 2003) and liquid-liquid extraction columns (LLEC) (Modes et al., 1999; Gerstlauer, 1999). In such unit operation equipment the dynamically changing behavior of the dispersed particles, or strictly speaking droplets (or bubbles), makes it necessary to consider a detailed mathematical rather than lumped modeling approach. These details are necessary to describe the discontinuous events occurring due to the interaction of the turbulent continuous and the dispersed phases constituents (droplets) such as breakage and coalescence. Loosely speaking, the term breakage considers the interaction of a single droplet with the turbulent continuous phase where the droplet undergoes breakage if the turbulent kinetic energy transmitted to the droplet exceeds its surface energy (Coulaloglou & Tavlarides, 1977). On the other hand, droplet coalescence is expected to occur due to the interaction between two droplets and the turbulent continuous phase. The coalescence between these two droplets is considered to occur if the intervening liquid film has sufficient contact time to be drained out (Chatzi & Lee, 1987). Consequently, it is expected to find a droplet size distribution along the spatial coordinate of the liquid-liquid contacting equipment making the models inherently assuming uniform droplet size distribution or based on some mean droplet diameter (*d32*) of little practical value (Alatiqi et al., 1995, Weinstein, Semiat & Lewin, 1998). Accordingly, the promising modeling of these phenomena, based on the population balances, offers not only the dispersed phase hold-up (volume concentration) but also any integral property associated with the resulting particle (droplet) distribution such as the mean droplet size and the specific interfacial area required for the calculation of mass and heat fluxes (Al Khani, Gourdon & Casamatta, 1988; Tsouris, Kirou & Tavlarides, 1994; Alopaeus et al., 2002).

The population balance approach could be applied for modeling the behavior of the interacting liquid-liquid dispersions in either two basic ways, namely; the stagewise and the differential models. In the stagewise models (Tsouris, Kirou & Tavlarides, 1994; Kentish, Stevens & Pratt, 1998; Steiner, Balmelli & Hartland, 1999) the multistage column is represented by a sequence of interacting stirred tanks with forward and backward flow components to compensate for the nonideal behavior of each tank. In this sense a population balance equation has to be written for each tank with the required boundary conditions. In the differential model approach (Casamatta & Vogelpohl, 1985; Al Khani, Gourdon & Casamatta, 1988, 1989; Cabassud, Gourdon & Casamatta, 1990; Modes et al., 1999), the PBE is usually formulated as a conservation law in terms of volume concentration (mass for constant dispersed phase density). The resulting differential model takes into account the droplet transport; breakage and coalescence as well as the necessary boundary conditions, though the latter are not clearly stated in the published literature. For a comprehensive review of mathematical modeling of liquid-liquid extraction columns, their advantages and disadvantages, the interested reader could refer to Mohanty (2000).

The application of the population balance approach is expected to provide invaluable information if no careful modeling of the breakage and coalescence, as well as droplet transport laws, is taken into consideration. However, due to the recent extensive research for determining the kinetics of droplet breakage and coalescence as well as droplet transport from single and swarm droplet experiments, it

becomes more possible than before to introduce more realistic models for these kinetic parameters and the transport laws (Cauwenberg, Degreve & Slater, 1997; Kentish, Stevens & Pratt,1998; Colella et al., 1999; Modes, 2000; Alopaeus et al. 2002; Biggs & Lant, 2002; Bart, 2003; Desnoyer, Masbernat & Gourdon, 2003; Mignard, Amin, & Ni, 2003). Actually, this detailed level of information is at the expense of the mathematical complexity and thus demands a high computational cost since no analytical solution is known for the general population balance equation. Consequently, a numerical solution is required if precise simulation of the dispersed phase processes is required. In the last two decades there are many published papers concerned with the numerical solution of many special cases of the PBE arising from the modeling of many chemical and physical processes (Gelbard & Seinfeld, 1978; Sastry & Gaschignard, 1981; Gelbard, Tambour & Seinfeld, 1980; Casamatta & Vogelpohl, 1985; Al Khani, Gourdon & Casamatta, 1988; Al Khani, Gourdon & Casamatta, 1989; Hounslow, Marshal & Ryall, 1988; Marchal et al., 1988; Guimaraes et al., 1990; Hounslow, 1990; Kronberger et al., 1994; Hill & Ng, 1995; Kronberger et al., 1995; Ribeiro et al., 1995; Zimmermann et al., 1995; Kumar & Ramkrishna, 1996a, b; Hill & Ng, 1996; van Peborgh Gooch & Hounslow, 1996; Zamponi & Stichlmair, 1996; Hill & Ng, 1997; Kumar & Ramkrishna, 1997; Liou, Srienc & Fredrickson, 1997; Ribeiro et al., 1997; Song, Steif & Weinspach, 1997; Nicmanis & Hounslow, 1998; Toutain et al., 1998; Vanni 1999; Vanni, 2000; Lee et al., 2001; Wulkow, Gerstlauer, Nieken, 2001; Bennet & Rohani, 2001; Liu & Cameron, 2001; Motz, Mitrovic, & Gills, 2002; Lim et al., 2002; Verkoeijen et al., 2002; Mahoney & Ramkrishna, 2002; Diemer & Olson, 2002a, b; Attarakih, Bart & Faqir, 2003a, b; Compas & Lage, 2003; Goodson & Kraft, 2003). Despite this intensive research, there no general numerical approach exist which is applicable to the general PBE when multivariate population distributions are necessary to be taken into account. The dependence of the average number distribution on droplet size, concentration, and perhaps age (Ribeiro et al., 1995; Gerstlauer, 1999) is an example of such multivariate distribution in liquid-liquid dispersions is. Moreover, the problem becomes more complicated when external coordinates appear as in the case of differential population balance models. By external coordinate it is meant the physical space (continuous phase) which is occupied by the droplets and hence it is distinguished from the internal coordinates describing the droplet properties such as size, concentration, age etc. (Hulburt & Katz, 1964). This independent set of coordinates is often referred to in the population balance literature as the droplet (particle) phase space. One attractive approach to reduce the dimensionality of the population balance equation is by averaging it with respect to selected internal coordinate through the use of the method of moments (Randolph & Larson, 1988; Diemer & Olson, 2002). The method of moments is considered very attractive from computational point of view especially when specific average properties of the population are the target of the calculations. Unfortunately, the method of moments is not without inherent problems due to the closure and the distribution reconstruction intricacies (Diemer & Olson, 2002).

5.1.1 Review of the available numerical methods

Apart from the method of moments, the most frequently used numerical methods for the solution of the PBE could be grouped into three categories: stochastic, higher order and zero order methods.

5.1.1.1 Stochastic methods

Stochastic approaches as differentiated from finite difference methods are simulation techniques designed to artificially realize the system behavior through the generation of random numbers used for the identification of the probability functions governing the system behavior (Ramkrishna, 2000). This stochastic simulation approach has the advantage of being capable of simulating the multivariate PBE with respect to internal coordinate when the other numerical methods become extremely expensive. A presentation of two currently used algorithms for stochastic simulation of the PBE in a batch stirred tank: the direct simulation and the mass flow algorithms is found in Goodson and Kraft (2003).

5.1.1.2 Higher order methods

Most of the higher order methods try to approximate the distribution function by a set of linearly independent functions of order greater than zero through the finite element method. Gelbard and SeinFeld (1978) solved the PBE for droplet coalescence in batch stirred tank using the orthogonal collocation on finite elements with cubic polynomials and by scaling the droplet diameter logarithmically. Nicmanis and Hounslow (1998) solved the PBE for continuous stirred tank at a steady state using the mixed Galerkin

and the orthogonal collocation methods on finite elements with cubic polynomials. Despite their accuracy, the major disadvantage of these methods is the excessive computational load imposed by evaluation of double integrals. This is particularly when the breakage and coalescence functions are dependent on some integral property associated with the population such as the dispersed phase hold-up (time dependent). Mahoney and Ramkrishna (2002) addressed this issue in addition to the difficulties associated with singularities of the integrand where suggestions are presented to remove these singularities for specific coalescence frequencies. Wulkow, Gerstlauer and Nieken (2001) solved the PBE for crystallization process using the Galerkin method on finite elements, which is adaptive in both droplet size and order (Galerkin-h-p). Hamilton, Curits and Ramkrishna (2003) used the orthogonal collocation method using the Hermite basis functions weighted with the log-normal distribution. Their numerical results showed that the method is very accurate; however, at the expense of computational cost due to the appearance of many double integrals in the source terms. The major draw back of this method like the other Galerkin based methods is the difficulty to decouple the time dependent frequencies (coalescence and breakage) from the time dependent variables, and hence the computational cost is increased excessively especially when more than one coordinate in the PBE is involved. An extensive review of these methods could be found in Ramakrishna (1985, 2000).

5.1.1.3 Zero order methods

Zero order methods as referred to by Kostoglou and Karabelas (1994) are methods concerned with representing the population distribution after dividing the droplet size into finite number of classes by a constant value (zero order polynomial) in each class. In this way the original integro-partial differential equation is transformed into a system of ODEs for which the numerical solution is well established. Zero order methods could be classified into two broad classes according to Kumar and Ramkrishna (1996a): internally consistent and inconsistent discretization schemes with respect to selected integral properties. By internal consistency it is meant that the desired integral property associated with the average number concentration obtained from the discrete PBE should be the same as that obtained from its continuous counterpart. This internal consistency is found to predict accurately the desired integral properties and at the same time improves the accuracy of the predicted droplet distribution on coarse grids (Hounslow, Marshal & Ryall, 1988; Lister, Smit & Hounslow, 1995; Kumar & Ramkrishna, 1996a, b; Attarakih, Bart & Faqir, 2003a, b). Hounslow, Marshal and Ryall (1988) are the first who introduced an internally consistent set of discrete PBEs with respect to total number and volume for droplet coalescence in batch stirred tank using a geometric grid of constant factor 2. Unfortunately, this method is not amenable to grid refinement and it was extended to variable geometric factor by a set of more complicated discrete equations by Lister, Smit and Hounslow (1995). Hill and Ng (1995, 1996) followed this line and derived a discretized PBE for droplet breakage and coalescence in a batch stirred tank with a major flaw that it is dependent on the type of the breakage functions for droplet breakage and the type of the grid for droplet coalescence. Their simple extension to continuous stirred tank is considered internally inconsistent, as we will show in this work. One of the earliest works to force internal consistency by conserving total droplet number and volume is presented in the paper by Sastry and Gaschignard (1981). These authors introduced two coupled sets of discrete PBEs for droplet coalescence in terms of number and volume balances with the appearance of double integrals in the source and sink terms and thus showing an excessive computational costs. Kumar and Ramkrishna (1996a) used the advantage of internal consistency and introduced a general framework of zero order discretization that is internally consistent with respect to any two integral properties irrespective of the grid structure. This scheme is called the fixed-pivot technique because it concentrates the droplet population in a given size range at a single point (called the pivot) through the use of Dirac delta function. The underlying idea in this approach is that when a droplet is formed by either breakage or coalescence on a discrete grid its resulting characteristic volume will never coincide with any of the representative volumes except for the linear grid. In the classical discretization approaches the resulting droplet volume is assigned to the nearest pivot and hence it could be shown that only one integral property could be conserved (Attarakih, Bart & Faqir, 2004). To conserve at least two integral properties the resulting droplet volume is linearly interpolated between two adjacent pivots such that any two integral properties are conserved. The fixed-pivot technique is found to be very powerful not only in predicting the unimodal but also the bimodal distributions when the other zero order methods fail to do that or become computationally expensive (Vanni, 2000). Another variation of this approach is introduced by the same authors (Kumar & Ramkrishna, 1996b) making use of the idea of Sastry and Gaschignard (1981) and that of internal consistency through the so-called moving-pivot technique. For example, when both total number and mass are the desired quantities to be conserved, the technique results in two sets of number and volume balances coupled through the pivots. These pivots are

now dynamic quantities and change their positions to reflect the changes in the average number distribution. Attarakih, Bart and Faqir (2003a) extended recently the moving-pivot technique to a continuous stirred tank with only droplet breakage. Despite the high accuracy of the scheme it is considered computationally expensive when applied to PBEs showing spatial variation of the distribution. Lee et al. (2001) exploited the advantages of the fixed-pivot technique and coupled it with an adaptive mesh method and the method of characteristics to simulate a batch crystallizer of potassium sulfate. Lim et al. (2002) also made use of the fixed-pivot technique and weighted essentially non-oscillatory (WENO) scheme applied to the growth term to solve the PBE for a batch crystallizer of potassium sulfate. Although these authors claimed that their method conserves the total crystal number and mass, the discrete equations for agglomeration and breakage they used conserve only the total number due to the erroneous expressions resulting when the size coordinate is transformed from mass to length. Most recently, Campos and Lage (2003) have also used the fixed-pivot technique in the simulation of a bubble column through a mixed Euler-Lagrangian formulation. However, they failed to take into account the problem of internal consistency due to the presence of the feed distribution. This means that the extension of either the fixed-pivot or moving-pivot techniques to continuous flow systems is not simply by plugging the discrete equations of the source term in the model. In our previous work (Attarakih, Bart & Faqir, 2003a) we have shown how the moving-pivot technique could be *correctly* extended to continuous flow systems.

It is worthwhile to mention some of the internally inconsistent methods such as the Galerkin method on finite elements with zero order polynomials (Kronberger, 1995), the finite difference method of Ribeiro (1995) and the wavelet-based method presented by Liu and Cameron (2001). The first method was introduced to discretize the PBE describing the hydrodynamics of liquid-liquid extraction columns. The method is not only less accurate than the fixed-pivot technique, but also it is computationally less efficient due to the many double integrals in the source term. Ribeiro et al.(1995) presented a simple first-order finite difference scheme for both droplet size and time to simulate the hydrodynamics of a continuous stirred tank. The algorithm is also extended to three internal coordinates: droplet volume, age and concentration where the method is only consistent with respect to total droplet volume (Ribeiro et al., 1997). The wavelet-based method is used to discretize the PBE by approximating the average number concentration and the coalescence frequency using a series of wavelets. Liu and Cameron (2001) reported that the resulting computational matrices resulting from the wavelet collocation algorithm are computed offline for time independent coalescence frequencies. The method is shown to have good prediction of the average number concentration and its associated moments when sufficient number of collocation points are used (greater than 67 for the case of constant coalescence frequency). The method was only compared to some analytical solutions and not with any competing approach for the solution of the PBE to assess its performance. Bennet and Rohani (2001) used the combined Lax-Wendroff and Crank-Nicholson methods to simulate an evaporative cooling crystallizer with fines dissolution. The convergence and accuracy of the method for general cases including breakage and coalescence were not considered. Motz, Mitrovic and Gilles (2002) applied the space-time conservation element and solution element (CE/SE) (Chang, Wang & Chow, 1999) to crystallization process with only crystal growth, attrition, dissolution and nucleation. Their numerical results for crystal growth simulation showed that this method is much superior to a second-order flux-limited upwind scheme (Koren, 1993), however; the method was not extended to include crystal agglomeration or breakage.

Compared to the above literature concerning the solution of the PBE of one internal coordinate, there is a few numbers of numerical studies with regard to PBE showing external coordinate dependency when interacting liquid-liquid dispersions are considered. For the numerical solution of stagewise models the interested reader could refer to Gerstlauer (1999) and Mohanty (2000). For differential PBE models, Al Khani, Gourdon and Casamatta (1988), Gourdon and Casamatta (1994) and Milot et al. (1990) used the finite difference methods for discretizing both the internal and external coordinate; however, they presented no detailed information about the algorithms. Milot et al. (1990) reported that the spatial finite difference scheme that he used shows spurious numerical oscillations unless fine grid is used around the dispersed and continuous phase inlets. Kronbeger et al. (1994, 1995) solved the PBE with spatial dependency using the Galerkin and the finite volume methods for discretization of the internal and external coordinates respectively. The resulting discrete set of PBEs was treated as a system of conservation laws. They used a first-order upwind scheme with flux vector splitting based on the sign of the local droplet velocity. However, the approximate Riemann solver of Roe they used requires the estimation of the eigenvalues of the convective flux Jacobian, which is computationally very expensive for large systems. At a steady state where mild gradients exist they reported that both schemes produced identical results. Moreover, the aforementioned authors used a limited flux-extrapolation scheme of

second order accuracy. In spite of limiting the numerical flux it still shows spurious oscillations at the dispersed phase inlet especially during the transient period where large gradients are expected to occur.
Apart from interacting liquid-liquid dispersions, recently Campos and Lage (2003) presented a mixed Euler-Lagrange formulation for solving the PBE of a bubble column including bubble breakage, coalescence and absorption. They considered only positive bubble velocities and used third order TVD (Total Variation Diminishing) scheme to discretize the convective term.
In this work we have developed a numerical algorithm to solve the PBE describing the hydrodynamics of interacting liquid-liquid dispersions showing both spatial and time dependencies as well as droplet interactions (breakage and coalescence). The underlying idea of this work is presented briefly by Attarakih, Bart and Faqir (2003b) and will be extended, numerically tested and experimentally validated in this work. From the literature review above, it is clear that the fixed-pivot offers the advantages of being relatively simple, accurate and computationally efficient and hence it will be *correctly* extended and efficiently applied to continuous flow systems. Unlike, the previous works reported for spatial discretization, which usually use upwind differencing schemes, we utilize a couple of first and second order accuracy central differencing schemes recently developed by Kurganov and Tadmor (2000). These schemes offer the advantage over the upwind schemes that they are free of any approximate Riemann solvers and hence are not tied to the eigenvalue structure of the Jacobian of the convective flux. In addition to these two central schemes a simple first-order upwind differencing scheme with flux vector splitting is derived based on the transport phenomena of the dispersed phase in a general liquid-liquid extraction column. The remaining body of this chapter is arranged as follows: in section 5.2 we present the general PBE for continuous flow systems and then it is simplified to the special cases of completely mixed continuous flow tank and a differential liquid-liquid extraction column (LLEC). The generalization of the fixed-pivot technique to continuous flow systems will be presented in section 5.3 stressing on how the feed source term is treated. In this section, the coalescence and breakage matrices are restructured to improve the scheme performance with special attention paid to the finite domain error. In section 5.4 we derive the semi-discrete PBEs based on the LLEC transport and the interactions of the dispersed and continuous phases along with the introduction of the central first and second order semi-discrete schemes, as well as the time discretization of the resulting system of ODEs. Section 5.5 is devoted to test the generalization of the fixed-pivot technique for droplet coalescence to continuous flow stirred tank, since Attarakih, Bart and Faqir (2004) extensively tested the GFP for droplet breakage. In section 5.6 we present three analytical solutions of the simplified PBE for LLECs against which the full discretization of the PBE is tested and validated. The experimental realization of the model is dealt with in section 5.7 by considering a laboratory scale LLEC of rotating disc type (RDC) for which the steady state hydrodynamic experimental data is available (Modes 2000). Finally in section 5.8 we present our conclusions and recommendations.

5.2 The general population balance equation

The PBE describing the hydrodynamics of a dispersed phase flowing in a continuous flow system in the absence of other transport phenomena such as mass transfer (no convective flux along the droplet internal coordinate) could be written as:

$$\frac{\partial n(v;\boldsymbol{r},t)}{\partial t}+\nabla\cdot\boldsymbol{F}=\nabla\cdot(\boldsymbol{D}_d\nabla n)+\rho\{n,v\} \tag{1}$$

where v is the droplet volume, $\boldsymbol{r}=[x, y, z]$, is a vector of external coordinate specifying the spatial variation of n. $n(v;\boldsymbol{r},t)\delta v=N(t,\boldsymbol{r})f(v)\delta v$ is the average number concentration associated with droplets having a volume between $v\pm\delta v$ at the time instant t and position in space $\boldsymbol{r}$ and its corresponding total number concentration is $N(t, \boldsymbol{r})$ while $f(v)$ is the average number density.
The second term on the left hand side represents the droplet transport by convection through surface of a given volume in space with velocity $\boldsymbol{U_d}=[U_{d,x}, U_{d,y}, U_{d,z}]$ and flux $\boldsymbol{F}=\boldsymbol{U_d}n$.
The first term on the right hand side is the droplet transport by diffusion characterized by the random movement of the individual droplets, in contrast to the convective transport by the turbulent eddies. The coefficient $\boldsymbol{D}_d$ appearing in this term is the Fick's diffusion tensor. The last term on the right hand side is the net number of droplet produced by either breakage or coalescence per unit time and unit volume and is given by (Valentas & Amundson, 1966):

$$\rho\{n,v\} = -\Gamma(v,\phi)n(v;z,t) + \int_{v}^{v_{\max}} \Gamma(v',\phi)\beta_n(v \mid v')n(v';z,t)\delta v' - n(v;z,t)\int_{v_{\min}}^{v_{\max}-v} \omega(v,v-v',\phi)n(v-v';z,t)\delta v' + \tfrac{1}{2}\int_{v}^{v_{\max}} \omega(v,v-v',\phi)n(v-v';z,t)n(v';z,t)\delta v' \quad (2)$$

The first and third terms in the above expression represent the rate at which the droplets are lost by breakage and coalescence per unit volume respectively, while the second and the fourth terms account for the rate of formation of droplets by breakage and coalescence per unit volume respectively. The breakage and coalescence frequencies are given by the functions, Γ and ω respectively and are dependent on the agitation intensity, internal tank (column) geometry, the system physical properties, and the dispersed phase hold-up: $\phi(\boldsymbol{r},t) = \int_{v_{\min}}^{v_{\max}} vn(v;\boldsymbol{r},t)\delta v$.

Note that the function $\beta_n(v|v')$ represents the distribution of the daughter droplets, given that a mother droplet of volume v' is broken and is assumed independent of time, but it may be function of the energy input and the system physical properties. This function should satisfy the usual number, volume and the physical ($\beta_n(v|v')=0$, $v>v'$) constraints (Ramkrishna, 2000).

5.2.1 The PBE for a completely mixed tank

The PBE for a completely mixed tank could be derived from Eq.(1) by integrating it over a finite some constant volume in space by making use of the divergence theorem to get:

$$\frac{\partial n(v;t)}{\partial t} = \frac{\left(\frac{\phi^{feed}}{v_f} f^{feed} - n\right)}{\tau} + \rho\{n,v\} \quad (3)$$

where τ is the vessel residence time, v_f is the average feed droplet volume, f^{feed} is the feed number density, and ϕ^{feed} is the dispersed phase hold-up entering the tank. The number concentration function is considered to satisfy the following two regulatory conditions:

$$n(v < v_{\min}, t) = 0 \quad (4)$$

$$n(v > v_{\max}, t) = 0 \quad (5)$$

these equations indicate that the number concentration function should vanish below and above minimum and maximum droplet volumes respectively. This is always true for turbulently interacting liquid-liquid dispersions in which both droplet breakage and coalescence mechanisms come to a local dynamic equilibrium. In this case droplets having volume less than v_{min} will coalesce and those greater than v_{max} will break up (Liu & Li, 1999). To complete the mathematical model of the completely stirred tank an initial condition must be specified. In this work only the continuous phase is present at the instant where the feed of the dispersed phase is switched on and thus corresponding to zero initial condition.

5.2.2 The PBE for a differential LLEC

The PBE for a countercurrent LLEC without mass transfer and showing spatial variation only along the column height could be simply deduced from Eq.(1):

$$\frac{\partial n}{\partial t} + \frac{\partial F}{\partial z} = \frac{\partial}{\partial z}\left(D_d \frac{\partial n}{\partial z}\right) + \frac{Q_d}{A_c}\left(\frac{n^{feed}}{v_f}\right)\delta(z - z_d) + \rho\{n,v\} \quad (6)$$

where $n(v;z,t)\delta v = N(t,z)f(v)\delta v$ is the average number concentration of droplets having a volume between $v \pm \delta v$ at the time instant t and column height z, and $N(t,z)$ is the total number concentration. The convective flux of these droplets along the column of a constant cross sectional area, A_c is represented by

$A_c F \delta v = A_c U_d n \delta v$, where U_d is the velocity of the dispersed phase relative the column walls and will be derived later on. The first term on the right hand side of Eq.(6) represents the axial dispersion of the dispersed phase due to the non-ideal flow in which a random movement of the fluid on the microscopic level is superimposed on the main flow (Zhu et al., 1983). This is assumed to follow Fick's law with a diffusion coefficient, D_d, and is distinguished from the forward mixing effect due to the droplet velocity distribution that is taken into account by the convective term (Zhang, Zhou & Su, 1985). The second term on the left hand side represents a number concentration rate of droplet entering as a feed of volumetric flow rate, Q_d, at the level z_d of the column. The positive direction of flow coincides with the dispersed phase flow from z_d to the top of the column. Note that the feed distribution is represented mathematically by a point source through the use of the Dirac delta function (Kronberger et al., 1994).
It should be noted that Eq.(6) is unlike the previous PBE models that are written directly in terms of volume rather than number concentration (eg. Casamatta & Vogelpohl, 1985 and Kronberger et al., 1994), since the internally consistent discrete PBEs in terms of any desired quantity are always derived from the number concentration PBE. Moreover, Eq.(6) is written in terms of the droplet volume rather than diameter as the internal coordinate to eliminate the complex expressions resulting from the internal coordinate transformation. However, we will simply project back the discrete PBEs onto the droplet diameter coordinate using the identity:

$$\int_{v_{i-1/2}}^{v_{i+1/2}} n(v;z,t)\delta v = \int_{d_{i-1/2}}^{d_{i+1/2}} n(d;z,t)\delta d \tag{7}$$

The boundary conditions are greatly simplified since the dispersed and the continuous phases are included in the model as point sources. So, the Danckwart's boundary conditions based on the discussion of Wilburn (1964) could be written by considering the LLEC to behave like a closed vessel between 0^+ and column height H:

$$0 = max(F,0) - D_d \frac{\partial n}{\partial z}, \quad at\ z = 0 \tag{8}$$

$$0 = -min(F,0) + D_d \frac{\partial n}{\partial z}, \quad at\ \ z = H \tag{9}$$

$$n(v;z,t) = n_0(v;z), \forall z \in [0,H] \tag{10}$$

The first boundary condition satisfies the continuity of the dispersed phase flux taking into account the possibility of droplet entrainment with the countercurrent continuous phase. The second boundary condition idealizes the situation at the top interface and simply means that the droplets with positive rise velocity reaching the level, H, will leave the column. However, realistic modeling of the mechanism of droplet coalescence at the interface needs more hydrodynamic considerations (Hartland & Jeelani, 1994).
In the above formulation, we also assume that the droplet breakage and coalescence are active only for $\forall z \in [z_d, z_c]$ and zero otherwise, where z_c is the continuous phase inlet. The regulatory conditions given by Eqs.(4) and (5) are also applicable for this case. The mathematical model given by Eq.(6) is also subjected to the initial condition implied by Eq.(10).

5.2.2.1 The dispersed and continuous phases velocities

The droplet rise velocity of the dispersed phase relative to the continuous one is given by:

$$U_r(d,z,\phi) = U_d \pm U_c \tag{11}$$

where the plus sign stands for countercurrent flow systems and the negative one stands for cocurrent systems. U_d and U_c are the actual dispersed and continuous phase velocities with respect to the column walls respectively. The relative velocity (also called the slip velocity) may be found from the single droplet terminal velocity modified such that the effect of the droplet swarm and the slowing effect due to the column internals are taken into account. Unfortunately, the form of this velocity is found dependent on the type of the column as well as the system physical properties. For comprehensive review of the slip velocity, as well as a simple guide for choosing the terminal droplet velocity, the reader could refer to Gourdon and Casamatta (1994). Nevertheless, we will assume a quite general form of the relative velocity

such that it could be simply adapted to the type of the column and the chemical system under investigation:

$$U_r(d,z,\phi) = K_v U_t(d,\boldsymbol{P}) f(\phi) \tag{12}$$

In the above equation K_v is droplet slowing factor having a value between zero and one which takes into account the internal column geometry and might be dependent on energy input, and the droplet diameter (Modes, 2000). U_t is the single droplet terminal velocity and is adequately described by some correlation such as Klee and Treybal (1956), Vignes (1965) and Grace, Wairegi and Nguyen (1976) depending on the system physical properties (Gourdon and Casamatta, 1994). The function $f(\phi)$ takes into account the effect of droplet swarm and is generally taken as $(1-\phi)^m$, where m is an empirical exponent (Godfrey and Slater, 1991), while the vector $\boldsymbol{P}$ may consist of all the system physical properties.
The remaining unknown in Eq.(11) is the continuous phase velocity which is usually determined in either two ways: The first one is due to Casamatta (1981) which is derived by making a total volume balance around a closed control volume spanning the column height from the base to an arbitrary level z. The derivation is accomplished by assuming that the variation of the continuous flow rate and hence U_c will cause an immediate change to the flow of the continuous phase. Kronberger (1995) presented a more mathematically sound derivation of this velocity model by coupling the dispersed and the continuous phases balances. This velocity model is valid at each instant of time and hence is suitable to transient column simulations although it shows oscillatory behavior in the transient hold-up due to the perfect control of the interface at the upper settling zone as shown in Fig.(1) (Hufnagl, McIntyre & Blass, 1991).

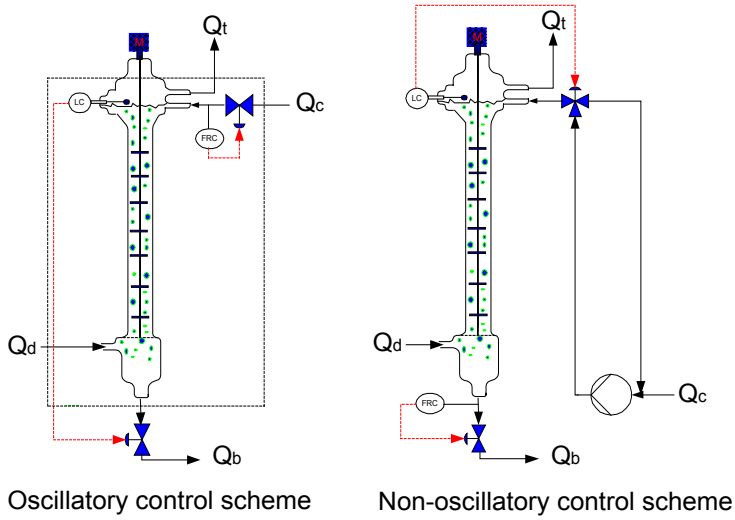

Fig.(1): Conventional and improved dispersed phase level controls (Hufnagl, McIntyre & Blass, 1991).

The second velocity model is more simple than the first one and is derived by assuming the continuous phase hold-up at a steady state and hence it is valid only for steady state simulations (Kronberger, 1995). The first model will be denoted as the oscillatory velocity model and the second one as a steady state velocity model, where both models are presented in Table 3 for the sake of clarity.
Hufnagl, McIntyre & Blass (1991) tried to improve the prediction of their lumped hydrodynamic model, which was unable to follow the oscillatory experimental hold-up behavior by suggesting an elegant interface level control scheme that proved experimentally to eliminate the transient oscillatory behavior of the dispersed phase hold-up. However, their idea was not mathematically formulated until 1998 when Weinstein, Semiat and Lewin (1998) included this idea in their lumped hydrodynamic model for a Kuhni LLEC. The stagewise dynamic population balance model of Gerstlauer (1999) was also neither able to follow the oscillatory behavior of the hold-up experimental profile nor to correctly eliminate it. The reason is simply that this author used the steady state continuous phase velocity model described above.
Accordingly, we present below an improved non-oscillatory continuous velocity model based on the control scheme of Hufnagl, McIntyre & Blass (1991). The idea of these authors is to manipulate the inlet

continuous feed flow rate rather than the traditional manipulation of the outlet continuous flow rate (see Fig.(1)). Now applying total volume balances around the control volume indicated by the dashed line on Fig.(1) we get the following two relations:

$$Q_{c,in} + Q_d = Q_t + Q_b \tag{13}$$

and note that:

$$Q_{c,out} = (1 - \phi_e) Q_b \tag{14}$$

where ϕ_e is the fraction of the dispersed hold-up entrained with continuous phase if any. By combining the above relations we get the required continuous phase flow rate in terms of the dispersed phase throughput:

$$Q_{c,in} = Q_t + \frac{1}{1-\phi_e} Q_{c,out} - Q_d \tag{15}$$

This equation when combined with the oscillatory velocity model given in Table 3 it provides the improved non-oscillatory velocity model. Now the dispersed phase velocity, U_d, could be obtained directly from Eq.(11) and hence the hydrodynamic model of the LLEC is completely formulated.

5.3 Model discretization with respect to internal coordinate

The population balance model given by Eq.(6) represents a nonlinear integro-partial differential equation (IPDE) of convective-diffusion type, where the source of nonlinearity is due to the convective and the source terms. To project this IPDE onto a finite set of PDEs, we discretize the droplet internal coordinate, v, according to the following discrete set: $\{v_{i-1/2} \mid i = 1, \ldots. M_x + 1\}$ with $v_{\min} = v_{1/2} < v_{3/2} < \ldots < v_{M_x+1/2} = v_{\max}$. Let the ith subdomain be defined as $V_i = [v_{i-1/2}, v_{i+1/2}),\ \mathrm{i} = 1, \ldots M_x$ and the population of the ith subdomain be concentrated at the middle of this subdomain such that $x_i = (v_{i-1/2} + v_{i+1/2})/2 = \pi d_i^3 / 6$ (see Fig. 2). Then the droplet size distribution is expanded using a point wise sampling of the distribution at the middle of the ith subdomain (also called the pivot) according to the following relation:

$$n(v; z, t) = \sum_{i=1}^{M_x} N_i(z,t) \delta(v - x_i) \tag{16}$$

where δ refers to the Dirac delta function and the set of the unknown coefficients, $N_i(z,t)$, refer to the total number concentration in the ith subdomain. Let us define the total quantity of droplets associated with a single droplet property $u_m(v)$ in the ith subdomain by:

$$\mathrm{I}_i(z,t) = \int_{v_{i-1/2}}^{v_{i+1/2}} u_m(v) n(v; z, t) dv = u_m(x_i) N_i(z,t),\ m = 1, 2 \tag{17}$$

where the volume fraction, $\varphi_i(z,t)$, and the number concentration, $N_i(z,t)$, in the ith subdomain follow directly by substituting $u_2(v)=v$ and 1 in the last equation respectively.

Kumar and Ramkrishna (1996a) showed that when the source term given by Eq.(2) is discretized by integrating it from $v_{i-1/2}$ to $v_{i+1/2}$ with respect to v, the source of internal inconsistency as described in section 5.1.1.3, results mainly due to the formation terms of breakage and coalescence but not due to the loss terms. They solved this problem through modifying the formation terms due to breakage and coalescence by multiply them with a triangular function that we may define as:

$$w_i(v) = \begin{cases} \gamma_i^{<i-1>}(v), & x_{i-1} \le v < x_i \\ \gamma_i^{<i>}(v), & x_i \le v < x_{i+1} \end{cases} \tag{18}$$

The set of linear functions, $\gamma_i^{<i-1>}(v)$ and $\gamma_i^{<i>}(v)$ should satisfy the constraints imposed by the conservation of any two integral properties associated with the number distribution function obtainable from those associated with the single droplet, $u_1(v)$ and $u_2(v)$:

$$\gamma_{i-1}^{<i-1)}(v)u_m(x_{i-1}) + \gamma_i^{<i-1>}(v)u_m(x_i) = u_m(v),\ m = 1,2 \tag{19}$$

Making use of these ideas we can integrate Eqs.(3) and (6) with respect to v from $v_{i-1/2}$ to $v_{i+1/2}$ with the aid of Eq.(16) and then multiplying both sides by the general desired discrete quantity, $u_m(x_i)$, to get the following sets of nonlinear ODEs and PDEs for a completely mixed tank and a differential LLEC respectively:

$$\frac{dI_i}{dt} = \frac{\left(\frac{\phi^{feed}}{v_f} I_i^{feed} - I_i\right)}{\tau} + \rho_i\{\boldsymbol{I},\boldsymbol{d}\} \tag{20}$$

$$\frac{\partial I_i}{\partial t} + \frac{\partial F_i}{\partial z} = \frac{\partial}{\partial z}\left(D_d \frac{\partial I_i}{\partial z}\right) + \frac{Q_d}{A_c}\left(\frac{I_i^{feed}}{v_f}\right)\delta(z - z_d) + \rho_i\{\boldsymbol{I},\boldsymbol{d}\} \tag{21}$$

where the source term for droplet breakage is transformed in terms of droplet diameter using Eq.(7) and is given by:

$$\rho_{b,i}(\boldsymbol{I}) = -\Gamma(d_i,\phi(t,z))I_i + \sum_{k=i}^{M_x} \pi_{i,k}^{<m>}\Gamma(d_k,\phi(t,z))I_k,\ \ i = 1,2,...M_x \tag{23}$$

$$\pi_{i,k}^{<m>} = \int_{d_{i-1}}^{d_i} \gamma_i^{<i-1>}(d)[\frac{u_m(d_i)}{u_m(d_k)}]\beta_n(d \mid d_k)\delta d + \int_{d_i}^{\min(d_k,d_{i+1})} \gamma_i^{<i>}(d)[\frac{u_m(d_i)}{u_m(d_k)}]\beta_n(d \mid d_k)\delta d \tag{24}$$

Note that the upper limit of integration on the second integral is set to satisfy the constraint: $\beta_n(d \mid d_k) = 0, d \geq d_k$. Similarly the source term for droplet coalescence could be written by introducing the idea of interaction coalescence matrix, $\boldsymbol{\Psi}$ as:

$$\rho_{c,i}(\boldsymbol{I}) = \sum_{k=1}^{i}\sum_{j=k}^{i} \Psi_{k,j}^{<i>}\omega_{k,j}I_kI_j - I_iu_m(x_i)\sum_{k=1}^{Mmax(i)} \frac{\omega_{i,k}}{u_m(x_k)u_m(x_i)}I_k,\ \ i = 1,2,..M_x \tag{25}$$

where $\boldsymbol{d}$ = $[d_1, d_2 \ ... \ d_{Mx}]$, $\boldsymbol{I}$=$[I_1, I_2, \ ... \ I_{Mx}]$ and the upper index on the loss term summation is the maximum integer such that: $Mmax(i) = \max_k(d_i^3 + d_k^3 \leq d_{Mx}^3);\ i,\ k = 1,\ 2..M_x$.

The significance of introducing the coalescence interaction matrix has two distinctive advantages over the original formulation of Kumar and Ramkrishna (1996a). The first one is that this three dimensional matrix is decoupled from the time dependent variables, $\boldsymbol{\omega}$ and $\boldsymbol{I}$ and hence it is always evaluated offline once a time. Second the ith coalescence interaction matrix, $\boldsymbol{\Psi}^{<i>}$, has a size $i \times i \times i$ which grows linearly as i increases and hence this saves the storage requirement instead of storing an $M_x \times M_x \times M_x$ matrix for each i. Moreover, the sparse nature of the ith coalescence interaction matrix will reduce the execution time considerably, as we will see later. This is because we carry the above summations only when the resulting volume of any two droplets of volumes x_k and x_j falls in the ith subdomain. Thus, the nonzero elements in the ith coalescence interaction matrix are the volumes of the coalescing droplets that report in the ith subdomain and are given by:

$$\boldsymbol{\Psi}_{k,j}^{<i>} = \begin{cases} \left[1 - \frac{1}{2}\delta_{k,j}\right]\frac{u_m(x_i)}{u_m(x_j)u_m(x_k)}\gamma_i^{<i-1>}(x_k + x_k), & \text{if} \quad d_{i-1}^3 \leq d_j^3 + d_k^3 < d_{i-1}^3 \\ \left[1 - \frac{1}{2}\delta_{k,j}\right]\frac{u_m(x_i)}{u_m(x_j)u_m(x_k)}\gamma_i^{<i>}(x_k + x_k), & \text{if} \quad d_i^3 \leq d_j^3 + d_k^3 < d_{i+1}^3 \end{cases} \tag{26}$$

where $\delta_{k,j}$ is the kronecker delta.
The two sets of Eqs.(20) and (21) are not internally consistent with respect to any two integral properties, $u_1(v)$ and $u_2(v)$ due to the presence of the feed distribution (Attarakih, Bart & Faqir, 2004). The internal consistency could be restored if we generalize the fixed-pivot technique by considering the appearance of the feed distribution as a formation (birth) term similar to those for breakage and coalescence. Making use of this, we can multiply the feed distribution by the triangular function given by Eq.(18) and integrating with respect to v from $v_{i-1/2}$ to $v_{i+1/2}$ and then multiplying it by $u_m(d_i)$ to get:

$$I_i^{feed} = \int_{d_{i-1}}^{d_i} \gamma_i^{<i-1>}(d)[u_m(d_i)] f^{feed}(d)\delta d + \int_{d_i}^{d_{i+1}} \gamma_i^{<i>}(d)[u_m(d_i)] f^{feed}(d\,|)\delta d \tag{27}$$

Now it is with this final equation the two sets of Eqs.(20) and (21) are internally consistent with their continuous counterparts Eqs.(3) and (6) with respect to any two integral properties obtainable from those of single droplets.

5.3.1 Restructuring of the discrete source term

The recognition of the sparse structure of the coalescence interaction matrix makes it possible to reduce the computational time drastically. The first double summation in Eq.(25) recognizes only the triangular structure of the *i*th interaction coalescence matrix and ignores its sparse nature. This sparse nature is due to the definite number of droplets falling in the *i*th subdomain through coalescence of droplets from the *k*th and *j*th subdomains. Since not all the coalescence events will lead to droplet volumes falling in the *i*th subdomain, then a number less than or equal to $i(i+1)/2$ always exists representing the maximum number of droplets falling in the *i*th subdomain. So, before we initiate the calculations, we will determine a set of vectors and matrices: *Kmin(i)*, *Kmax(i)*, *M(i)*, *Jmin(i,k),* and *Jmax(i,k)* representing the locations of the nonzero elements of the *i*th interaction matrix once the grid structure becomes available. Hence, we modify the limits of the summations in the coalescence formation term as follows:

$$\rho_{c,i}(\boldsymbol{I}) = \sum_{k=Kmin(i)}^{Kmax(i)} \sum_{j=Jmin(i,k)}^{Jmax(i,k)} \Psi_{k,j}^{<i>} \omega_{k,j} I_k I_j - I_i u_m(x_i) \sum_{k=1}^{Mmax(i)} \frac{\omega_{i,k}}{u_m(x_k) u_m(x_i)} I_k \tag{28}$$

Similarly the source term for droplet breakage could be written in terms of the breakage interaction matrix that have an upper triangular structure with the following elements:

$$A_{i,k} = \begin{pmatrix} \left[\pi_{i,i}^{<m>} - 1\right] \\ \pi_{i,k}^{<m>} \end{pmatrix},\ i = 1,2..M_x,\ k = i,\ i+1...M_x \tag{29}$$

Like the coalescence interaction matrix it is independent of time and thus it is generated only once a time offline. The complete source term could now be written in a compact matrix form as follows:

$$\boldsymbol{\rho}(\boldsymbol{I}) = \begin{pmatrix} \boldsymbol{I}^T\left[\left(\boldsymbol{\omega} \bullet \boldsymbol{\Psi}^{<1>}\right)\boldsymbol{I}\right] \\ \boldsymbol{I}^T\left[\left(\boldsymbol{\omega} \bullet \boldsymbol{\Psi}^{<2>}\right)\boldsymbol{I}\right] \\ \cdots\cdots\cdots\cdots \\ \boldsymbol{I}^T\left[\left(\boldsymbol{\omega} \bullet \boldsymbol{\Psi}^{<M_x>}\right)\boldsymbol{I}\right] \end{pmatrix} - \boldsymbol{I}^T \bullet \left[\boldsymbol{\omega}\left(\boldsymbol{\zeta} \bullet \boldsymbol{I}\right)\right] + \boldsymbol{A}[\boldsymbol{\Gamma} \bullet \boldsymbol{I}] \tag{30}$$

where:

$$\zeta_k = \frac{1}{u_m(x_k)} \tag{31}$$

and the symbol $\bullet$ appearing in Eq.(30) denotes an element by element matrix multiplication.

5.3.2 The finite domain error

Due to the presence of the boundary conditions (regulatory conditions) there would be an inevitable underestimation of the integral properties obtained from the number distribution if these boundary conditions are not exactly satisfied. This failure of taking into account the nonzero values of the portions of the distribution below d_{min}, and above d_{max} (if these droplet sizes are not properly chosen) is termed the finite domain error (FDE) (Gelbard & Seinfeld, 1978; Nicmanis & Hounslow, 1998; Attarakih, Bart & Faqir, 2003a). The subsequent erroneous estimation of d_{min}, and d_{max} such that the regulatory conditions are not approximately satisfied will result in an underestimation of the predicted integral quantities of interest. So, we present the following approximate relation to safely estimate the minimum and maximum internal coordinate sizes at fixed number of subdomains, M_x, such that the total FDE is below a specified tolerance *TOL*:

$$FDE(d_{\min}, d_{\max}, M_x) = FDE^L + FDE^U \le TOL \tag{32}$$

where:

$$FDE^L \approx \sum_{m=1}^{2}\sum_{i=1}^{2}\frac{1}{\Delta d_i}u_m(d_i)N_i(z,t) + \sum_{m=1}^{2}\sum_{i}^{2}\frac{1}{\Delta d_i}\left(\int_{d_{i-1/2}}^{d_{i+1/2}}u_m(d)n^{feed}(d)\delta d + \int_{d_{i-1/2}}^{d_{i+1/2}}u_m(d)n^{ic}(d)\delta d\right) \tag{33}$$

$$FDE^U \approx \sum_{m=1}^{2}\sum_{i=M_x-1}^{M_x}\frac{1}{\Delta d_i}u_m(d_i)N_i(z,t) + \sum_{m=1}^{2}\sum_{i=M_x-1}^{M_x}\frac{1}{\Delta d_i}\left(\int_{d_{i-1/2}}^{d_{i+1/2}}u_m(d)n^{feed}(d)\delta d + \int_{d_{i-1/2}}^{d_{i+1/2}}u_m(d)n^{ic}(d)\delta d\right) \tag{34}$$

The derivation of these relations is shown in Appendix B.
Unfortunately, for a dispersed process in which both breakage and coalescence are active, the estimation of d_{min} and d_{max} has an iterative nature. First start with an initial estimation at fixed M_x, solve the complete problem, and check if the condition implied by Eq.(32) is satisfied. If it is not satisfied, then d_{min}, will be reduced and d_{max} will be increased by a small amount and the problem is solved again until Eq.(32) is satisfied. It should be noted that a minimum number of subdomains (M_x) that satisfies Eq.(32) at a specified tolerance, *TOL*, always exists.
A particular advantage of this approach is that the above condition is checked at each integration step or perhaps at regular time steps. So, once this condition is violated the calculations should be stopped and restarted again with an improved estimation of d_{min} and d_{max}. This reduces the computational time significantly while at the same time achieving an automatic FDE estimation. Moreover, another obvious advantage of the estimation of the total FDE is to minimize it at a specified simulation time by keeping the lower and upper finite domain errors approximately equal (Attarakih et al., 2003a).

5.4. Model discretization with respect to external coordinate

The discrete sets of ordinary and partial differential equations given by Eqs.(20) and (21) are now in terms of any discrete quantity, $u_m(d_i)$ associated with the discrete number concentration, $N_i(z,t)$. The question that presents itself at this stage is which discrete quantity, $u_m(d_i)$ that is suitable for the discretization of Eq.(21) with respect to the external coordinate? This question might be answered if we are guided by the volume approach for the PBEs presented recently by Verkoeijen et al. (2002). These authors have pointed out that the volume distribution based on droplet volume as an internal coordinate is the most suitable when the PBE is coupled with a fluid dynamics model such that in our case. This volume distribution becomes inevitable since the finite volume numerical approach is the most feasible one for external coordinate discretization for the system of PDEs given by Eq.(21) (Toro, 1999). This is because Eq.(21) represents a system of nonlinear conservation laws coupled through the convective and source terms when the volume (mass) distribution is chosen to describe the droplet population evolution in space and time. It should not be confused that the droplet diameter appearing in Eqs.(21) contradicts the above conclusions since we projected the volume onto the diameter coordinate only after the internal coordinate discretization . Thus, we preserved all the advantages of using the droplet volume as internal coordinate discussed by Verkoeijen et al. (2002) such as the additive property of droplet volumes.
So, in the following section the finite volume numerical approach is used to discretize the PBEs with respect to the external coordinate (column height) using a volume distribution function by setting $u_1(v)=1$and $u_2(v)=v$ corresponding to total number and volume conservation and hence:

$$I_i = \varphi_i(z,t) = x_i N_i(z,t) \tag{35}$$

5.4.1 Spatially first and second order discrete LLEC models

The system of conservation laws given by Eq.(21) is actually dominated by the convective term for typical values of D_d which are in the order of $10^{-4} m^2/s$ (Modes, 2000) (Peclet No. $\approx 1\times10^3\ H$ - $2\times10^3\ H$). Due to this and the presence of the point source term imposed by the feed at the location z_d it is expected that the total transient hold-up (and hence the hold-up of the different internal subdomains) will move along the column height with a steep front. Accordingly, high-resolution schemes are required to capture this moving front since first order schemes are known to suffer from excessive numerical diffusion (front smearing) (Toro, 1999). However, it will be very useful in the first step of spatial discretization is to consider only a first-order accurate scheme which is based on droplet volume balance on discrete space (spatial cell). So recall that the *i*th convective flux is given by:

$$F_i = U_d(d_i, \phi)\varphi_i(z,t) \tag{36}$$

and consider the general staggering spatial grid (cell-centered finite volume approach) given in Fig.(2): $z_{l\pm1/2} = z_l \pm \Delta z_l / 2,\ l = 1,2..L$ and let the average cell hold-up be given as:

$$\varphi_{i,l}(t) = \frac{1}{\Delta z_l}\int_{z_{l-1/2}}^{z_{l+1/2}} \varphi_i(z,t)dz \tag{37}$$

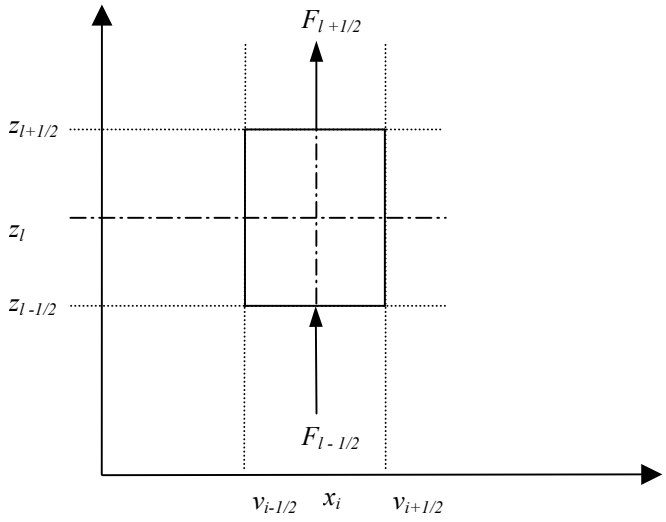

Fig.(2): External and internal coordinates discretization cell.

Now it is possible to consider the unsteady state droplet volume balance across the *l*th cell boundaries shown in Fig.(2) and the net volume (mass) generation of the dispersed phase in it. This cell volume could be considered small enough so that the spatial variation within it could be neglected. Since the droplet rise velocity, U_d, might be negative at any cell boundary due to the effect of the droplet swarm and/or the continuous phase velocity as indicated by Eq.(11), it is necessary to split the convective flux into negative and positive components:

$$F_{i,l+1/2} = F^+_{i,l} + F^-_{i,l+1} \tag{38}$$

where:

$$F_{i,l}^{+} = max\left(U_i(d_i, \phi_l(t))\varphi_{i,l}(t), 0\right) \tag{39}$$

$$F_{i,l+1}^{-} = min\left(U_i(d_i, \phi_{l+1}(t))\varphi_{i,l+1}(t), 0\right) \tag{40}$$

Note that the direction of these fluxes is from the bottom to top if positive and from the top to the bottom of the cell if negative, and there exists only one flux at the same cell boundary. The total flux at the *l*th cell boundary may be extended to include the diffusive flux which is always positive in the direction of flow (Rice, 1995) and hence:

$$F_{t,i,l+1/2}^{+} = F_{i,l}^{+} - \frac{D_d}{2}\frac{\partial \varphi_i}{\partial z}\bigg|_{l+1/2} \tag{41}$$

$$F_{t,i,l-1/2}^{-} = F_{i,l}^{-} + \frac{D_d}{2}\frac{\partial \varphi_i}{\partial z}\bigg|_{l-1/2} \tag{42}$$

By applying the conservation of mass to the *l*th cell shown in Fig.(2) and making use of the fluxes definitions above, one could obtain the following set of ODEs:

$$\frac{d\varphi_{i,l}}{dt} + \frac{F_{i,l+1/2} - F_{i,l-1/2}}{\Delta z_l} = \frac{D_d \partial \varphi_i / \partial z)_{l+1/2} - D_d \partial \varphi_i / \partial z)_{l-1/2}}{\Delta z_l} + \frac{Q_d}{A_c}\frac{\varphi_i^{feed}}{v_f}\frac{\delta_{l,l_d}}{\Delta z_l} + \rho(\boldsymbol{\varphi}_l, \boldsymbol{d}) \tag{43}$$

where i=1, 2, ..M_x, l =1,2, … L, and the spatial derivatives of the diffusive flux might be approximated as a difference between the centers of two adjacent cells where the hold-up values are known:

$$D_d \frac{\partial \varphi_i}{\partial z}\bigg|_{l+1/2} \approx D_{d,l+1/2}\frac{\varphi_{i,l+1} - \varphi_{i,l}}{\Delta^* z_l} \tag{44}$$

Note that $\Delta z_l = z_{l+1/2} - z_{l-1/2}$, which is the same as $\Delta^* z_l = z_{l+1} - z_l$ only for uniform spatial cells. Also note that the discrete source term given by Eq.(43) is evaluated at the center of the *l*th spatial cell; that is, at z=z_l.

To complete the model, the discrete boundary conditions corresponding to Eqs.(8) and (9) could be easily written in terms of volume concentration as follows:

$$0 = F_{i,0}^{+} - D_d \frac{\partial \varphi_i}{\partial z}\bigg|_{1/2}, \quad at\ z = 0 \tag{45}$$

$$0 = -F_{L+1}^{-} + D_d \frac{\partial \varphi_i}{\partial z}\bigg|_{L+1/2}, \quad at\ \ z = H \tag{46}$$

The discrete model given by Eq.(43) is an integral approximation to the system of conservation laws given by Eq.(21). This integral approximation exactly satisfies the conservation of volume and hence it presents no numerical difficulties (except its low accuracy) around the discontinuity caused by the feed point source. More interestingly, this model is exactly the same as that derived by Kronberger et al. (1995) and Kronberger (1995) based on first-order upwind differencing and flux vector-splitting scheme. This scheme as its name indicates uses the information available from grid points on the side from which the information flows. Thus for positive numerical flux the upwind side is the lower cell center and for negative flux the upwind side is the upper cell center. Despite the low accuracy of this scheme for unsteady state simulation it is stable, simple and accurate for steady state calculations where sharp profiles are not likely to occur. Moreover, the present semi-discrete scheme for a general LLEC could be easily related to the backflow-cell models by suitably relating the dispersion (diffusion) coefficient, D_d and the backflow fraction relative to the forward flow (McSwain & Durbin, 1966).

To circumvent the problem of numerical diffusion inherently existing in the first-order schemes, high-resolution schemes are required to lessen this numerical diffusion and hence sharpen the predicted moving front. This is done by increasing the order of spatial discretization of the numerical flux without violating the physical behavior of the phenomena under investigation. This violation comes from the fact that *linear* differencing schemes of order greater than one introduces spurious oscillation around large gradients according to the Godunov's theorem (Toro, 1999). Thus higher order upwind numerical fluxes are nonlinear and require more information by resorting to a complicated characteristic decomposition of the numerical flux more than the simplified approach presented above.

Recently, Kurganov and Tadmor (2000) presented a high-resolution central difference scheme of first and second order accuracy. These central differencing schemes offer universal black-box solvers for general systems of conservation laws such that given by Eq.(21). Moreover, the use of central differencing schemes in the presence of the diffusion as well as the source terms does not call for the operator splitting technique suffering from the traditional splitting limitations; that is, it requires a small time step that is comparable to the diffusion time scale (Karlsen et al., 2001). Unlike the upwind differencing schemes, the central differencing schemes do not require the time-consuming characteristic decomposition called for by the approximate Riemann solvers (Toro, 1999). Additionally, the spatial numerical derivatives required for the high-resolution implementation could be evaluated in a componentwise manner in a way similar to the scalar nonlinear limiters. Similarly, the evaluation of the numerical flux Jacobian is not necessary, but instead the approximate flux derivatives are evaluated in a componentwise manner based on the neighboring discrete values of the numerical flux: $F(\varphi_{i,l-1},\phi_{l-1}), F(\varphi_{i,l},\phi_l)$ and $F(\varphi_{i,l+1},\phi_{l+1})$.

The main idea behind these central differencing schemes is in the way that it evolves in time the reconstructed piecewise-polynomial values at the cell boundary from their known values at the cell centers. This evolution step is realized by sampling the reconstructed values at the cell boundaries by including more precise information about the local propagation speeds ($S_{l\pm1/2}$). Kurganove and Tadmor (2000) used these ideas to construct the following numerical flux approximation:

$$F_{i,l+1/2} = \frac{F(\varphi^+_{i,l+1/2}) + F(\varphi^-_{i,l+1/2})}{2} - \frac{S_{i,l+1/2}}{2}\left(\varphi^+_{i,l+1/2} - \varphi^-_{i,l+1/2}\right) \tag{47}$$

where:

$$\varphi^+_{i,l+1/2} = \varphi_{i,l+1} - \frac{\Delta^* z_{l+1}}{2}\left.\frac{\partial \varphi_i}{\partial z}\right|_{l+1} \tag{48}$$

$$\varphi^-_{i,l+1/2} = \varphi_{i,l} + \frac{\Delta^* z_l}{2}\left.\frac{\partial \varphi_i}{\partial z}\right|_{l} \tag{49}$$

and the propagation local speeds (irrespective of the direction of propagation) are estimated from the following relation:

$$\boldsymbol{S}_{l+1/2} = \max\left\{ r\left(\frac{\partial F(\boldsymbol{\varphi}^-_{l+1/2})}{\partial \boldsymbol{\varphi}}\right), r\left(\frac{\partial F(\boldsymbol{\varphi}^+_{l+1/2})}{\partial \boldsymbol{\varphi}}\right)\right\} \tag{50}$$

where r denotes the spectral radius of the Jacobian matrix.

The spatial derivatives appearing in Eqs.(48) and (49) are evaluated using a minmod-like limiter (Kurganov & Tadmor, 2000) that is given by:

$$\left.\frac{\partial \varphi_i}{\partial z}\right|_l = minmod\left(\theta\frac{\varphi_{i,l} - \varphi_{i,l-1}}{z_l - z_{l-1}}, \frac{\varphi_{i,l+1} - \varphi_{i,l-1}}{z_{l+1} - z_{l-1}}, \theta\frac{\varphi_{i,l+1} - \varphi_{i,l}}{z_{l+1} - z_l}\right), \quad 1 \le \theta \le 2 \tag{51}$$

where θ is s TVD parameter with a value equals 2 corresponding to the least dissipative limiter, while the value of unity guaranties that the scheme is free from any spurious oscillations. For definition of the minmod limiter the reader could refer to Kurganov and Tadmor (2000).

Note that the above numerical flux (Eq.(47)) is of second order accuracy and could be simply made first order by setting the numerical derivatives in Eqs.(48) and (49) to zeros. Moreover, the estimation of the local propagation speeds, $S_{i,l\pm1/2}$, is carried out based on a crude estimation of the Jacobian such that its eigenvalues are approximately given by: $\lambda_i \approx U_{d,i}, i = 1,2..M_x$ in a similar way as we did in section 5.4.1 in Eqs.(39) and (40).
It is worthwhile to mention that the above numerical flux could be reduced exactly to that of Kurganov and Tadmor (2000) when uniform spatial grid is used.

5.4.2 Model discretization with respect to time

The semi-discrete model given by the set of ODEs (Eq.(43)) and the first-order upwind numerical fluxes appearing in Eqs.(38) through (40) as well as the central numerical fluxes given by Eqs.(47) through (51) admits the use of efficient time discretization schemes by contrast to its fully discrete versions. Although higher order time differencing schemes offer high accuracy and time step control, they may violate the solution positivity, especially at high level of space discretization unless very small time steps are to be used. So, as a first simple time discretization, we apply the implicit Euler method by lagging the nonlinear terms appearing in the convective and source terms. The discrete system could be written in a standard tridiagonal form in space for each internal coordinate subdomain as follows:

$$-q^n_{i,l,l-1}\varphi^{n+1}_{i,l-1} + q^n_{i,l,l}\varphi^{n+1}_{i,l} - q^n_{i,l,l+1}\varphi^{n+1}_{i,l+1} = \varphi^n_{i,l} + \Delta t R^n_{i,l}, \quad i = 1,2..M_x,\ l = 1,2..L,\ n = 0,1..N_t \tag{52}$$

where:

$$q^n_{i,l,l-1} = \Delta t a(\varphi^n_{i,l-1}),\ q^n_{i,l,l} = 1 + \Delta t b(\varphi^n_{i,l}),\ q^n_{i,l,l+1} = \Delta t c(\varphi^n_{i,l+1}) \tag{53}$$

The nonlinear terms *a*, *b*, *c*, and *R* appearing in the above equations are dependent on the numerical flux type and could be easily deduced by comparing Eqs.(52) and (53) with the time-discretized version of Eq.(43).
The above tridiagonal system could be resolved using the standard Thomas algorithm at each time step followed by the fixed-point iteration method to improve the predicted solution due to lagging of the nonlinear terms. An accelerating convergence technique such as the bounded Wegstein method may be used. This iterative technique is only required for unsteady state simulations, since for steady state calculations the above algorithm converges always to the solution irrespective of the time step size. Moreover, since the above tridiagonal system is diagonally dominant (Kronberger, 1995) with positive right hand side, it is found to converge to the steady state solution without any risk of having negative values ensuring the solution positivity.

5.5 Discrete model validation

The convergence and accuracy of the discrete model in both internal and external coordinates is tested in this section against analytical solutions whenever it is possible. Eight case studies are considered of which seven have analytical solutions. The first four cases are devoted to test the generalized fixed-pivot technique (GFP) for a continuous stirred tank (CST) with a particular stress on treating the feed source term, the initial conditions and droplet coalescence. The droplet breakage was tested in detail in chapter 3 (see Attarakih, Bart & Faqir, 2004) and will not be repeated here. In this work we present three analytical solutions for the LLEC for the cases of neither droplet breakage nor coalescence, only droplet breakage, and droplet coalescence alone with uniform dispersed phase velocity. Case 8, which has no known analytical solution, considers a more practical situation where both breakage and coalescence mechanisms are active.
In all the following results the average number or volume distributions are obtained using the following relation:

$$\bar{I}_i = \frac{u_m(d_i)N_i}{\Delta d_i} \tag{54}$$

where $u_m(d_i)$=1 and $\pi d_i^3/6$ for the average number and volume concentrations respectively, which are the conserved integral quantities according to the GFP. Consequently, the convergence tests are carried out based on the systematic error in terms of *d30* as a mean droplet diameter. This choice of the mean droplet diameter includes the effect of both the conserved quantities on the error behavior. The systematic error is defined as:

$$SysErr = \left| d30^a - d30^n \right| \tag{55}$$

where the *a* and *n* superscripts on *d30* refer to the analytical and numerical values respectively.
In all the cases given below, unless explicitly stated, we discretized the droplet diameter logarithmically with lower and maximum droplet diameters that were chosen such that the total FDE given by Eq.(32) is less than 0.1%:

$$d_{i-1/2} = d_{\min}\left(\frac{d_{\max}}{d_{\min}}\right)^{\frac{i-1}{Mx}}, \quad i = 1,2...M_x + 1 \tag{56}$$

5.5.1 Case 1: CST without droplet breakage or coalescence

This case study is the simplest among all the cases and its analytical solution is trivial by considering Eq.(3) with zero source term. The objective of this case is to isolate the effect of inconsistent discretization of the feed term. The feed distribution of this case is simply the Weibull distribution: $n^{feed} = 3d^2e^{-d^3}$, d_{min}=0.01, d_{max}=5 mm, τ = 1 s, Φ^{feed}=0.524 and we used uniform grid for the droplet diameter with 20 subdomains. For this simple case the discrete numerical solution is exactly the same as that obtained from the analytical solution. The time integration is performed using the implicit Euler method with Δt=0.1 s. Fig.(3) shows the over predicted vessel hold-up (Φ) obtained from the number concentration when the PBE is only consistent with total number concentration. However, due to the internal consistency with respect to the total number concentration, the total number concentration is exactly predicted for this simple case. On the other hand the GFP predicts correctly both the number and volume concentrations using the same number of subdomains.

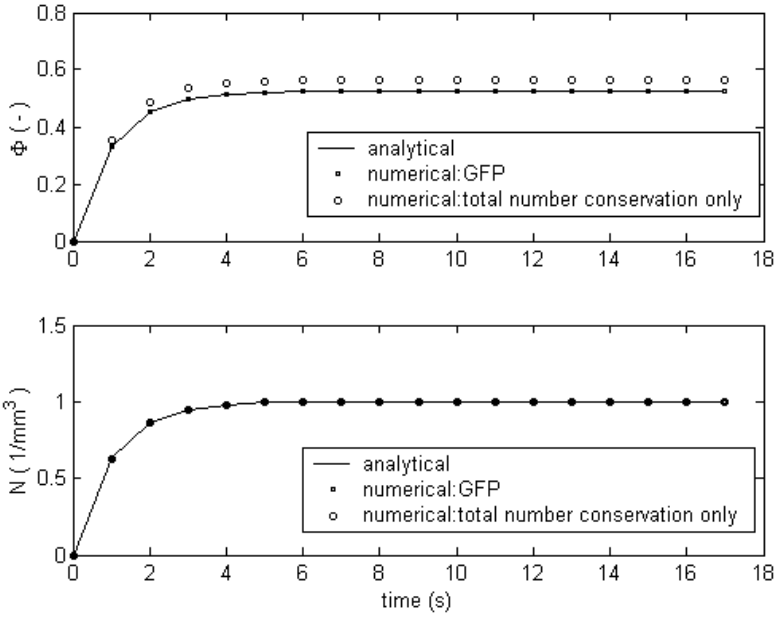

Fig.(3): The effect of the feed conservative discretization on the response of the total volume and number concentrations in a continuous stirred tank without coalescence or breakage (case 1).

5.5.2 Case 2: CST with droplet coalescence

In this case, we consider droplet coalescence in a continuous stirred tank with constant coalescence frequency: $\omega=\omega_0$, zero initial condition and a feed distribution that is given by:

$$n^{feed}(d)=\frac{N_0^f}{v_0}\left(\frac{\pi d^2}{2}\right)\exp(-v/v_0) \tag{57}$$

with N_0^f=1, v_0=1, Φ^{feed}=1 , and Δt=1 s.
The integration is carried out until a steady state is approached with tolerance of 10^{-6}, and compared to the analytical solution given by Hounslow (1990) at different vessel residence times in Fig.(4). It is clear that there is good agreement between the predicted solution using the GFP technique and the analytical one. The systematic error as predicted by Eq.(55) is shown in Table 1 at different vessel residence times. It is clear that this systematic error is in fact relatively small for all the residence times considered and thus elucidates the good performance of the technique even for small number of subdomains. It should be pointed out that the GFP technique is designed to accurately predict specific integral properties of the distribution but without destroying it. This fact is evident from these results since despite the small error appearing in the average number concentrations (see Fig.(4)), the integral properties (total number and volume) are still accurately predicted as indicated in Table 1.
As pointed out in section 5.3.1, the restructuring of the coalescence source term by introducing the idea of the coalescence interaction matrices reduced significantly the execution time especially when high level of discretization is used. We used the parameters of this case to see the effect of structured and non-structured coalescence interaction matrices. All the numerical runs are carried using PC Pentium III 750 MHz performing single task with Compaq visual FORTRAN compiler version 6.6. Fig. (5) shows the superior performance of the structured matrices when compared with the unstructured ones.

5.5.3 Case 3: CST with droplet breakage and coalescence

In this case, we consider the GFP technique to droplet breakage and coalescence with size dependent frequency. The breakage and coalescence frequencies are given by: $\Gamma(d)=K_b v(d)$ and $\omega=\omega_0\left(v(d)+v(d')\right)$ with K_b=1 and ω_0=20, and uniform daughter droplet distribution: $\beta_n(d\mid d')=6\frac{d^2}{d'^3}$ (binary breakage) and zero initial condition. The feed droplet distribution is the same as that of case 1.
Since no analytical solution is available for this case we only introduce the total number and volume concentration expressions N and φ respectively:

$$\frac{dN}{dt}=\frac{N^{feed}-N}{\tau}+K_b\varphi-\omega_0 N\varphi \tag{58}$$

$$\frac{d\varphi}{dt}=\frac{\varphi^{feed}-\varphi}{\tau} \tag{59}$$

Note that obtaining expressions for the other integral quantities is not possible since the equations become unclosed. Now, Eq.(58) could be easily integrated with the desired accuracy along the exact solution of Eq.(59) and hence we can compare the transient responses of the average number and volume concentrations to the predicted ones. However, at a steady state one could easily derive the mean droplet diameter, *d30* to get:

$$d30=\left(\frac{1+\tau\omega_0\varphi^{feed}}{N^{feed}+\tau K_b\varphi^{feed}}\left(\frac{6}{\pi}\right)\right)^{\frac{1}{3}} \tag{60}$$

Fig.(6) shows the response of the total volume and number concentrations using the GFP technique with 30 subdomains, τ = 10 s and Δt=0.1 s as compared to the solution of Eqs.(58) and (59). The two solutions agree very well for the whole simulation period despite the sharp changes in the number concentration.

The peak in the response of the number concentration is due to three competing effects: breakage, coalescence and the feed source terms. Since in this example droplet breakage is dominated by coalescence ($\omega_0 > K_b$), the number concentration at the beginning is not sufficient to induce high rate of coalescence and the addition of droplets by the feed is dominant. When the number concentration reaches a sufficiently high value the overall coalescence rate exceeds that of the feed after which equilibrium is reached between these two effects. Table 1 shows the systematic error for different vessel residence times at a steady state. Again the discrepancy between the predicted and exact total quantities is indeed small even at low level of discretization.

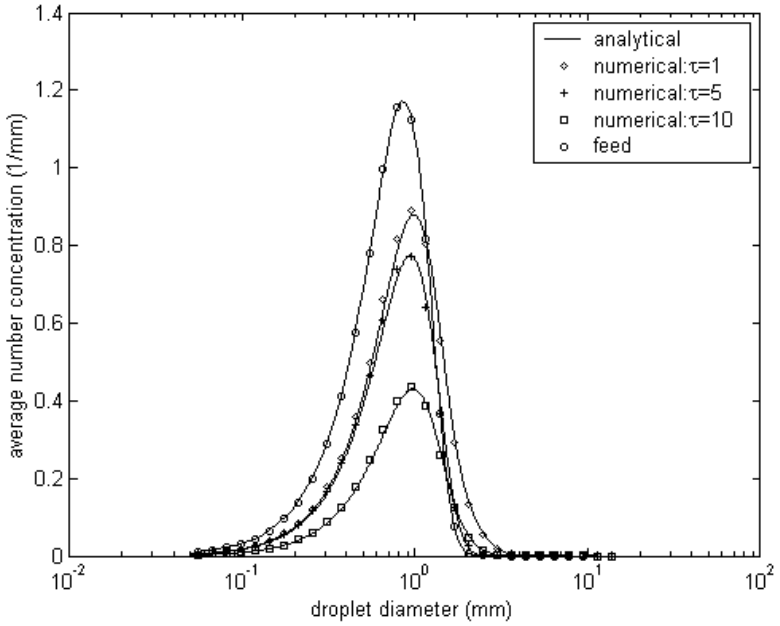

Fig.(4): The steady state droplet number distribution for pure coalescence in a continuous stirred tank with $M_x = 30$.The analytical solution is given by Hounslow (1990) (case 2).

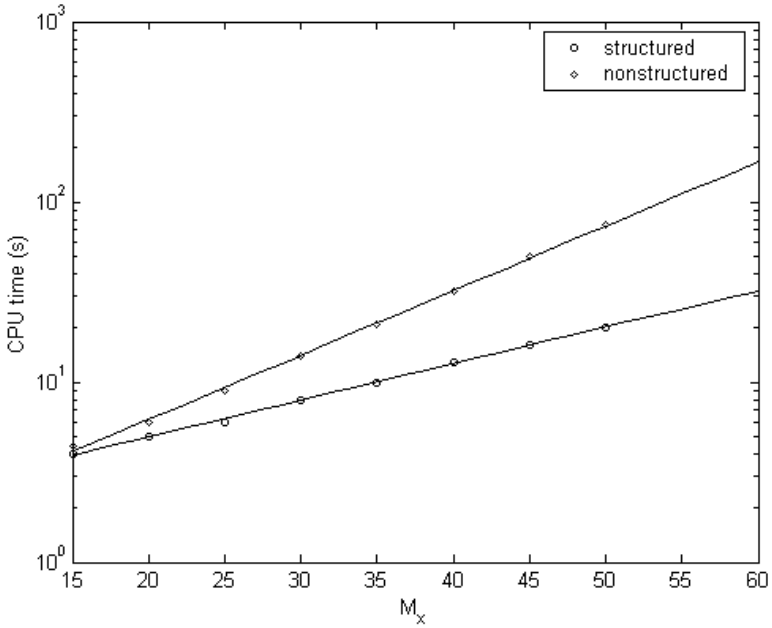

Fig.(5): The effect of restructuring the coalescence interaction matrices on the CPU time (750 MHz Pentium III processor) requirements for droplet coalescence in a CST using the parameters of case 2.

5.5.4 Case 4: Droplet coalescence plus first order removal in batch stirred tank

This case is selected to show how the internal inconsistency of the initial condition discretization results in an increase of error in the predicted conserved quantities. The initial condition is the same as that given by Eq.(57), the coalescence frequency is: $\omega = \omega_0 \left(v(d) + v(d') \right)$ with ω_0=1, and the first order removal coefficient is taken as unity. Fig.(7) shows the predicted solution using the GFP technique compared to the analytical solution (Gelbard and SeinFeld, 1978) at different simulation times with 30 subdomains and Δt=0.05s, where excellent agreement between these solutions is evident. Note that in the production of these results the initial condition is discretized so that it is consistent with respect to the total number and volume concentrations. Table 1 shows the steady state systematic error for this case at different simulation times with and without internal consistency of the initial condition. It is clear how the systematic error grows wildly when the initial condition discretization is only consistent with respect to one integral property (number concentration).

Table 1: The steady state systematic error at different vessel residence times for different numerical case studies.

Case	Vessel type	τ^a	% SysErr in *d30*	$[d_{min}, d_{max}]$	Minimum M_x such that FDE<0.1% as given by Eq.(32)
2	continuous	1	0.0011	0.03, 15	20
		5	0.0013	0.03, 15	20
		10	0.0014	0.03, 15	20
3	continuous	1	0.0148	0.01, 26	20
		5	0.0082	0.01, 26	20
		10	0.0048	0.01, 26	20
4	batch	0.5	0.0436 (3.1221)*	0.05, 26	25
		1	0.0598 (4.3240)*	0.05, 26	25
		2	0.0595 (4.3495)*	0.05, 26	25

a: For the batch vessel τ is the final simulation time.
*:The discrete initial condition is consistent only with respect to total number concentration.

5.6 Discrete model validation: LLEC

To get more insight into the performance of the GFP as well as the spatial discretization techniques, we present four cases in this section, three of which have analytical solutions, as we will show below. In all the cases that follow we assumed zero initial condition at the instant where the dispersed phase feed is switched on. The column dimensions used in this work are that of a laboratory scale RDC column having geometrical specifications shown in Table 2.
The chemical system used is the EFCE test system: water-toluene for which the physical properties are available online (http://www.dechema.de/Extraktion). The spatial numerical schemes are denoted as follows: the first order upwind scheme with flux vector splitting is UW1FVS, the first and second order central differencing schemes of Kurganov and Tadmor (2000) are denoted by KT1 and KT2 respectively. The TVD parameter θ used in the reconstruction step of the KT2 method is set 1.7 as a compromise value between dissipative and oscillatory free solution behavior. Also, the two dimensional grid with respect to spatial and droplet diameter is denoted as $L \times M_x$ respectively.

5.6.1 Case 5: LLEC without breakage and coalescence

First we start to solve the PBE given by Eq.(6) by dropping the diffusive and source terms, and we assume the dispersed phase is flowing through a stagnant continuous phase (Q_c=0) at low hold-up such that the swarm effects are negligible. For the droplet terminal velocity the rigid sphere law interpolated between the viscous and inertial regions (Wesselingh & Bollen, 1999) is used:

$$U_t = \left[\left(\frac{g(\rho_c - \rho_d)d^2}{18\mu_c} \right)^{-0.85} + \left(\sqrt{\frac{1.74g(\rho_c - \rho_d)d}{\rho_c}} \right)^{-0.85} \right]^{\frac{-1}{0.85}} \tag{61}$$

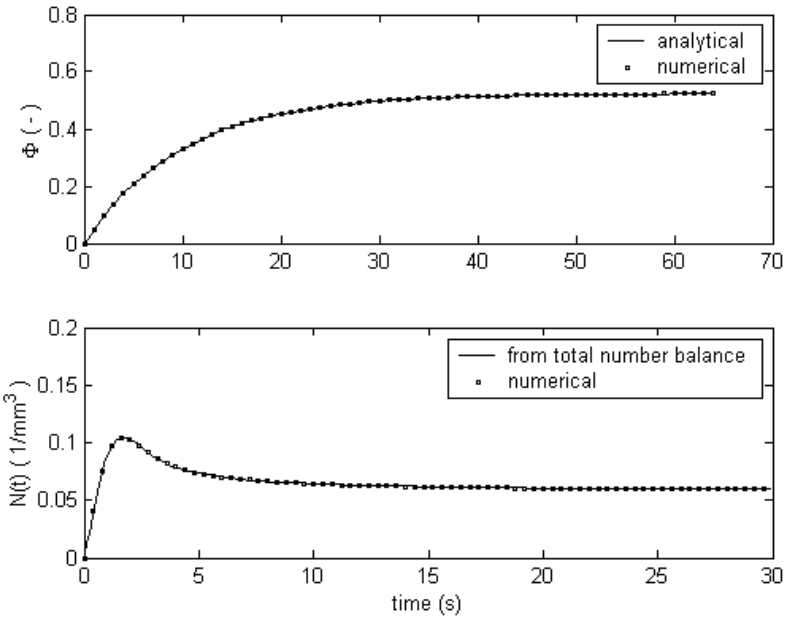

Fig.(6): The response of the total volume and number concentrations in a continuous stirred tank with size dependent coalescence frequency and linear breakage rate (with respect to volume): $\tau = 10$, $\omega_0 = 20$, $K_b = 1$, and $M_x = 30$ (case 3)

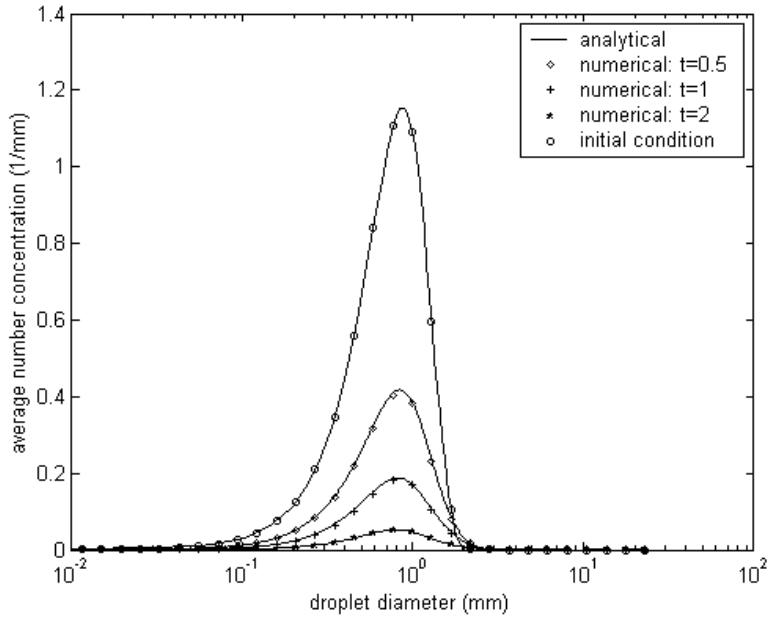

Fig.(7): Droplet distribution for coalescence with sum frequency and first order removal rate in a batch stirred tank with $M_x = 30$. The analytical solution is reported by Gelbard and Seinfeld (1978) (case 4).

where the first term inside the brackets is simply the Stokes's law for viscous range and the second term is the droplet velocities in the inertial range and the various symbols are defined in the nomenclature.
The analytical solution for this simplified PBE is obtained using Laplace transform with respect to time followed by solving the resulting linear ODE with respect to spatial coordinate. In terms of volume distribution *p(d;z,t)*, the analytical solution could be written as:

$$p(d,z,t)=\frac{Q_d}{A_c U_t(d)}\,p^{feed}u(t-\tau(d,z)) \tag{62}$$

where:

$$u(t-\tau(d,z))=\begin{cases}1, & t-\tau(d,z)\geq 0\\ 0, & otherwise\end{cases} \tag{63}$$

$$\tau(d,z)=\begin{cases}\dfrac{z-z_d}{U_t(d)}, & z-z_d\geq 0\\ 0, & otherwise\end{cases} \tag{64}$$

The inlet feed is taken as the Weibull distribution: $n^{feed}=\alpha\beta d^{\beta-1}e^{-\alpha d^{\beta}}$ with α =1.1×10^{-3}and β =8. The minimum and maximum droplet diameters are 0.25 and 4.0 mm respectively, Q_d=1.111×10^{-4}m^3/s, and Δt=0.05s.

Table 2: RDC column geometry.

Column diameter	(m)	0.15	Column height	(m)	2.550
Stator diameter	(m)	0.105	Dispersed phase inlet	(m)	0.250
Rotor diameter	(m)	0.090	Continuous phase inlet	(m)	2.250
Compartment height	(m)	0.030			

Fig.(8) shows the dispersed phase hold-up and the number concentration profiles at t = 15 s as compared to the analytical solution given by Eqs.(62) through (64). First, the two first order upwind and central differencing schemes (UW1FVS and KT1) show identical predictions of the profiles on a two-dimensional grid of size 150×30. This is because it is easy to show that the central first order scheme is reduced exactly to the first order upwind scheme for linear convective problems. Due to their first order accuracy the two schemes show numerical diffusion around the sharp moving front as expected. The use of the second order central differencing scheme (KT2) eliminates almost the entire diffusing luggage accompanying the first order schemes.
Fig.(9) shows the exact and numerical average volume distribution along the column height at t =15 s using the KT2 scheme. The two solutions are almost identical and the forward mixing of the dispersed phase is also predicted. Large droplets travel faster than the small ones and hence they possess different residence times as it is observed experimentally (Zhang et al., 1985; Qian & Wang, 1992).
Fig.(10) shows the transient total volume and number concentration profiles along the column using the KT2 scheme. First the moving front is correctly tracked out when compared to the analytical solution given by Eq.(62). Second the true volume and number concentration profiles are actually smearing as they move along the column due to the droplet forward mixing (different droplet velocities). This actually makes the numerical solution less difficult than predicting hypothetical profiles resulting from the uniform droplet velocity distribution as we will see in the cases 6 and 7.
Fig.(11) shows the convergence characteristics of the central differencing schemes KT1 and KT2. It is clear that both methods are converging in the sense of the L1-error ($L_1(t)=\sum_{i=1}^{M_x}\sum_{l=1}^{L}|\varphi_{i,l}^{<analyt>}(t)-\varphi_{i,l}^{<num>}(t)|\,\Delta d_l\Delta z_i$). The KT2 has an L1-error that is about 40% less than that of KT1. The L1-error for the UW1FVS is the same as that of KT1 and so it is not shown here.

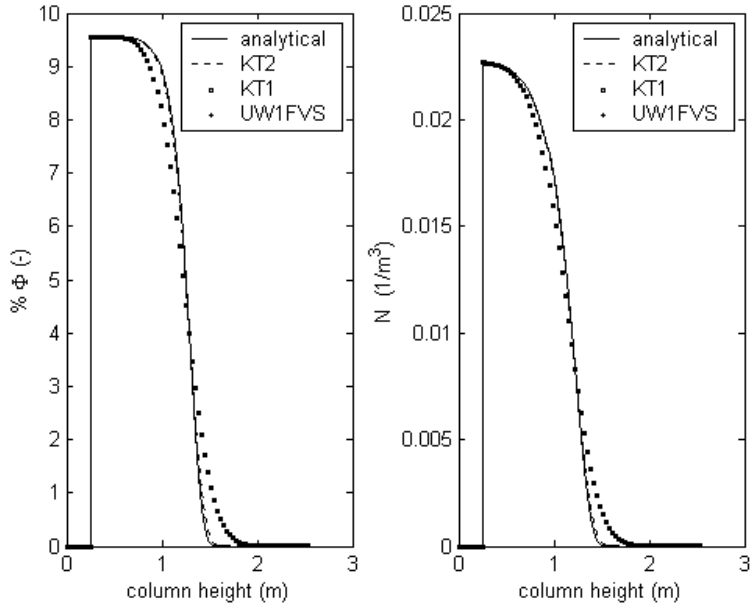

Fig.(8): Test of the spatial discretization algorithms using the simplified analytical solution of the PBE with grid dimensions:150×30 (nonuniform and uniform grids) for internal and external coordinates respectively, t =15s, Δt =0.05s, rigid sphere law terminal velocity, Q_c=0 and Q_d=1.111×10^{-4}m^3/s (case 5).

5.6.2 Case 6: LLEC with droplet breakage and uniform dispersed phase velocity

As it is shown in appendix A an analytical solution of the PBE given by Eq.(6) is possible in the presence of droplet breakage source term if the dispersed phase velocity considered to have a uniform distribution as it is hypothesized in the classical LLEC models. So, in this case we retain all the assumptions used in case 5 except that U_d=Q_d/A_c , $\Gamma = K_b^{'} U_d v(d)$, $\beta_n(d \mid d') = 6\frac{d^2}{d'^3}$, and $n^{feed} = N_0^f e^{-\alpha v(d)/v_0} / v_0$ with $N_0^f = 1$, $v_0 = \alpha^2 / N_0^f$ to insure feed volume distribution normalization, $K_b^{'}$=1, and α = 1. Based on these simplifications the analytical solution for this case is given by:

$$p(d,z,t) = \left(\frac{d}{d_0}\right)^3 \left(\frac{\pi d^2}{2}\right) \left[\frac{\alpha + K_b^{'}(z - z_d)}{\alpha}\right]^2 \exp\left[-\left(\alpha + K_b^{'}(z - z_d)\right)\left(\frac{d}{d_0}\right)^3\right] u\left[t - \tau(d,z)\right] \tag{65}$$

where the unit step function u is the same as that given by Eqs.(63) and (64) with $U_t = U_d$.
The minimum and maximum droplet diameters are 0.05 and 3.0 mm respectively, Q_d=1.111×10^{-4}m^3/s, Δt=0.05s and the final simulation time is 120 s.
In this case the total volume and number concentration profiles have a discontinuity that is moving along the column with a velocity U_d=Q_d/A_c. This hypothesized problem is very difficult to solve because of this moving discontinuity and hence it represents a severe test to the spatial discretization schemes as well as the GFP.
Fig.(12) shows the analytical and predicted volume and number concentrations using the GFP technique and the UW1FVS, KT1 and KT2 schemes. It is clear that the first order schemes are suffering from some numerical diffusion and need more spatial grid points to reduce it. On the other hand, the second order scheme has a much better performance near the discontinuities in both volume and number concentrations. In comparison to case 5 we need only 150 spatial cells to almost eliminate the numerical diffusion because the moving front is rather more flat than in this case. Moreover, it seems that both droplet breakage and the nonuniform velocity distribution that are responsible for the nonuniform volume concentration profile. This is because when a volume concentration is obtained from the PBE, the source

term due to droplet breakage disappears to satisfy the conservation of volume (mass), but this is not the case for the total number concentration. Hence, the total number concentration increases linearly along the column height.

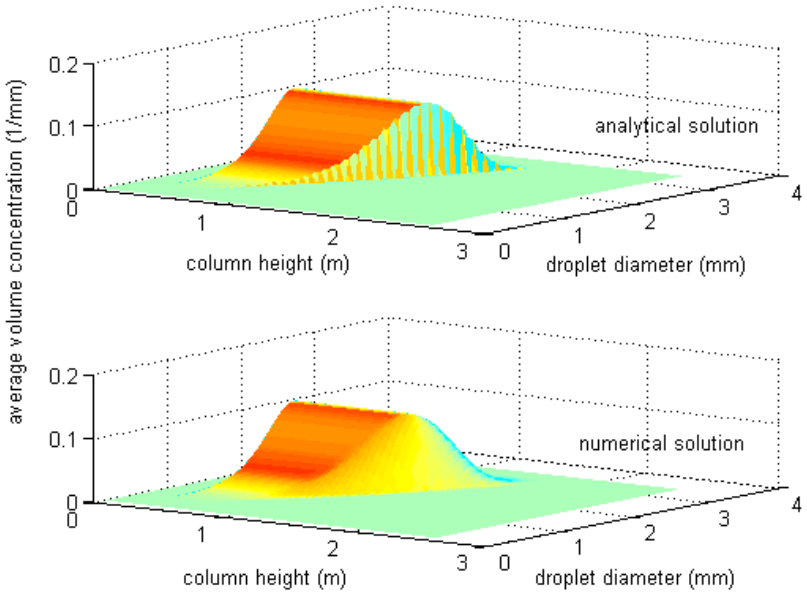

Fig.(9): Comparison of the numerical and exact transient behavior of the average volume concentration using the GFP and the second order central difference scheme (KT2) of case 5 with grid dimension:150×30 for internal and external coordinates respectively, t = 15 s, Δt =0.05s, Q_c=0 and Q_d=1.111×10^{-4}m^3/s.

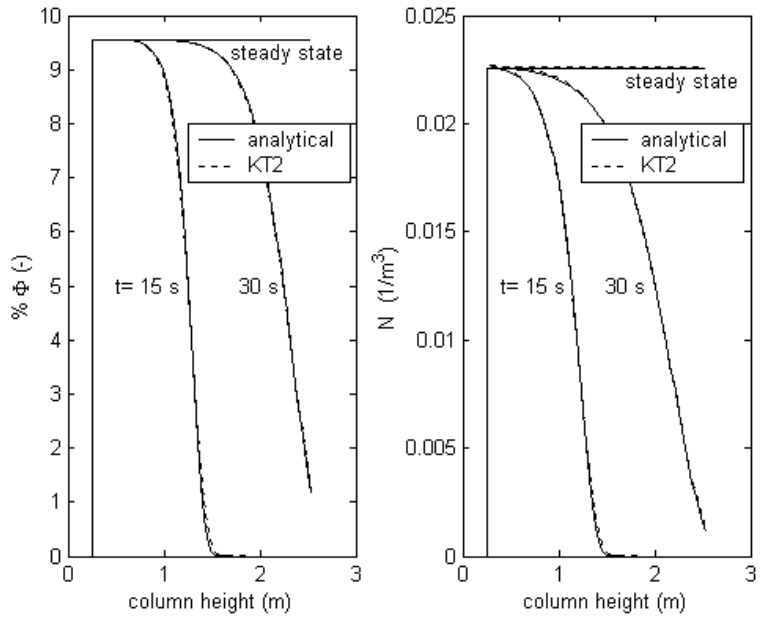

Fig.(10): Comparison between the transient total volume and number concentration profiles and the analytical solution of the PBE (case 5) using the second order discretization scheme with grid dimension: 150×30 for internal and external coordinates respectively with Δt = 0.05s, Q_c = 0 and, Q_d=1.111×10^{-4}m^3/s.

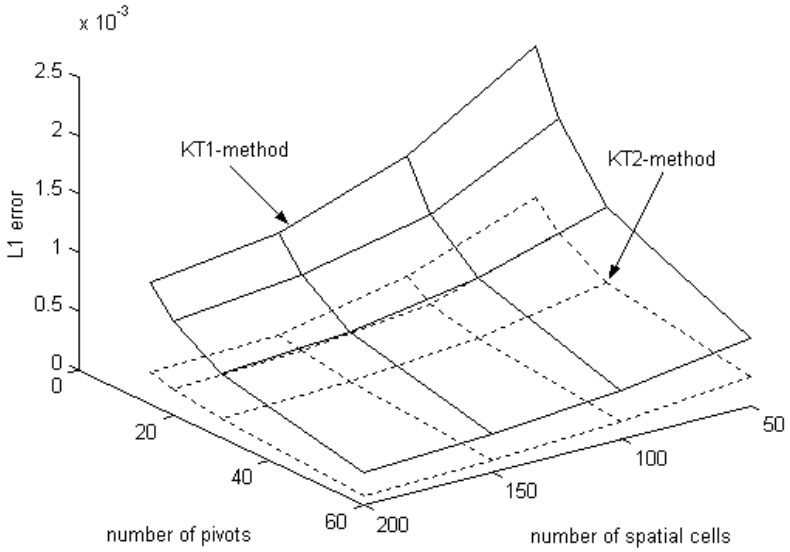

Fig.(11): The convergence characteristics of the first and second order (KT1 & KT2) central differencing schemes using the analytical solution given by Eq.(62) at t = 10 s, Δt =0.05 s, uniform droplet diameter, nonuniform spatial grids, Qc=0.0 and Q_d=1.111×10^{-4}m^3/s.

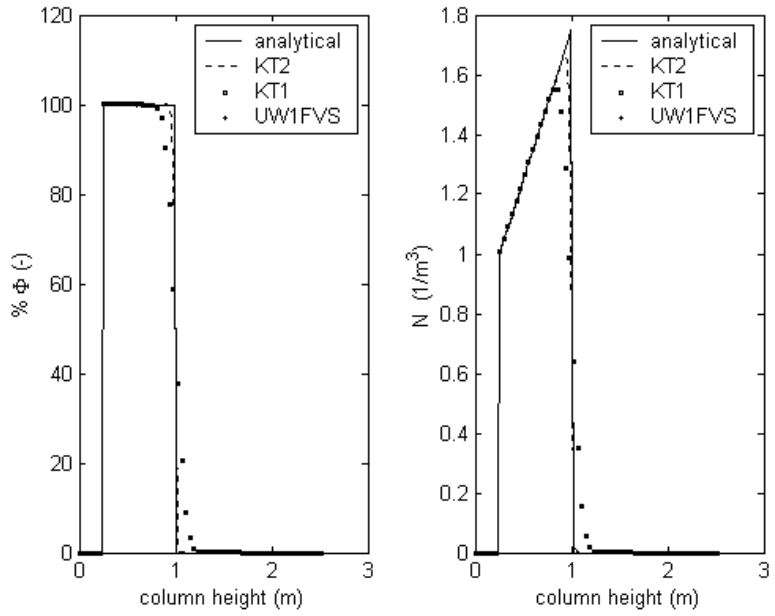

Fig.(12): Comparison between numerical and analytical solutions using the GFP and the spatial discretization schemes for droplet breakage of case 6 on grid with dimension: 300 × 30, t = 120s, Δt =0.05s, Q_c=0, Q_d=1.111×10^{-4}m^3/s and U_d= Q_d/A_c.

Fig.(13) shows the average volume distribution along the column at t=120 s where the sharp moving front (because of the uniform velocity distribution) seems to be accurately predicted when the analytical (exact) and numerical solutions are compared.
The steady state convergence of the average volume distribution as compared to the analytical solution at selected positions along the column is shown in Fig.(14), where the steady state is achieved to a tolerance of 10^{-6}. It is evident that there is a good agreement between the predicted and the analytical solutions, and thus elucidating our trust in the GFP even when the distribution becomes sharp as we ascend the column.

5.6.3 Case 7: LLEC with droplet coalescence and uniform dispersed phase velocity

This case is devoted to test the presence of droplet coalescence as source term in the PBE given by Eq.(6). All the assumptions imposed on the PBE in case 6 are applicable here except that the breakage term is set equal to zero. The coalescence frequency is $\omega = K_c U_d$, where K_c=1×10^{-9} m^2, the minimum and maximum droplet diameters are 0.1 and 5.0 mm respectively, the final simulation time is t = 120 s and Δt=0.1 s.
The analytical solution is derived in Appendix A and is given by:

$$p(d,z,t) = N_0^f \left(\frac{d}{d_0}\right)^3 \left(\frac{\pi d^2}{2}\right) \left(\frac{2}{2+N_0^f K_c (z-z_d)}\right)^2 \exp\left(\frac{-2\left(\frac{d}{d_0}\right)^3}{2+N_0^f K_c (z-z_d)}\right) u\left[t-\tau(d,z)\right] \qquad (66)$$

where u is the unit step function given by Eq.(63) with $U_t = U_d$.

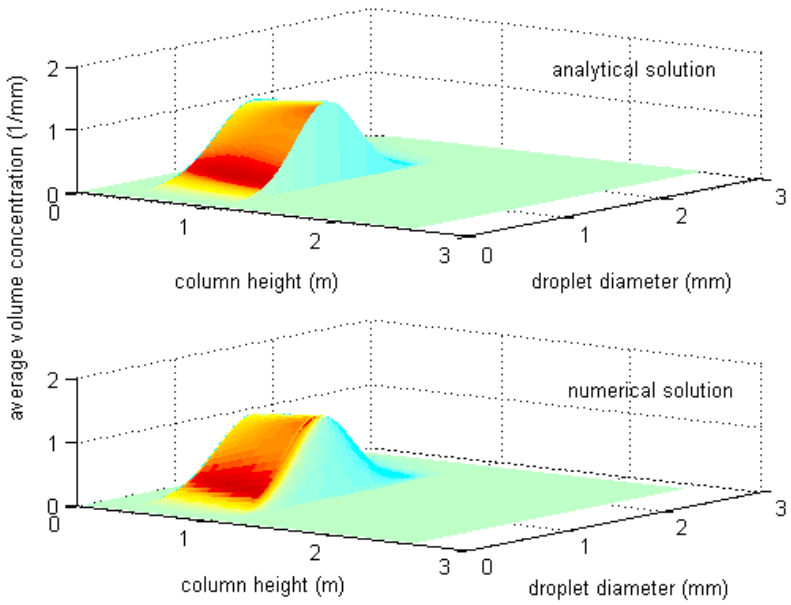

Fig.(13): Comparison of the numerical and exact transient behavior of the average volume concentration using the GFP and the second order central difference scheme (KT2) of case 6 with grid dimensions: 300×30 for internal and external coordinates respectively, t = 120 s, Δt = 0.05 s, Q_c= 0 and Q_d=1.111×10^{-4}m^3/s.

Fig.(15) shows the predicted total volume (Φ) and number (N) concentrations using UW1FVS, KT1, and KT2 along with the analytical solution given by Eq.(66). As in case 6, since the dispersed phase velocity distribution is uniform, both these profiles move along the column with a discontinuity having a speed of

$U_d=Q_d/A_c$. This makes the numerical solution using the first order schemes more dissipative than the second order one (KT2). Since the total volume of droplet is conserved its concentration profile along the column is uniform; however, the number concentration profile is proportional to the inverse of z, since droplet coalescence is accompanied by droplet number reduction.
Fig.(14) shows the convergence of the volume distribution as predicted by the KT2 (external coordinate) and the GFP (internal coordinate) schemes at a steady state using grid with dimension: 300×30. It is clear how the volume distribution is shifted to the large droplet size as the dispersed phase ascends the column.

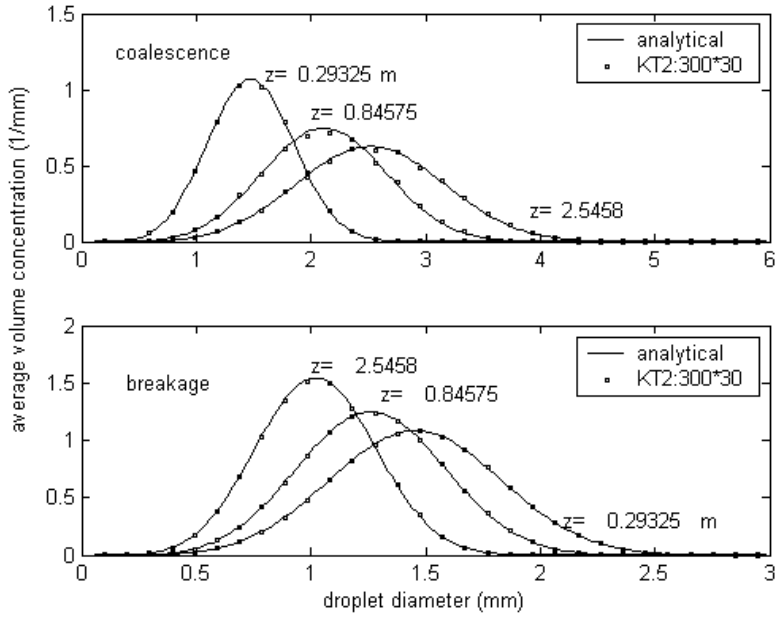

Fig.(14): The steady state comparison between numerical and analytical solutions using the GFP and the KT2 spatial discretization scheme for droplet breakage (bottom) and coalescence (top) for cases 6 and 7 respectively on grid with dimensions: 300×30, t = 120s, Δt = 2 s, Q_c= 0 , Q_d= 1.111×10^{-4}m^3/s, and
U_d= Q_d/A_c.

5.6.4 Case 8: LLEC with droplet breakage and coalescence

In this case we consider a more realistic case including both droplet breakage and coalescence as well as a rigid sphere velocity law given by Eq.(61) with swarm effect function $f = (1-\phi)$ and slowing factor K_v = 1. The feed is given by Weibull distribution with parameters the same as those given in case 5, the breakage frequency is given by $\Gamma = \frac{\pi^2 K_b}{36} d^6$ s^{-1} where K_b = 0.02 m^{-6}/s, d is in mm and the daughter droplet distribution is the same as that in case 6. The coalescence frequency is given by $\omega = K_c(d^3 + d'^3)$ with K_c = 0.5 m^{-6}/s where d is in mm and the dispersion coefficients are D_c=D_d = 10^{-4} m^2/s. The minimum and maximum droplet diameters are 0.25 and 4 mm where breakage and coalescence are active, and 0.25 and 6.5 mm only when droplet coalescence is active. The time step is taken as 0.05 and 2 s for all the transient and steady state simulations respectively with tolerance of 10^{-6} as a criterion for a steady state approach. Since no analytical solution is available for this case, the numerical convergence is tested through doubling the grid dimensions such that the two consecutive grids produce almost the same solution.
First the discrete models are tested using the non-oscillatory velocity model given in Table 3. Fig.(16) shows the convergence of the GFP and the spatial discretization schemes UW1FVS and KT2 for the prediction of total volume and number concentrations at t = 15 s.
It is clear that the GFP and the KT2 schemes converge to the solution since the two consecutive grids: 150×25 and 300×50 produced almost the same results. However, the UW1FVS needs a grid of dimension

900×25 to almost converge to the same solution due to its dissipative nature. It should be noted that the moving front in this practical case is not very sharp due to the forward mixing and axial dispersion.

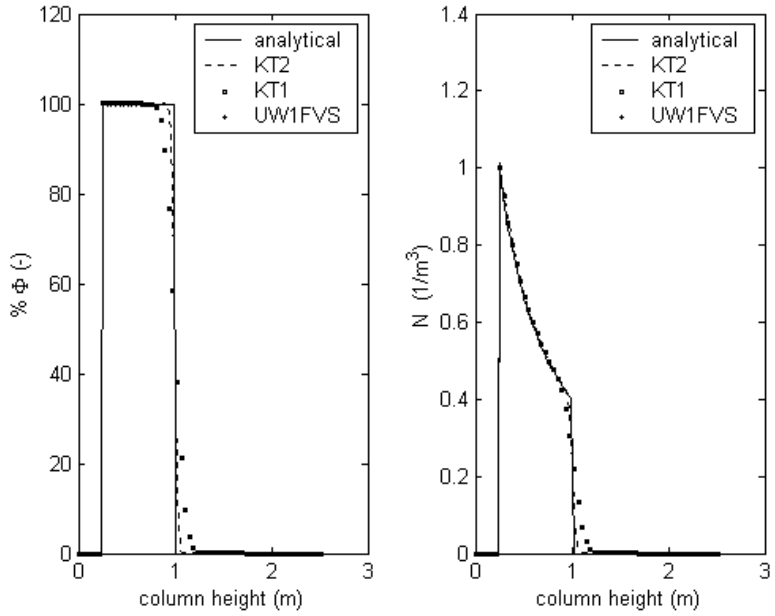

Fig.(15): Comparison between numerical and analytical solutions using the GFP and the spatial discretization schemes for droplet coalescence of case 7 on grid with dimensions:300×30, t = 120s, Δt =0.05s, Q_c=0 , Q_d=1.111×10^{-4}m^3/s, and U_d= Q_d/A_c.

Table 3: Available continuous phase velocity models.

Continuous phase velocity model	Reference
1- Oscillatory: $U_c = \frac{Q_t}{A_c} - \alpha_c \frac{Q_{c,in}}{A_c} - \alpha_d \frac{Q_{d,in}}{A_c} - \int_{d_{\min}}^{d_{\max}} v(d) U_r(d,\phi,\boldsymbol{P}) n(d;z,t) \delta d$	Casamatta (1981)
2- Steady state: $U_c = \alpha_c \frac{Q_c}{A_c(1-\phi)} + \frac{D_c}{1-\phi}\frac{\partial \phi}{\partial z}$	Kronberger (1995)
$Q_t = \int_{d_{\min}}^{d_{\max}} v(d) U_r(d;\phi(H,t),\boldsymbol{P}) n(d;H,t) \delta d$	
$\alpha_c = \begin{cases} 1, & z \le z_c \\ 0, & z > z_c \end{cases}$ and $\alpha_d = \begin{cases} 1, & z \le z_d \\ 0, & z > z_d \end{cases}$	

Fig.(17) shows the steady state convergence of the GFP and the spatial discretization schemes in the presence of different droplet interaction mechanisms. The KT1 scheme is found to produce identical results as UW1FVS and hence it is not shown here. First the solution is converging for different droplet interactions on consecutive grids: 70×25 and 150×50 for both total volume and number concentrations, indicating that the first order schemes are accurate enough to predict the hydrodynamic behavior of LLECs at a steady state. Second, the discrete model behavior seems to correctly reflect the different droplet interactions in the column. For droplet breakage alone the volume and number concentration profiles change sharply along the column height. This is because as the droplets ascend the column the droplets break up and hence their rise velocity is reduced resulting in an increased total volume and number concentrations.

The reverse situation could be said when only droplet coalescence is active. Since in reality, both droplet breakage and coalescence are active, we expect the volume and number concentrations profiles to lie

within the limits of the two previous cases as shown in Fig. (17) which is observed experimentally in Kühni (Gerstlauer, 1999) and RDC columns (Modes, 2000).

Fig.(18) shows the convergence of the GFP technique at fixed spatial grid using the KT2 scheme for spatial discretization. It is clear that the GFP technique is converging on consecutive grids: 70×25 and 70×70 for various droplets interaction mechanism along the column. Table 4 sheds more light on the quantitative convergence characteristics of the internal and external discretization schemes as well as the

Table 4: The steady state convergence of the GFP and the spatial discretization schemes based on case 8 with nonuniform and uniform spatial and droplet diameter grids respectively.

	Systematic error			CPU time (s)		
$L \times M_x$	FVS	KT1	KT2	FVS	KT1	KT2
50×15	0.00611	0.00062	0.00091	5	5	6
100×30	0.00171	0.00038	0.00016	28	29	31
150×45	0.00065	0.00032	0.00013	148	156	159

* CPU time measured under Compaq Visual FORTRAN 6.6 on a 750 MHz Pentium III PC

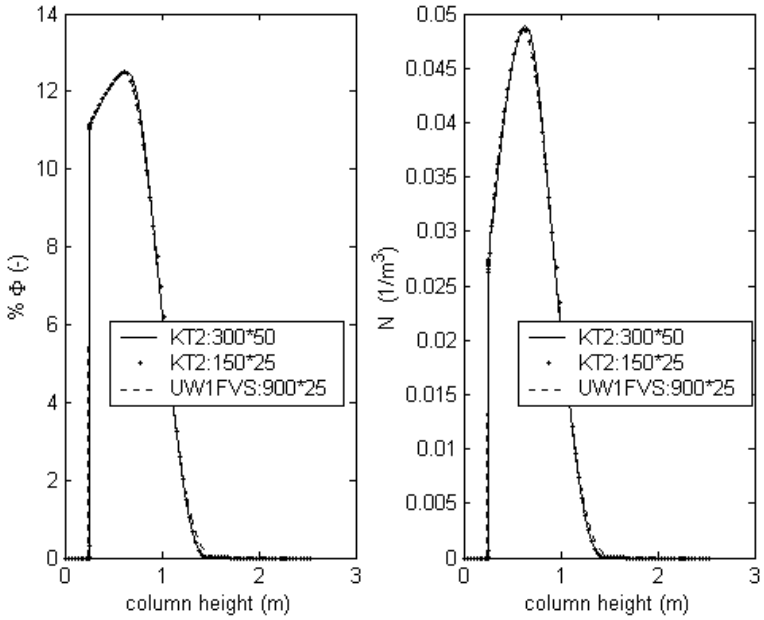

Fig.(16):Convergence of volume and number concentrations using the GFP and the spatial discretization schemes at t = 15 s for droplet breakage and coalescence of case 8 with Δt =0.05 s, $Q_c = 0.28 \times 10^{-4} m^3/s$, $Q_d = 1.111 \times 10^{-4} m^3/s$ with uniform droplet diameter and nonuniform spatial grids.

CPU time requirements. The convergence test is based on the mean droplet diameter $\overline{d30}$ with respect to diameter and column height. Since no analytical solution is available, we used a reference solution on grid whose dimension is 300×60 at a steady state. It is clear that the discretization in both dimensions is converging with small systematic errors, where the KT2 scheme is the most accurate one. It is also interesting to note that the CPU time requirements for the second order scheme KT2 using 500 integration steps is almost the same as that of the first order schemes: KT1 and UW1FVS with the gain of higher accuracy.

To see the difference between the conventional and the improved velocity models given by Eq.(15) and Table 3, we simulate these two models using the parameters of this case. Fig.(19) shows the response of the dispersed phase flow rate at the top of the column using oscillatory and non oscillatory velocity models. It is clear how the improved velocity model eliminates completely the oscillation behavior of the dispersed phase by simply manipulating the inlet continuous phase flow rate. This oscillatory behavior due to manipulating the continuous flow rare at the bottom of the column (Fig.(1)) is observed

experimentally by many authors and the interested reader could refer to Hufnagl, McIntyre and Blass (1991), Weinstein, Semiat and Lewin (1998) and Gerstlauer (1999).

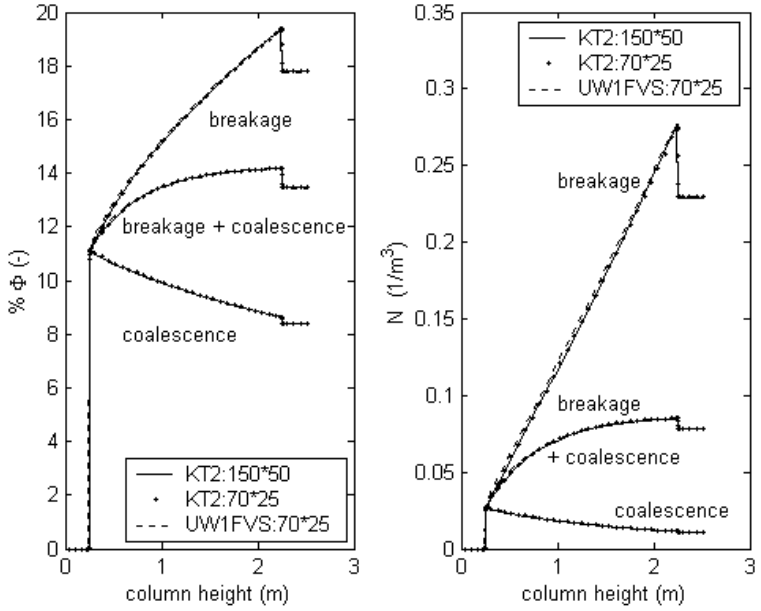

Fig.(17): The steady state convergence of volume and number concentrations using the GFP and the spatial discretization schemes for droplet breakage and coalescence of case 8 with Δt = 2 s, Q_c = 0.28 $\times 10^{-4} m^3/s$, Q_d = $1.11 \times 10^{-4} m^3/s$ with uniform droplet diameter and nonuniform spatial grids.

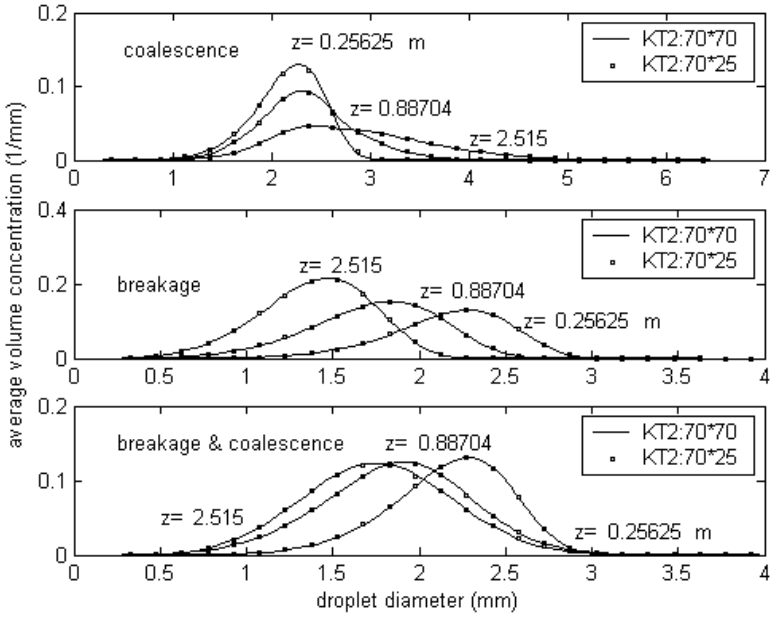

Fig.(18): The steady state convergence of the average volume distributions along the column using the GFP and the KT2 spatial schemes for droplet breakage and coalescence of case 8 with Δt = 2 s,
Q_c = 0.28 $\times 10^{-4} m^3/s$, Q_d = $1.11 \times 10^{-4} m^3/s$ with uniform droplet diameter and nonuniform spatial grids.

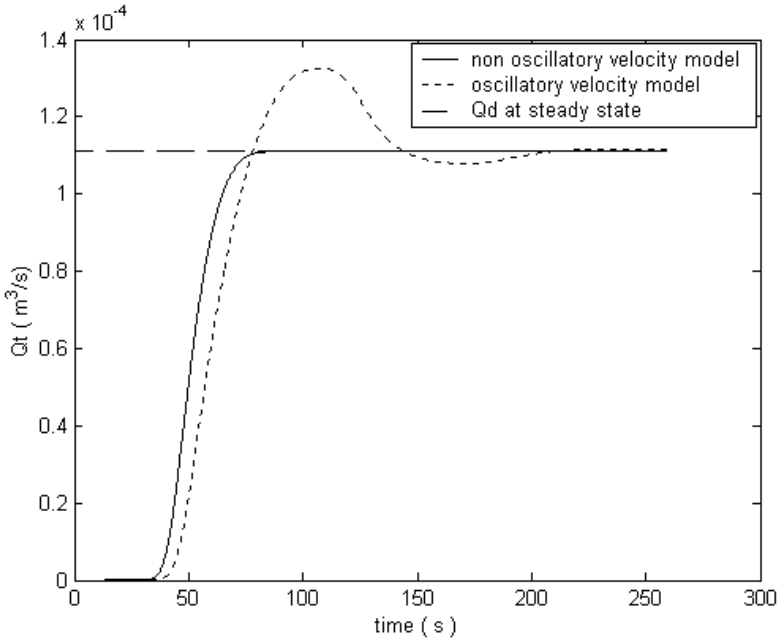

Fig.(19): Comparison between the oscillatory and non oscillatory velocity models using KT2 scheme for droplet breakage and coalescence of case 8 with Δt = .1 s, $Q_c = 0.28 \times 10^{-4}$m^3/s, $Q_d = 1.11 \times 10^{-4}$m^3/s using uniform droplet diameter and nonuniform spatial grids of dimension 150×30.

5.7 Experimental validation

In order to get more trust in the present population balance model and its discrete counterparts, we compare its predictions to some of the available experimental work in the published literature. From this, is the recent experimental data of Modes (2000) for the steady state hydrodynamics of a laboratory scale RDC column whose dimensions are shown in Table 2.

The experimentally correlated droplet transport functions, the breakage frequency, and the daughter droplet distribution will be used for model validation. These were determined based on single droplet experiments carried out in a column segment having five compartments of total height 0.15 m. The droplet rise velocity and the breakage probability functions are determined using digital image processing, while the axial dispersion coefficient of the dispersed phase is determined using residence time analysis for a monodispersion of droplets of specified diameters (Modes et al., 1999). Due to the relative high interfacial tension of the used chemical system (water-toluene), the low values of dispersed phase hold-up, and in the absence of mass transfer, the droplet coalescence could be safely neglected. Additionally, Modes (2000) recommended the use of Vignes (1965) velocity law to estimate the terminal droplet velocity multiplied by (1-ϕ) to take into account the droplet swarm effect (see Eq.(12)). This author correlated the slowing factor, K_v, and the axial dispersion coefficient, D_d, with the energy input and the droplet diameter as follows:

$$K_v(d, N^*) = 1 - 1.037\left(N^{*3} D_R^5\right)^{0.12} - 0.62\left(\frac{d}{D_s - D_R}\right)^{0.44} \tag{67}$$

$$\frac{D_d}{U_d H} = 0.0138 + 8.26 \times 10^{-7}\left(\frac{N^* D_R}{U_d}\right)^{3.3} \tag{68}$$

where N^* is the rotor speed (s^{-1}), D_R, and D_s are the rotor and stator diameters respectively whose values are shown in Table 2.

The droplet breakage frequency and the daughter droplet distribution are correlated based on single droplet experiments and are given by:

$$\Gamma(d,\phi) = P_r(d,N^*)\frac{U_d(d,\phi)}{H_c} \tag{69}$$

where the breakage probability, P_r, is correlated with the system physical properties, the energy dissipation in the following form:

$$\frac{P_r}{1-P_r} = 6.04\times10^{-4}\left(\frac{\rho_c^{0.8}\mu_c^{0.2}dD_R^{1.6}\left(\omega_R^{1.8}-\omega_{R,crit}^{1.8}\right)}{\sigma}\right)^{1.595} \tag{70}$$

while $\omega_{R,crit}$ is the critical rotor speed below which the breakage probability falls to zero (Modes, 2000) and H_c is the RDC compartment height.
The daughter droplet distribution (based on number) is assumed to follow the beta distribution, which is given by:

$$\beta_n(d\mid d') = 3\vartheta(\vartheta-1)\left[1-\left(\frac{d}{d'}\right)^3\right]^{(\vartheta-2)}\frac{d^2}{d'^3} \tag{71}$$

where ϑ is the mean number of daughter droplets produced upon breakage of mother droplet of diameter d'. It is experimentally correlated and found dependent on the energy dissipation and having a value ≥ 2. Note that when ϑ is equal 2 the above daughter droplet distribution is reduced to the uniform distribution with respect to droplet volume as internal coordinate.
In all the numerical simulations presented in this section the inlet feed distribution is based on the measured values and for the convergence tests we find the log normal distribution fits will the experimental data. The integration is carried out until a steady state using the column dimensions shown in Table 2 with a time step Δt=2 s. The UW1FVS discrete model with uniform grid having a dimension of 70×20 is used for spatial discretization, where doubling of the grid size shows no principal differences in the predicted results. The minimum droplet diameter is chosen to lie below the critical droplet diameter, and the maximum droplet size is estimated based on the initial and feed droplet distributions such that Eq.(32) is satisfied.

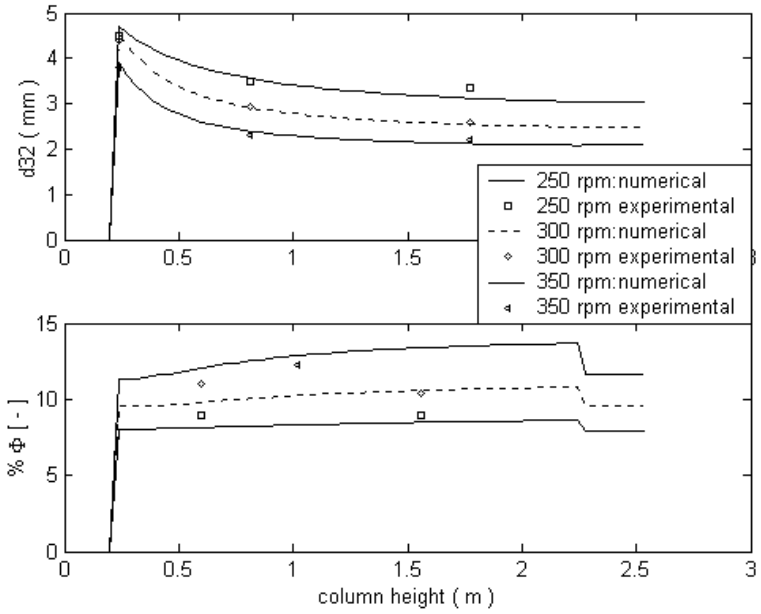

Fig.(20): The steady state comparison between experimental data and the model prediction with two energy inputs using grid dimension: 70×20 and Q_c=2.78×10^{-5} , Q_d=3.33×10^{-5} m^3/s. The experimental data is from Modes (2000).

Fig.(20) compares the predicted mean droplet diameter, *d32*, and the dispersed phase hold-up at three rotor speeds, 250, 300 and 350 rpm. The predicted and experimental values of the mean droplet diameter seems to be in good agreement with the experimental data, however, the predicted hold-up values are not as good as the predicted *d32*. This is because the errors in the volume distribution seem to cancel when the *d32* is calculated since it involves the ratio of droplet volume to its surface area. Nevertheless, the model correctly follows the experimental trend where the hold-up increases as the rotor speed increases indicating an increase in the droplet breakage.
Fig.(21) shows the predicted and experimental droplet volume densities at rotor speed 300 rpm corresponding to the measuring points along the column. The model predicts fairly well the volume distribution along the column; however, the error increases as the droplet is shifted to the left indicating the breakage of the droplets as they ascend the column.
In Fig.(22), we examined the effect of different droplet terminal velocity laws on the predicted mean droplet diameter and the dispersed phase hold-up. Again, it seems that the error cancellation, when calculating the mean droplet diameter, makes it less sensitive to the type of the velocity law than the dispersed phase hold-up. Anyhow, we need more experimental hold-up data to select the right terminal velocity law that well describe the chemical system under investigation.

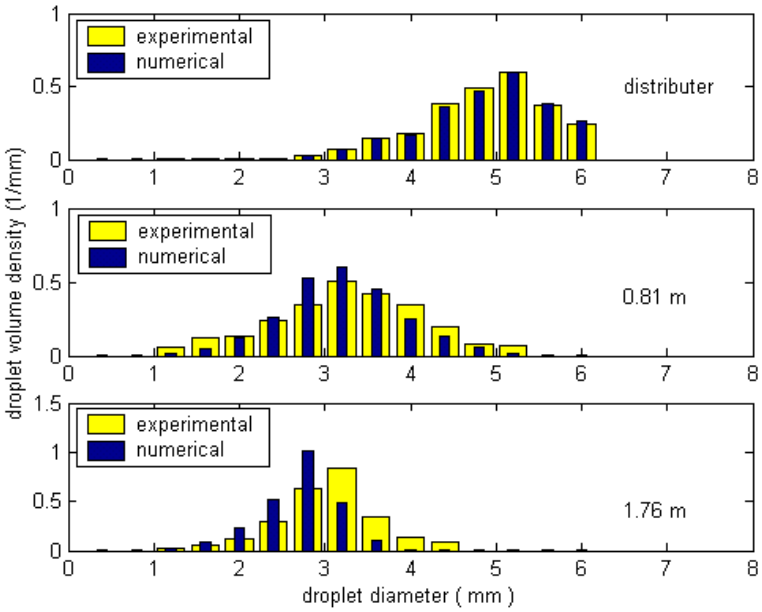

Fig.(21):The steady state comparison between experimental data and the model prediction at 300 rpm using grid dimension: 70×20, Q_c=1.39×10^{-5} and Q_d=3.33×10^{-5} m^3/s. The experimental data is from Modes (2000).

Note that the sensitivity analysis of the model predictions with respect to certain parameters such as, K_v, D_d, Γ, and ϑ is not considered in this work since this issue is analyzed by (Modes, 2000). He found that the greatest model sensitivity is with respect to the droplet-slowing factor, K_v. It should also be pointed out that the model predicts the flooding behavior of the column when an excessive entrainment of the dispersed phase is observed at the bottom of the column. However, further flooding analysis can be found in Gourdon and Casamatta (1994) and will not be detailed here.

5.8 Conclusions

- The comprehensive literature review of the available numerical techniques showed that the zero order methods that are inherently consistent with respect to specific droplet integral properties posses the simplicity, robustness, and accuracy for solving the general PBEs. Among these methods the fixed-pivot technique of Kumar and Ramkrishna (1996a) is the most candidate for

this task. So, in this work we generalized the fixed-pivot technique to solve the general PBE for continuous flow systems showing both internal and external coordinates dependency.

- The external coordinate discretization is carried out using simplified upwind and central differencing schemes where the latter having the advantage of being free of any approximate Riemann solvers.
- The combined internal and external discretization schemes are found very efficient in solving extremely difficult cases in CSTs and LLECs including droplet breakage and coalescence.
- The discrete models are validated using eight cases, of which seven have known analytical solutions, where three of which are derived in this work. In all these case studies the discretization schemes were able to predict the analytical solutions and found convergent to solutions on fine grids where the analytical solutions are not available. The second order central differencing scheme (KT2) is found the most accurate to capture the moving profiles along the column; however, the three differencing schemes have almost the same accuracy for steady state simulations when sharp profiles are not likely to appear. Moreover, the CPU time requirement for the second order scheme was found comparable to the first order ones with a remarkable high accuracy.
- The transient behavior of the dispersed phase hold-up is found dependent on the type of the continuous phase velocity model. In this work, we derived a continuous phase velocity model that is non oscillatory based on the idea of Hufnagl, McIntyre and Blass (1991), and hence it is superior to the oscillatory model derived by Casamatta (1981).

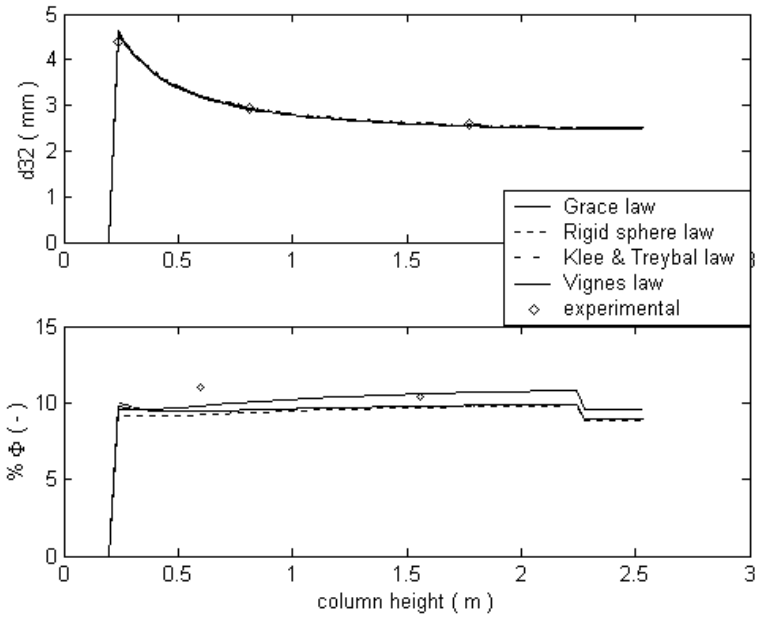

Fig.(22): The effect of the different velocity models (Grace et al., 1976, Klee and Treybal, 1956, Vigness, 1965) on the steady state *d32* and the total column hold-up with grid dimensions:70×20, Q_c=2.78×10^{-5} and Q_d=3.33×10^{-5} m^3/s. The experimental data is from Modes (2000).

- The comparison of the upwind first order central differencing scheme with the experimental data at a steady state was found very satisfactory. The model is found to well predict the general LLEC hydrodynamic behavior at different rotor speeds.
- So, it is concluded that the combination of the GFP and UW1FVS provides a powerful and robust solver for the PBE describing the hydrodynamic behavior of general LLECs. Due to this we are currently extending these schemes to the more general case when mass transfer is included.

Nomenclature

$\boldsymbol{A}$	breakage interaction matrix, Eq.(29)
A_c	column cross sectional area
D_c, D_d	diffusion coefficients for the continuous and dispersed phases respectively, $m^2.s^{-1}$
D_R, D_s	rotor and stator diameters respectively, m
$\boldsymbol{d}$	characteristic droplet diameter vector
d, d'	droplet diameter, mm
d_0	mean droplet diameter of the initial or feed droplet distribution, mm
d_i, $d_{i+1/2}$	the characteristic droplet diameter and the right boundary of the ith subdomain respectively, mm
d_{min}, d_{max}	minimum and maximum droplet diameters, mm
$d30$, $d32$	mean droplet diameters, mm
$\overline{d30}$	mean droplet diameter with respect to d and column height, mm
F	the convective flux: $U_d n$ or $U_d p$, $s^{-1}m^{-3}$ or s^{-1}
FDE^L, FDE^U	average lower and upper finite domain errors, Eq.(32)
f^{feed}	inlet feed distribution, m^{-1}
g	the acceleration of gravity, $m.s^2$
H, H_c	column and single compartment heights respectively, m
I_i	integral quantity based on the property $u_m(d_i)$ in the ith subdomain
$\overline{I_i}$	average integral quantity based on the property $u_m(d_i)$ in the ith subdomain, Eq.(54)
K_b, K_c	breakage and coalescence frequency constants
L	number of external (spatial) coordinate cells
M_x	number of subdomain of the internal coordinate (pivots)
N_0^f	number concentration in the inlet feed, m^{-3}
N_i	droplet number concentration in the ith subdomain, mm^{-3}
N^*	rotor speed, s^{-1}
n	number distribution function, m^{-4}
n_0, n^{ic}	initial number distribution function, m^{-1}
n^{feed}	feed number distribution function, m^{-1}
$\boldsymbol{P}$	physical properties vector
P_r	breakage probability, Eq.(70)
p	volume distribution function, m^{-1}
Q_b	dispersed phase flow rate at bottom of the column, $m^3.s^{-1}$
Q_d	dispersed phase flow rate, $m^3.s^{-1}$
Q_c,	continuous phase flow rate, $m^3.s^{-1}$
Q_t	dispersed phase flow rate at top of the column, $m^3.s^{-1}$
$\boldsymbol{r}$	external coordinate victor:[x, y, z]
r	spectral radius of the Jacobian matrix
$\boldsymbol{S}$	local propagation speed, Eq.(50)
$SysErr$	systematic error, Eq.(55)
t	time, s
U_c	continuous phase velocity relative to the column walls, $m.s^{-1}$
U_d	dispersed phase velocity relative to the column walls, $m.s^{-1}$
U_r	relative droplet (slip) velocity, $m.s^{-1}$
U_t	terminal droplet velocity, $m.s^{-1}$
u_m	any property associated with single droplet
v,v'	droplet volumes, m^3
v_0, v_f	mean droplet volume of the initial condition and feed distributions, m^3
v_{min}, v_{max}	minimum and maximum droplet volume, m^3
x_i	the characteristic droplet volume in the ith subdomain, m^3
z	spatial coordinate, m
z_d	dispersed feed inlet, m
z_c	continuous phase inlet, m

Greek symbols

α	parameter in the Weibull and inlet feed distributions
α_c, α_d	as defined in Table 3
β	parameter in the Weibull distribution
β_n	daughter droplet distribution based on droplet number, mm^{-1}
Γ	droplet breakage frequency, s^{-1}
$\Psi^{<i>}$	the *i*th coalescence interaction matrix, Eq.(26)
ϕ, Φ	dispersed phase hold-up
ϕ_e	dispersed phase hold-up entrained with the continuous phase
φ_i	dispersed phase hold-up in the *i*th subdomain
$\gamma_i^{<i-1>}$, $\gamma_i^{<i>}$	linear functions satisfying Eq.(19)
ρ, $\rho_{b,i}$, $\rho_{c,i}$	breakage and coalescence source terms, Eqs.(2), (23), and (25)
ρ_c, ρ_d	density of the continuous and dispersed phases respectively, $kg.m^{-3}$
μ_c	continuous phase viscosity, $kg.m^{-1}.s^{-1}$
ω	droplet coalescence frequency, $m^3.s^{-1}$
ω_R, $\omega_{R,crit}$	rotor and critical rotor speeds respectively, s^{-1}
σ	interfacial tension, $N.m^{-1}$
ζ	as defined by Eq.(31)
τ	residence time, s
θ	TVD parameter between 1 and 2.
$\vartheta(v')$	average number of droplets produced when mother droplet of volume, v', is broken

Appendix A. Analytical solution of the simplified PBE

To the best of the author's knowledge there is no analytical solution to the general PBE given by Eq.(6). However, Campos and Lage (2003) tried to solve it for droplet breakage and growth using the successive generation method of Liu, Srienc and Fredrickson (1997) by neglecting the diffusion term and assuming constant U_d. Unfortunately, they were not able to obtain an analytical solution in the closed from, and hence their semi-analytical solution requires further sophisticated programming as they pointed out. In this section we present an efficient methodology for solving the PBE with uniform dispersed phase velocity in a stagnant continuous phase, negligible diffusion flux and zero initial condition. So, let us simplify Eq.(6) based on these assumptions to get:

$$\frac{\partial n}{\partial t} + U_d \frac{\partial n}{\partial \zeta} = \rho\{n, v\} \tag{A1}$$

where $\zeta = z - z_d$. , $U_d = Q_d/A_c$ and the boundary condition is given by:

$$n(v, 0, t) = \frac{Q_d}{A_c} n^{feed} \quad \text{at} \quad \zeta = 0 \tag{A2}$$

Due to the convective nature of Eq.(A1) with uniform droplet velocity, it is well known that the response of the dispersed phase cannot occur until the local residence time, ζ/U_d is exceeded. So, let us define the relative time, η as:

$$\eta(t, \zeta) = t - \frac{\zeta}{U_d} \tag{A3}$$

Now making the necessary variable transformation using the chain rule, Eq.(A1) could be reduced to:

$$U_d \frac{\partial n(v; \eta, \zeta)}{\partial \zeta} = \rho\{n(v; \eta, \zeta), v\} \tag{A4}$$

with the following boundary condition:

$$n(v, 0, \eta) = \frac{Q_d}{A_c} n^{feed} \quad \text{at} \quad \zeta = 0 \text{ and } \eta > 0 \tag{A5}$$

Note that we can treat the spatial variable ζ as a like time variable and hence the first order IPDE given by Eqs.(A4) and (A5) could be solved in the same way as we solve the PBE for a batch stirred tank. It is then this important analogy between Eq.(A4) and the batch PBE that makes our approach very general and effective in obtaining an analytical solution whenever it is possible to solve the batch PBE. For example, all the analytical solutions reported by Gelbard and Seinfeld (1978) are valid solutions to Eqs.(A4) and (A5) by simply replacing the time variable in it by ζ. Following this methodology, we can derive the analytical solutions for case 6 by simply using the analytical solution for droplet breakage in a batch stirred tank that is given by Ziff and McGrady (1985) after transforming it in terms of droplet diameter:

$$n(d, \zeta, \eta) = \left(\frac{\pi d^2}{2}\right)\left[\frac{\alpha + K_b' \zeta}{\alpha}\right]^2 \exp\left[-\left(\alpha + K_b' \zeta\right)\left(\frac{d}{d_0}\right)^3\right] u[\eta] \tag{A6}$$

Note that the unit step function, u, is used since $\eta \geq 0$ and the part of the column in front of the moving dispersed phase is completely empty because of the zero initial condition. Now rewriting this equation in terms of the original variables and the volume distribution p we get:

$$p(d,z,t)=\left(\frac{d}{d_0}\right)^3\left(\frac{\pi d^2}{2}\right)\left[\frac{\alpha+K_b^{'}(z-z_d)}{\alpha}\right]^2\exp\left[-\left(\alpha+K_b^{'}(z-z_d)\right)\left(\frac{d}{d_0}\right)^3\right]u\left[t-\tau(d,z)\right] \tag{A7}$$

This is exactly the same as Eq.(65) and the unit step function is defined by Eqs.(63) and (64).
Similarly, Eq.(66) is derived by using the analytical solution for droplet coalescence in batch stirred tank as reported by Gelbard and Seinfeld (1978) after transforming it in terms of droplet diameter:

$$n(d,\zeta,\eta)=N_0^f\left(\frac{\pi d^2}{2}\right)\left(\frac{2}{2+N_0^f K_c\zeta}\right)^2\exp\left(\frac{-2\left(\frac{d}{d_0}\right)^3}{2+N_0^f K_c\zeta}\right)u\left[\eta\right] \tag{A8}$$

By substituting η and ζ in the above equation and rewriting it in terms of volume distribution p we recover exactly Eq.(66).
It should be pointed out that the droplet growth could be included in Eq.(A1) in a straight forward manner, and hence we could also get solutions for Eq.(A1) whenever this is possible in batch stirred tank.

Appendix B. Estimation of the total finite domain error (FDE)

Let us start from the average lower and upper FDEs as given by (Attarakih, Bart & Faqir, 2003a):

$$FDE = \frac{1}{\Delta d}\sum_{m=1}^{2}\int_{0}^{d_{\min}} u_m(d)n(d;z,t)\delta d + \lim_{d\to\infty}\frac{1}{\Delta d}\int_{d_{\max}}^{d} u_m(d)n(d;z,t)\delta d = \sum_{m=1}^{2}\left(FDE_m^L + FDE_m^U\right) \tag{B1}$$

In breakage and coalescence process, the minimum and maximum droplet sizes could be initially estimated based on the inlet feed and initial condition distributions such that $FDE_m^U < TOL/2$ (m=1, 2), where TOL is real and small positive number. These upper and lower residuals could be fairly approximated using the available values of the discrete distributions as follows:

$$FDE^L = \sum_{m=1}^{2}\sum_{i=1}^{2}\frac{1}{\Delta d_i}u_m(d_i)N_i(z,t) + \frac{1}{\Delta d}\sum_{m=1}^{2}\int_{0}^{d_{\min}} u_m(d)n(d;z,t)\delta d \tag{B2}$$

$$FDE^U = \sum_{m=1}^{2}\sum_{i=M_x-1}^{M_x}\frac{1}{\Delta d_i}u_m(d_i)N_i(z,t) + \lim_{d\to\infty}\frac{1}{\Delta d}\sum_{m=1}^{2}\int_{d_{\max}}^{d} u_m(d)n(d;z,t)\delta d \tag{B3}$$

Note that:

$$\sum_{m=1}^{2}\sum_{i=1}^{2}\frac{1}{\Delta d_i}\int_{d_{i-1/2}}^{d_{i+1/2}} u_m(d)n(d;z,t)\delta d > \frac{1}{\Delta d}\sum_{m=1}^{2}\int_{0}^{d_{\min}} u_m(d)n(d;z,t)\delta d \tag{B4}$$

Since the number distribution function should be monotone increasing at least for $d \in [0\ ,\ d_{min} + 2\Delta d]$ because of the lower boundary condition. This makes the following condition always valid:

$$\sum_{m=1}^{2}\sum_{i=1}^{2}\frac{1}{\Delta d_i}\int_{d_{i-1/2}}^{d_{i+1/2}} u_m(d)n(d;z,t)\delta d \le TOL/2 \Rightarrow \frac{1}{\Delta d}\sum_{m=1}^{2}\int_{0}^{d_{\min}} u_m(d)n(d;z,t)\delta d < TOL/2 \tag{B5}$$

Similarly:

$$\sum_{m=1}^{2}\sum_{i=M_x-1}^{M_x}\frac{1}{\Delta d_i}\int_{d_{i-1/2}}^{d_{i+1/2}} u_m(d)n(d;z,t)\delta d > \lim_{d\to\infty}\frac{1}{\Delta d}\sum_{m=1}^{2}\int_{d_{\max}}^{d} u_m(d)n(d;z,t)\delta d \tag{B6}$$

Since the number distribution function should be monotone decreasing at least for $d \in [\, d_{max} - 2\Delta d,\ d_{max},]$ because of the upper boundary condition, it follows that:

$$\sum_{m=1}^{2}\sum_{i=M_x-1}^{M_x}\frac{1}{\Delta d_i}\int_{d_{i-1/2}}^{d_{i+1/2}} u_m(d)n(d;z,t)\delta d \le TOL/2 \Rightarrow \lim_{d\to\infty}\frac{1}{\Delta d}\sum_{m=1}^{2}\int_{d_{\max}}^{d} u_m(d)n(d;z,t)\delta d < TOL/2 \tag{B7}$$

and hence d_{min} and d_{max} could be safely estimated at fixed M_x and TOL from the following relations:

$$FDE(d_{\min}, d_{\max}, M_x) = FDE^L + FDE^U \le TOL \tag{B8}$$

$$FDE^L \approx \sum_{m=1}^{2}\sum_{i=1}^{2}\frac{1}{\Delta d_i}u_m(d_i)N_i(z,t) + \sum_{m=1}^{2}\sum_{i}^{2}\frac{1}{\Delta d_i}\left(\int_{d_{i-1/2}}^{d_{i+1/2}} u_m(d)n^{feed}(d)\delta d + \int_{d_{i-1/2}}^{d_{i+1/2}} u_m(d)n^{ic}(d)\delta d\right) \tag{B9}$$

$$FDE^U \approx \sum_{m=1}^{2}\sum_{i=M_x-1}^{M_x}\frac{1}{\Delta d_i}u_m(d_i)N_i(z,t) + \sum_{m=1}^{2}\sum_{i=M_x-1}^{M_x}\frac{1}{\Delta d_i}\left(\int_{d_{i-1/2}}^{d_{i+1/2}} u_m(d)n^{feed}(d)\delta d + \int_{d_{i-1/2}}^{d_{i+1/2}} u_m(d)n^{ic}(d)\delta d\right) \tag{B10}$$

which are the required ones given by Eqs.(32) through (34).

References

Alatiqi, I., Aly, G., Mjalli, F., & Mumford, C. J. (1995). Mathematical modeling and steady-state analysis of a Scheibel extraction column. *Can. J. Chem. Engng.*, **73,** 523-533.

Al Khani, S. D., Gourdon, C., & Casamatta, G. (1988). Simulation of hydrodynamics and mass transfer of disks and rings pulsed column. *Ind. Engng. Chem. Res.*, **27,** 329-333.

Al Khani, S. D., Gourdon, C., & Casamatta, G. (1989). Dynamic and steady-state simulation of hydrodynamics and mass transfer in liquid-liquid extraction column. *Chem. Engng. Sci.*, **44,** 1295-1305.

Alopaeus, V., Koskinen, J., Keskinen, K. I., & Majander, J. (2002). Simulation of the population balances for liquid-liquid systems in a nonideal stirred tank: Part 2- parameter fitting and the use of multiblock model for dense dispersions. *Chem. Engng. Sci.*, **57,** 1815-1825.

Attarakih, M. M., Bart, H. J., & Faqir, N. M. (2003a). Optimal moving and fixed grids for the solution of discretized population balances in batch and continuous systems: droplet breakage. *Chem. Engng. Sci.*, **58,** 1251-1269.

Attarakih, M. M., Bart, H.-J., & Faqir, N. M. (2003b). Solution of the population balance equation for liquid-liquid extraction columns using a generalized fixed-pivot and central difference schemes.

Kraslawski, A. & Turunen, I. (Ed.), *European symposium on computer aided process engineering-13*, Computer-aided chemical engineering 14 (pp. 557-562). Elsevier, Amsterdam.

Attarakih, M. M., Bart, H. J., & Faqir, N. M. (2004). Solution of the droplet breakage equation for interacting liquid-liquid dispersions: a conservative discretization approach. *Chem. Engng. Sci.*, **59**, 2547-2565.

Bart, H.-J. (2003). Reactive extraction in stirred columns: A review. *Chem. Engng. Tech.*, **26,** 723-731.

Bennett, M. K. , & Rohani, S. (2001). Solution of population balance equations with a new combined Lax-Wendroff/Crank-Nicholson method. *Chem. Engng. Sci.*, **56,** 6623-6633.

Biggs, C. A. , & Lant, P. A. (2002). Modelling activated sludge flocculation using population balances. *Powder Tech.*, **14,** 201-211.

Cabassud, M., Gourdon, C., & Casamatta, G. (1990). Single drop break-up in a Kühni column. *Chem. Engng. J.*, **44,** 27-41.

Campos, F. B. , & Lage, P. L. C. (2003). A numerical method for solving the transient multidimensional population balance equation using Euler-Lagrange formulation. *Chem. Engng. Sci.*, **58,** 2725-2744.

Casamatta, G., (1981): Comportement de la population des gouttes dans une colonne d'extraction: Transport, rupture, coalescence, transfer de matiere, Dissertation, Institut National Polytechnique De Toulouse.

Casamatta, G. , & Vogelpohl, A. (1985). Modelling of fluid dynamics and mass transfer in extraction columns. *Ger. Chem. Engng.*, **8,** 96-103.

Cauwenberg, V., Degreve, J., & Slater, M. J. (1997). The interaction of solute transfer, contaminants and drop break-up in rotating disc contactors: Part I. Correlation of drop breakage probabilities. *Can. J. Chem. Engng.*, **75,** 1046-1055.

Chang, S.-C., Wang, X.-Y., and Chow, C.-Y. (1999). The space-time conservation element and solution element method: A new high-resolution and genuinely multidimensional paradigm for solving conservation laws. *J. Com. Phys.*, **156**, 89-136.

Chatzi, E. , & Lee, J. M. (1987). Analysis of interactions for liquid-liquid dispersions in agitated vessels. *Ind. Engng. Chem. Res.*, **26,** 2263-2267.

Colella, D., Vinci, D., Bagatin, R., & Masi, M. (1999). A study on coalescence and breakage mechanisms in three different bubble columns. *Chem. Engng. Sci.*, **54,** 4767-4777.

Coulaloglou, C. A. , & Tavlarides, L. L. (1977). Description of interaction processes in agitated liquid-liquid dispersions. *Chem. Engng. Sci.*, **32,** 1289-1297.

Desnoyer, C., Masbernat, O., & Gourdon, C. (2003). Experimental study of drop size distribution at high phase ratio in liquid-liquid dispersions. *Chem. Engng. Sci.*, **58,** 1353-1363.

Diemer, R. B. , & Olson, J. H. (2002a). A moment methodology for coagulation and breakage problems: Part 1- analytical solution of the steady-state population balance. *Chem. Engng. Sci.*, **57,** 2193-2209.

Diemer, R. B. , & Olson, J. H. (2002b). A moment methodology for the coagulation and breakage problems: Part 2-moment models and distribution reconstruction. *Chem. Engng. Sci.*, **57,** 2211-2228.

Gelbard, F. , & Seinfeld, J. H. (1978). Numerical solution of the dynamic equation for particulate systems. *J. Comput. Phys.*, **28,** 357-375.

Gelbard, F., Tambour, Y., & Seinfeld, J. H. (1980). Sectional representation of simulating aerosol dynamics. *J. Colloid & Interface Sci.*, **76,** 541-556.

Gerstlauer, A., (1999): Herleitung und Reduktion populationsdynamischer Modelle am Beispiel der Fluessig-Fluessig-Extraktion. Fortschritt-Berichte VDI Reihe, 3, 612.

Godfrey, J. C. , & Slater, M. J. (1991). Slip velocity relationships for liquid-liquid extraction columns. *Trans. Inst. Chem. Engng.*, **69,** 130-141.

Goodson, M. , & Kraft, M., (2003): Stochastic simulation of coalescence and breakage processes: a practical study. Preprint No. 9, pp. 1-30. Cambridge center for computational chemical engineering, Cambridge.

Gourdon, C. , & Casamatta, G. (1994). Population balance based modeling of solvent extraction columns. *Liquid-liquid extraction equipment***,** pp. 136-226, John Wiley, New York

Grace, J. R., Wairegi, T., & Nguyen, T. H. (1976). Shapes and velocities of single drops and bubbles moving freely through immiscible liquids. *Trans. Inst. Chem. Engng.*, **54**, 167-173.

Guimaraes, M. M., Cruz-Pinto, J. J. C., Regueiras, P. F. R., & Madureira, C. M. N. (1992). The simulation of interacting liquid-liquid dispersions- A new algorithm and its potentiality. Sekine T.(Ed.), *Solvent extraction 1990*, Part B, p. 1241-1246, Elsevier, Amsterdam .

Hamilton, R. A., Curits, J. S., & Ramkrishna, D. (2003). Beyond log-normal distributions: Hermite spectra for solving population balances. *AIChE J.*, **49,** 2328-2343.

Hartland, S. , & Jeelani, S. A. K., (1994): Gravity settlers. *Liquid-liquid extraction equipment*, Godfrey J. C. & Slater M. J., (Eds.), John Wiley, New York

Hill, P. J. , & Ng, K. M. (1995). New discretization procedure for the breakage equation. *AIChE J.*, **41,** 1204-1216.

Hill, P. J. , & Ng, K. M. (1996). New discretization procedure for the agglomeration equation. *AIChE J.*, **42,** 727-741.

Hill, P. J. , & Ng, K. M. (1997). Simulation of solids processes accounting for particle -size distribution. *AIChE J.*, **43,** 715-726.

Hounslow, M. J. (1990). A discretized population balance for continuous systems at steady state. *AIChE J.*, **36,** 106-116.

Hounslow, M. J., Marshall, V. R., & Ryall, R. L. (1988). A discretized population balance for nucleation, growth, and aggregation. *AIChE J.*, **34,** 1821-1832.

Hufnagl, H., McIntyre, M., & Blass, E. (1991). Dynamic behaviour and simulation of a liquid-liquid extraction column. *Chem. Engng. Tech.*, **14,** 301-306.

Hulburt, H., & Katz, S. (1964). Some problems in particle technology. A statistical mechanical formulation. *Chem. Engng. Sci.*, **19**, 555-574.

Karlsen, K. H., Lie, K.-A., Natvig, J. R., Nordhaug, H. F., & Dahle, H. K. (2001). Operator splitting methods for systems of convective-diffusion equations: nonlinear error mechanisms and correction strategies. *J. Comput. Phys.*, **173,** 636-663.

Kentish, S. E., Stevens, G. W., & Pratt, H. R. C. (1998). Estimation of coalescence and breakage rate constants within a Kühni column. *Ind. Engng. Chem. Res.*, **37,** 1099-1106.

Klee, A. J. , & Treybal, R. E. (1956). Rate of rise or fall of liquid drops. *AIChE J.*, **2,** 444-447.

Koren, B., (1993): A robust upwind discretization method for advection, diffusion and source terms. *Numerical methods for advection-diffusion problems*, Vreugdenhil C. B. & Koren B. (Eds.), (pp. 117-138), Vieweg & Sohn, Braunschweig.

Kostoglou, M. , & Karabelas, A. J. (1994). Evaluation of zero order methods for simulating particle coagulation. *J. Colloid Interface Sci.*, **163,** 420-431.

Kronberger, T., Ortner, A., Zulehner, W., & Bart, H.-J. (1994). Numerical determination of drop size distribution in extraction columns. Fasano A. (Ed.), *7th European Conference on Mathematics in Industry,* p. 247-254, B. G. Teubner Stuttgart.

Kronberger, T., (1995): Numerische Simulation von Tropfenpopulationen in Extraktionskolonnen, Dissertation, Johannes Kepler Universitat Linz, Linz 1995.

Kronberger, T., Ortner, A., Zulehner, W., & Bart, H. (1995). Numerical simulation of extraction columns using a drop population model. *Comput. Chem. Engng.*, **19,** S639-S644.

Kumar, S. , & Ramkrishna, D. (1996a). On the solution of population balance equations by discretization-I. A fixed pivot technique. *Chem. Engng. Sci.*, **51,** 1311-1332.

Kumar, S. , & Ramkrishna, D. (1996b). On the solution of population balance equations by discretization-II. A moving pivot technique. *Chem. Engng. Sci.*, **51,** 1333-1342.

Kumar, S. , & Ramkrishna, D. (1997). On the solution of population balance equations by discretization-III. Nucleation, growth and aggregation of particles. *Chem. Engng. Sci.*, **52,** 4659-4679.

Kurganov, A. , & Tadmor, E. (2000). New high-resolution central schemes for nonlinear conservation laws and convective diffusion equations. *J.Comput. Phys.*, **160,** 241-282.

Lee, G., Yoon, E. S., Lim, Y. I., Le Lann, J. M., Meyer, X. M., & Joulia, X. (2001). Adaptive mesh method for the simulation of crystallization processes including agglomeration and breakage: the potassium sulfate system. *Ind. Engng. Chem. Res.*, **40,** 6228-6235.

Lim, Y. I., Le Lann, J. M., Meyer, X. M., Joulia, X., Lee, G., & Yoon, E. S. (2002). On the solution of population balance equations (PBE) with accurate front tracking methods in practical crystallization processes. *Chem. Engng. Sci.*, **57,** 3715-3732.

Liou, J.-J., Srienc, F., & Fredrickson, A. G. (1997). Solutions of population balance models based on a successive generations approach. *Chem. Engng. Sci.*, **52,** 1529-1540.

Lister, J. D., Smit, D. J., & Hounslow, M. J. (1995). Adjustable discretized population balance for growth and aggregation. *AIChE J.*, **41,** 591-603.

Liu, Y. , & Cameron, T. (2001). A new wavelet-based method for the solution of the population balance equation. *Chem. Engng. Sci.*, **56,** 5283-5294.

Liu, S. , & Li, D. (1999). Drop coalescence in turbulent dispersions. *Chem. Engng. Sci.*, **54,** 5667-5675.

Mahoney, A. W. , & Ramkrishna, D. (2002). Efficient solution of population balances equations with discontinuities by finite elements. *Chem. Engng. Sci.*, **57,** 1107-1119.

McSwain, C. V. , & Durbin, L. D. (1966). The backflow-cell model for continuous two-phase nonlinear axial holdup and mixing effect. *Sep. Sci.*, **1,** 677-700.

Mignard, D., Amin, L., & Ni, X.-D. (2003). Population balance modelling of droplets in an oscillatory baffled reactor- using direct measurements of breakage rates constants. *J. Chem. Technol. Biotechnol.*, **78,** 364-369.

Milot, J. F., Duhamet, J., Gourdon, C., & Casamatta, G. (1990). Simulation of a pneumatically pulsed liquid-liquid extraction column. *Chem. Engng. J.*, **45,** 111-122.

Modes, G., (2000): Grundsatzliche Studie zur Populationsdynamik einer Extraktionskolonne auf Basis von Einzeltropfenuntersuchungen, Dissertation, Shaker Verlag.

Modes, G., Bart, H.-J., Rodrigue-Perancho, D., & Broder, D. (1999). Simulation of the fluid dynamics of solvent extraction columns from single droplet parameters. *Chem. Engng. Tech.*, **22,** 231-236.

Mohanty, S. (2000). Modeling of liquid-liquid extraction column: A review. *Rev. Chem. Engng.*, **16,** 199-248.

Motz, S., Mitrovic, A., & Gilles, E.-D. (2002). Comparison of numerical methods for the simulation of dispersed phase systems. *Chem. Engng. Sci.*, **57,** 4329-4344.

Nicmanis, M. , & Hounslow, M. J. (1998). Finite-element methods for steady-state population balance equations. *AIChE J.*, **44,** 2258-2272.

Qian, Y. , & Wang, J. (1992). Modelling of mass transfer in extraction columns with drop forward-mixing and coalescence-redispersion. *Can. J. Chem. Engng.*, **70,** 88-96.

Ramkrishna, D. (1985). The status of population balances. *Rev. Chem. Engng.*, **5,** 49-95.

Ramkrishna, D. (2000). *Population balances: Theory and applications to particulate systems in engineering*. San Diego: Academic Press.

Randolph, A. D. , & Larson, M. A. (1988). *Theory of particulate process*. 2nd Ed. San Diego: Academic Press.

Ribeiro, L. M., Regueiras, P. F. R., Guimaraes, M. M. L., Madureira, C. M. C., & Cruz-Pintu, J. J. C. (1995). The dynamic behavior of liquid-liquid agitated dispersions-I. The hydrodynamics. *Comput. Chem. Engng.*, **19,** 333-343.

Ribeiro, L. M., Regueiras, P. F. R., Guimaraes, M. M. L., Madureira, C. M. N., & Cruz-Pinto, J. J. C. (1997). The dynamic behavior of liquid-liquid agitated dispersions II. Coupled hydrodynamics and mass transfer. *Comput. Chem. Engng.*, **21,** 543-558.

Rice, G. R. , & Do, D. D. (1995). *Applied mathematics and modeling for chemical engineers*. New York: John Wiley.

Sastry, K. V. S. , & Gaschignard, P. (1981). Discretization procedure for the coalescence equation of particulate process. *Ind. Engng. Chem. Fundam.*, **20,** 355-361.

Song, M., Steif, A., & Weinspach, P.-M. (1997). A very effective method to solve the population balance equation with particle size growth. *Comput. Chem. Engng.*, **52,** 3493-3498.

Steiner, L., Bamelli, M., & Hartland, S. (1999). Simulation of hydrodynamic performance of stirred extraction column. *AIChE J.*, **45,** 257-267.

Toro, E. F. (1999). *Riemann solvers and numerical methods for fluid dynamics*. 2nd ed. Berlin: Springer.

Toutain, J., Lann, J. M. L., Gourdon, C., & Joulia, X. (1998). Maxwell-Stefan approach coupled drop population model for the dynamic simulation of liquid-liquid extraction pulsed column. *Comput. Chem. Engng.*, **22,** S379-S386.

Tsouris, C., Kirou, V. I., & Tavlarides, L. L. (1994). Drop size distribution and holdup profiles in a multistage extraction column. *AIChE J.*, **40,** 407-418.

Valentas, K. J. , & Amundson, A. R. (1966). Breakage and coalescence in dispersed phase systems. *Ind. Engng. Chem. Fundam.*, **5,** 533-542.

Vanni, M. (1999). Discretization procedure for the breakage equation. *AIChE J.*, **45,** 916-919.

Vanni, M. (2000). Approximate population balances equations for aggregation-breakage processes. *J.Coll. Int. Sci.*, **221,** 143-160.

van Peborgh Gooch, J. R. , & Hounslow, M. J. (1996). Monte Carlo simulation of size-enlargement mechanics in crystallization. *AIChE J.*, **42,** 1864-1874.

Verkoeijen, D., Pauw, G. A., Meesters, G. M. H., & Scarlett, B. (2002). Population balances for particulate processes- a volume approach. *Chem. Engng. Sci.*, **57,** 2287-2303.

Vignes, A. (1965). Hydrodynamique des dispersions. *Genie Chimique*, **93,** 129-142.

Weinstein, O., Semiat, R., & Lewin, D. R. (1998). Modeling, simulation and control of liquid-liquid extraction columns. *Chem. Engng. Sci.*, **53,** 325-339.

Wesselingh, J. A. , & Bollen, A. M. (1999). Single particles, bubbles and drops: Their velocities and mass transfer coefficients. *Trans. Inst. Chem. Engng.*, **77,** 89-96.

Wilburn, N. P. (1964). Mathematical determination of concentration profiles in two-phase continuous countercurrent extractors. *Ind. Eng. Chem. Fundam.*, **3,** 189-195.

Wulkow, M., Gerstlauer, A., & Nieken, U. (2001). Modeling and simulation of crystallization process using parsival. *Chem. Engng. Sci.*, **56,** 2575-2588.

Zamponi, G., Stichlmair, J., Gerstlauer, A., & Gilles, E.-D. (1996). Simulation of the transient behaviour of a stirred liquid/liquid extraction column. *Comput. Chem. Engng.*, **20**, S963-S968.

Zhang, S. H., Yu, S. C., Zhou, Y. C., & Su, Y. F. (1985). A model for liquid-liquid extraction column performance- The influence of drop size distribution on extraction efficiency. *Can. J. Chem. Engng.*, **63,** 212-226.

Zhu, F. G., Ni, X. D., Zhou, Y. C., Yu, S. C., & Su, Y. F. (1984). A modified rotating disc contactor with wire mesh coalescers. Akell, R. & King, C. J. (Eds.), *New developments in liquid-liquid extractors: Selected papers from ISEC '83*, **80**, (pp. 115-123). AIChE, New York.

Zimmermann, A., Joulia, X., Gourdon, C., & Gorak, A. (1995). Maxwell-Stefan approach in extractor design. *Chem. Engng. J.*, **57,** 229-236.

CHAPTER 6

LLECMOD: A Windows-Based Program for Hydrodynamics Simulation of Liquid-Liquid Extraction Columns

6.1 Introduction

The simulation of chemical engineering processes is now widely used to shed some light on the dynamic or steady state performance as well as equipment scale up of many unit operation equipment. This is because in most cases the actual running of these is very expensive or sometimes prohibitive due to safety reasons even at the laboratory scale. One of the most industrially important unit operations in chemical engineering is the liquid-liquid extraction that finds many significant applications in mining, petroleum, food and pharmaceutical industries (Seader & Henley, 1998). The hydrodynamics as well as the mass transfer in such unit operations is fundamentally influenced by the behavior of the dispersed phase consisting of populations of distributed rather than lumped characteristics in droplet phase space. Consequently, the natural framework of modeling of such dispersed phase processes is based on the population balances (Jiricny et al.,1979; Casamatta, 1981; Attarakih et al., 2003). Although such modelling framework is rich in the information it furnishes, it is still expensive from computational point of view since the full population balance models are normally integral partial differential equations (IPDE) of stretched type (Hwang & Shih, 1982). These IPDEs have only limited number of analytical solutions (Ramkrishna, 2000) that are in most cases strongly simplified and hence become physically unrealistic. Consequently, for realistic liquid-liquid extraction column (LLEC) simulation based on the population balance modelling, it is inevitable to seek for numerical solutions. In such cases the need for numerical solutions imposes two levels of difficulties due to the convective, droplet breakage and coalescence events occurring simultaneously. The convective nature in dispersed phase systems is actually dominant when compared to the axial dispersion and hence sharp front profiles describing the number or volume concentration distributions are expected to develop along the spatial coordinate in the direction of flow. At the same time the evolution of these distributions is governed by the breakage and coalescence mechanisms involving linear integral expressions for breakage and nonlinear ones for droplet coalescence. These issues are fully discussed by Attarakih et al. (2004) where an efficient numerical algorithm based on the generalized fixed-pivot technique and the central differencing schemes of Kuganove and Tadmor (2000) is presented and extensively tested. For user-friendly implementation of such numerical algorithm we introduce in this work the basics of a windows-based computer code that is called **L**iquid-**L**iquid **E**xtraction **C**olumn **MOD**ule (**LLECMOD**). The basic feature of this program is to provide the simulation of the hydrodynamics of LLECs based on the population balance approach for both transient and steady state through an interactive windows input dialogs. The LLECMOD is not restricted to a certain type of liquid-liquid extraction column since it is built in the most general form that allows the user to input the various droplet interaction functions. These functions include droplet terminal velocity taking into account the swarm effect and the slowing factor due to column geometry, the breakage frequency and daughter droplet distribution, the coalescence frequency and the axial dispersion coefficients.

6.2 The mathematical model

The population balance equation (PBE) based on the number concentration distribution along the column could be formulated as follows (Attarakih et al., 2003):

$$\frac{\partial n}{\partial t}+\frac{\partial F}{\partial z}=\frac{\partial}{\partial z}\left(D_d\frac{\partial n}{\partial z}\right)+\frac{Q_d}{A_c}\left(\frac{n^{feed}}{v_f}\right)\delta(z-z_d)+\rho\{n,v\} \tag{1}$$

where $n(v;z,t)\delta v=N(t,z)f(v)\delta v$ is the average number concentration associated with droplets having a volume between $v\pm\delta v$ at the time instant t and column height z, $N(t,z)$ is the total number concentration and $f(v)$ is the droplets number density. The convective flux of these droplets along the column of a constant cross sectional area, A_c, is represented by $A_cF\delta v = A_cU_dn\delta v$, where U_d is the velocity of the dispersed phase relative to the column walls. The first term on the right hand side of Eq.(1) represents the axial dispersion of the dispersed phase due to the non-ideal flow in which a random movement of the fluid on the microscopic level is superimposed on the main flow (Zhu et al., 1983). This is assumed to follow Fick's law with a diffusion coefficient, D_d, and is distinguished from the forward mixing effect due to the droplet velocity distribution that is taken into account by the convective term (Zhang et al., 1985). Where as the second term on the left hand side represents a number concentration rate of droplet entering as a feed of volumetric flow rate, Q_d, at the level z_d of the column. The positive direction of flow coincides with the dispersed phase flow from z_d to the top of the column. Note that the feed distribution is represented mathematically by a point source through the use of the Dirac delta function (Kronberger et al., 1994). The last term on the right hand side of Eq.(1) represents the net rate of the number of droplets generated by breakage and coalescence events per unit volume and is reported in detail by Attarakih et al. (2004).

The boundary conditions are greatly simplified since the dispersed and the continuous phases are included in the mathematical model given by Eq.(1) as point sources. Accordingly, the Danckwart's boundary conditions based on the discussion of Wilburn (1964) could be written by considering the LLEC to behave like a closed vessel between 0^+ and column height H:

$$0=max(F,0)-D_d\frac{\partial n}{\partial z},\quad at\ z=0 \tag{2}$$

$$0=-min(F,0)+D_d\frac{\partial n}{\partial z},\quad at\ \ z=H \tag{3}$$

$$n(v;z,t)=n_0(v;z),\forall z\in[0,H] \tag{4}$$

The first step in the numerical solution of these equations is to project the infinite system (with respect to droplet volume or diameter) of IPDEs given by Eq.(1) onto a finite system of partial differential equations (PDE) using the generalized fixed pivot technique. The idea in this technique is to divide the internal droplet coordinate (volume) into a contiguous finite subdomians covering the range of this internal coordinate. In each subdomain, the total volume concentration is obtained by integrating the volume concentration distribution with respect to volume (diameter) over the boundaries of this subdomain. This local volume concentration is then concentrated at a single point in this subdomain called the fixed-pivot, x_i, (see Fig.(2))and is given by:

$$\varphi_i(z,t)=\int_{v_{i-1/2}}^{v_{i+1/2}}v(v)n(v;z,t)dv=v(x_i)N_i(z,t),\quad i=1,2\ ...\ M_x \tag{5}$$

This replaces the IPDE given by Eq.(1) by M_x finite number of PDEs that are nonlinearly coupled through the convective and the source terms. These PDEs are then discretized based on upwind and central differencing schemes resulting in the following semidiscrete formulation:

$$\begin{aligned}&\frac{d\varphi_{i,l}}{dt}+\frac{F_{i,l+1/2}-F_{i,l-1/2}}{\Delta z_l}=\\&\qquad\frac{D_d\partial\varphi_i/\partial z\big|_{l+1/2}-D_d\partial\varphi_i/\partial z\big|_{l-1/2}}{\Delta z_l}+\frac{Q_d}{A_c}\frac{\varphi_i^{feed}}{v_f}\frac{\delta_{l,l_d}}{\Delta z_l}+\rho(\boldsymbol{\varphi}_l,\boldsymbol{d}),\ i=1,2..M_x,\ l=1,2..L\end{aligned} \tag{6}$$

The expressions for the numerical and diffusive fluxes are treated in detail by Attarakih et al.(2004). In addition, the source term takes into account the conservation of any two integral properties, u_1 and u_2 and is given by:

$$\boldsymbol{\rho}(\boldsymbol{\varphi}) = \begin{pmatrix} \boldsymbol{\varphi}^T \left[\left(\boldsymbol{\omega} \bullet \boldsymbol{\Psi}^{<1>} \right) \boldsymbol{\varphi} \right] \\ \boldsymbol{\varphi}^T \left[\left(\boldsymbol{\omega} \bullet \boldsymbol{\Psi}^{<2>} \right) \boldsymbol{\varphi} \right] \\ ..... \\ \boldsymbol{\varphi}^T \left[\left(\boldsymbol{\omega} \bullet \boldsymbol{\Psi}^{<M_x>} \right) \boldsymbol{\varphi} \right] \end{pmatrix} - \boldsymbol{\varphi}^T \bullet \left[\boldsymbol{\omega} \left(\boldsymbol{\zeta} \bullet \boldsymbol{\varphi} \right) \right] + \boldsymbol{A}[\boldsymbol{\Gamma} \bullet \boldsymbol{\varphi}] \tag{7}$$

where:

$$A_{i,k} = \begin{pmatrix} \left[\pi_{i,i}^{<m>} - 1 \right] \\ \pi_{i,k}^{<m>} \end{pmatrix}, i = 1,2..M_x, k = i, i+1...M_x \tag{8}$$

$$\pi_{i,k}^{<m>} = \int_{d_{i-1}}^{d_i} \gamma_i^{<i-1>}(d)[\frac{u_m(d_i)}{u_m(d_k)}]\beta_n(d \mid d_k)\delta d + \int_{d_i}^{\min(d_k, d_{i+1})} \gamma_i^{<i>}(d)[\frac{u_m(d_i)}{u_m(d_k)}]\beta_n(d \mid d_k)\delta d \tag{9}$$

$$\zeta_k = \frac{1}{u_m(x_k)} \tag{10}$$

$$\Psi_{k,j}^{<i>} = \begin{cases} \left[1 - \frac{1}{2}\delta_{k,j} \right] \frac{u_m(x_i)}{u_m(x_j)u_m(x_k)} \gamma_i^{<i-1>}(x_k + x_k), & \text{if} \quad d_{i-1}^3 \le x_j + x_k < d_{i-1}^3 \\ \left[1 - \frac{1}{2}\delta_{k,j} \right] \frac{u_m(x_i)}{u_m(x_j)u_m(x_k)} \gamma_i^{<i>}(x_k + x_k), & \text{if} \quad d_i^3 \le x_j + x_k < d_{i+1}^3 \end{cases} \tag{11}$$

$$\Gamma_i = \Gamma(d_i, \phi(t,z)), \quad i = 1,2,...M_x \tag{12}$$

$$\omega_{i,k} = \omega(d_i, d_k, \phi(t,z)), \quad i,k = 1,2,...M_x \tag{13}$$

$\gamma_i^{<i-1>}$ and $\gamma_i^{<i>}$ are triangular functions defined in Attarakih et al. (2004). Note that the above mathematical model conserves the total droplet number and volume by setting $u_1 = 1$ and $u_2 = v$

6.3 User input data and functions

The above discrete formulation requires grid structure input for both droplet diameter and column height: d_i, i=1, 2, ... M_x; z_l, l=1, 2, ... L; the breakage frequency function $\Gamma(d_i, \phi(z_l,t))$; the coalescence frequency $\omega(d_i,d_j,\phi(z_l,t))$, and the droplet rise velocity. All these parameters and functions must be defined in a user supplied input module called: UserFunctionsMod where a sample of which is given in appendix A.

6.3.1 Grids generation

The grid structure depends on the column geometry as shown in Fig.(1) as well as the minimum and maximum droplet diameters prevailing in the column. The program provides two types of grids for both column height and droplet diameter. For droplet diameter geometric and uniform droplet discretizations are available:

$$d_{i-1/2} = d_{\min}\left(\frac{d_{\max}}{d_{\min}}\right)^{\frac{i-1}{Mx}}, \quad i = 1,2...M_x + 1 \tag{14}$$

$$d_{i-1/2} = d_{\min} + \left(\frac{d_{\max} - d_{\min}}{M_x}\right)(i-1), \quad i = 1,2...M_x + 1 \tag{15}$$

For the column height the uniform grid structure has the same form as that given by Eq.(15) by replacing d with z. However, the nonuniform grid structure is constructed by a combination of uniform grids to produce relatively fine structure around the dispersed and continuous phases inlets where permanent discontinuities appear. This provides sharp resolution of these discontinuities at steady state conditions without excessive increase in the number of grid points. The above grids are internally generated by LLECMOD and the user is only required to input the parameters: d_{min}, d_{max}, z_0, z_d, z_c, H, M_x, and L.

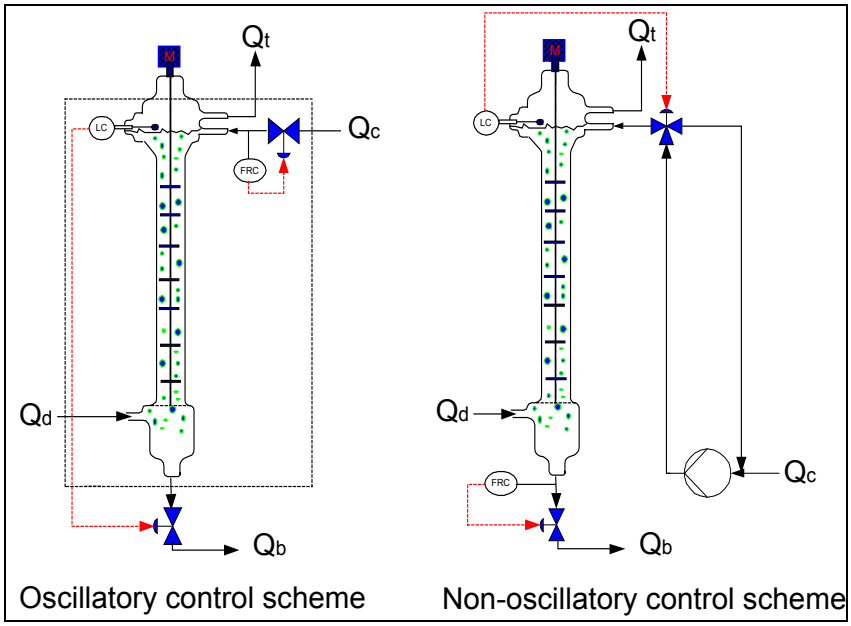

Fig.(1): Conventional and improved dispersed phase level controls (Hufnagl et al., 1991).

6.3.2 Dispersed and continuous phases chemical components

The physical properties required for the evaluation of droplet transport and interactions (breakage and coalescence) are loaded from a simple database containing ten and three chemical components for the dispersed and continuous phases respectively. However, the user could add the physical properties for any new chemical component by editing the files: LLECMOD\CompData. The required information for the use of these files is shown in Table 1. Note that alphabetical letters precede the names of the components and are arranged alphabetically to be distinguished by the LLECMOD text reader. This means that when any component is added to the database it should be consistent with this rule. The physical property of any chemical component should be added to the related file in Table 1 at the corresponding position.

Table 1: Continuous and dispersed phase physical properties files.

File name	Description.
CompNameCont.txt	contains the names of the continuous phase components.
CompNameDisp.txt	contains the names of the dispersed phase components.
PhysPropCont.txt	contains the densities and viscosities of the continuous phase components.
PhysPropdisp.txt	contains the densities and viscosities of the dispersed phase components.
PhysPropSurfTension.txt	contains the surface tension of any combination between the continuous and dispersed phase components.

6.3.3 Inlet feed distribution

The inlet feed distribution appearing in Eq.(1) could be supplied by the user in either two ways: First by representing the data in tabulated form where the first column is the characteristic droplet diameter in mm and the second column is the feed population density (mm^{-1}) corresponding to the given droplet diameter in the first column. The LLECMOD generates the grid and compares the number of read pivots M_x with the input ones, and if they are not equal, an error message is displayed. The discrete feed distribution is generated and normalized internally according to the relation:

$$\varphi_i^{feed} = \frac{\overline{\varphi_i}\Delta d_i}{\sum_{i=1}^{M_x} \overline{\varphi_i}\Delta d_i} \tag{16}$$

The second form of the feed input is in the form of three frequently used distributions to fit the liquid-liquid distributors or droplet distributions in agitated columns: the normal, lognormal and Weibull distributions (see Fig.2). Depending on his choice the user is asked to input the parameters for the selected distribution. Note that the number of pivots M_x , the type of the grid (uniform or geometric), the minimum and maximum droplet diameters must be input by the user.

6.3.4 The terminal droplet velocity: SDVel

The LLECMOD has four terminal droplet velocity laws (SDVel functions) that could be easily chosen by the user. These velocity laws are: Klee and Treybal (1956), Vignes (1965), Grace et al. (1976) and the rigid sphere law (Wesswlingh & Bollen, 1999). If the user does not choose any of these laws, the LLECMOD automatically chooses by default the suitable velocity law based on the selection chart detailed in the book of Godfrey and Slater (1994). Moreover, if the user has a specific velocity law he could add it simply to the user input module as shown in appendix A. Note that the unit of the terminal droplet velocity should be in $m.s^{-1}$ and so the input droplet diameter must be transformed from mm to m.

6.3.5 The continuous phase velocity models

The continuous phase velocity models are required to calculate the dispersed phase velocity U_d are shown in Table 2. The first velocity model corresponds to the interface level control as shown in Fig.(1). In this control scheme the outlet continuous flow rate is manipulated to control the position of the interface at the top of the column. The velocity model corresponding to this scheme shows an oscillatory behaviour in the dispersed phase hold up as reported both experimentally (Hufnagl et al., 1991; Gerstlauer, 1999) and theoretically (Weinstein et al., 1998; Attarakih et al., 2004). The second velocity model assumes that the continuous phase is at steady state and hence it is not applicable for transient simulations, while the third velocity model is based on the control scheme shown in Fig.(1) by manipulating the inlet continuous flow rate. This resulting oscillation in the dispersed phase hold up could be explained as follows (Weinstein et

al., 1998): At the instant of introducing the dispersed phase at z_d the outlet flow rate of the continuous phase increases immediately because it is displaced by the dispersed phase ($\phi_d + \phi_c = 1$), at the same time the dispersed phase hold up is propagated along the column causing an increase in the top flow rate, Q_t. At $z = z_d$ and according to the velocity model 1 shown in Table 2, $Q_{c,out} = A_c U_c$ start to decrease to satisfy the total volume balance (Note that $n(d;z<z_d,t) = 0$ away from flooding conditions). As a result this reduction in the continuous phase flow rate at the bottom of the column will decrease the dispersed phase hold up according to $U_d = U_r - U_c$.

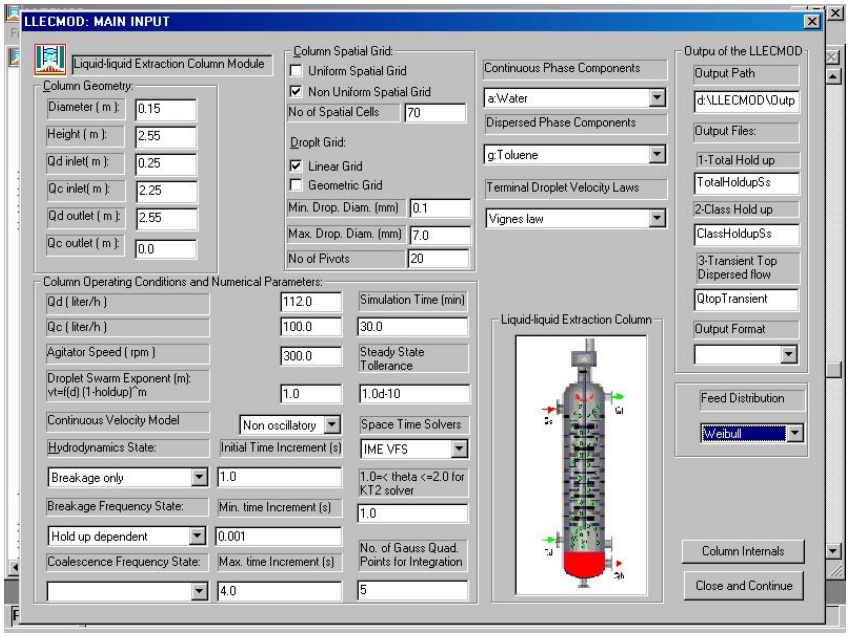

Fig.(2): The main input dialog of the LLECMOD showing the input of the present sample problem.

Accordingly, this decrease in the dispersed phase hold up will propagate along the column and hence causing the top flow to decrease. This causes the continuous flow rate at the bottom to increase and hence the dispersed phase hold up will increase again and the process repeats itself with decreasing amplitude that is damped when the steady state is approached.
The non-oscillatory velocity model gets rid of this resonance behaviour by keeping the continuous phase flow rate at the bottom of the column at a constant value and hence it allows the inlet flow rate to vary according to: $Q_{c,in} = Q_t + \frac{1}{1-\phi_e} Q_{c,out} - Q_d$ (Attarakih et al., 2004). This is found to eliminate completely the oscillatory behavior of the dispersed phase hold up since its magnitude at the base of the column is maintained constant as long as Q_d is constant.

6.3.6 Axial dispersion coefficients: Dc and Dd

The axial dispersion coefficients, D_c and D_d for the dispersed and continuous phases respectively are defined in the user input module as functions Dc and Dd as shown in appendix A. These coefficients are allowed only to vary with the column height in the present version of LLECMOD. The dependency on droplet diameter or velocity will be taken into account in the future versions.

Table 2: Available continuous phase velocity models.

Continuous phase velocity model	Reference
1- Oscillatory: $U_c = \frac{Q_t}{A_c} - \alpha_c \frac{Q_{c,in}}{A_c} - \alpha_d \frac{Q_{d,in}}{A_c} - \int_{d_{\min}}^{d_{\max}} v(d) U_r(d,\phi,\boldsymbol{P}) n(d;z,t) \delta d$ $Q_t = \int_{d_{\min}}^{d_{\max}} v(d) U_r(d;\phi(H,t),\boldsymbol{P}) n(d;H,t) \delta d$	Casamatta (1981)
2- Steady state: $U_c = \alpha_c \frac{Q_c}{A_c(1-\phi)} + \frac{D_c}{1-\phi} \frac{\partial \phi}{\partial z}$	Kronberger (1995)
3-Nonoscillatory: $U_c = \frac{Q_t}{A_c} - \alpha_c \frac{Q_{c,in}}{A_c} - \alpha_d \frac{Q_{d,in}}{A_c} - \int_{d_{\min}}^{d_{\max}} v(d) U_r(d,\phi,\boldsymbol{P}) n(d;z,t) \delta d$ with $Q_{c,in} = Q_t + \frac{1}{1-\phi_e} Q_{c,out} - Q_d$ $\alpha_c = \begin{cases} 1, & z \le z_c \\ 0, & z > z_c \end{cases}$ and $\alpha_d = \begin{cases} 1, & z \le z_d \\ 0, & z > z_d \end{cases}$	Attarakih et al. (2004)

6.3.7 Breakage frequency and daughter droplet distribution: GamaF and BetaF

The breakage frequency function $\Gamma(d,U_d,\phi(z,t))$ could be easily defined by the user as shown in the user input module in appendix A (GamaF). This function must have a unit of s^{-1} and so U_d must be in $m.s^{-1}$ and d must be in m. All the physical properties are declared internally and they need not to be redeclared in this function. The daughter droplet distribution (BetaF) must be based on number rather than volume as a requirement of the GFP technique. Its unit should be in mm^{-1} and so there is no need to convert its input argument from mm to m. Note that the number of daughter droplets produced during breakage must be included in this function.

For the case that the breakage frequency is independent from the dispersed phase hold up or the dispersed phase velocity we call it separable; that is, $\Gamma=\Gamma(d)$. In this case we choose from the input menu: *Breakage frequency state/Hold up independent*, which is the default. On the other hand, if $\Gamma=\Gamma(d,\phi(z,t))$, we choose: *Breakage frequency state/Hold up dependent*.

6.3.8 The coalescence frequency: OmegaF

The coalescence frequency function $\omega(d,d',\phi(z,t))$ is defined in the user input module as shown in appendix A as OmegaF. The unit of this function is $m^3.s^{-1}$ and so the input droplet diameters must be transformed from mm to m. For constant coalescence frequency, it must be multiplied by 10^{-9} to take into account this unit conversion. For the case that the coalescence frequency is independent from the dispersed phase hold up we call it separable; that is, $\omega=\omega(d,d')$. In this case we choose from the input menu: *coalescence frequency state/Hold up independent*, which is the default. On the other hand, if $\omega=\omega(d,d`,\phi(z,t))$ we choose: *coalescence frequency state/Hold up dependent*.

6.4 Droplet phase space-time solvers

The LLECMOD provides three droplet phase space-time solvers to discretize droplet diameter, column height and time as shown in Table 3. The algorithms on which these solvers are built are fully described and extensively tested by Attarakih et al. (2004). The user could choose from the drop list menu provided by the input dialog the suitable solver with IME FVS as the default one. The minimum and maximum time steps, the final simulation time, the steady state tolerance, and the TVD (total variation diminishing) parameter θ for IME KT2 solver could also be chosen by the user from the input dialog. The value of the

TVD parameter ranges from 1 to 2 with value 2 for the least dissipative behaviour while the value 1 guarantees a non-oscillatory scheme.

Table 3: Available phase space-time solvers in LLECMOD.

Solver	Order	Description
IME FVS	First order in time and space	Upwind differencing with flux vector splitting with implicit Euler method.
IME KT1	First order in time and space	Non-oscillatory central differencing with implicit Euler method.
IME KT2	First order in time and second order in space	Non-oscillatory central differencing scheme with implicit Euler method.

6.5 The LLECMOD output

The output from the LLECMOD is of two types: the first one is graphical output consisting of the most important simulation results. These are the inlet feed distribution, the relative droplet velocity taking into account the slowing factor K_v, the hold up along the column, the mean droplet diameter (*d32*) along the column, and the droplet volume distribution at selected positions along the column. The second output is written to three output files: the total hold up and the mean droplet diameter of the dispersed phase along the column, the droplet volume distribution along the column, and the transient top flow rate. Moreover, in the directory LLECMOD\Output\Plot the user could find a MATLAB file written using MATLAB version 6.1 to plot the two dimensional droplet distribution and the other aforementioned outputs. If this MATLAB script is to be used, the option *unFormt* should be chosen from the input dialog since for *Format* option the volume distribution matrix will be written four columns per page for ease of print out.

6.6 Sample problem

In this section we consider a sample problem to illustrate the basic features of the LLECMOD including the main input parameters, the user input functions, and the output of the program. For this purpose we will use the case study reported by Attarakih et al. (2004) used for experimental validation of his presented numerical algorithm. This experimental data is based on the work of Modes (2000) for the steady state hydrodynamics of a laboratory scale RDC column whose dimensions are shown in Table 4.

Table 4: RDC column geometry.

Column diameter	(m)	0.15	Column height (m)	2.550
Stator diameter	(m)	0.105	Dispersed phase inlet (m)	0.250
Rotor diameter	(m)	0.090	Continuous phase inlet (m)	2.250
Compartment height	(m)	0.030		

The experimental data for the system water-toluene was compared to the simulated results by Attarakih et al. (2004) and hence will not be repeated here. The experimentally correlated droplet transport functions, the breakage frequency, and the daughter droplet distribution will be used. These were determined based on single droplet experiments carried out in a column segment having five compartments of total height 0.15 m. The droplet rise velocities and the breakage probability functions are determined using digital image processing, while the axial dispersion coefficient of the dispersed phase is determined using residence time analysis for a monodispersion of droplets of specified diameters (Modes et al., 1999). The chemical system used is the EFCE test system: water-toluene whose physical properties are available online (http//www.dechema.de/Extraktion). Due to the relative high interfacial tension of this system, the low values of the dispersed phase hold up, and in the absence of mass transfer, the droplet coalescence could be safely neglected. Accordingly, Modes (2000) recommended the use of Vignes (1965) velocity

law to estimate the terminal droplet velocity multiplied by (1-ϕ) to take into account the droplet swarm effect. This author correlated the slowing factor, K_v, and the axial dispersion coefficient, D_d, with the energy input and the droplet diameter as follows:

$$K_v(d,N^*) = 1 - 1.037\left(N^{*3}D_R^5\right)^{0.12} - 0.62\left(\frac{d}{D_s - D_R}\right)^{0.44} \tag{17}$$

$$\frac{D_d}{U_d H} = 0.0138 + 8.26\times10^{-7}\left(\frac{N^* D_R}{U_d}\right)^{3.3} \tag{18}$$

where N^* is the rotor speed (s^{-1}), D_R, and D_s are the rotor and stator diameters respectively whose values are shown in Table 4.
The droplet breakage frequency and the daughter droplet distribution are correlated based on single droplet experiments and are given by:

$$\Gamma(d,\phi) = P_r(d,N^*)\frac{U_d(d,\phi)}{H_c} \tag{19}$$

The breakage probability, P_r, is correlated with the system physical properties and the energy dissipation in the following form:

$$\frac{P_r}{1-P_r} = 6.04\times10^{-4}\left(\frac{\rho_c^{0.8}\mu_c^{0.2}dD_R^{1.6}\left(\omega_R^{1.8} - \omega_{R,crit}^{1.8}\right)}{\sigma}\right)^{1.595} \tag{20}$$

where $\omega_{R,crit}$ is the critical rotor speed below which the breakage probability falls to zero (Modes, 2000) and H_c is the RDC compartment height.
The daughter droplet distribution (based on number) is assumed to follow the beta distribution, which is given by:

$$\beta_n(d \mid d') = 3\vartheta(\vartheta-1)\left[1-\left(\frac{d}{d'}\right)^3\right]^{(\vartheta-2)}\frac{d^2}{d'^3} \tag{21}$$

where ϑ is the mean number of daughter droplets produced upon breakage of mother droplet of diameter d'. It is experimentally correlated and found dependent on the energy dissipation and having a value ≥ 2. Note that when ϑ equals 2 the above daughter droplet distribution is reduced to the uniform distribution with respect to droplet volume as internal coordinate.
In all the numerical simulations presented in this section the inlet feed distribution is based on the measured values and for the convergence tests we find the log normal distribution fits well the experimental data. The numerical integration is carried out until steady state using the column geometry shown in Tables 4 and Fig.(3). The IME FVS solver is used with grid having a dimension of 70×20, where doubling of the grid size shows no principal differences in the predicted results. The minimum droplet diameter is chosen to lie below the critical droplet diameter predicted by Eq.(20). The user input parameters using the LLECMOD main input dialog are shown in Fig.(2). The detailed internal RDC column geometry is shown in Fig.(3) which is based on the values indicated in Table 4. The input parameters and data shown in Figs.(2) and (3) are echoed off on the LLECMOD working window as shown in Fig.(4) before the space time integrator is started.

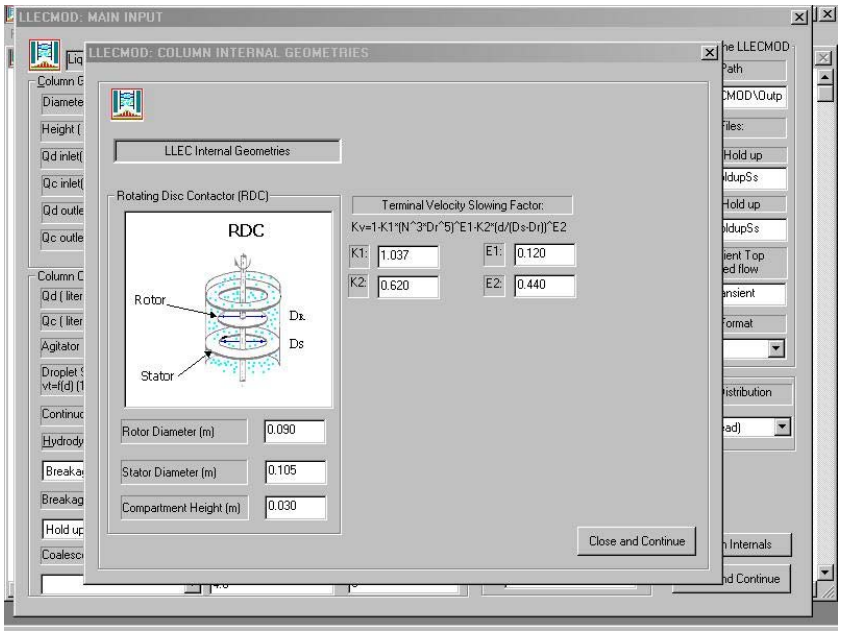

Fig.(3): The LLECMOD input dialog for internal RDC column geometries.

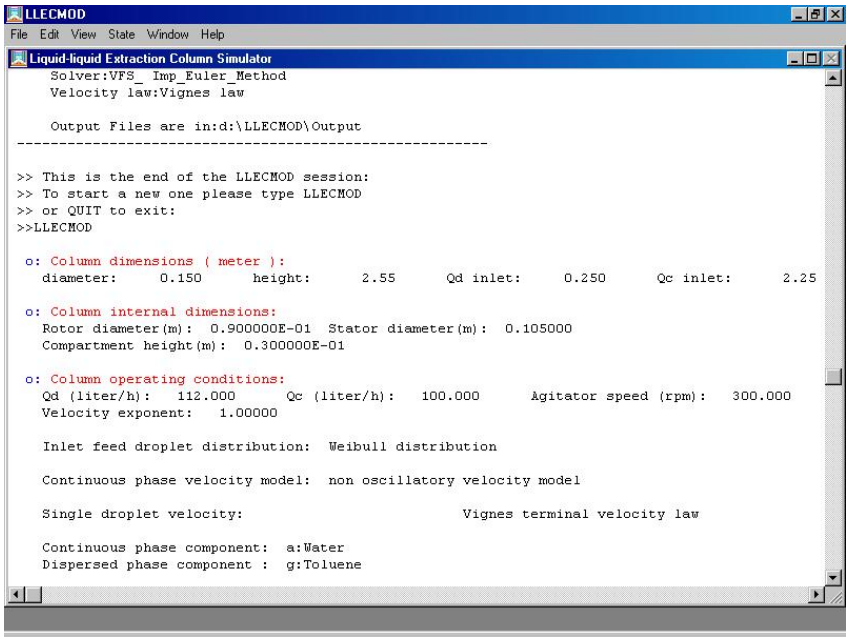

Fig.(4): Echo off of the user input data.

So, if any mistake is made during the input the user could return to the main dialog to correct it. Once all the input is echoed off the user is asked either to continue the LLECMOD session or to restart again. If *Y* (*Yes*) is chosen then the LLECMOD starts the space time integration using the user input parameters and displays the current simulation time and the evolution of the top flow rate. Once the final simulation time is exceeded or the steady state tolerance is achieved the LLECMOD presents the results in graphical form as shown in Figs.(6) through 9. In addition to these figures a summary of the simulation is displayed in a separate window as shown in Fig.(5). This figure shows the dispersed phase flow rate at the top of the column is almost the same as the throughput; however, the steady state is not achieved according to the chosen tolerance (10^{-10}) since the final simulation time is exceeded (30 minuets). Fig.(6) shows the evolution of the dispersed phase flow rate at the top of the column as generated by the LLECMOD

graphics library. This graphics library is an improved and modified version of the SIGRAPH library provided with the Compaq visual FORTRAN version 6.6. The non-oscillatory and oscillatory behaviours of the top flow rate are clear based on the discussion of section 6.3.5. Fig.(7) shows the terminal droplet velocity as generated by LLECMOD taking into account the effect of the slowing factor, K_v, due to the column internal geometry (Eq.(17)). Since the terminal droplet velocity increases as the droplet diameter increases and the slowing factor decreases at the same time, it follows then that the product of these functions passes through a maximum as it is evident in Fig.(7).
Fig.(8) shows the steady state dispersed phase hold up and the mean droplet diameter where the discontinuities due to the dispersed and continuous phases inlets are highly resolved due to the nonuniform spatial grid used in the simulation (see Fig.(2)). Since breakage is dominant (no coalescence) for the toluene–water system the hold up increases along the column indicating that as the droplets ascend the column they break up due to the input energy dissipation in the continuous phase. This is naturally accompanied by a decrease in the mean droplet diameter (*d32*) as it is clear in Fig.(8). This fact is further elucidated by referring to Fig.(9) where the cumulative droplet volume distribution is depicted at selected positions along the column. It is evident that rapid droplet breakage is found to occur between 10 and 60 % of the column active height. Since no droplet breakage is assumed in the upper settling zone, the cumulative population densities at the continuous phase inlet and outlet of the column are identical.
The CPU time requirements on PC of 750 MHz speed for this case is 128 s as shown in the output of the LLECMOD in Fig.(5). However, this time could be reduced if the steady state tolerance is set smaller than 10^{-10}. The performance of the other solvers is extensively tested by Attarakih et al. (2004) and are found to produce identical results at steady state. However, for transient simulations it is found that the first order solvers (IME FVS and IME KT1) are suffering from numerical diffusion due to the steep moving fronts of the droplets hold up of different sizes. This numerical diffusion is greatly reduced when the second order solver (IME KT2) is used and thus the moving fronts could be captured correctly.

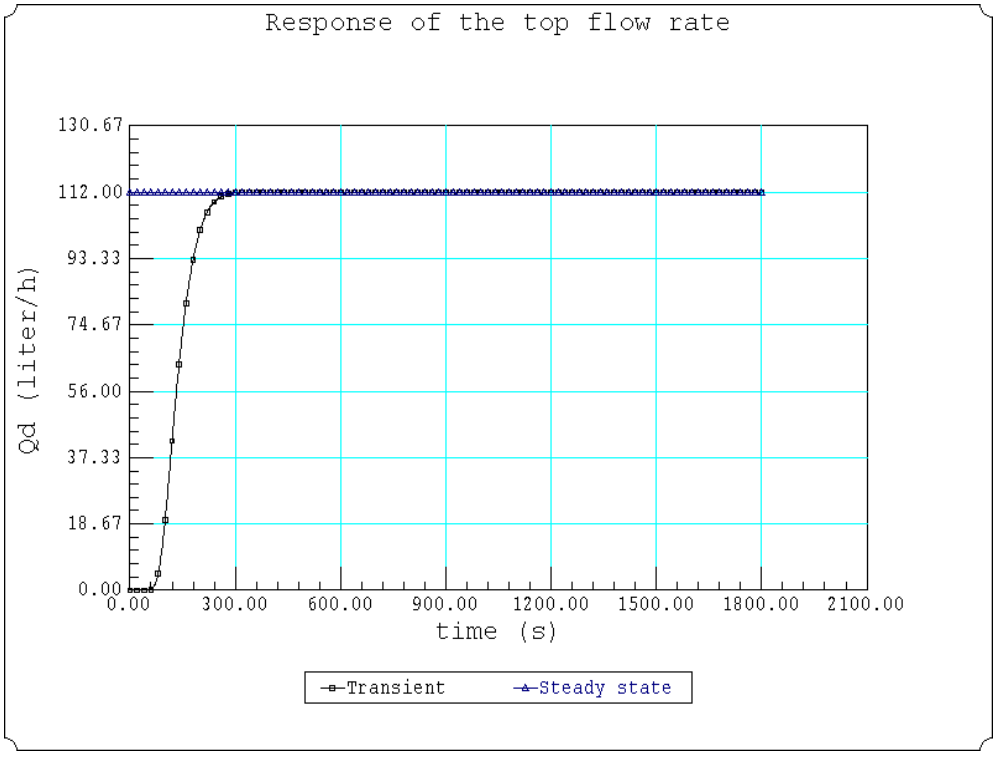

Fig.(6):a- The dispersed phase response at the top of the column using the non-oscillatory velocity model.

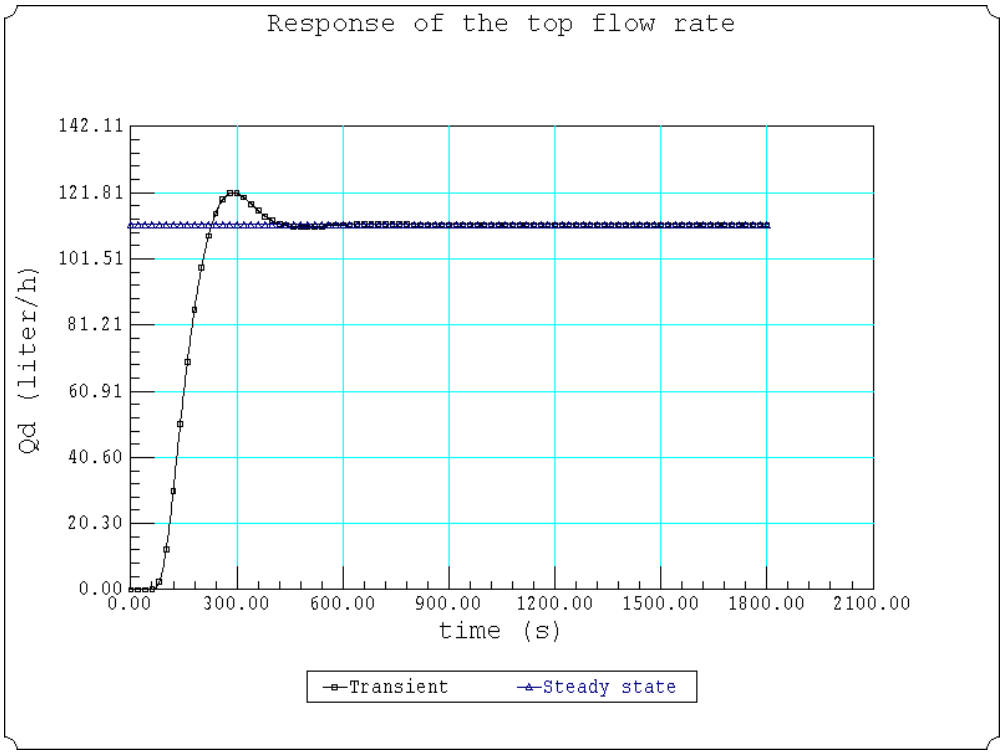

Fig.(6):b- The dispersed phase response at the top of the column using the oscillatory velocity model.

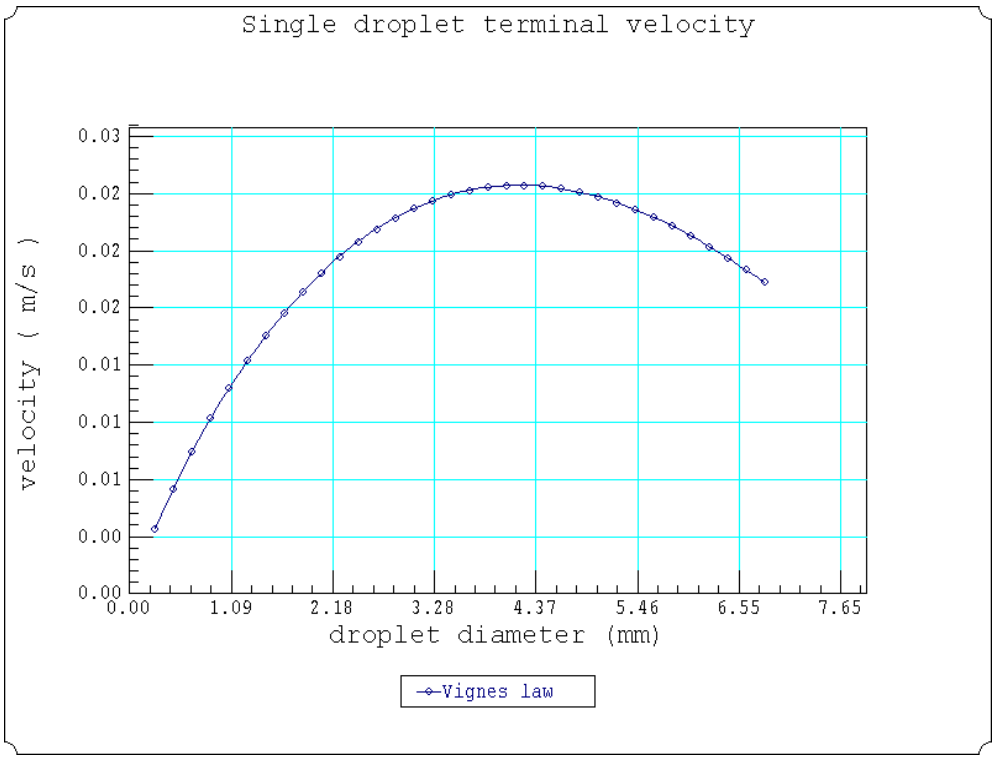

Fig.(7): The terminal droplet velocity multiplied by the slowing factor, K_v.

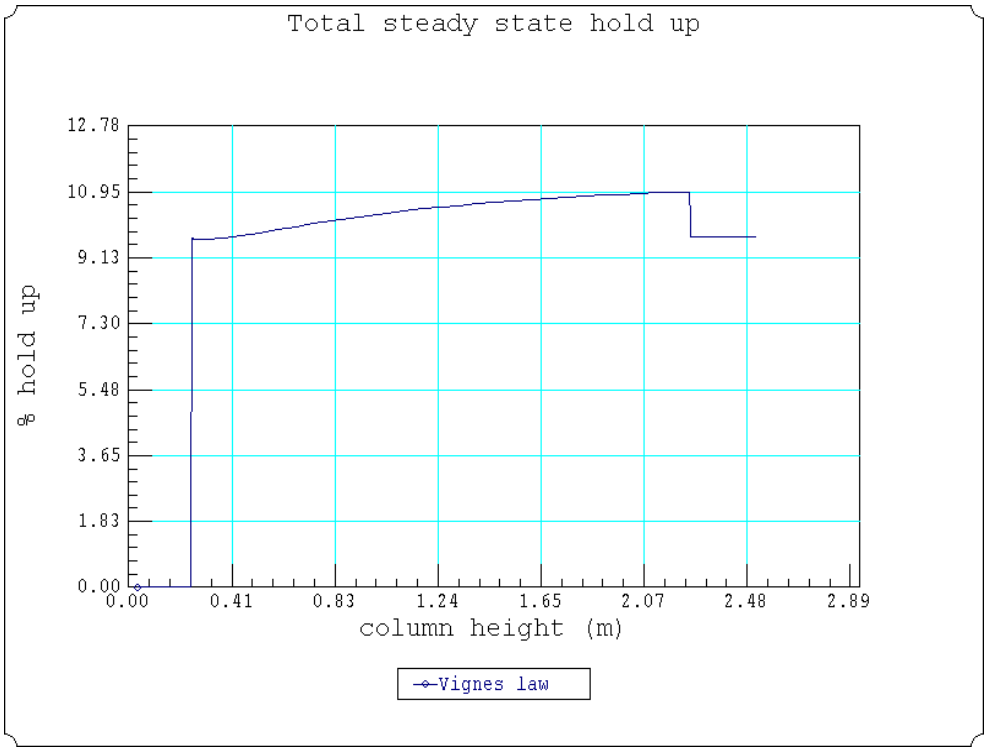

Fig.(8): a- Steady state dispersed phase hold up.

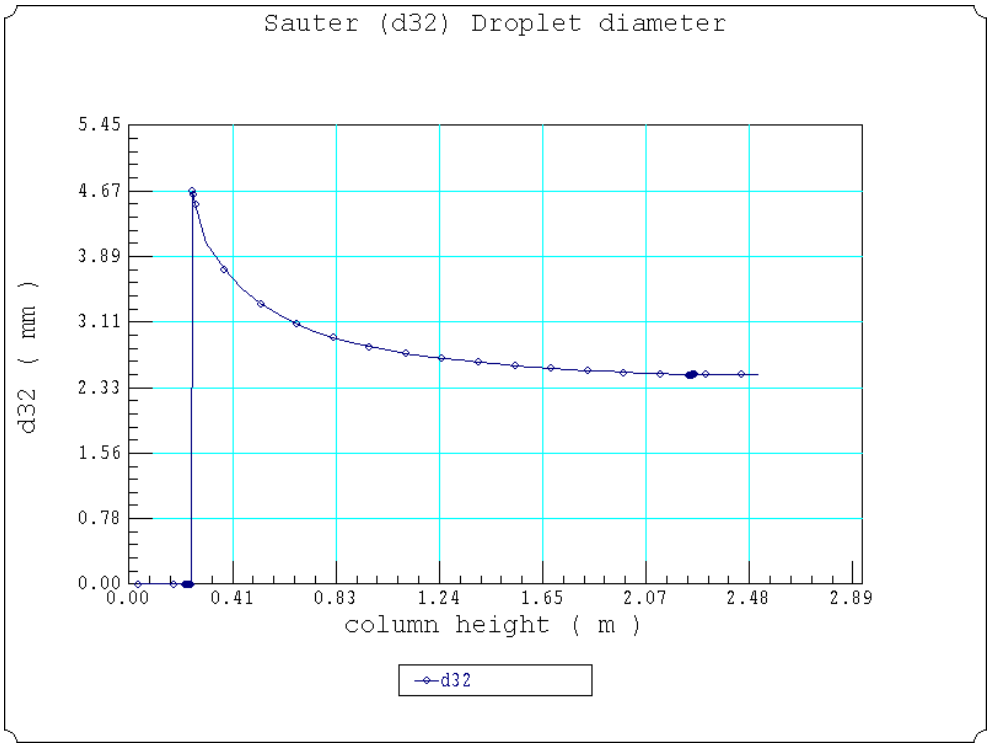

Fig.(8): b- Steady state mean droplet diameter.

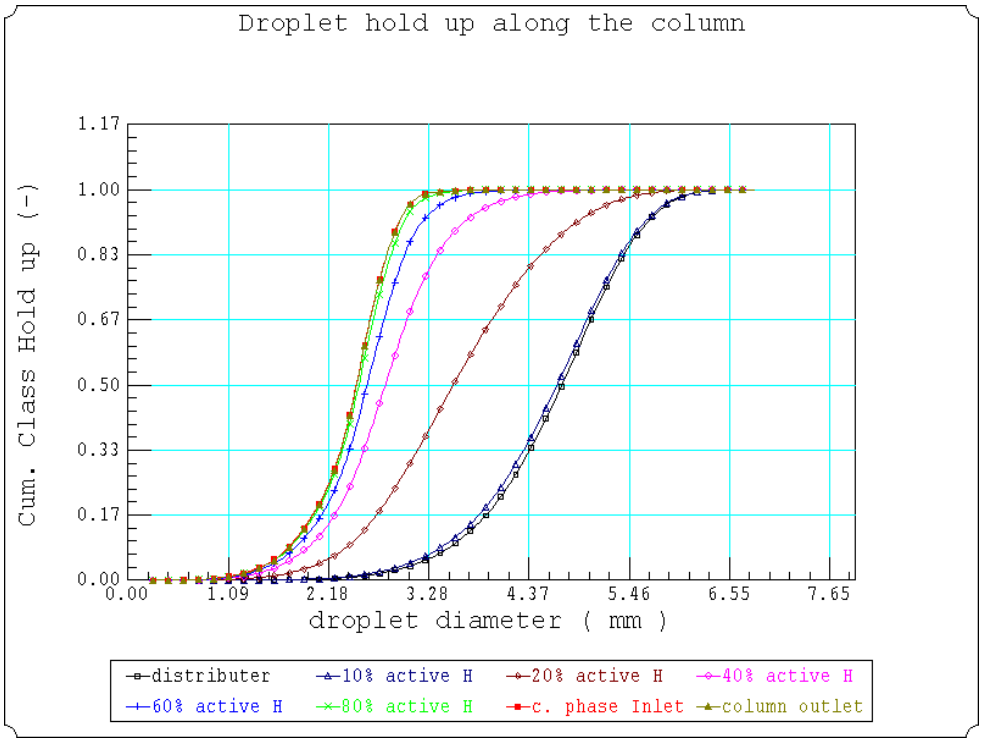

Fig.(9): The cumulative droplet volume density at different positions in the column.

6.7 Conclusions

In this paper we exploited successfully the numerical algorithm developed by Attarakih et al. (2004) to develop the basic features of a windows-based program LLECMOD for the hydrodynamics simulation of general liquid-liquid extraction columns. The LLECMOD program is based on the population balance approach to model the hydrodynamics of interacting liquid-liquid dispersions taking into account droplet transport as well as the breakage and coalescence in the most general way. The user-friendly input dialogs and the user functions input module make the program very general and simple to use. For steady state simulation purposes, the IME FVS solver is found to be the best when very sharp hold up profiles are not expected to occur. However, the accuracy of the spatial second order solver (IME KT2) makes it very attractive for transient simulations without appreciable increase in the CPU time (Attarakih et al., 2004). Due to these reasons the program is now being extended to include mass transfer as well as parameter optimization of the coalescence and breakage functions.

Nomenclature

$\boldsymbol{A}$	breakage interaction matrix, Eq.(8)
A_c	column cross sectional area
D_c, D_d	diffusion coefficients for the continuous and dispersed phases respectively, $m^2.s^{-1}$
D_R, D_s	rotor and stator diameters respectively, m
$\boldsymbol{d}$	characteristic droplet diameter vector
d, d'	droplet diameter, mm
d_i	the characteristic droplet diameter in the ith subdomain, mm
d_{min}, d_{max}	minimum and maximum droplet diameters, mm
$d32$	mean droplet diameter, mm
F	the convective flux
$f(v)$	droplet number density function
H, H_c	column and single compartment heights respectively, m
L	number of external (spatial) coordinate cells
M_x	number of subdomain of the internal coordinate (pivots)
$N(t,z)$	total droplets number concentration at time t and location z
N^*	rotor speed, s^{-1}
n	number distribution function, m^{-4}
n^{feed}	feed number distribution function, m^{-1}
$\boldsymbol{P}$	physical properties vector
P_r	breakage probability, Eq.(20)
Q_b	total flow rate at bottom of the column, $m^3.s^{-1}$
Q_d	inlet dispersed phase flow rate, $m^3.s^{-1}$
$Q_{c,in}$, $Q_{c,out}$	inlet and outlet continuous phase flow rates, $m^3.s^{-1}$
Q_t	dispersed phase flow rate at top of the column, $m^3.s^{-1}$
t	time, s
U_c	continuous phase velocity relative to the column walls, $m.s^{-1}$
U_d	dispersed phase velocity relative to the column walls, $m.s^{-1}$
U_r	relative droplet (slip) velocity, $m.s^{-1}$
u_m	any mth property associated with single droplet
v,v'	droplet volumes, m^3
v_f	mean droplet volume of the feed distribution, m^3
v_{min}, v_{max}	minimum and maximum droplet volume, m^3
x_i	the characteristic droplet volume in the ith subdomain, m^3
z	spatial coordinate, m
z_0	continuous phase outlet, m
z_d	dispersed feed inlet, m
z_c	continuous phase inlet, m

Greek symbols

α_c, α_d	as defined in Table 2
β_n	daughter droplet distribution based on droplet number, mm^{-1}
Γ	droplet breakage frequency, 1/s
$\Psi^{<i>}$	the ith coalescence interaction matrix whose elements are given by Eq.(11)
ϕ	dispersed phase hold up
ϕ_e	dispersed phase hold up entrained with the continuous phase
$\boldsymbol{\varphi}$	local volume concentration vector whose elements are given by Eq.(5)
$\gamma_i^{<i-1>}$, $\gamma_i^{<i>}$	triangular functions to satisfy conservation of any two integral properties
$\boldsymbol{\rho}$	breakage and coalescence source term
ρ_c, ρ_d	density of the continuous and dispersed phases respectively, $kg.m^{-3}$
μ_c	continuous phase viscosity, $kg.m^{-1}.s^{-1}$
ω	coalescence frequency, $m^3.s^{-1}$
ω_R, $\omega_{R,crit}$	rotor and critical rotor speeds respectively, s^{-1}

σ	interfacial tension, $N.m^{-1}$
θ	TVD parameter between 1 and 2.
$\vartheta(d')$	mean number of daughter droplets produced upon breakage of mother droplet of diameter d'.

Appendix A. Sample of the FORTRAN 90 user input module

```
!-----------------------------------------------------------------------------------------------------------------------
!   This is the Main Function Input file for the LLECSMOD that simulate
!   the hydrodynamics of Liquid-Liquid Extraction Columns base on the
!   Droplet Population Balances.
!   Example 1: The breakage correlations are from Modes (2000) and
!   the coalescence frequency is from Coulaloglou and Tavlarides (1977).
!-----------------------------------------------------------------------------------------------------------------------
!
!   File Name:BreakModesCoalCouloglou.for
!   File Location: LLECMOD\Examples
!
!   $Version:151202$
!-----------------------------------------------------------------------------------------------------------------------
!
!   Functions:
!
!   SDVel               : single droplet velocity
!   Dd                  : dispersed phase dispersion coefficient
!   Dc                  : continuous phase dispersion coefficient
!   FeedF               : feed distribution
!   BetaF               : daughter droplet distribution
!   GamaF               : breakage frequency
!   OmegaF              : coalescence frequency function
!
!   Uses CommonVarMod in which the common variables are declared.
!
!   Common variables
!
!   RevPerMin           : agitator speed, rmp
!   RotarDiameter       : rotor diameter, m
!   StatorDiameter      : stator diameter, m
!   MuC                 : continuous phase viscosity, kg.m-1.s-1
!   MuD                 : dispersed phase viscosity, kg.m-1.s-1
!   RhoC                : continuous phase density, kg.m-3
!   RhoD                : dispersed phase density, kg.m-3
!   SigmaCD             : interfacial tension, N.m-1
!   CompartHeight       : single compartment height, m
!   VelocityLaw         : string containing the name of the velocity law
!
!  Dimensionless numbers
!
!   Eo                  : Eötvös number
!   We                  :Weber number
!   Wecrit              :critical Weber number
!   Wem                 :modified Weber number
!
!-----------------------------------------------------------------------------------------------------------------------
    module UserFunctionsMod

    use CommonVarMod
    contains
!-----------------------------------------------------------------------------------------------------------------------
```

```
!-----------------------------------------------------------------------------------------------------------------------
!    1-The droplet terminal velocity:(Godfrey & Slater,1994), user defined velocity law.
!-----------------------------------------------------------------------------------------------------------------------
!
      doubleprecision function SDVel(dmm)
!
!    Declare the subroutine arguments
!
     doubleprecision,intent(in)::dmm
!
!    Declaration of the internal variables
!
!    d:in mm and RelVel in m.s-1, so change:d(mm) ------> d(m)
!    in the subroutiens
!
!    vignes law
!
      call Vignes(dmm,SDVel)

      endfunction SDVel
!-----------------------------------------------------------------------------------------------------------------------
      subroutine Vignes(dmm,SDVel)
!-----------------------------------------------------------------------------------------------------------------------
!    Vignes velocity law
!-----------------------------------------------------------------------------------------------------------------------
      doubleprecision,intent(in)::dmm
      doubleprecision,intent(out)::SDVel
      doubleprecision::d,dRho,Eo,dvmax,SDVelKT,SDVelmax
!     doubleprecision::Dr,Ds,Nrpm,Kv
!
!     d:in mm and RelVel in m.s-1, so change:d(mm) ------> d(m)
!
      VelocityLaw='Vignes law'
      d=dmm*1.0d-3
!
!     The slowing factor for RDC column:Kv as given by Modes (2000) and is calculated
!     internally.
!
!     Dr=RotarDiameter
!     Ds=StatorDiameter
!     Nrpm=RevPerMin/60.0d0                                    !min-1 ---> s-1
!
!     Kv=1.0d0-1.037d0*(Nrpm**3.0d0*Dr**5.0d0)**0.12d0
!     Kv= max(0.0d0,Kv-0.62d0*(d/(Ds-Dr))**0.44d0)
!
      dRho=RhoC-RhoD
!     maximum d where the Vignes velocity is maximum
      dvmax=dsqrt(2.0d0*SigmaCD/g/dRho)

      Eo=g*dRho*d*d/SigmaCD
      SDVel=(RhoC/MuC)**(1.0d0/3.0d0)*(g*dRho/RhoC)**(2.0d0/3.0d0)
      SDVel=SDVel*(1.0d0-Eo/6.0d0)*(d/4.2d0)
      SDVelKT=4.98d0*dRho**0.28d0*MuC**0.10d0*                 &
&     SigmaCD**0.18d0/RhoC**0.55d0
!
      Eo=g*dRho*dvmax*dvmax/SigmaCD
      SDVelmax=(RhoC/MuC)**(1.0d0/3.0d0)*(g*dRho/RhoC)**(2.0d0/3.0d0)
      SDVelmax=SDVelmax*(1.0d0-Eo/6.0d0)*(dvmax/4.2d0)
```

```
!
!    Combined Vignes and Klee & Treybal velocity laws
!
     if (SDVel .le. SDVelKT .and. d .ge. dvmax) then
        if (SDvelmax .gt. SDVelKT) then
          SDVel= SDVelKT
          VelocityLaw='Vignes+Klee & Treybal'
        else
!    Keep Vignes velocity at the maximum value
          SDVel=SDVelmax
          VelocityLaw='Vignes Law'
        endif
     endif

     SDVel=SDVel
     end subroutine Vignes
!-----------------------------------------------------------------------------------------------------------------------------
!    2-The dispersed phase dispersion coefficient:Dd                (m2.s-1)
!-----------------------------------------------------------------------------------------------------------------------------
     doubleprecision Function Dd(zp)
     doubleprecision,intent(in)::zp

!    Dispersion coefficiet of the dispersed phase  assumed independent of zp

     Dd=1.0d-5+zp*0.0d0                                            ! m2.s-1

     end Function Dd
!-----------------------------------------------------------------------------------------------------------------------------
!    3-The continuous phase dispersion coefficient:Dc (m2.s-1)
!-----------------------------------------------------------------------------------------------------------------------------
     doubleprecision Function Dc(zp)
     doubleprecision,intent(in)::zp

!    Dispersion coefficiet of the dispersed phase assumed independent of zp

     Dc=1.0d-4+zp*0.0d0                                            ! m2.s-1

     end Function Dc
!-----------------------------------------------------------------------------------------------------------------------------
!    5-Breakage daughter droplet distribution (mm-1)
!-----------------------------------------------------------------------------------------------------------------------------
     doubleprecision function BetaF(dmm,dmmp)
     doubleprecision,intent(in)::dmm, dmmp
     doubleprecision::Nue,Dr,Wer,Nrpm
!
!    dmm          :daughter droplet diameter (inpt)
!    dmmp         :mother droplet diameter          (input)
!    BetaF        :daughter droplet distribution based on number (output)
!    Nue          :Average No. of daughter droplets  (output)
!
     Dr=RotarDiameter
     Nrpm=RevPerMin/60.0d0                                         !(min-1 ----> s-1)
     We=RhoC*Dr**3*Nrpm**2/SigmaCD
     dcrit=0.981d0*Dr*We**(-0.55d0)*1000.0d0                       !mm
     if (dmmp .lt. dcrit) then
        Nue=2.0d0
     else
        Nue=2.0d0+0.17d0*((dmmp/dcrit)-1.0d0)**1.83d0
```

```
      endif

      BetaF=((1.0d0-(dmm/dmmp)**3.0d0))**(Nue-2.0d0)
      BetaF=3.0d0*Nue*(Nue-1.0d0)*BetaF*(dmm/dmmp)**2.0d0/dmmp

       end function BetaF
!-----------------------------------------------------------------------------------------------------------------------
!    4-Droplet breakage frequency (s-1)
!-----------------------------------------------------------------------------------------------------------------------
      doubleprecision function GamaF(dmm,holdup,Vd)

      doubleprecision,intent(in)::dmm,holdup,Vd
      doubleprecision::Dr,Nrpm,W,Wecrit,Wem,pi,P
!
      d=dmm*1.0d-3                                                    ! mm -----> m
      pi=22.0d0/7.0d0
      Dr=RotarDiameter
      Nrpm=RevPerMin/60.0d0                                           !(min-1 ----> s-1)

      Wecrit=2.0d0*pi*0.738d0*(RhoC*Dr**3/SigmaCD)**(-.50d0)*          &
&          (d/Dr)**(-.99d0)

      W=2.0d0*pi*Nrpm
      Wem=RhoC**0.8d0*MuC**0.2d0*Dr**1.6d0*d*(W**1.8d0-Wcrit**1.8d0)
      Wem=max(0.0d0,Wem/SigmaCD)

      P=6.04d-4*Wem**1.595d0/(1.0d0+6.04d-4*Wem**1.595d0)
      GamaF=P*Vd/CompartHeight+0.0d0*holdup
!
      end function GamaF
!-----------------------------------------------------------------------------------------------------------------------
!    5.-The coalescence frequency function:Omega(d,dp,holdup):(m3.s-1)
!-----------------------------------------------------------------------------------------------------------------------
      doubleprecision function OmegaF(d,dp,holdup)
!
!    Declaration of the function arguments
!
!    doubleprecision::holdup,d,dp
!
!    Declaration of the function variables
!
      doubleprecision::pi, C3,C4,Np,Ns,Dr,VT,phi,CoalEff
      doubleprecision::muec,sigma,eps1,dm,dmp,term1,term2,h,h1,h2
!
!    Evaluate droplets coalescence frequency (m3.s-1)
!    The coalescence frequency function is given by:
!     Coulaloglou and Tavlarides (1977) ; and Alopaeus et al. ( 1999, 2002)
!
!    C3                  :dimensionless constant
!    C4                  :constant (m-2)
!    Dr                  :impeller diameter (m)
!    dm                  :characteristic droplet diameter, m
!    dmp                 :characteristic droplet diameter, m
!    muec                :continuous phase viscosity (kg.(m.s)-1)
!    Np                  :power number
!    Nr                  :impeller speed (s-1)
!    phi                 :dispersed phase holdup
!    RhoC                :continuous phase density (kg.m-3)
```

```
!   sigma                :interfacial tension for the system (J.m-2)
!  VT                    :comportement volume (m3)
!
     pi=22.0d0/7.0d0
     C3=1.55d-3
     C4=2.0d6
!
     Np=5.0d0
     Ns=RevPerMin/60.0d0                                    !(min-1 ----> s-1)
     Dr=RotarDiameter
     VT=(pi*d_col**2.0d0)/4.0d0*CompartHeight
     phi=holdup
     muec=MuC
     sigma=SigmaCD
!
     phi=holdup
     eps1=phi*Np*Dr**5.0d0*Ns**3.0d0/VT
!
     dm=d*1.0d-3                                            !mm ----> m
     dmp=dp*1.0d-3                                          !mm ----> m
!
     h1=C3*eps1**(1.0d0/3.0d0)*(dm+dmp)**2.0d0
     h2=h1*(dm**(2.0d0/3.0d0)+dmp**(2.0d0/3.0d0))**(1.0d0/2.0d0)
     h=h2/(1.0d0+phi)
     term1=C4*muec*RhoC*eps1/(1.0d0+phi)**3.0d0/sigma**2.0d0
     term2=((dm*dmp)/(dm+dmp))**4.0d0
     CoalEff=dexp(-term1*term2)
     OmegaF=h*CoalEff
     end function OmegaF
!-------------------------------------------------------------------------------------------------------------------------
     end module UserFunctionsMod
!-------------------------------------------------------------------------------------------------------------------------
```

References

Alopaeus, V., Koskinen, J., & Keskinen, K. I. (1999). Simulation of population balances for liquid-liquid systems in a nonideal stirred tank. Part1 description and qualitative validation of model. *Chem. Engng Sci.*, **54,** 5887.

Alopaeus, V., Koskinen, J., Keskinen, K. I., & Majander, J. (2002). Simulation of the population balances for liquid-liquid systems in a nonideal stirred tank: Part 2- parameter fitting and the use of multiblock model for dense dispersions. *Chem. Engng. Sci.*, **57,** 1815.

Attarakih, M. M., Bart, H.-J., & Faqir, N. M. (2003). Solution of the population balance equation for liquid-extraction columns using a generalized fixed-pivot and central difference schemes. Kraslawski, A. & Turunen, I. (Ed.), *European symposium on computer aided process engineering-13*, Computer-aided chemical engineering 14 (pp. 557). Elsevier, Amsterdam.

Attarakih, M. M., Bart, H.-J. & Faqir, N. M. (2004). Numerical solution of the spatially distributed population balance equation describing the hydrodynamics of interacting liquid-liquid dispersions. *Chem. Engng. Sci*., **59**, 2567.

Casamatta, G., (1981): Comportement de la population des gouttes dans une colonne d'extraction: Transport, rupture, coalescence, transfer de matiere, Dissertation, Institut National Polytechnique De Toulouse.

Coulaloglou, C. A. , & Tavlarides, L. L. (1977). Description of interaction processes in agitated liquid-liquid dispersions. *Chem. Engng Sci.*, **32,** 1289.

Gerstlaur, A., (1999): Herleitung und Reduktion populationsdynamischer Modelle am Beispiel der Fluessig-Fluessig-Extraktion. Fortschritt-Berichte VDI Reihe, 3, 612.

Godfrey, J. C. , & Slater, M. J. (1994). *Liquid-liquid extraction equipment*. New York :John Wiley.

Grace, J. R., Wairegi, T., & Nguyen, T. H. (1976). Shapes and velocities of single drops and bubbles moving freely through immiscible liquids. *Trans. Inst. Chem. Engng*, **54**, 167.

Hufnagl, H., McIntyre, M., & Blass, E. (1991). Dynamic behavior and simulation of a liquid-liquid extraction column. *Chem. Eng. Tech.*, **14,** 301.

Hwang, C., & Shih, Y-P. (1982). Solution of population balance equations via block pulse functions. *The Chem. Engng J., **25***, 39.

Jiricny, v., Kratky, M., & Prochazka, J. (1979). Counter-current flow of dispersed and continuous phase I. Discrete polydispersed model. *Chem. Engng. Sci.*, **34,** 1141.

Klee, A. J. , & Treybal, R. E. (1956). Rate of rise or fall of liquid drops. *AIChE*, **2,** 444.

Kronberger, T., Ortner, A., Zulehner, W., & Bart, H.-J. (1994). Numerical determination of drop size distribution in extraction columns. Fasano A.(Ed.), *7th European Conference on Mathematics in Industry* p. 247-254, B. G. Teubner Stuttgart.

Kurganov, A. , & Tadmor, E. (2000). New high-resolution central schemes for nonlinear conservation laws and convective diffusion equations. *J.Com. Phys.*, **160,** 241.

Modes, G., Bart, H.-j., Rodrigue-Perancho, D., & Broder, D. (1999). Simulation of the fluid dynamics of solvent extraction columns from single droplet parameters. *Chem. Eng. Tech.*, **22,** 231.

Modes, G., (2000): *Grundsatzliche Studie zur Populationsdynamik einer Extraktionskolonne auf Basis von Einzeltropfenuntersuchungen*. Aachen: Shaker.

Ramkrishna, D. (2000). *Population Balances: Theory and applications to particulate systems in engineering*. San Diego: Academic Press.

Seader, J. D. , & Henley, E. J. (1998). *Separation process principles*. New York: John Wiley.

Vignes, A. (1965). Hydrodynamique des dispersions. *Genie Chimique*, **93,** 129.

Weinstein, O., Semiat, R., & Lewin, D. R. (1998). Modeling, simulation and control of liquid-liquid extraction columns. *Chem. Engng. Sci.*, **53,** 325.

Wesselingh, J. A. , & Bollen, A. M. (1999). Single particles, bubbles and drops: Their velocities and mass transfer coefficients. *Trans. Inst. Chem. Engng*, **77,** 89.

Wilburn, N. P. (1964). Mathematical determination of concentration profiles in two-phase continuous countercurrent extractors. *Ind. Engng. Chem. Fundam.*, **3,** 189.

Zhang, S. H., Yu, S. C., Zhou, Y. C., & Su, Y. F. (1985). A model for liquid-liquid extraction column performance- The influence of drop size distribution on extraction efficiency. *Can. J. Chem. Engng*, **63,** 212.

Zhu, F. G., Ni, X. D., Zhou, Y. C., Yu, S. C., & Su, Y. F. (1984). A modified rotating disc contactor with wire mesh coalescers. Akell, R. & King, C. J. (Eds.), *New developments in liquid-liquid extractors: Selected papers from ISEC '83*, **80**, (pp. 115-123). AIChE, New York.

Curriculum Vitae

Personal data:

Name **:** Menwer M. Attarakih

Date of birth : 10.09.1967
Place of birth : Wadi Sseer-Jordan
Marital status: married with three children
Nationality : Jordanian

Education:

- Bachelor Degree in Chemical Engineering, The University of Jordan, Jordan: 1993
- Master Degree in Chemical Engineering, The University of Jordan, Jordan: 1998
- Ph.D. Student: Institute of Process Engineering, University of Kaiserslautern, Germany: Since Sep. 2000-2004.
-

Experience

- Process Engineer in Oil Splitting, Fatty Acids and Glycerin Distillation Plants, Jordan Industrial Resources Company, Jordan: 1994-1999
- Assistant Lecturer, Al-Balqa Applied University, Jordan:1999- Sep. 2000.

Language:

1-Arabic : mother tongue.
2- English : very good in reading, writing and speaking.
3-German : passed the DSI examination.